Viscoelastic properties and compaction behaviour of pharmaceutical particulate materials

Tsardaka, Ekaterini D.

Award date:
1990

Awarding institution:
University of Bath

VISCOELASTIC PROPERTIES
AND
COMPACTION BEHAVIOUR
OF
PHARMACEUTICAL PARTICULATE MATERIALS

Submitted by Ekaterini D. Tsardaka
for the degree of PhD
of the University of Bath
1990

ProQuest LLC
789 East Eisenhower Parkway
P.O. Box 1346
Ann Arbor, MI 48106-1346

To my parents ...

SUMMARY

The viscoelastic behaviour of particulate solids is of major relevance in powder compaction. When designing a pharmaceutical tablet formulation, it is highly undesirable for the tablet properties to be markedly affected by changes in compaction rate on different tablet presses, if problems are to be avoided during scale-up and manufacture. In order to be able to predict and minimise the time-dependent deformation of pharmaceutical powders, a full understanding of such behaviour is needed.

For comparative purposes, a range of materials with differing compaction properties were studied.

Heckel plots were extended in order to study the consolidation behaviour of materials during compression, decompression and after ejection. A number of derived parameters were proposed as a useful means of assessing the viscoelastic characteristics of materials.

The mechanical properties of the tablets produced were assessed by means of both a diametral loading test and a direct tension test, in order to study the homogeneity of tablets with respect to strength and toughness.

Fitting stress relaxation data to a hyperbolic equation enabled the asymptotic value of relaxed stress and the rate of stress relaxation at short times to be determined.

Creep analysis was found to be a most useful method in quantifying the viscoelastic properties of materials. Creep experiments were used to separately quantify the ability of a material to undergo elastic, viscoelastic and plastic deformation at constant stress. Analysis of the viscoelastic compliance provided a time constant and an equilibrium value.

Spectral analysis of the creep data was an alternative method of studying viscoelastic behaviour, since analysis in the frequency domain revealed hidden periodicities of mechanisms possibly related to viscoelastic behaviour.

A detailed study of several forms of modified starch addressed factors which may influence its viscoelastic behaviour, including manufacturing process variables such as particle size, moisture content and degree of pregelatinisation.

ACKNOWLEDGEMENTS

In the course of my research, I have drawn on the time and experience of many people. They made this work possible, one way or another. I wish to thank them all.

Above all, I would like to express my gratitude to my family for their total encouragement and financial support throughout these years. Also, my beloved Mr. J. Karydas for his precious love, support, encouragement and actual help at the early stages of this work.

I would like to thank my academic supervisor Professor J.E. Rees for his direction and understanding during my studies. His support and creative criticism are greatly appreciated. Special thanks are due to Mrs. J.P. Hart for her valuable friendship, help, advice and time spent on this project. I would also like to thank Mrs. S.J. Carter for her encouraging discussions and Miss S.B. Alston and Miss A. Tsoufi for their assistance.

I wish to acknowledge Miss J. Clarke's help during my introduction to spectral analysis. Also, Dr. J.N. Staniforth's useful suggestions at the start of this work. In addition, Miss E.M. Stevens and Miss C.L. Hughes for their contribution to parts of this project. The advice of Miss K. Tzioli of the School of Mathematical Sciences is also greatly appreciated. I would also like to thank Dr. J.E. Hogan of Colorcon Ltd., for supplying the samples requested, as well as for providing useful information regarding Starch 1500 and Micromeritics U.K. Ltd. for performing a number of particle density measurements.

Many thanks are due to Mr. G.E.C. Venn and Mr. A.K. Shave of the Science Schools workshop for their technical assistance in various parts of the work, and Mr. H.R. Perrott of the School of Materials Science for his advice in the use of the scanning electron microscope.

I wish to thank Mr. R.M. Sadler for making the slides often needed during the research and always handed to him in "the last minute". I am particularly endebted to Mr. C.W. Wilson and Mrs. T. Mehaffey of the Photography unit for always completing the work requested in "no time". Finally, I am grateful to my godfather, Mr. T. Lambropoulos for offering his expertise in three-dimensional graphs.

Last but not least, I wish to thank Mrs. A. Kralli for her special "contribution" and Mrs. M. Gallop for her hospitality and motherly attention during my stay with her.

LIST OF CONTENTS

	page
SUMMARY	i
ACKNOWLEDGEMENTS	ii
LIST OF CONTENTS	iii
LIST OF TABLES	viii
LIST OF FIGURES	ix
LIST OF APPENDICES	xv
LIST OF SYMBOLS	xx
KEY OF SYMBOLS USED ON GRAPHS	xxiii

CHAPTER ONE

GENERAL INTRODUCTION	1
1.1 THEORY OF COMPACTION	3
1.1.1 Force transmission and utilisation during compaction	3
1.1.2 Mechanisms of powder consolidation	3
1.1.2.1 Particle rearrangement and closer packing	5
1.1.2.2 Elastic deformation	6
1.1.2.3 Plastic deformation	7
1.1.2.4 Brittle fracture	12
1.1.2.5 Deformation of materials without dislocations	13
1.1.3 Compact formation	16
1.1.3.1 Mechanisms of bonding	16
1.1.3.2 Lamination and capping	18
1.2 MECHANICAL PROPERTIES OF TABLETS	21
1.2.1 Factors affecting the mechanical properties of tablets	22

1.2.1.1 Crystal properties 22
1.2.1.2 Moisture 25
1.2.1.3 Particle size and shape 27
1.2.2 Methods for characterising the compaction process 30
1.2.2.1 Energy of compaction 30
1.2.2.2 Compression cycles 34
1.2.2.3 Heckel plots 38
1.2.3 Methods for characterising finished compacts 46
1.2.3.1 Friability test 46
1.2.3.2 Indirect tension test by diametral loading 46
1.2.3.3 Direct tension test 57
1.2.3.4 Other indices of tableting performance 62
1.2.3.5 Scanning electron microscopy 66

1.3 VISCOELASTIC BEHAVIOUR 67

1.3.1 Nature of viscoelastic behaviour 67
1.3.2 Analysis of viscoelastic behaviour 71
1.3.2.1 Stress relaxation 71
1.3.2.2 Creep analysis 78

1.4 HIGH SPEED COMPACTION SIMULATOR 85

CHAPTER TWO

MATERIALS AND METHODS

2.1 MATERIALS 88

2.1.1 List of materials 88
2.1.2 Characterisation of particulate solids 90
2.1.2.1 Bulk density 90
2.1.2.2 Tapped density 90
2.1.2.3 Particle density 93
2.1.2.4 Particle size analysis 94
2.1.2.5 Moisture content 100
2.1.2.6 Conditioning of powders 100

2.2 METHODS 104

2.2.1 Tablet compression 104
2.2.1.1 Data acquisition and manipulation 107
2.2.1.2 Elastic distortion during compaction 115
2.2.2 Diametral loading test 124
2.2.2.1 Data acquisition and manipulation 124
2.2.3 Direct tension test 132
2.2.3.1 Data acquisition and manipulation 132
2.2.4 Stress relaxation 135
2.2.4.1 Data acquisition and manipulation 135
2.2.5 Creep test 138
2.2.5.1 Data acquisition and manipulation 138

RESULTS AND DISCUSSION

CHAPTER THREE

BEHAVIOUR OF MATERIALS DURING COMPACTION

3.1 WORK DURING COMPACTION 145

3.2 BEHAVIOUR OF MATERIALS AT PEAK LOAD 158

3.3 EXTENDED HECKEL PLOTS 160

3.3.1 Low pressures 165
3.3.2 Linear region 166
3.3.3 High pressures 171
3.3.4 Decompression curve 171
3.3.5 Other areas derived from extended Heckel plots 176

CHAPTER FOUR

ASSESSMENT OF THE MECHANICAL STRENGTH OF TABLETS

4.1 DIAMETRAL LOADING TEST 179

4.1.1 Diametral loading of compacts 179
4.1.2 Effect of platen rate on diametral loading results obtained for Avicel PH102 compacts 189

4.2 DIRECT TENSION TEST 192

4.3 SCANNING ELECTRON MICROSCOPY 199

CHAPTER FIVE

STRESS RELAXATION

5.1 STRESS RELAXATION CURVES 201

5.2 LINEARISATION OF STRESS RELAXATION DATA 205

CHAPTER SIX

CREEP ANALYSIS

6.1 PARAMETERS AFFECTING CREEP EXPERIMENTS 218

6.1.1 Effect of applied load and test duration 218
6.1.2 Creep testing of powder and preformed compacts 219
6.1.3 Effect of powder mass 220
6.1.4 Effect of loading rate 221
6.1.5 Effect of tooling dimensions 225

6.2 CREEP BEHAVIOUR OF MATERIALS 227

6.3 SPECTRAL ANALYSIS OF CREEP DATA 249

6.3.1 Introduction 249
6.3.2 Creep spectra 258

CHAPTER SEVEN

FACTORS AFFECTING THE PHYSICO-MECHANICAL PROPERTIES OF STARCH

7.1 INTRODUCTION 263

7.2 PARTICLE SIZE 265

7.3 MOISTURE CONTENT 274

7.4 DEGREE OF PREGELATINISATION 282

CHAPTER EIGHT

CONCLUSIONS 296

SUGGESTIONS FOR FURTHER WORK 300

REFERENCES 301

PUBLICATIONS 319

APPENDICES

APPENDIX A 320

APPENDIX B 321

APPENDIX C 333

APPENDIX D 343

APPENDIX E 353

APPENDIX F 356

367

LIST OF TABLES

The following Tables are presented in Chapter Two.

		page
Table 2.1	Density measurements for the materials tested.	91
Table 2.2	Particle size analysis of Avicel PH102, Emcocel 90M, and Starch 1500.	97
Table 2.3	Particle size analysis of sodium chloride, sodium bicarbonate, anhydrous lactose and Emcompress.	98
Table 2.4	Particle size analysis of amylose, amylopectin and batches of Starch 1500 containing different proportions of cold water solubles.	99
Table 2.5	Moisture content of materials equilibrated at 53% relative humidity.	101
Table 2.6	Substances used to provide a range of relative humidities at 25C.	103
Table 2.7	Weights of the materials used in experiments.	106
Table 2.8	Calibration data for the strain gauges.	109
Table 2.9	Calibration data for 10mm LVDT (Sangamo Instr. Ltd.).	112
Table 2.10	Correction applied for the elastic distortion of the punch assemblies of the tableting machine.	120
Table 2.11	Calibration data for 5mm LVDT (Sangamo Instr. Ltd.).	129
Table 2.12	Calibration data for 5mm LVDT (RDP Instr. Ltd.).	140

Other Tables are presented in the Appendix section.

LIST OF FIGURES

CHAPTER ONE

Fig. 1.1	Various stages during the compaction of particulate materials according to Seelig and Wulff (1946).	4
Fig. 1.2	Plastic deformation by means of a translational slip in crystals.	8
Fig. 1.3	Edge and screw dislocations in crystals.	10
Fig. 1.4	Crack stop mechanism in materials proposed by Cook and Gordon (1964).	15
Fig. 1.5	Force-displacement curve during compaction of materials used by Higuchi et al (1952) for the assessment of the work done during compaction.	31
Fig. 1.6	Heckel plot and relevant parameters (Heckel, 1961a and b).	40
Fig. 1.7	Assessment of the consolidation behaviour of materials based on the effect of particle size on their Heckel plot, according to Hersey and Rees (1971), and York and Pilpel (1973).	44
Fig. 1.8	Failure patterns during diametral loading of tablets (Newton et al, 1971) and stress distribution in pure tensile failure (Frocht, 1948).	48
Fig. 1.9	Force-displacement curve during diametral loading of tablets used by Rees and Rue (1978c) for the assessment of work of failure.	52
Fig. 1.10	Theoretical curves for some area-ratio values according to Moschos (1985).	55
Fig. 1.11	Tensile testing apparatus used by Nystrom et al (1977) for direct tension testing of tablets.	58
Fig. 1.12	Mechanical models used to represent the elastic and viscous behaviour of materials.	68
Fig. 1.13	Mechanical models used to represent the viscoelastic behaviour of semisolids.	70
Fig. 1.14	Decrease in force with time during stress relaxation experiments.	72
Fig. 1.15	A typical creep curve annotated to show discrete deformation mechanisms, and a mechanical model which can be used to describe creep behaviour.	79

CHAPTER TWO

Fig. 2.1	Instrumented E2 Manesty tableting machine with associated data acquisition and processing	105

system.
Fig. 2.2 Calibration curve for the strain gauges. 110
Fig. 2.3 Close-up of the tableting machine showing the position of the LVDT on the die table. 111
Fig. 2.4 Calibration curve for 10mm LVDT (Type AG/10, Sangamo Instr. Ltd.). 113
Fig. 2.5 Upper punch assembly showing the initial and improved position of the LVDT contact arm. 114
Fig. 2.6 Experimental systems used to determine the elastic distortion of the punch assemblies under load. 117
Fig. 2.7 Elastic distortion of the different systems used to calculate the individual distortions of the upper and lower punch assemblies during compaction. 119
Fig. 2.8 Calculation of areas derived from extended Heckel plots. 123
Fig. 2.9 Mechanical testing machine used to assess the mechanical properties of tablets. 125
Fig. 2.10 Digital micrometer used to measure tablet dimensions. 126
Fig. 2.11 Experimental system used for diametral loading of tablets, showing the position of the LVDT on the moving crosshead of the mechanical testing machine. 128
Fig. 2.12 Calibration curve for 5mm LVDT (AG/5, Sangamo Instr. Ltd.). 130
Fig. 2.13 Mechanical testing machine with associated data acquisition and processing system. 131
Fig. 2.14 Experimental system used for direct tension testing of tablets. 133
Fig. 2.15 Ball and socket structure used to ensure axial alignment during direct tension testing of tablets. 134
Fig. 2.16 Mechanical testing machine equipped with a compression cage and constant stress module. 136
Fig. 2.17 Lower punch and die used with the compression cage. 137
Fig. 2.18 Compression cage showing the position of the LVDTs during creep testing. 139
Fig. 2.19 Calibration curve for 5mm LVDT (D5/500A, RDP Electr. Ltd.). 141
Fig. 2.20 Original creep curve and the derived curve describing compliance due to retarded elastic deformation as a function of time. 143

CHAPTER THREE

Fig. 3.1 "True" work done on the lower punch during compaction at a range of compaction forces. 147
Fig. 3.2 "True" power of compaction at a range of 149

compaction forces.
Fig. 3.3 Expansion work undergone by materials during decompression at a range of compaction forces. 150
Fig. 3.4 "True" work of compaction as a percentage of the total work of compaction at a range of compaction forces. 152
Fig. 3.5 Expansion rate of materials during decompression at a range of compaction forces. 153
Fig. 3.6 Power of expansion of materials during decompression at a range of compaction forces. 154
Fig. 3.7 Effect of compaction force on the relative density of the produced tablets. 157
Fig. 3.8 Extended Heckel plots obtained for Avicel PH102, Emcocel 90M and Starch 1500 at 18kN. 161
Fig. 3.9 Extended Heckel plots obtained for sodium chloride, sodium bicarbonate, anhydrous lactose and Emcompress at 18kN. 162
Fig. 3.10 Three-dimensional profile of $\ln[1/(1-D)]$, plotted against pressure and time for Starch 1500 at 18kN. 163
Fig. 3.11 Three-dimensional profile of $\ln[1/(1-D)]$, plotted against pressure and time for Emcompress at 18kN. 164
Fig. 3.12 Yield pressure values at a range of compaction forces. 168
Fig. 3.13 Values for the intercept A of the Heckel equation at a range of compaction forces. 169
Fig. 3.14 Extended Heckel plot obtained for a rubber plug at 18kN. 173
Fig. 3.15 Chord area values expressed as a percentage of the square area at a range of compaction forces. 175
Fig. 3.16 Values of the area above the decompression curve expressed as a percentage of the square area at a range of compaction forces. 178

CHAPTER FOUR

Fig. 4.1 Radial tensile strength values at a range of compaction forces. 180
Fig. 4.2 Deformation before failure during diametral loading of tablets at a range of compaction forces. 183
Fig. 4.3 Radial work of failure values at a range of compaction forces. 184
Fig. 4.4 Corrected work of failure during diametral loading of tablets at a range of compaction forces. 186
Fig. 4.5 Apparent failure viscosity values obtained during diametral loading of tablets at a range of compaction forces. 187

Fig. 4.6 Effect of loading rate on the tensile strength of Avicel PH102 tablets at a range of compaction forces. 190
Fig. 4.7 Effect of loading rate on the radial work of failure of Avicel PH102 tablets at a range of compaction forces. 191
Fig. 4.8 Axial tensile strength values at a range of compaction forces. 193
Fig. 4.9 Strength isotropy ratio values at a range of compaction forces. 196
Fig. 4.10 Work of failure during direct tension testing of tablets at a range of compaction forces. 197

CHAPTER FIVE

Fig. 5.1 Stress relaxation curves for the materials loaded to 2kN at 10mm/min. 202
Fig. 5.2 Relative force drop and rate of force decay to half force drop during stress relaxation experiments. 204
Fig. 5.3 Stress relaxation data plotted as F_t/F_{min} against lnt. 206
Fig. 5.4 Slope and intercept values obtained from a plot of F_t/F_{min} against lnt. 207
Fig. 5.5 Hyperbola and its linear transformation. 209
Fig. 5.6 Stress relaxation data plotted as $t/(F_{max}-F_t)$ against t. 212
Fig. 5.7 Slope and intercept values obtained from a plot of $t/(F_{max}-F_t)$ against t. 213
Fig. 5.8 Values for the parameters a and b of the hyperbolic equation used to describe stress relaxation data. 214
Fig. 5.9 Values for the product a·b of the parameters a and b of the hyperbolic equation. 215

CHAPTER SIX

Fig. 6.1 Effect of initial loading rate on the viscosity coefficient and J_i values of Avicel PH102, Starch 1500 and Emcompress. 224
Fig. 6.2 Creep curves for the materials at approximately 0.7 porosity. 228
Fig. 6.3 J_o values for the materials at a range of relative densities. 229
Fig. 6.4 J_r values for the materials at a range of relative densities. 230
Fig. 6.5 J_n values for the materials at a range of relative densities. 231
Fig. 6.6 Viscosity coefficient values for the materials at a range of relative densities. 234

Fig. 6.7 Elastic modulus values for the materials at a range of relative densities. 236
Fig. 6.8 Effect of porosity on $\ln G^*$ values. 239
Fig. 6.9 Effect of porosity on $\ln \eta$ values. 241
Fig. 6.10 k_2 values for the materials at a range of relative densities. 245
Fig. 6.11 J_i values for the materials at a range of relative densities. 247
Fig. 6.12 Significance of peaks in a spectrum. 252
Fig. 6.13 An example of spectral analysis of a time series. 254
Fig. 6.14 Typical print-out of a creep curve. 259
Fig. 6.15 Creep spectra for Emcompress and anhydrous lactose. 260
Fig. 6.16 Creep spectra for Starch 1500 and Avicel PH102. 261

CHAPTER SEVEN

Fig. 7.1 Yield pressure values for some particle size fractions (<125μm, 125-180μm and >180μm) of Starch 1500. 266
Fig. 7.2 Radial work of failure for some particle size fractions (<125μm, 125-180μm and >180μm) of Starch 1500. 267
Fig. 7.3 "True" work of compaction for some coarse particle size fractions (>710μm and >1680μm) of Starch 1500. 269
Fig. 7.4 Yield pressure values for some coarse particle size fractions (>710μm and >1680μm) of Starch 1500. 270
Fig. 7.5 Elastic modulus values for some coarse particle size fractions (>710μm and >1680μm) of Starch 1500. 271
Fig. 7.6 Viscosity coefficient values for some coarse particle size fractions (>710μm and >1680μm) of Starch 1500. 272
Fig. 7.7 Radial work of failure values for some coarse particle size fractions (>710μm and >1680μm) of Starch 1500. 273
Fig. 7.8 Effect of moisture on the yield pressure of Starch 1500. 275
Fig. 7.9 Effect of moisture on the elastic modulus of Starch 1500. 276
Fig. 7.10 Effect of moisture on the viscosity coefficient of Starch 1500. 277
Fig. 7.11 Effect of moisture on the J_i values of Starch 1500. 279
Fig. 7.12 Effect of moisture on the k_2 values of Starch 1500. 280

Fig. 7.13 Effect of moisture on the radial work of failure of Starch 1500. 281
Fig. 7.14 Effect of the amount of cold water solubles on the yield pressure of Starch 1500. 284
Fig. 7.15 Effect of the amount of cold water solubles on the viscosity coefficient of Starch 1500. 285
Fig. 7.16 Effect of the amount of cold water solubles on the radial work of failure of Starch 1500. 286
Fig. 7.17 Yield pressure values for Starch 1500 and National 1551 at a range of compaction forces. 288
Fig. 7.18 % chord area values for Starch 1500 and National 1551 at a range of compaction forces. 289
Fig. 7.19 Elastic modulus values for Starch 1500 and National 1551 at a range of relative densities. 290
Fig. 7.20 Viscosity coefficient values for Starch 1500 and National 1551 at a range of relative densities. 292
Fig. 7.21 J_i values for Starch 1500 and National 1551 at a range of relative densities. 293
Fig. 7.22 k_2 values for Starch 1500 and National 1551 at a range of relative densities. 294
Fig. 7.23 Radial work of failure for Starch 1500 and National 1551 at a range of compaction forces. 295

LIST OF APPENDICES

page

APPENDIX A

Table A.1 Work and related parameters obtained during compression for Avicel PH102, Emcocel 90M and Starch 1500. 322

Table A.2 Work and related parameters obtained during compression for sodium chloride, sodium bicarbonate, anhydrous lactose and Emcompress. 323

Table A.3 Results obtained for a rubber plug compressed at 18kN. 324

Table A.4 Parameters related to elastic recovery, obtained during decompression for Avicel PH102, Emcocel 90M and Starch 1500. 325

Table A.5 Parameters related to elastic recovery, during decompression for sodium chloride, sodium bicarbonate, anhydrous lactose and Emcompress. 326

Table A.6 Time-related parameters, obtained during compression for Avicel PH102, Emcocel 90M and Starch 1500. 327

Table A.7 Time-related parameters, obtained during compression for sodium chloride, sodium bicarbonate, anhydrous lactose and Emcompress. 328

Table A.8 Extended Heckel plot results for Avicel PH102, Emcocel 90M and Starch 1500. 329

Table A.9 Extended Heckel plot results for sodium chloride, sodium bicarbonate, anhydrous lactose and Emcompress. 330

Table A.10 Yield pressure values for Tablettose, obtained at 50 - 200MPa using several high speed compaction simulators (Bateman, 1988). 331

Table A.11 Yield pressure values for Tablettose at a range of compaction forces. 332

APPENDIX B

Table B.1 Diametral loading results for Avicel PH102, Emcocel 90M and Starch 1500. 334

Table B.2 Diametral loading results for sodium chloride and sodium bicarbonate. 335

Table B.3 Diametral loading results for anhydrous lactose and Emcompress. 336

Table B.4 Effect of loading rate on the radial tensile strength of Avicel PH102 compacts. 337

Table B.5 Effect of loading rate on the radial work of 338

failure of Avicel PH102 compacts.
Table B.6 Direct tension test results for Avicel PH102, Emcocel 90M and Starch 1500. 339
Table B.7 Direct tension test results for sodium chloride and sodium bicarbonate. 340
Table B.8 Direct tension test results for anhydrous lactose and Emcompress. 341
Table B.9 Strength isotropy ratio values for the materials subjected to both a direct and an indirect tension test. 342

APPENDIX C

Fig. C.1 Scanning electron micrographs of Avicel PH102 and Emcocel 90M powder and the surface of a fractured tablet. 344
Fig. C.2 Scanning electron micrographs of Starch 1500 and National 1551 powders and the surface of a fractured tablet. 345
Fig. C.3 Scanning electron micrographs of Starch 1500 (>710μm) powder at low and high magnification, and the surface of a fractured tablet. 346
Fig. C.4 Scanning electron micrographs of Starch 1500 (>1680μm) powder at low and high magnification, and the surface of a fractured tablet. 347
Fig. C.5 Scanning electron micrographs of amylose powder at low and high magnification, and the surface of a fractured tablet. 348
Fig. C.6 Scanning electron micrographs of amylopectin powder at low and high magnification, and the surface of a fractured tablet. 349
Fig. C.7 Scanning electron micrographs of sodium chloride powder at low and high magnification, and the surface of a fractured tablet. 350
Fig. C.8 Scanning electron micrographs of sodium bicarbonate and anhydrous lactose powder and the surface of a fractured tablet. 351
Fig. C.9 Scanning electron micrographs of Emcompress powder at low and high magnification, and the surface of a fractured tablet. 352

APPENDIX D

Table D.1 Stress relaxation results for Avicel PH102, Starch 1500, anhydrous lactose and Emcompress. 354
Table D.2 Results obtained from linearisation of stress relaxation data for Avicel PH102, Starch 1500, anhydrous lactose and Emcompress. 355

APPENDIX E

Table E.1	Effect of test duration on the parameters derived from creep data for Starch 1500 and Emcompress.	357
Table E.2	Effect of powder mass on the parameters derived from creep data for Starch 1500 and Emcompress.	358
Table E.3	Effect of upper punch concavity on the parameters derived from creep data for Starch 1500 and Emcompress.	359
Table E.4	Effect of punch and die diameter on the parameters derived from creep data for Starch 1500 and Emcompress.	360
Table E.5	Creep results for Avicel PH102, Emcocel 90M and Starch 1500.	361
Table E.6	Creep results for sodium chloride, sodium bicarbonate, anhydrous lactose and Emcompress.	362
Table E.7	Parameters derived from creep data for Avicel PH102, Emcocel 90M and Starch 1500.	363
Table E.8	Parameters derived from creep data for sodium chloride, sodium bicarbonate, anhydrous lactose and Emcompress.	364
Table E.9	Elastic modulus values obtained using the equation proposed by Spriggs (1961).	365
Table E.10	Viscosity coefficient values obtained using the equation proposed by Spriggs (1961).	366

APPENDIX F

Table F.1	Work and related parameters obtained during compression for some particle size fractions of Starch 1500 (B.N. 611002).	368
Table F.2	Parameters related to elastic recovery, obtained during decompression for some particle size fractions of Starch 1500 (B.N. 611002).	369
Table F.3	Time-related parameters, obtained during compression for some particle size fractions of Starch 1500 (B.N. 611002).	370
Table F.4	Extended Heckel plot results for some particle size fractions of Starch 1500 (B.N. 611002).	371
Table F.5	Diametral loading results for some particle size fractions of Starch 1500 (B.N. 611002).	372
Table F.6	Work and related parameters obtained during compression for some particle size fractions of Starch 1500 (Batch F).	373
Table F.7	Parameters related to elastic recovery, obtained during decompression for some particle size fractions of Starch 1500 (Batch	374

F).
Table F.8 Time-related parameters, obtained during compression for some particle size fractions of Starch 1500 (Batch F). 375
Table F.9 Extended Heckel plot results for some particle size fractions of Starch 1500 (Batch F). 376
Table F.10 Creep results for some particle size fractions of Starch 1500 (Batch F). 377
Table F.11 Parameters derived from creep data for some particle size fractions of Starch 1500 (Batch F). 378
Table F.12 Diametral loading results for some particle size fractions of Starch 1500 (Batch F). 379
Table F.13 Moisture content of Starch 1500 at a range of relative humidities. 381
Table F.14 Work and related parameters obtained during during compression for Starch 1500 stored at different humidity conditions. 382
Table F.15 Parameters related to elastic recovery, obtained during decompression for Starch 1500 stored at different humidity conditions. 383
Table F.16 Time-related parameters, obtained during compression for Starch 1500 stored at different humidity conditions. 384
Table F.17 Extended Heckel plot results for Starch 1500 stored at different humidity conditions. 385
Table F.18 Creep results for Starch 1500 stored at different humidity conditions. 386
Table F.19 Parameters derived from creep data for Starch 1500 stored at different humidity conditions. 387
Table F.20 Diametral loading results for Starch 1500 stored at different humidity conditions. 388
Table F.21 Work and related parameters obtained during compression for batches of Starch 1500 containing different proportions of cold water solubles. 390
Table F.22 Parameters related to elastic recovery, obtained during decompression for batches of Starch 1500 containing different proportions of cold water solubles. 391
Table F.23 Time-related parameters, obtained during compression for batches of Starch 1500 containing different proportions of cold water solubles. 392
Table F.24 Extended Heckel plot results for batches of Starch 1500 containing different proportions of cold water solubles. 393
Table F.25 Work and related parameters obtained during compression for amylose and amylopectin. 394
Table F.26 Parameters related to elastic recovery, obtained during decompression for amylose 395

and amylopectin.
Table F.27 Time-related parameters, obtained during compression for amylose and amylopectin. 396
Table F.28 Extended Heckel plot results for amylose and amylopectin. 397
Table F.29 Creep results for batches of Starch 1500 containing different proportions of cold water solubles. 398
Table F.30 Parameters derived from creep data for batches of Starch 1500 containing different proportions of cold water solubles. 399
Table F.31 Creep results for amylose and amylopectin. 400
Table F.32 Parameters derived from creep data for amylose and amylopectin. 401
Table F.33 Diametral loading results for batches of Starch 1500 containing different proportions of cold water solubles. 402
Table F.34 Diametral loading results for amylose and amylopectin. 404
Table F.35 Parameters obtained during compression of 1500 (B.N. 306015) and National 1551. 405
Table F.36 Parameters derived from creep data for Starch 1500 (B.N. 306015) and National 1551. 406
Table F.37 Diametral loading results for Starch 1500 (B.N. 306015) and National 1551. 407

LIST OF SYMBOLS

γ = strain
γ_1 = elastic strain
γ_2 = viscous strain
$\gamma_n(t)$ = creep strain in the viscous region
$\gamma_o(t)$ = creep strain in the elastic region
$\gamma_r(t)$ = creep strain in the viscoelastic region
$\dot{\gamma}$ = shear rate
δ = constant related to compressibility
ϵ = porosity
η = shear viscosity
η_o = viscosity coefficient at zero porosity
η_t = viscosity coefficient at tapped density
$\eta_{0.3}$ = viscosity coefficient at 0.3 porosity
μ = shear modulus
π = 3.1415927
σ = stress
σ_1 = stress in the spring
σ_2 = stress in the dashpot
σ_τ = tensile strength of a compact without a hole
σ_{τ_o} = tensile strength of a compact with a hole
σ_a = axial tensile strength
σ_r = radial tensile strength
σ_x = tensile stress
σ_y = compressive stress
σ_z = shear stress
σ^2 = variance of the time series
ϕ_2 = solid fraction
χ^2 = value of the χ^2 distribution

a, b = constants of a hyperbolic equation

a_l-e_l = constants of the polynomial equation describing the elastic distortion of the lower punch

a_u-e_u = constants of the polynomial equation describing the elastic distortion of the upper punch

a_a, b_b = spacings between atoms in crystals

A = constant of the Heckel equation

AFV = apparent failure viscosity

B, n = coefficients

BFP = brittle fracture propensity

BI = bonding index

C = constant

CW_f = corrected work of failure

C^2 = value of the modified χ^2 distribution

d_b = bulk density

d_p = particle density

d_t = tapped density

d.f. = degrees of freedom

D = relative density

D_a = relative density of the compact when $\ln[1/(1-D)] = A$

D_b = densification due to particle rearrangement prior to the application of an appreciable force

D_o = relative density of the loose powder at zero pressure

D_t = tablet diameter

DI = disruption index

ERI = elastic recovery index

f = friability

ΔF = amount of the compressional force left in the viscoelastic region at time t

F_{max} = force at t=0 during a stress relaxation experiment

F_{min} = force at the end of a stress relaxation experiment

ΔF_o = amount of the compressional force at time t=0

F_t = force at time t during a stress relaxation experiment

g = gravitational constant

G = elastic modulus

G_o = elastic modulus at zero porosity

G_t = elastic modulus at tapped density

$G_{0.3}$ = elastic modulus at 0.3 porosity

h_i = initial height of the indenter

h_r = rebound height of the indenter

h_t = tablet thickness

H_m = tablet thickness at maximum load

H_t = tablet thickness at t=30s

J_i = asymptotic value of $J_v(t)$ at infinity

J_m = creep compliance of each Voigt element

J_n = creep compliance in the viscous region

J_o = creep compliance in the elastic region

J_r = creep compliance in the viscoelastic region

$J(t)$ = creep compliance as a function of time

$J_v(t)$ = creep compliance due to retarded elastic deformation as a function of time

k = relaxation coefficient

k_1 = slope of the linear region of the creep curve

k_2 = time constant in the viscoelastic region
K = proportionality constant of the Heckel equation
LPF = lower punch force
m = size of sets of estimates to be averaged in a spectral window
m_i = mass of the indenter
N = number of observations
p = probability
P = axial pressure during compaction
P_a = load required to cause axial failure
P_c = compression pressure
P_f = power of failure
P_i = indentation hardness
P_m = magnitude of P_i at zero porosity
P_o = pressure at time t=0
P_r = load required to cause radial failure
P_t = pressure at time t
P_v = relative pressure
P_z = axial pressure at zero porosity
Py = yield pressure
Py_1 = yield pressure at minimum punch velocity
Py_2 = yield pressure at maximum punch velocity
PS = power specrum of a time series
r = empirical constant of the Spriggs equation
r_c = chordal radius of the dent produced
r_i = radius of the indenter
r_t = tablet radius
R_a = area-ratio
S_e = stress at equilibrium
S_t = stress at time t
S_v = relative stress
SIR = strength isotropy ratio
SRS = strain rate sensitivity index
t = time
T_m = retardation time of each Voigt element
UPF = upper punch force
v = Burger's vector
V = sample volume
V_b = volume of the poured powder
V_p = volume of the powder excluding void spaces
V_t = volume of the powder including void spaces
W = sample weight
W_a = sample weight after testing
W_d = weight of the dried powder sample
W_f = work of failure
W_o = original sample weight
x = punch displacement, relative platen movement
X = independent variable
x_e = displacement reading as force deviates below threshold
x_m = displacement reading at maximum force
x_s = first displacement reading as force deviates above threshold
Y = dependent variable

KEY OF SYMBOLS USED ON GRAPHS

Unless indicated otherwise, the following symbols will be used:

ANHYDROUS LACTOSE	■
AVICEL PH102	●
EMCOCEL 90M	○
EMCOMPRESS	□
SODIUM CHLORIDE	△
SODIUM BICARBONATE	▲
STARCH 1500	✳

Note: Error bars on graphs indicate ± 95% confidence intervals.

CHAPTER ONE

GENERAL INTRODUCTION

Tablets represent a convenient and acceptable way for administering drugs to the body. They are solid dosage forms containing a precise amount of one or more drugs and some other inert ingredients, called excipients. These are diluents, binders and adhesives, disintegrants, lubricants and glidants, colours, flavours and sweeteners. Tablets provide several advantages:

- relatively low production cost
- ease of packaging
- minimal storage space requirements
- ease of dispensing
- convenience of use and optimum portability
- flexibility in dosage
- accuracy and precision of dosage

Tablet design and manufacture has always been a challenge because of the many competing objectives of this dosage form. Factors such as bioavailability, resistance to abrasion, as well as appearance, have to be taken into consideration. The formulation scientist has, therefore, to consider the use of the

most suitable components and procedures in order to design the best possible product.

There are three common approaches to tablet manufacture. Direct compression involves simple mixing of the ingredients and compression into tablets. In contrast, during dry granulation, mixtures are normally compressed into large, relatively weak compacts which are then milled to produce smaller aggregates; these are then compressed into tablets. The third approach, wet granulation, is the most widely used method. It involves wet massing and drying of the materials and requires screening at various stages. The main purpose of the methods which utilise granulation is to improve the flow and compression properties of the starting materials and reduce the risk of constituent powder segregation.

Some materials cannot be compressed into tablets without prior treatment. Others produce tablets of inadequate properties. So far, "trial and error" methods have generally been used in order to overcome such problems. The lack of full understanding of the compaction mechanisms seems to be the major cause of these limitations. Justified crucial decisions can only be taken when the compaction behaviour of materials is mathematically modelled and the relationships between formulation and manufacturing variables are fully understood.

1.1 THEORY OF COMPACTION

1.1.1 Force Transmission and Utilisation During Compaction

Initially, within a powder bed there are essentially only point contacts between the particles. When an external force is applied, it is transmitted through such interparticle contacts. Stress is, therefore, concentrated around these points, resulting in local deformation of the material. The type of deformation depends on the rate of application, duration and, of course, magnitude of the locally created stress, as well as the physico-mechanical properties of the material.

In practice, there are certain factors which limit the full utilisation of the applied force, such as frictional effects and even adhesion on the surfaces of the die wall and punch faces. To eliminate such undesirable effects, additives, known as anti-adhesives and lubricants, are often used.

1.1.2 Mechanisms of Powder Consolidation

Following die-filling (Fig. 1.a), the compaction of a material involves various processes, as summarised by Seelig and Wulff (1946):

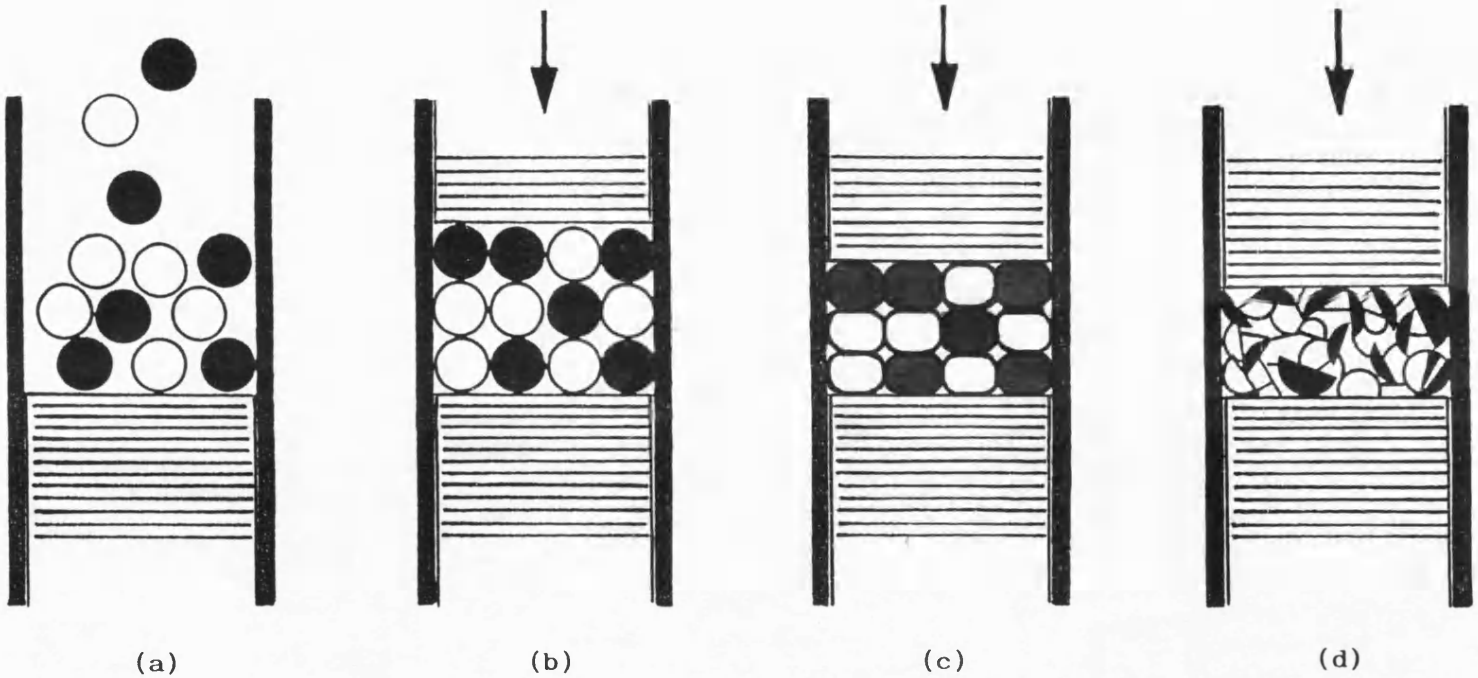

FIG. 1.1 Various stages during the compaction of particulate materials according to Seelig and Wulff (1946).

- particle rearrangement (Fig. 1.1b)
- elastic and plastic deformation (Fig. 1.1c)
- bond formation through cold-working, with or without fragmentation (Fig. 1.1d)

Train (1956) stated that different stages of powder compaction can be distinguished by studying changes in the slope of a plot of the logarithm of applied pressure against relative volume. He distinguished four stages:

- closer packing of particles
- formation of temporary struts, columns and vaults
- crushing or plastic deformation of particles
- consolidation due to the compressibility of the solid

He considered that at higher loads elastic deformation of the densified compact may occur.

Cole et al (1975), however, noted that depending on the material, the different consolidation mechanisms may overlap as compression takes place. Therefore, none of the mathematical expressions proposed so far could describe adequately the compaction process for all powders.

1.1.2.1 Particle Rearrangement and Closer Packing

During the initial stages of force application, consolidation takes place due to the particles sliding past each other, thus achieving closer packing. The extent to which this

will occur is greatly influenced by the frictional properties of the sliding surfaces, since interparticle attractive forces which result in friction and adhesion must be overcome. Surface irregularities will obstruct free movement by giving rise to substantial frictional forces.

Furthermore, the particle size distribution of the powder is also important. Samples with a wide range of particle size will pack more closely, due to the smaller particles occupying the interparticle voids between the larger ones. On the other hand, small or irregular particles will give rise to electrostatic effects, thus preventing close packing.

1.1.2.2 Elastic Deformation

When pressure is applied to a powder bed, particle rearrangement is soon followed by deformation. Initially, elastic deformation occurs, the extent of which depends on the elastic modulus, G, of the material. According to Hooke's law, in the elastic region the stress, σ, is proportional to the strain, γ:

$$\gamma = \sigma/G \qquad \text{Eq. 1.1}$$

If G is high, there is relatively little deformation and the system is rigid. If G is low, large temporary distortion occurs which recovers immediately at load release.

1.1.2.3 Plastic Deformation

When the elastic limit is exceeded at the yield point of the material, irreversible deformation takes place until the cross-sectional area of the material normal to the applied load is capable of supporting that stress.

Many crystals deform plastically by means of a translational slip (Fig. 1.2), where one part of a crystal slides against an adjacent part. Ideally, the crystal orientations within the different parts remain unchanged. The surfaces on which slip occurs form the slip plane. Crystals often slip simultaneously along two or more slip planes. This happens when deformation on one set of planes causes the shear stress on another set to increase sufficiently to initiate slip on this second set. Such a multiple slip is called twinning.

In many materials, plastic deformation occurs due to the movement of serious mobile defects, known as dislocations. According to the "dislocation theory" (Cottrell, 1953), these defects are responsible for the fact that the observed stress required to cause atomic planes to slide past each other within crystals, is several orders of magnitude lower than the following relationship would predict:

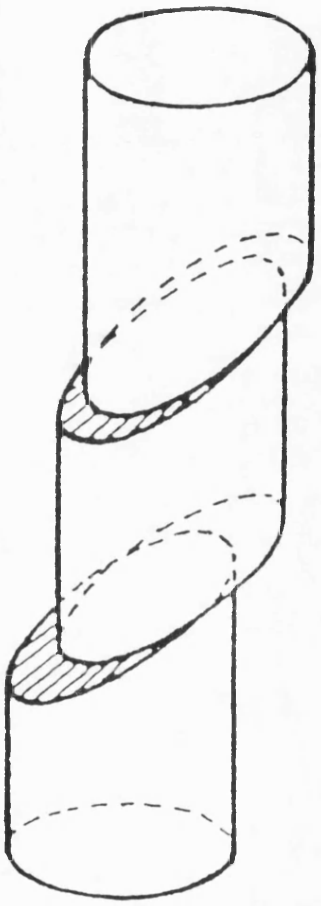

FIG. 1.2 Plastic deformation by means of a translational slip in crystals.

$$\text{shear stress} = a_a/b_a \cdot \mu/2\pi \quad \text{Eq. 1.2}$$

where,

a_a, b_a = spacings between atoms

μ = shear modulus

Only in very fine fibres or single crystal whiskers, have stresses approaching the ideal shear strength been observed. This led to the development of fibre reinforced solids for engineering purposes. When dislocations move, or attempt to move in the direction that would enable the crystal to give way to the applied force, the resistance that the crystal lattice offers to their movement is much smaller than the shear strength. The reason for this is as follows. The forces between the atoms in a crystal lattice balance only when the dislocation lies in a position of symmetry with respect to the atoms in the slip plane. Between these positions of symmetry, the forces are not fully balanced and only a small applied force is needed to drive the dislocation forward.

The nature of a dislocation is characterised by Burger's vector, v (Henderson, 1972). This specifies the direction and distance by which atoms of the slip plane move with respect to others on the same slip plane. An edge dislocation results when a row of atoms is either removed from the crystal or displaced by a unit distance in such a way, that under the action of a shear stress, movement occurs along a slip plane in the direction of the applied force (Fig. 1.3a). In comparison, when the movement of a dislocation occurs in a direction normal to

(a)

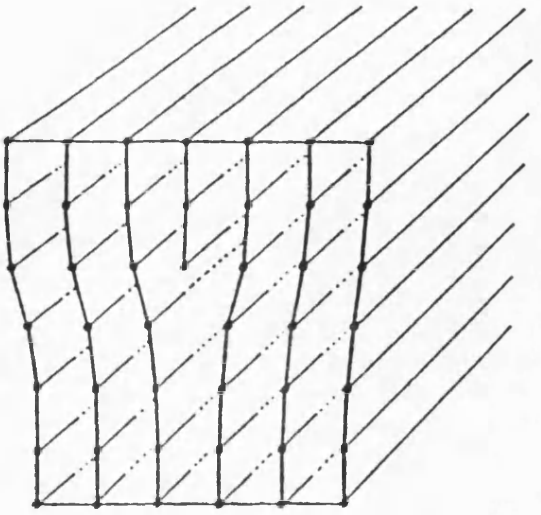

(b)

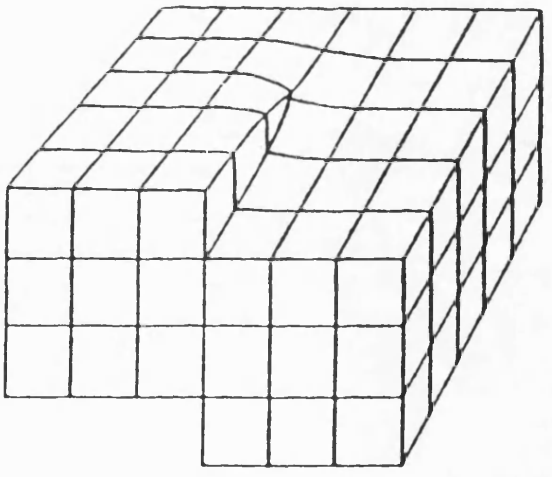

FIG. 1.3 Edge (a) and screw (b) dislocations in crystals.

the applied force, a screw dislocation is formed. A strain pattern of a screw dislocation may be visualised as in Fig. 1. 3b. Dislocations in a real crystal are likely to have both an edge and a screw character, their proportions varying as they move within the crystal lattice.

Apart from mobile dislocations, non-mobile ones are also situated randomly within a crystal and can obstruct the movement of other dislocations. Such distortions, as well as intersecting slip planes can cause interlocking of dislocations. If further movement of dislocations follows, a pile-up of dislocations is produced. The resulting increase in dislocation density, together with the reduced mobility due to the pile-ups, reduces dramatically the ability of the material to undergo plastic deformation and relieve stress. This can lead to brittle fracture of a normally plastic material, a phenomenon known as work-hardening. It has been suggested as a predominant failure mechanism occuring in sodium chloride crystals (Rosenberg, 1984).

Work hardening may have a significant effect on the behaviour of particulate solids under load (Rees et al, 1972). During a powder compaction process, the resulting embrittlement increases the number of contact points and thus, the area over which the load is applied and may, therefore, be responsible for the reported reduction in bond strength.

Finally, an important element in understanding dislocation movement is the fact that atoms in a slip plane do not move

simultaneously but consecutively. The reason for this is the non-uniform applied stress which causes some areas to attempt to move first followed by the rest of the plane at some finite speed.

Concluding, the nature of dislocations within crystals and their mobility pattern in particular, could contribute to the explanation of the time-dependent plastic deformation of many crystalline materials. The dislocation density is one of the parameters used to quantify such crystal imperfections.

Plastic deformation in various crystalline materials has been substantiated by means of photographic evidence. Gregory (1962), Hardman and Lilley (1973) and, more recently Duberg and Nystrom (1982) are some of the workers who have used scanning electron micrography to provide evidence for plastic deformation in materials.

1.1.2.4 Brittle Fracture

If the rate of force application is sufficiently rapid and its magnitude exceeds a certain threshold value, the material will be incapable of deforming plastically to accomodate the induced strain. According to Griffith's Crack Theory, under such conditions, rapid crack propagation and, therefore, fracture of the particles will occur.

This mechanism was first proposed by Griffith (1920) in

order to explain the differences between the theoretical and observed strength values for glass. He calculated that if the elastic strain energy released by the increase in crack size exceeded the surface energy required for the production of the two new surface areas, crack growth could proceed.

As a result of fragmentation, particle size is reduced and the number of contact points within a powder bed increases substantially. Under these circumstances, the formation of a compact may be achieved by interparticle bonding between points being in close proximity.

Photographic proof of brittle fracture in materials during compaction was published by Hardman and Lilley (1970). Furthermore, a rise in the specific surface area of sulphathiazole granules in response to a compaction load was attributed to brittle fracture (Higuchi et al, 1953). This conclusion was also supported by Armstrong and Haines-Nutt (1970) for magnesium carbonate compacts.

1.1.2.5 Deformation of Materials Without Dislocations

Although the "dislocation theory" can explain the deformation properties of many crystalline materials under stress, Gordon (1983) stated that this is probably not the case with polysaccharides, such as celluloses and starches. Cook and Gordon (1964) proposed the "theory of weak interfaces" to

explain the behaviour of such materials. According to this, such materials contain regions where bonding between two sections of the material is weaker than within the sections themselves. In such a case, if a crack is initiated within these sections, the weak interface will break and a "crack stop mechanism" will result (Fig. 1.4). The resultant crack will be normal to the interface and there will be little tendency for crack propagation.

In contrast, if the adhesive strength of the interface is large, the interface may remain intact and the crack will propagate by crossing it. In this case, the material will behave in a brittle manner.

According to the above authors, for materials such as celluloses and starches, deformation is facilitated by slippage of the entangled branched molecules. Sections of the polymer chains slide past each other causing rearrangements of local nature as well as long range disruptions. It was also suggested that the viscoelastic nature of these materials is due to the different time required for these rearrangements to occur in crystals.

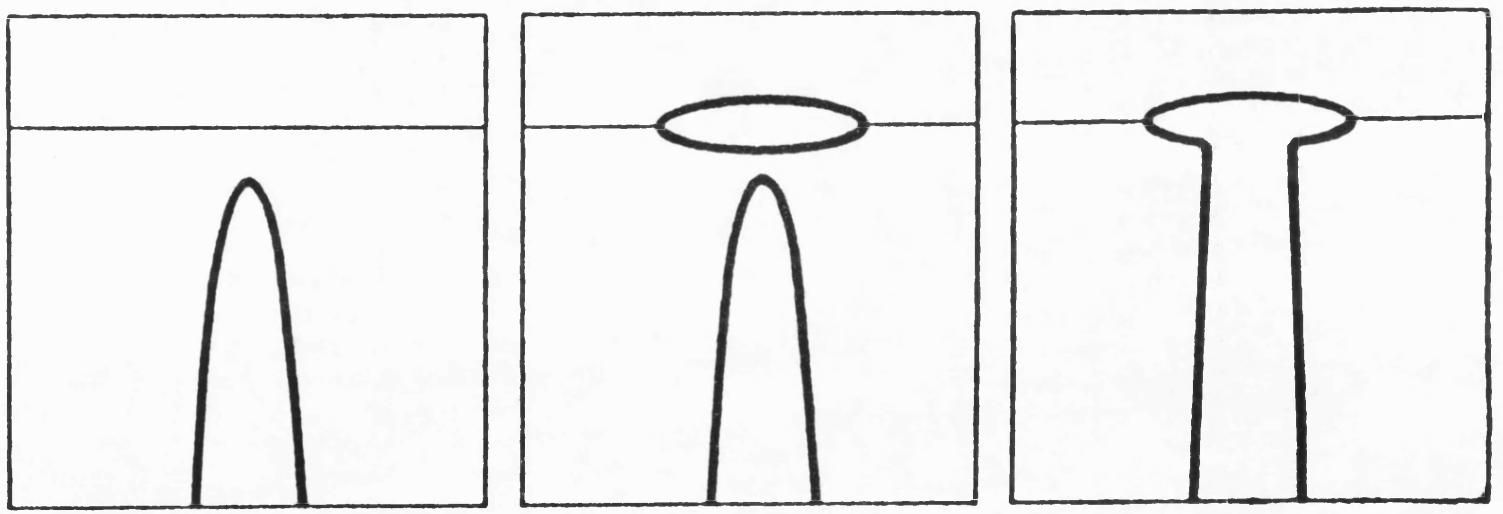

FIG. 1.4 Crack stop mechanism in materials proposed by Cook and Gordon (1964).

1.1.3 Compact Formation

1.1.3.1 Mechanisms of Bonding

In 1721, Newton stated that "the parts of all homogeneal, hard bodies which fully touch one another stick together very strongly". Also, Bowden and Tabor (1954) showed that, in theory, perfectly clean surfaces adhere to each other with a strength equal to the strength of the material.

In practice, however, surfaces are not so clean since they are almost always contaminated with moisture, gases, oxides, grease and other surface contaminants (Orr, 1966). Shotton and Rees (1966) and Rees and Shotton (1970) stated that an increase in the moisture content of sodium chloride crystals decreased the tablet crushing strength, probably by reducing the interparticle bonding.

During compression, the applied force brings adjacent surfaces into close contact. Shearing of particles in addition to elastic and plastic deformation allows a number of bonds to be formed, due to the increased contact area. Furthermore, brittle materials fracture under load resulting in the creation of clean, new surfaces in close proximity, the conditions for rebonding being excellent.

An interesting study reported by Johnson et al (1971), emphasised that bonding releases energy rather than consuming

it. Although energy is needed to bring particles sufficiently close to bond, the actual bonding process releases energy. This is analogous to a chemical reaction and the associated activation energy.

According to Orr (1966), molecular forces are mainly responsible for bonding. He discounted the role of interlocking, a fact also supported by Train and Lewis (1962). This mechanism proposed by Seth (1956) can only be effective with particles of excessively irregular shape containing particularly strong asperities and projections which can resist shear forces during compression. This is not the case for most pharmaceutical particulate solids.

Van der Waals forces and hydrogen bonding have been suggested to be the major bonding mechanisms that hold pharmaceutical compacts together. Reier and Shangraw (1966) attributed the good compaction properties of microcrystalline cellulose to extensive hydrogen bonding over large areas of contact. In brittle materials, a large number of points support the applied load so that the resultant stress at each point is relatively low (Cole et al, 1975). This minimises the plastic deformation which occurs locally and limits the area of true contact and bonding.

For some materials, softening or melting may occur at asperities, if high pressure produces a localised high temperature, at least equal to the softening or melting point of the material (Rankell and Higuchi, 1968). The release of

pressure will cause the solidification of the fused material and the formation of solid bridges between the particles. This type of bonding is common for materials with low melting points. Work reported by Jayasinghe et al (1969), York and Pilpel (1972), York and Pilpel (1973) and Britten and Pilpel (1978) showed that there is a relationship between the tensile strength of compacts, the formation temperature of the powder bed and the melting point of the material.

In addition, increase in pressure may cause an increase in the solubility of the material in the film of moisture on its surface. Decompression will result in crystallisation and again, the formation of strong solid bridges between the particles (Shotton and Rees, 1966).

Finally, according to the mechanical activation theory (Huttenrauch, 1978; Huttenrauch and Jacob, 1977; Huttenrauch and Keiner, 1976a, b and c; 1979a and b), material produced by milling, drying, mixing or any other manufacturing process that disrupts its crystal structure, shows improved bonding due to a reduced degree of order of the crystal lattice.

1.1.3.2 Lamination and Capping

Lamination and capping are two phenomena often encountered during compaction of pharmaceutical particulate materials. Lamination occurs when the tablet splits along one or more

planes normal to the axis of compression. In comparison, capping takes place when one or both crowns separate themselves from the remainder of the tablet. The precise mechanism of capping for many materials has not been fully elucidated.

As early as 1954, Bowden and Tabor suggested that capping was due to the expansion of elastically deformed particles and the subsequent rupture of interparticle bonds. Gregory (1962) attributed lamination in coal briquettes to entrapped gases. However, other studies (Shotton and Ganderton, 1961; Ritter and Sucker, 1980) have shown that vacuum does not affect the capping tendency of materials. On the other hand, Mann et al (1983) reported that sub-atmospheric pressure conditions resulted in an increase in the capping pressure of the formulations they studied. They used a high speed compaction simulator and tooling which ensured air entrapment within the granule bed.

Shotton and Ganderton (1961) attributed the capping of paracetamol tablets to failure of strong interparticle bonds under recovery stresses that propagate across the particles. This was contradicted by a subsequent report that this material shows a low degree of plastic deformation and bonding (Obiorah and Shotton, 1976).

Parmentier (1980) has considered the influence of die-wall friction, compression speed, anisotropic deformation characteristics and elasticity on the capping phenomenon.

Several methods have been used to predict the capping tendency of materials (Forlano and Chavkin, 1960; Seitz and

Flessland, 1965). In 1978, Nystrom et al suggested the use of the strength isotropy ratio as a means of predicting the capping tendency of materials. This ratio was obtained by subjecting replicate tablets to a direct tension test as well a diametral loading test. More recently, Krycer et al (1982) proposed the capping index, defined as the gradient of a plot of the percentage elastic recovery versus the residual die wall pressure.

1.2 MECHANICAL PROPERTIES OF TABLETS

When powdered materials are formed into compacts, adjacent particles are pressed into close proximity so that at points of contact, interacting surface forces can be strong enough to produce a stable structure. This is manifested as the mechanical strength of the new entity.

The magnitude of the attractive forces and the area over which they act are both very important and depend mainly on the physico-chemical properties of the material and the applied load. The mechanical properties of tablets are heavily dependent on the type of deformation the materials undergo during compaction. Fracture of particles leads to the creation of clean new surfaces, while plastic deformation results in an increase in true contact area.

The extent of bonding during compaction is not, however, the only important factor to be considered. The energy stored as elastic strain during compression is responsible for the disruption of a number of bonds during decompression. Therefore, although some materials undergo extensive plastic flow during compression, relatively weak tablets are produced, due to massive elastic recovery and failure of a large number of bonds. As mentioned earlier, the elastic characteristics of materials are also responsible for tablet capping during ejection.

1.2.1 Factors Affecting the Mechanical Properties of Tablets

A number of factors affect the compressional characteristics of materials and, therefore, the mechanical properties of the finally produced tablets. They include the intrinsic properties of materials, as well as the processing steps during the manufacturing procedure. Material variability and inadequate control of such processes contribute to batch-to-batch variation and cause serious problems during the scaling-up of a formulation. The practical significance of lot-to-lot differences in powder properties was emphasised by Jones (1981). The most important of these factors are discussed below.

1.2.1.1 Crystal Properties

A raw material may exist as different polymorphs, i.e. solid crystalline phases resulting from the different possible arrangements of the same molecules, atoms or ions in the solid state. Such polymorphs are produced by different conditions of crystallisation and subsequent storage, and differ in properties such as melting point, density and crystal hardness (Haleblian, 1975). They may, therefore, differ in their compaction properties, too.

Crystals of the same polymorph may exist in different habits, i.e. although the arrangement of the molecules in the lattice is the same, the crystal shape may be different. This may be due to the solvent of crystallisation or the presence of impurities that affect the growth rate of different crystal faces to various extents (Mullin, 1979). Furthermore, both the presence of inclusions and residual surface impurities are very common (Mullin, 1972). This was also emphasised by Hersey and Krycer (1980). In all of the above cases the compressibility of the materials may be affected.

Crystal defects such as point defects and dislocations can also affect the compaction properties of crystalline materials (Henderson, 1972; Gordon, 1983). The extent, nature and state of such defects depend mainly on the manufacturing process and the handling history of the material in general.

According to the activation theory proposed by Huttenrauch (1978), Huttenrauch and Keiner (1976a, b, c and d, 1977, 1979a and b), whenever a powder is handled, crystallised, dried, milled, granulated, mixed or compressed, there is always the possibility that mechanical activation will occur. This tendency is increased by moisture (Huttenrauch and Keiner, 1976c and d) and in small particle size fractions (Huttenrauch, 1977) but reduced by surfactants (Huttenrauch and Jacob, 1977). Activation results in the partial breakdown of the crystal structure to the amorphous state, producing crystal lattice irregularities. These may occur either throughout the entire

crystal or only at the particle surface. Such changes are often manifested as development of static charge, agglomeration tendency, moisture adsorption and even chemical and physical reactivity; bonding by sintering may also be favoured. Attention is drawn to the fact that surface changes, although not readily recognisable, can have pronounced effects on surface energy and other parameters.

York and Grant (1985) proposed a "disruption index" (DI) in order to quantify the disorder induced by low level additives in a host crystal lattice. According to them, high DI values suggest a major disruptive effect of the guest molecules. Such an effect could be related to other properties including the compressional properties of the crystalline material.

Finally, regions within the crystals acting as stress concentrators, such as cracks and half cracks, are very important since they often initiate fracture under stress.

The influence of crystallinity, polymerisation degree, and other factors related to the preparation technique, on the tableting properties of celluloses was studied by Doelker et al (1987). They concluded that there is no direct correlation between the mechanical properties and crystallinity of these materials.

In conclusion, although the chemical and crystalline structure play a major role in the behaviour of powders under pressure, no general relationship has yet been derived to allow the prediction of the compressional characteristics of

materials. Better characterisation of the raw materials as well as a fuller understanding of the processing variables are undoubtedly of the utmost importance.

1.2.1.2 Moisture

The influence of moisture on the consolidation behaviour and the bonding properties of powdered materials has been emphasised by many workers.

According to York (1981), apart from the water absorbed into materials, water can interact with solids in two ways i.e., at low humidities, as fairly tightly bound (monolayer adsorbed) water and at higher humidities, as more movable (solvent-like) water. Zografi (1988), however, pointed out that such a model is a simplification of the water-solid interaction.

Moisture has been suggested as affecting the deformation properties of materials. It has been claimed that it causes a kind of internal lubrication within a powder bed which facilitates slippage and flow of adjacent individual crystals (Shotton and Rees, 1966; Armstrong and Haines-Nutt, 1974). Increased moisture content has been shown to result in a lower yield pressure (Ragnarson and Sjogren, 1985). This was also attributed to facilitated deformation coupled with reduced interparticulate friction. On the other hand, it has been suggested that moisture uptake can reduce particle fragmentation during compression (Armstrong and Haines-Nutt, 1974).

Furthermore, Patel and Armstrong ((1987) stated that for materials which mainly fragment during compaction, an increase in moisture caused initially a decrease in their elastic recovery to a minimum, attributed to greater plasticity and surface tension forces. After a certain critical point depending on the material, elastic recovery increased again, possibly due to the water opposing consolidation. Finally, absolutely dry granulations have been shown to have poor compressional characteristics (Smith, 1949).

The number of bonds and, therefore, the compact strength also depend on the amount of water present. Solid bridges, formed on recrystallisation of dissolved material have been suggested to be responsible for increasing the tablet strength of sodium chloride compacts (Shotton and Rees, 1966; Rees and Hersey, 1972). On the other hand, dissolution of these bridges was claimed to cause a reduction in compact strength (Rees and Hersey, 1972). Liquid bridges can also cause interparticulate adhesion and, therefore, an increase in compact strength at low loads (Rumpf, 1962; Turner and Balasubramian, 1974).

However, water vapour adsorption can have a negative effect on particle-particle interaction as reported by Herrmann (1971/ 1972) and by Ahlneck and Alderborn (1989). This is propably due to the formation of multilayers of water on the particle surfaces (Zografi et al, 1984) acting as a lubricant and disturbing or reducing intermolecular attraction forces (Coelho and Harnby, 1978). Khan et al (1981) attributed capping of

microcrystalline cellulose compacts of high moisture content compressed at 163MPa, to the condensed moisture being sqeezed out on to the particle surface reducing particle bonding and increasing elastic recovery.

It seems that the effect of moisture on the compaction properties of materials as a whole, is a complicated phenomenon. Extreme humidity conditions can cause a dramatic change in the mechanical properties of compacts. The available evidence suggests that moisture can either increase or decrease the compact strength depending on the material. Understanding of the interactions between water and solid materials subjected to compression is, therefore, of vital importance. A specific moisture content must be guaranteed for each formulation in order to obtain compacts of optimum physico-mechanical qualities.

1.2.1.3 Particle Size and Shape

Particle size is one of the most important sources of lot-to-lot variation and is generally considered to be a processing effect.

Shotton and Ganderton (1961) described the role of particle size in the compressional behaviour of a material. They stated that for granular materials which bonded as strongly as bonding within the crystal lattice, leading to fracture across the grain when the tablets were subjected to a diametral loading test,

smaller granules formed stronger tablets than larger ones. However, when granules retained their identity, so that fracture occured at the bonding surface between these granules, the strength of the tablet produced was independent of the size of the original granules.

McKenna and McCafferty (1982) studied the effect of particle size on the compaction properties of a range of materials. The larger particles of spray dried lactose gave weaker tablets whereas, microcrystalline cellulose showed no particle size effect. Fell and Newton (1968) also showed an increase in the tensile strength of lactose compacts with a decrease in particle size.

Shlanta and Milosovich (1964) reported different degrees of stress relaxation for different particle size fractions of salicylamide and sodium chloride, suggesting greater plasticity of the smaller particles. This was supported by Hardman and Lilley (1970 and 1973) who stated that smaller particles are more plastic. Rue and Rees (1978), using Heckel plots, found the yield strength to increase with decreasing particle size. They attributed this to a lower probability of cracks being present in smaller particles which, therefore, withstood higher loads before fracture.

Alderborn and Nystrom (1982b) showed that for materials such as Emcompress and saccharose, which fragment extensively during compaction, tablet strength was almost independent of particle size. For acetylsalicylic acid, sodium citrate and

lactose, tablet strength decreased with an increase in particle size. The opposite was observed for sodium chloride and Starch 1500.

Marshall and Sixsmith (1974) and Sixsmith (1982) stated that particle size variation is only one factor causing differences in the Heckel plots of various grades of a microcrystalline cellulose (Avicel). Particle shape was considered to play an important role in their deformation properties. Other investigators have also studied the effect of particle shape on the compaction properties of plastically deforming materials. According to Alderborn and Nystrom (1982a) and Alderborn (1985), it seems that more irregular particles give rise to higher friction and shear forces, hence producing stronger tablets. For materials which mainly fragment during tableting, compactibility seems to be independent of the shape of the original particles. Furthermore, Shotton and Obiorah (1973) found differences in the compaction properties of sodium chloride, a plastically deforming material, which they attributed to variation in the material's particle shape.

Thus far, many of the statements produced by various workers appear to be contradictory. More work is, therefore, needed to define the precise effect of particle size and shape on both the deformation and bonding properties of materials.

1.2.2 Methods for Characterising the Compaction Process

1.2.2.1 Energy of Compaction

Several workers have tried to assess the compaction process by quantifying the amount of energy involved in it. One of the most widely used methods of determining the energy of compaction is the calculation of the area under the force-displacement curves (Fig. 1.5) during compaction. From such plots, Higuchi et al (1952), determined the mechanical work of compression, which they said, should be equal to the sum of the energy dissipated in the form of thermal energy and that retained in the tablet in the form of increased surface energy. No attempt was made at the time, however, to correlate such data with tablet performance.

De Blaey and Polderman (1971a) suggested a series of energy consuming processes during tableting:

- particle rearrangement
- inter-particle friction
- particle-die wall friction
- elastic deformation
- non-recoverable deformation

They showed that the amount of energy involved in the first two stages was negligible. They also introduced the following calculations (1971a and b):

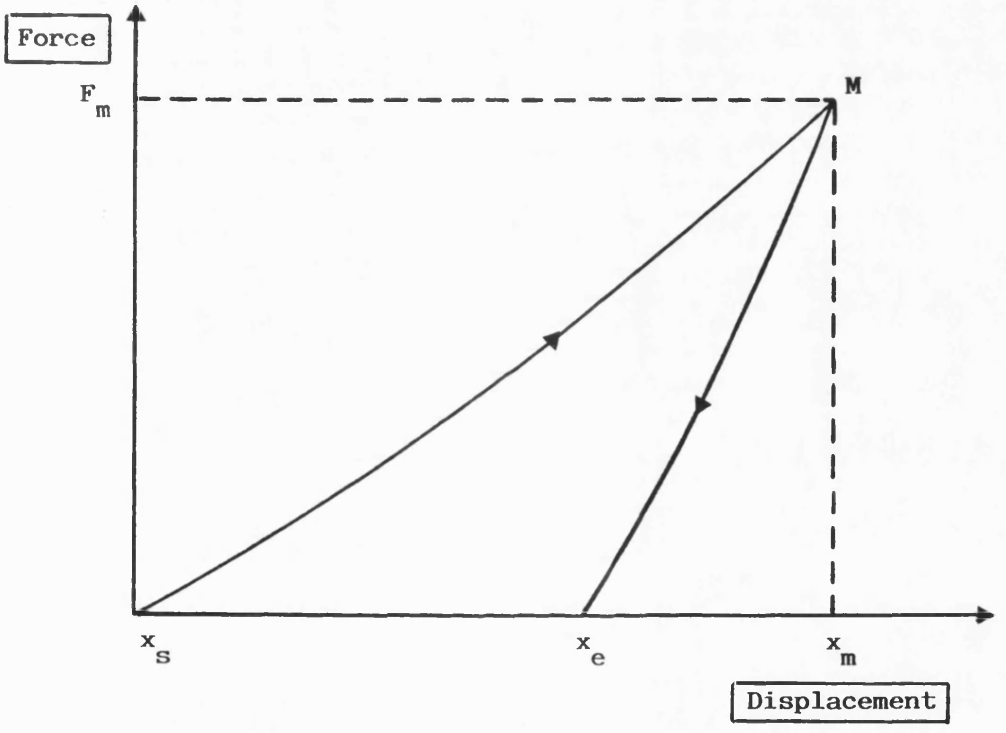

FIG. 1.5 Force-displacement curve during compaction of materials used by Higuchi et al (1952) for the assessment of the work done during compaction.

$$\text{Gross Work} = \int_{x_s}^{x_m} \text{UPF} \cdot dx \qquad \text{Eq. 1.3}$$

$$\text{Expansion Work} = \int_{x_m}^{x_e} \text{UPF} \cdot dx \qquad \text{Eq. 1.4}$$

$$\text{Friction Work} = \int_{x_s}^{x_m} (\text{UPF} - \text{LPF}) \cdot dx \qquad \text{Eq. 1.5}$$

where,

UPF = upper punch force

LPF = lower punch force

x = upper punch displacement

x_s = first displacement reading as force deviates above threshold

x_m = displacement reading at maximum force

x_e = displacement reading as force deviates below threshold

The same workers (1970) suggested that a second compression should be performed without the ejection of the tablet, in order to measure the work required for the elastic deformation. They stated that the tablet does not recover at the same rate as the moving upper punch. Therefore, the area $x_e M x_m$ in Fig. 1.5 represents only part of the elastic recovery of the tablet. They calculated the true (net) work of compaction, by also subtracting the frictional work from the gross work:

$$\text{net work} = \int_{x_s}^{x_m} UPF_1 \cdot dx - \int_{x_s}^{x_m} UPF_2 \cdot dx - \int_{x_s}^{x_m} (UPF_1 - LPF_1) \cdot dx \quad \text{Eq. 1.6}$$

1 and 2 refer to the first and second compression respectively.

According to De Blaey and Polderman (1971b):

$$\text{net work} = \int_{x_s}^{x_m} (LPF_1 - LPF_2) \cdot dx \quad \text{Eq. 1.7}$$

In this case, only lower punch force is monitored, hence taking into account die-wall friction which leads to a reduction in the force finally transmitted from the upper to the lower punch. They stated that the total net work, or a part of it, is used for bond formation. Therefore, the good correlation that they found between net work and tablet crushing strength, would have been expected.

The use of a second compression for the calculation of net work is associated with the assumption that work done during recompression is purely elastic and no more non-recoverable deformation takes place. Furthermore, it is assumed that the time elapsed before the second compression is sufficient for the complete elastic recovery of the tablet.

Patel et al (1985), however, showed that not all materials attain constant work for elastic deformation in the second compression. Carless and Leigh (1974) had concluded that for

some materials, elastic recovery of the tablet continues after ejection. According to Guyot (1978), a comparison of the slope and shape of force-displacement curves, between materials compressed under identical conditions, can be related to the mechanical properties of the produced tablets. More recently, however, Ragnarsson and Sjogren (1985) concluded that there is no simple correlation between the net work and the deformation properties of a material. The net work was found to be substantially affected by particle interactions when particle size, lubrication and moisture content were varied.

Therefore, the net work appears rather unsuitable for general evaluation of the deformation properties of materials. It could however, be useful for detecting batch-to-batch variation in their compaction properties.

1.2.2.2 Compression Cycles

Many workers study compression cycles by comparing the transmitted die wall pressure or the lower punch pressure as a function of the applied pressure. The "force ratio", i.e. the ratio of radial to axial stress has been used to study the compressional properties of materials, die wall friction and pressure transmission during compression.

Nelson (1955) used a third punch and a force-measuring transducer to measure the force transmitted to the die wall. Although he reported that about 30% of the pressure transmitted

to the lower punch was transmitted to the die wall, he did not attempt a comparative study of different materials. This percentage was increased when magnesium stearate was added. He also stated that the marked difference between the die wall pressure and the lower punch pressure indicates that the bond strength in planes parallel and normal to the direction of compression will not be the same; it should, however, be proportional to the difference in die wall and lower punch pressures.

Windheuser et al (1963) related the transmitted pressure to measurements of die expansion using strain gauges. Their system offered the advantage of not altering the internal die bore and not including measurements which depended on extrusion characteristics. Apparent yield values were derived from the initial linear portions of plots of radially transmitted force versus upper punch force. They also concluded that, in general, materials with rather good conversion of normal pressure to lateral pressure tend to form good tablets. According to these workers, such measurements may provide a useful indication of the compression characteristics of various materials.

Higuchi et al (1965) studied several topics, such as the relationship between the exerted pressure and the lateral pressure during compression, the decay of residual die wall pressure, the correlation between the residual die wall pressure and ejection force and the pressure transmission characteristics under repeated loading of the formed tablet. They were able to

state, but only qualitatively, that softer substances seemed to give higher die-wall pressures. They concluded that such studies yield useful information in understanding the compression characteristics of materials.

Radial pressure measurements allowed Leigh et al (1967) to distinguish between an ideal elastic material, a constant yield stress material, and a Mohr body for which the yield stress in shear is a function of the applied normal stress.

Ridgway et al (1969) showed that the die wall pressure increased as the Vickers hardness of the crystalline materials they studied decreased. Their method involved the application of photoelastic stress analysis using the stress patterns, observed by means of polarised light in the wall of a perspex die.

The development and transmission of radial pressure during loading and unloading of a powder bed was related by Carless and Leigh (1974) to the yield and elastic behaviour of several powders. These workers stated that the recovery pattern and the influence of the physical properties of the material on its compaction properties could be studied using parameters such as the stress ratio and the radial pressure relaxation behaviour.

Carless and Leigh (1969) used the compression modulus expressed as $\log(P_z/P)/[(1/D)-1]$, proposed by Bal'shin (1938) to describe the compressional properties of materials.

where,

P = axial pressure

P_z = axial pressure at zero porosity

D = relative density at pressure P

Such a treatment was, however, criticised by Rees (1970) who stated that caution is needed when a parameter of this type is used, unless the actual relations between pressure and relative volume are also considered.

Long (1960) and Leigh et al (1967) analysed the theoretical relationships between these pressures, assuming that powders are analogous to non porous solids. Based on the above assumption, Carstensen (1980) and Carstensen and Toure (1980) showed that a plot of the radially transmitted pressure versus the applied pressure produces a hysteresis area that is linear with respect to the maximum applied pressure, if plastic deformation occurs. If, brittle fracture takes place, a quadratic relationship exists. Later studies, however, suggested that such relationships are no more valid than the assumptions made (Carstensen et al, 1981).

Finally, the influence of size, configuration and positioning of die wall strain gauges on the measurement of radially transmitted stress was recently investigated by Huckle and Summers (1985). The dependence of die wall response on compact position was shown to decrease with multiple gauges mounted along the die length and connected to form a single gauge on each side of the die.

1.2.2.3 Heckel Plots

During tableting operations, pressure is applied on a certain amount of powder or granular material in a die. This may eventually lead to the formation of a compact. Several investigators have tried to express the compaction behaviour of powders. The terms "compressibility" and "compactibility" have been used to describe the ability to form a powder compact. In order to prevent confusion, Schwarzkopf (1947) proposed that "compressibility" be defined as the extent to which the density of a powder is increased by a given pressure, and "compactibility" as the minimum pressure needed to produce a compact of a given strength. "Compression ratio" is probably the most widely used compaction parameter. It is defined as the ratio of the compact density obtained by pressing the material at a given pressure to the apparent density of the loose powder. However, any one of these parameters will only provide limited information about the whole compaction process, because it refers to just one specific condition, such as a certain compact strength or a given pressure.

The details of the consolidation process during compaction have been investigated by many workers. Die filling is recognised as the first step, followed by particle rearrangement. With further increase in pressure, particles will deform elastically. When their elastic limit is reached, either

brittle fracture or plastic deformation or both will occur, resulting in the creation of a large number of bonds necessary to form a compact. This stage is dependent mainly upon the material.

A quantitative evaluation of each of these stages has been attempted by several workers, as reviewed by Kawakita and Tsutsumi (1966). A more meaningful approach was made, however, by Heckel (1961a). He considered the compaction of powders to be analogous to a first-order chemical reaction, with pores being the reactants and densified material being the product. The "kinetics" of the process would then be described by a proportionality between the change in density with pressure and the pore fraction:

$$dD/dP = K\cdot(1-D) \qquad \text{Eq. 1.8}$$

where,

D = relative density

1-D = pore fraction

P = pressure

K = proportionality constant

Eq. 1.8 leads to Eq. 1.9.

$$\ln[1/(1-D)] = K\cdot P + \ln[1/(1-D_o)] \qquad \text{Eq. 1.9}$$

where,

D_o = relative density of the loose powder at zero pressure.

According to Heckel (1961a and b), Eq. 1.9 does not describe the compaction process quantitatively (Fig. 1.6). The replacement of the term $\ln[1/(1-D_o)]$ with a constant A, gives

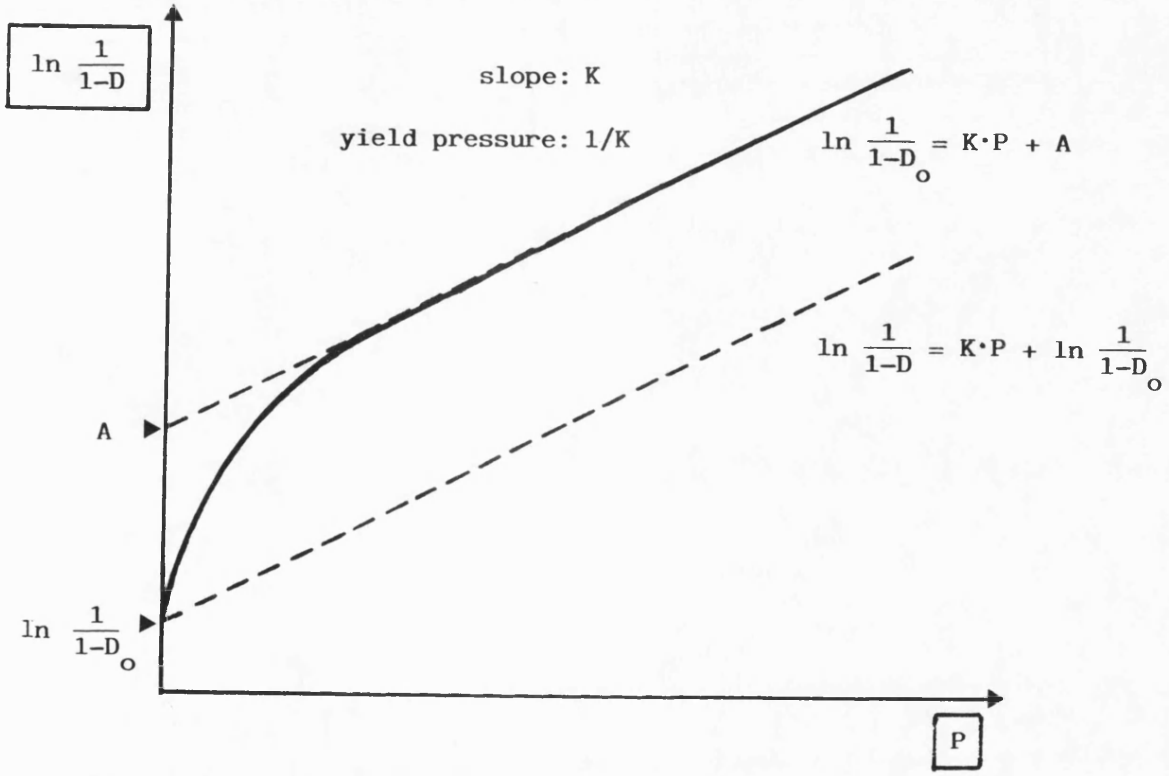

FIG. 1.6 Heckel plot and relevant parameters (Heckel, 1961a and b).

Eq. 1.10 which is valid except at the lowest pressures.

$$\ln[1/(1-D)] = K \cdot P + A \qquad \text{Eq. 1.10}$$

The constants A and K can be calculated from the intercept and the slope respectively of the extrapolated linear part of the plot (Fig. 1.6). According to Heckel (1961b), A combines the densification effects caused by the die filling ($\ln[1/(1-D_o)]$) and by individual particle movement (B) at low pressures before any appreciable interparticle bonding occurs.

Therefore,

$$A = \ln[1/(1-D_o)] + B \qquad \text{Eq. 1.11}$$

where,

$$D_a = D_o + D_b \qquad \text{Eq. 1.12}$$

D_a = relative density when $\ln[1/(1-D)] = A$

D_a can be calculated from Eq. 1.13:

$$D_a = 1-e^{-A} \qquad \text{Eq. 1.13}$$

D_o may be determined experimentally and D_b can be calculated from Eq. 1.12.

Heckel's results with metal powders indicated that D_o, D_a and D_b are sensitive to differences in particle size and shape whereas, K seemed to be a material constant. Finally, he concluded that the compaction process may be described by two parameters. One (A) is related to low pressure densification caused by interparticle movement, and the other (K) is a measure of the ability of the material to densify plastically after appreciable bonding has occurred.

Duberg and Nystrom (1985) stated that the fragmentation

tendency of materials can be expressed by the correlation coefficient calculated from linear regression of Heckel plots in the pressure range 5-50MPa. A value close to unity would correspond to a material consolidating mainly by plastic (and/or elastic) deformation. Low values would be indicative of an high fragmentation propensity. A prerequisite for the validity of such a statement is to make the calculations at low pressures, where fragmentation normally is pronounced.

The slope K, of the straight line portion, is often expressed as a reciprocal and is referred to as the mean yield pressure, Py:

$$Py = 1/K \qquad \text{Eq. 1.14}$$

Roberts and Rowe (1985) studied the effect of punch velocity on the constants derived from the Heckel equation in order to describe the compaction behaviour of several materials. They noted that some materials showed a rapid curvature of the Heckel plot as the density of the material approached the true density and the term $\ln[1/(1-D)]$ approached infinity. This was considered to be a consequence of the limitations of the Heckel equation. It was stated that high values of yield pressure (Py) are indicative of materials that consolidate by brittle fracture. Furthermore, change in the Py values with punch velocity, would only occur with materials deforming plastically. For these materials, Py would increase because of a reduction in the amount of plastic deformation due to the time-dependent

nature of plastic flow. This led to a strain rate sensitivity index (SRS), for ranking materials in terms of their brittle and ductile behaviour. SRS was calculated according to Eq. 1.15:

$$SRS = [(Py_2 - Py_1)/Py_2] \cdot 100 \qquad \text{Eq. 1.15}$$

where,

Py_2 = yield pressure at maximum punch velocity

Py_1 = yield pressure at minimum punch velocity

According to Hersey and Rees (1971), it is possible to differentiate between plastically deforming and brittle materials from the effect of particle size on their Heckel plots.

- Type A materials (Fig. 1.7a) consolidate by plastic deformation. Initial particle size is retained in the absence of fragmentation, thus giving different A values but the same K values.

- Type B materials (Fig. 1.7a) are considered to consolidate by fragmentation. The initial particle size is reduced by fragmentation, giving the same A and K values.

- Type C (Fig. 1.7b) was reported by York and Pilpel (1973) when they studied the compressional properties of four fatty acids. The densification of the materials was considered to be due to both plastic deformation and asperities melting. The initial steep linear incline seemed to be dependent on the individual fatty acid concerned.

Roberts and Rowe (1986b) also used the Heckel constants to study the effect of both particle size and mechanical

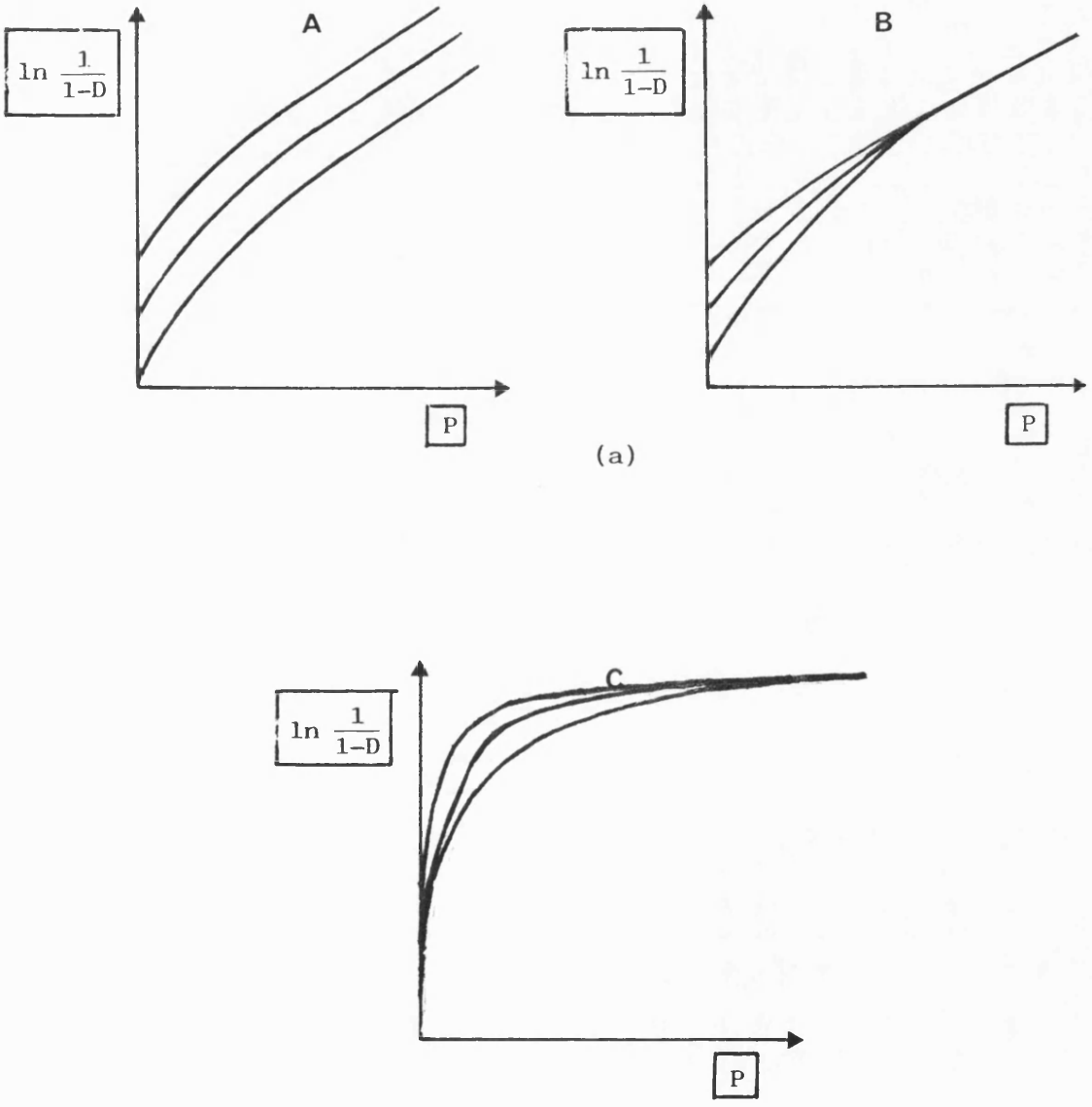

FIG. 1.7 Assessment of the consolidation behaviour of materials based on the effect of particle size on their Heckel plot, according to (a) Hersey and Rees (1971), and (b) York and Pilpel (1973).

pretreatement on the mechanical properties of powders. Duberg and Nystrom (1985), however, emphasised that Py values can be erroneously interpreted if materials consolidate by more than one major mechanism.

Several materials have been classified with respect to their consolidation mechanism based on the above hypothesis. However, a few years later, Rue and Rees (1978) stated that caution is necessary when attempting to draw any conclusions from such data, since the type of Heckel plots produced for many materials will vary with the experimental conditions. Contradictory results were obtained for several materials when dies of different sizes were used. It was also noted that different particle size fractions of the same material may exhibit variation in the predominant consolidation mechanism, ranging from brittle fracture to plastic deformation (Gregory, 1962). Fell and Newton (1971) stated that different Heckel plots were obtained for crystalline lactose by using different compaction rates. These Heckel plots were also dependent on whether volume was measured under load or after ejection. Finally, Rue and Rees (1978) stated that Heckel plots could be used in order to quantify the amount of plastic deformation the materials undergo, by measuring the areas under the curves obtained at different "contact times" (Jones, 1977). This would form the basis for comparing the plastic deformation of a range of materials. Such a comparison would be much more reliable than the classification of materials into types A, B or C.

1.2.3 Methods for Characterising Finished Compacts

1.2.3.1 Friability Test

A parameter relevant to the potential behaviour of tablets during coating, packaging and transport is the resistance to surface abrasion. This may be evaluated using the friability test, which involves measuring the weight loss when tablets are subjected to a standardised agitation procedure. Friability, f, is then calculated according to Eq. 1.16:

$$f = ((W_o - W_a)/W_o) \cdot 100 \qquad \text{Eq. 1.16}$$

where,

W_o = original weight of a sample of tablets

W_a = sample weight after testing

This method, however, although often used during industrial production, does not provide the detailed information required to explain and predict the tableting behaviour of particulate materials.

1.2.3.2 Indirect Tension Test by Diametral Loading

During the diametral loading test, which was introduced as a means of determining the strength of powder compacts, a cylindrical compact is compressed diametrally between two flat platens. Initially, instruments used for this purpose were

manually operated but, later, motorised ones were developed. However, it was not possible to compare the results obtained for specimens of different size, because their dimensions were disregarded. Also, differences in testing instruments and operators added to the unreliability of the results. It became necessary to introduce a testing method from which realistic and meaningful, quantitative comparisons of the strength of materials could be made.

In 1953, Carneiro and Barcellos introduced the indirect tensile test (Brazilian Disc test). It involved the diametral loading of a cylinder of concrete between flat platens at a slow rate. They stated that if a uniform stress was introduced to the specimen it was then observed to split in two along the loading diameter. In their analysis of the diametral loading test, Rudnick et al (1963) emphasised the requirements for tensile failure. According to Newton et al (1971), when a tablet is compressed diametrically, it may fracture in any of the ways shown in Fig. 1.8a. When it fails by mechanism 1, which is pure tensile fracture, the stress distribution within the tablet can be calculated (Frocht, 1948), as shown in Fig. 1.8b. The applied load may be resolved into three components:

a. tensile stress (σ_x) applied normal to the loaded diameter

b. compressive stress (σ_y)

c. shear stress (σ_z)

Under ideal line loading, compressive and shear stresses are particularly high just below loading points C_1 and C_2, and

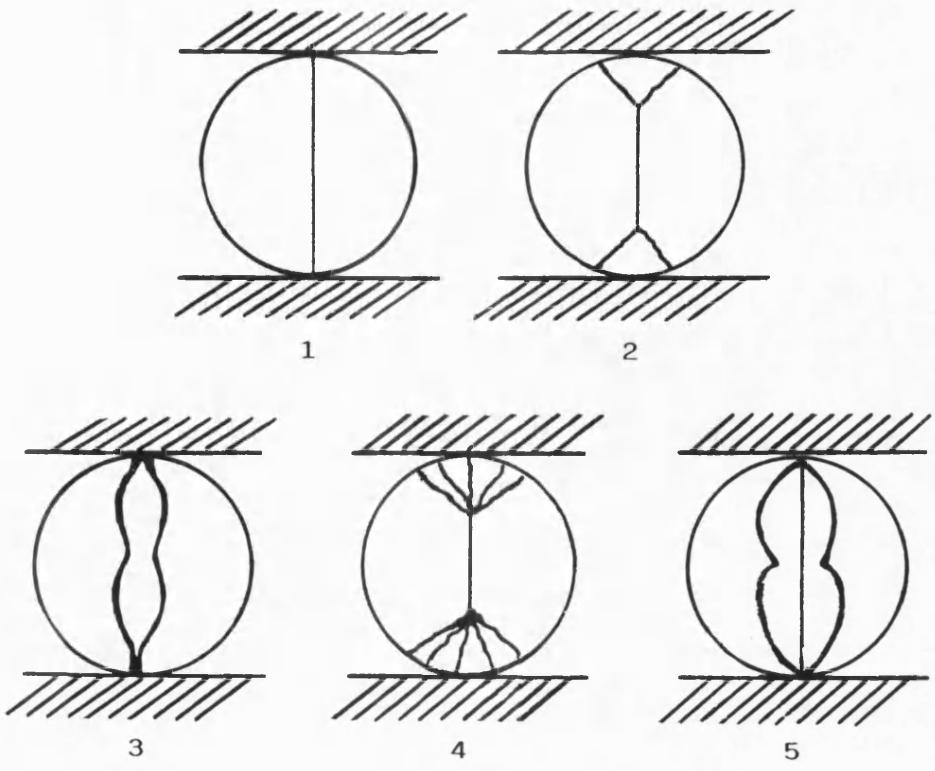

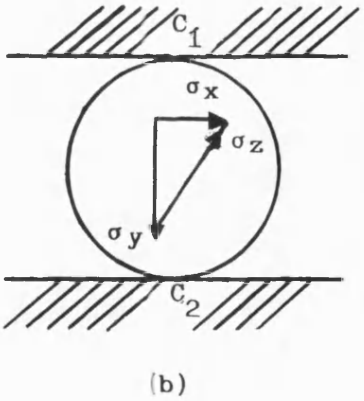

FIG. 1.8 Failure patterns (a) during diametral loading of tablets (Newton et al, 1971) and stress distribution (b) in pure tensile failure (Frocht, 1948).

are minimised around the centre of the loading diameter. Fell and Newton (1970b) stated that ideal line loading rarely occurs in practice. Pharmaceutical tablets are relatively soft compared to the platens of the device, thus allowing the load to be distributed over a large contact area. As a consequence, compressive and shear stresses are minimised and tensile failure occurs.

The tensile strength of the tablet is calculated according to Eq. 1.17:

$$\sigma_r = 2P_r/\pi \cdot D_t \cdot h_t \qquad \text{Eq. 1.17}$$

where,

σ_r = radial tensile strength of the specimen (normal to the loading diameter)

P_r = load required for the radial failure of the tablet

D_t = tablet diameter

h_t = tablet thickness

σ_r has the units N/m^2, designated Pa.

Rowe et al (1973) suggested a correction to Eq. 1.17 to allow for a comparison of compacts of different porosities. The inclusion of the correction factor $1/(1-\varepsilon)$ was meant to account for changes in the area of contact between particles as porosity changes:

$$\sigma_r = 2P_r/\pi \cdot D_t \cdot h_t \cdot (1-\varepsilon) \qquad \text{Eq. 1.18}$$

where,

ε = porosity

A few years later, however, Newton (1974) criticised this correction for allowing neither for the distribution of porosity nor for the true contact area within the specimen.

Inevitably, the diametral loading test was used to assess the mechanical properties of pharmaceutical tablets. It is the most widely used method for tablet strength determination, since it is relatively easy, quick and reproducible. Further work led to the prediction of tensile strength of mixed component systems (Fell and Newton, 1970) and of tablets of different dimensions (Newton et al, 1971). Empirical equations were reported, describing the tensile failure of deep concave tablets (Newton et al, 1972) and doubly-convex discs (Pitt et al, 1988) during diametral loading. Finally, tablet strength variability, often encountered in brittle materials, was described successfully by the Weibull distribution (Newton and Stanley, 1974).

Several workers recognised, however, that tensile strength - often incorrectly described by pharmaceutical technologists as "hardness" - is not a parameter which describes completely the mechanical properties of a pharmaceutical compact.

Rees and Rue (1978c) studied platen displacement as a means of assessing tablet deformation during the diametral loading test. A displacement transducer recorded the relative movement of the platens until failure occured. Load, P_r, was plotted against displacement, x. The area under the curve, calculated by integrating the load with respect to platen movement (Eq. 1.19), represented the work done on the tablet to cause its failure:

$$W_f = \int_{0}^{P_r} P_r \cdot dx \qquad \text{Eq. 1.19}$$

where,

P_r = load required to cause radial failure

x = relative movement of the platens

W_f has the units Joules.

The work has been related to the "toughness" of the tablet, defined as the ability of the material to absorb energy in the elastic and plastic region. However, since the measured displacement is not a tensile strain, but a deformation of the compact in the direction of compressive loading, Rees and Rue (1978c) used the term "work of failure" instead.

Rees et al (1977) modified Eq. 1.19 in a similar way to Eq. 1.17, in order to correct for the size of a circular cylindrical specimen:

$$CW_f = 2/\pi \cdot D_t \cdot h_t \int_{0}^{P_r} P_r \cdot dx \qquad \text{Eq. 1.20}$$

where,

D_t = tablet diameter

h_t = tablet thickness

CW_f has the units Joules m^{-2}.

Although x is not a tensile displacement, this "corrected" work of failure may be considered to represent the work done by the platens to cause tensile failure.

Rees and Rue (1978c) concluded that materials with similar tensile strength values may show markedly different work of

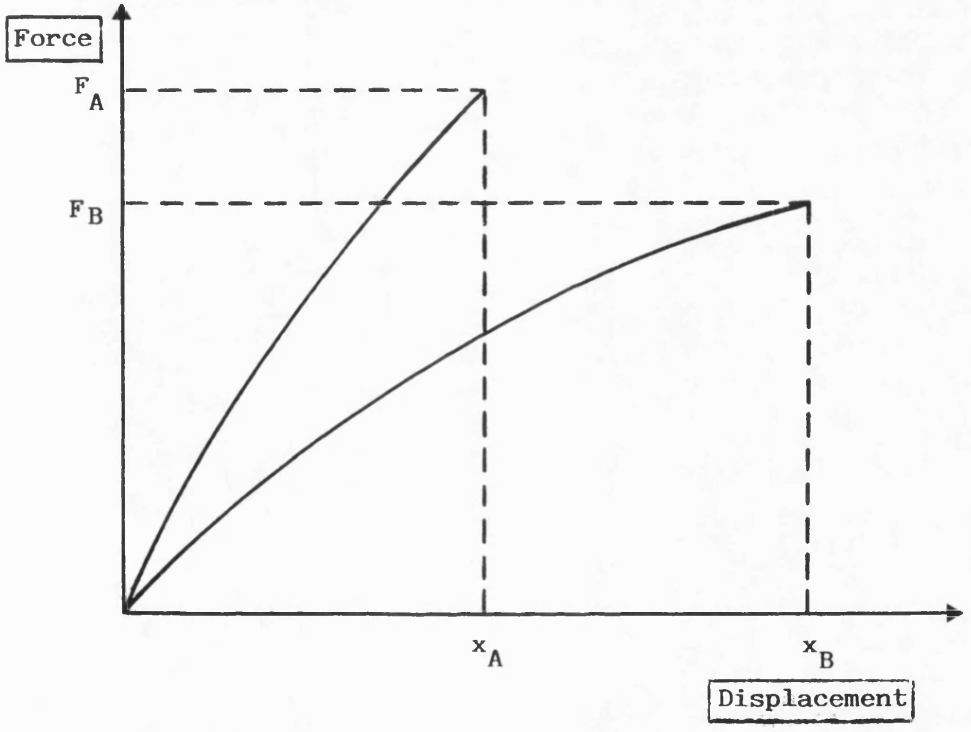

FIG. 1.9 Force-displacement curve during diametral loading of tablets used by Rees and Rue (1978c) for the assessment of work of failure.

failure values, due to variations in their resistance to deformation prior to failure. Furthermore, a material A may have a slightly higher tensile strength than material B, but it may undergo considerably less deformation before failure. The area under the force-displacement curve for material B may then be larger than for material A (Fig. 1.9), indicating that the work which can be done on material B prior to its failure, is greater than in the case of material A. In general, materials which consolidate mainly by plastic deformation during compaction tend to show high work of failure values. This is due to a combination of high tensile strength values and large deformation before failure during the diametral loading test. In contrast, materials consolidating mainly by fragmentation during compaction tend to show low work of failure values.

In order to simulate conditions to which tablets may be subjected in practice during coating, packaging and transport, Rees and Rue (1978c) exposed the tablets to a semi-empirical multiple impact test. A mass of 240g was allowed to drop onto the edge of a tablet placed diametrally between two parallel metal platens. The number of impacts needed for the tablet to fail was counted. A linear relationship was found to exist between tensile strength and this impact number, but the relationship was specific to a particular tablet composition. However, work of failure values were linearly related to the number of impacts required to cause failure, irrespective of tablet size and composition. The authors concluded that work of

failure is a more useful means of quantitative assessment of a tablet's mechanical resistance to damage than tensile strength.

An interesting study of the force-displacement curves was made by Moschos (1985). The parameter Ra was derived, described as the area-ratio and calculated according to Eq. 1.21:

$$R_a = (P_r \cdot x/2)/W_f \qquad \text{Eq. 1.21}$$

where,

P_r = load required to cause radial failure

x = platen displacement before failure

W_f = work of failure

R_a has no units.

Moschos (1985) stated that this ratio characterised the curvature of force-displacement curves by comparing the two areas $P_r \cdot x/2$ and W_f. The theoretical curves for some area-ratio values are given in Fig. 1.10. It is evident that tablets with $R_a > 1$ undergo extensive deformation at the beginning of loading whereas, tablets with $R_a < 1$ show resistance to deformation at the beginning, and then an increase in deformation near the breaking point. He reasoned, therefore, that no valid conclusions may be drawn about the failure deformation of a material from a sub-failure test. As a result, the 75% breaking load data obtained earlier by Rees and Rue (1978a) could not be extrapolated to 100% of the breaking load to provide valid data relevant to failure.

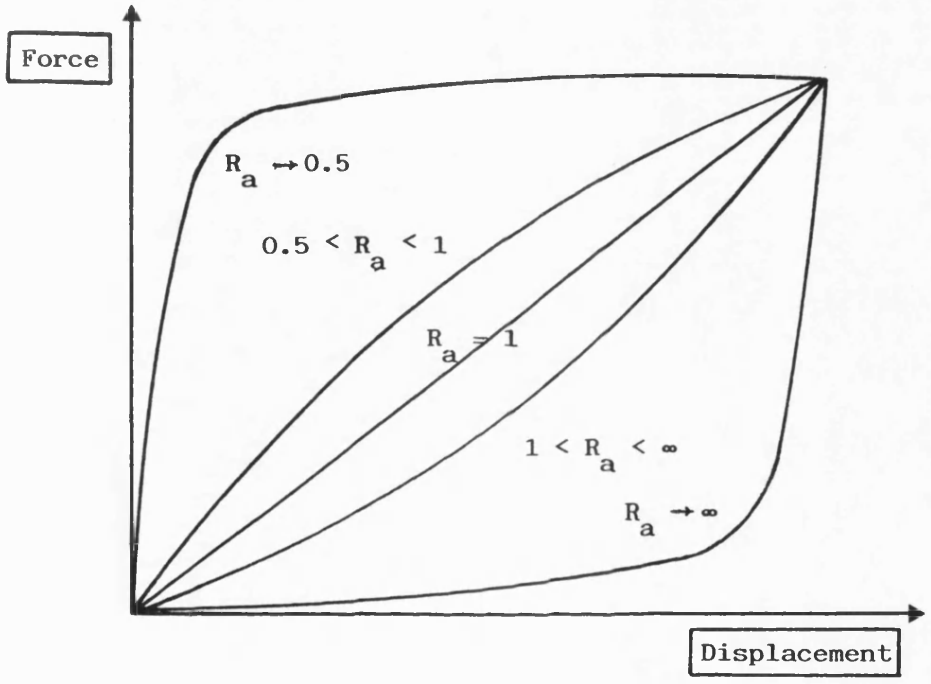

FIG. 1.10 Theoretical curves for some area-ratio values according to Moschos (1985).

Another parameter which may be derived from a diametral loading test, is the power of failure, P_f. It is defined as the product of the work of failure, W_f, and the reciprocal of the time, t, required for a tablet to break:

$$P_f = W_f/t \qquad \text{Eq. 1.22}$$

P_f has the units Joules/s.

P_f was found to lack the necessary sensitivity to discern small differences in plastic behaviour (Patel, 1986).

Apparent failure viscosity, AFV, is defined as the product of tensile strength, σ_x, and time, t, required for tablet failure:

$$AFV = \sigma_x \cdot t \qquad \text{Eq. 1.23}$$

AFV has the units Pa•s.

Patel and Staniforth (1987) concluded that AFV is a useful parameter since it provides information about both the strength and the deformation ability of compacts. It gives, therefore, a good indication of the plasticity of different excipients.

Finally, the effect of strain rate on the mechanical strength of tablets has been studied by many workers. It has been reported (Ritschel et al, 1969; Newton et al, 1986) that, in many cases, increase in strain rate causes a reduction in tensile strength. This has been shown to be dependent on the brittle or the plastic nature of the specimens (Moschos and Rees, 1985). Accurate control of the test conditions is, therefore, vital especially when comparison of data obtained by different workers is attempted.

1.2.3.3 Direct Tension Test

The direct tension test is mainly used for the evaluation of tensile strength of materials such as metals and polymeric materials. The specimens are held at each end and they fail under a direct tensile force. The applied tensile stress is determined as load/area. The major advantage of this method is the application of a uniaxial tensile stress. Pure tensile failure occurs because compressive and shear stresses are negligible.

The use of such a method in strength determination of powder compacts is associated with several problems. If the specimen is not aligned properly, bending stresses will be added. Premature fracture may also occur if gripping of the specimen causes any high localised stresses. It is essential that the whole method of sample preparation and alignment does not lead to the introduction of any weak planes in the compact.

It is well known that uniaxial compaction results in the production of heterogeneous compacts regarding stress distribution and porosity. Nystrom et al (1977) constructed the testing machine illustrated in Fig. 1.11 in order to measure the pure axial tensile strength of pharmaceutical tablets. They used normal-sized, flat-faced tablets which were fixed between a pair of adapters by means of a cyanoacrylate adhesive. By applying a tensile force to the adapters, the tablets were strained until

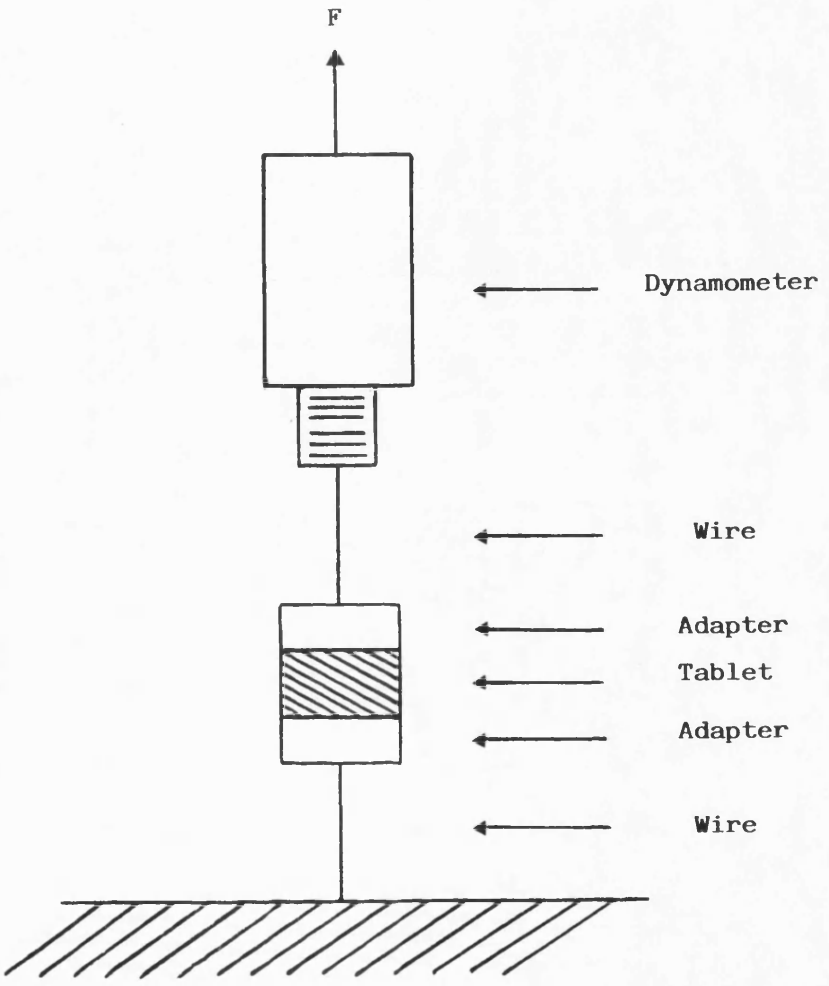

FIG. 1.11 Tensile testing apparatus used by Nystrom et al (1977) for direct tension testing of tablets.

they broke in a plane normal to their axes. The maximum force applied was measured by spring balances. In order to compare axial and radial tensile strength values, replicate tablets were subjected to diametral crushing in a Heberlein test apparatus.

It was shown that above a certain limit, an increasing compaction load could result in a considerable decrease in the axial tensile strength of the tablets, while their radial tensile strength was either unchanged or continued to increase. Capping is attributed to the presence of internal tensile strains in the tablets, normal to the plane of capping. Nystrom et al (1977), therefore, suggested that a measurement of the axial strength rather than the radial strength is more appropriate for investigating capping tendency, and that a quantitive measurement ought, therefore, to be included frequently in tablet strength determinations.

Further experiments by Nystrom et al (1978) supported that hypothesis. Isotropic materials such as blackboard chalk were also used in order to check the agreement between axial and radial tensile strength of an homogeneous body. The following equations were used to derive values from the two tests respectively:

$$\sigma_a = 4P_a/\pi \cdot D_t \qquad \text{Eq. 1.24}$$

$$\sigma_r = 2P_r/\pi \cdot D_t \cdot h_t \qquad \text{Eq. 1.25}$$

where,

σ_a = axial tensile strength

σ_r = radial tensile strength

P_a = load required to cause axial failure

P_r = load required to cause radial failure

D_t = tablet diameter

h_t = tablet thickness

It was emphasised that it is not sufficient to compare axial and radial tensile strength values obtained at a single specific compaction load, but that values over a wide range of loads should be considered. The same workers suggested the use of the strength isotropy ratio, calculated according to Eq. 1.26, as an expression of the homogeneity of the tablets and as a measure of their capping tendency.

$$\text{Strength Isotropy Ratio (SIR)} = \frac{\text{axial tensile strength}}{\text{radial tensile strength}} \qquad \text{Eq. 1.26}$$

This ratio should be as close to unity as possible over the whole range of compaction loads. In 1982, Duberg and Nystrom studied several ways of characterising the fragmentation tendency of a number of materials during compaction. They concluded that strength isotropy ratio seemed to be a parameter providing fairly easily a quantitative measure of this tendency. According to these workers, fragmentation during compaction results in a better packing arrangement of the material in the die and also produces an increased number of contact points.

This leads to a decreased local pressure at each point. Brittle materials are, therefore, believed to form relatively homogeneous tablets. This increase in stress homogeneity leads to an increased strength isotropy ratio. Results obtained by the same workers in 1985 were also in agreement with these conclusions. They stated that the strength isotropy ratio reflects the degree of homogeneity in the bond distribution throughout the compact. This homogeneity is a function of both consolidation mechanism and bonding properties. According to them, high isotropy ratios were obtained for tablets bonding with weak attraction forces, i.e. for:

a. Brittle materials, showing no (or minor) elastic recovery and producing a large number of weak bonds e.g. Emcompress and lactose.

b. Plastically deforming materials, producing a small number of weak bonds e.g. sodium bicarbonate and to which a small quantity of a dry binder has been added. In such a case, a high isotropy ratio will be obtained due to an increase in the number of bonds within the compact.

Low isotropy ratios were obtained for tablets in which the stress distribution is non-uniform, i.e. for:

a. Plastically deforming materials in which a small number of strong bonds are formed on compaction, e.g. sodium chloride, or in which a large number of strong bonds are formed due to mechanical interlocking and sintering phenomena.

b. Those brittle materials which undergo extensive elastic

recovery leading to bond rupture.

c. Mixtures of compounds and additives bonding by strong attraction forces.

Duberg and Nystrom (1982) believe, therefore, that their results indicate a necessity to study other aspects of tablet strength than just the radial strength. It must, however, be emphasised that although the way the specimen is mounted between the adapters does not seem to have any effect on the tensile strength evaluation, it may introduce problems in the associated strain evaluation. In other words, it may be difficult to assess whether the movement measured during the test is due only to deformation of the specimen and not to the stretching of the adhesive.

1.2.3.4 Other Indices of Tableting Performance

Tabor (1948 and 1951) described an impact method for assessing the mean pressure under an indenter (indentation hardness). Hiestand et al (1971) confirmed the applicability of this method to porous compacts using a pendulum to achieve impact. The indentation hardness, P_i, is calculated according to Eq. 1.27:

$$P_i = \frac{4m_i \cdot g \cdot r_i}{r_c^4} \left(h_i - \frac{3h_r}{8}\right) \qquad \text{Eq. 1.27}$$

where,

m_i = mass of the indenter

g = gravitational constant

r_i = radius of the spherical indenter

r_c = chordal radius of the dent produced

h_i = initial height of the indenter

h_r = rebound height of the indenter

Leuenberger et al (1981) found that P_i varies with the porosity of the compact and suggested Eq. 1.28 relating the indentation hardness to the applied pressure and the relative density of the compact, to account for such variations:

$$P_i = P_m (1-e^{-P_m}) \qquad \text{Eq. 1.28}$$

where,

P_m = magnitude of P_i at zero porosity

P_c = compression pressure

ϕ = solid fraction

δ = constant related to compressibility

This relationship was based on the concept of effective bonding at contact points across the cross-sectional area of a compact. They showed this equation to be valid for a number of different substances. Leuenberger (1982) and Leuenberger and Jetzer (1984) proposed the above-mentioned method for pure substances as well as for binary mixtures, with the use of interaction terms. They reported good agreement between experimental data and the above equation.

The Bonding Index (BI) is a parameter calculated from tensile strength and indentation hardness values (Hiestand and Smith, 1984). Basically, this ratio compares the compact strength after elastic recovery with a measure of the shear strength under a compressive load. This can be interpreted as indicating the relative survival of the true areas of contact established at maximum pressure during compression. For this reason, Jetzer and Leuenberger (1984) proposed its use for the prediction of capping and/or lamination tendency of materials. However, BI values vary with the porosity of the compact. Furthermore, Jetzer and Leuenberger (1984) found a discontinuity of BI values when fracture occurs. In addition, Jetzer et al (1985) showed differences in these two parameters at two different tableting and test conditions. Although qualitative conclusions could still be drawn, absolute values of these parameters varied. This was attributed more to differences in the compression-decompression-ejection cycle than in the test procedures. Finally, such a treatment, although useful in some respects, depends on experimental results only and is not deduced from theory.

Hiestand et al (1977) introduced the concept of Brittle Fracture Index in order to quantify the tendency of materials to laminate or cap during ejection. They stated that when a square compact is made with a hole in it, most of the residual stresses are concentrated around this hole. As a result, a compact without a hole has a higher tensile strength than that with a

hole. The Brittle Fracture Index (BFI) relates these two tensile strength values:

$$BFI = [(\sigma_T/\sigma_T)_o - 1]/2 \qquad \text{Eq. 1.29}$$

where,

σ_T = tensile strength of the square compact without a hole

σ_{T_o} = tensile strength of the square compact with a hole

These workers considered BFI to be an assessment of the material's stress relief ability due to its plastic flow. Values close to zero are indicative of a "plastic" material, whereas values approaching unity, indicate that the material has a tendency to laminate. It must be emphasised that for the Brittle Fracture Index to be meaningful, the only significant stress in the compact must be the one around the introduced hole. It is important that additional stress relief at pores within the compact should be minimised. Hiestand and Smith (1984) found an increase in the BFI with an increase in relative density of sucrose and spray-dried lactose. They did not question the validity of the concept, but proposed that BFI measurements should be made at a single relative density for all materials and preferably at a relative density of 0.85-0.90. At such high density values values the shape and orientation of pores are likely to vary less, resulting in more homogeneous stress relief throughout the compact.

More recently, Roberts and Rowe (1986a) extended the test to compacts of "tablet-sized" dimensions. This test had the obvious advantage of measuring the BFI at strain rates and

conditions approaching those normally used in tableting. Their results from such tests were in good agreement with those of Hiestand et al (1977) and Hiestand and Smith (1984).

The determination of the above mentioned parameters and indices allows a meaningful qualitative comparison of the compaction properties of materials as well as a guide in the prediction of these properties. However, each one of them alone does not seem to be adequate to describe fully a material's tableting performance. A combination of various parameters is necessary for a better understanding of compaction behaviour.

1.2.3.5 Scanning Electron Microscopy (S.E.M.)

S.E.M. can contribute to the study of the compaction mechanisms of materials. A material can be examined before and after compaction in order to assess whether the original particles have undergone plastic deformation, or if brittle fracture has led to particle size reduction. Duberg and Nystrom (1982) studied sodium chloride and were able to identify discrete primary particles with approximately the same size as before compaction, although there was a slight change in shape. For Emcompress and dendritic sodium chloride, none of the original particles could be observed after compaction, indicating a large degree of fragmentation. Lactose, sodium citrate and saccharose seemed to behave as intermediates and the degree of fragmentation was difficult to define.

1.3 VISCOELASTIC BEHAVIOUR

1.3.1 Nature of Viscoelastic Behaviour

There would appear to be an increasing need for a better rheological control of pharmaceutical solids. Because of their complex heterogeneous nature, the classic rheological treatments cannot adequately quantify their properties. In fact, many pharmaceutical materials behave both as solids and liquids and are, therefore, defined as viscoelastic or semi-solid materials. Mechanical models are often used to represent elastic and viscous behaviour (Kuhn, 1947). The deformation of a spring is analogous to the elastic rheological behaviour (Fig. 1.12a):

$$\gamma = \sigma / G \qquad \text{(Hooke's law)} \qquad \text{Eq. 1.30}$$

where,

γ = strain

σ = stress

G = Young's modulus

Viscous flow is usually represented by a dashpot containing a Newtonian fluid (Fig. 1.12b):

$$\gamma/t = \sigma/\eta \qquad \text{(Newton's law)} \qquad \text{Eq. 1.31}$$

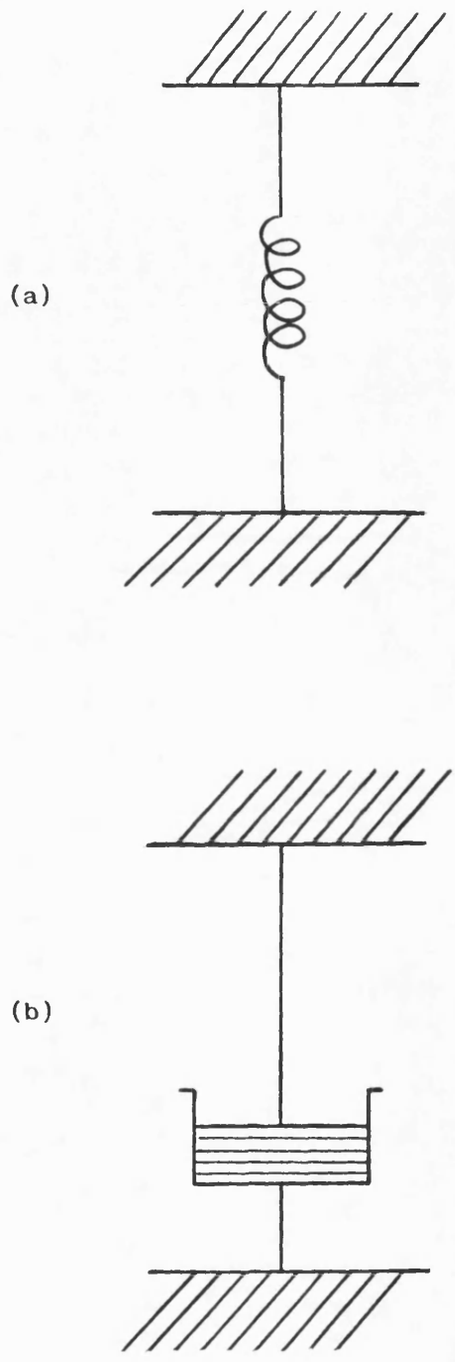

FIG. 1.12 Mechanical models used to represent the elastic (a) and viscous (b) behaviour of materials.

where,

γ/t = shear rate

σ = stress

η = shear viscosity

The behaviour of pharmaceutical powders under stress can also be described by mathematical models. The Maxwell model (Fig. 1.13a) represents a material which exhibits both elastic and viscous behaviour and consists of an elastic spring in series with a dashpot containing a viscous liquid. The stress in the spring equals that in the dashpot, whereas the total strain is the sum of the strains in the spring and the dashpot:

$$\gamma = \gamma_1 + \gamma_2 \qquad \text{Eq. 1.32}$$

where,

γ = total strain

γ_1 = elastic strain

γ_2 = viscous strain

The Voigt (Kelvin) model (Fig. 1.13b) consists of a spring and a dashpot connected in parallel. The strain in the spring equals that in the dashpot, whereas the total stress is the sum of the stresses in the spring and the dashpot:

$$\sigma = \sigma_1 + \sigma_2 \qquad \text{Eq. 1.33}$$

where,

σ = total stress

σ_1 = stress in the spring

σ_2 = stress in the dashpot

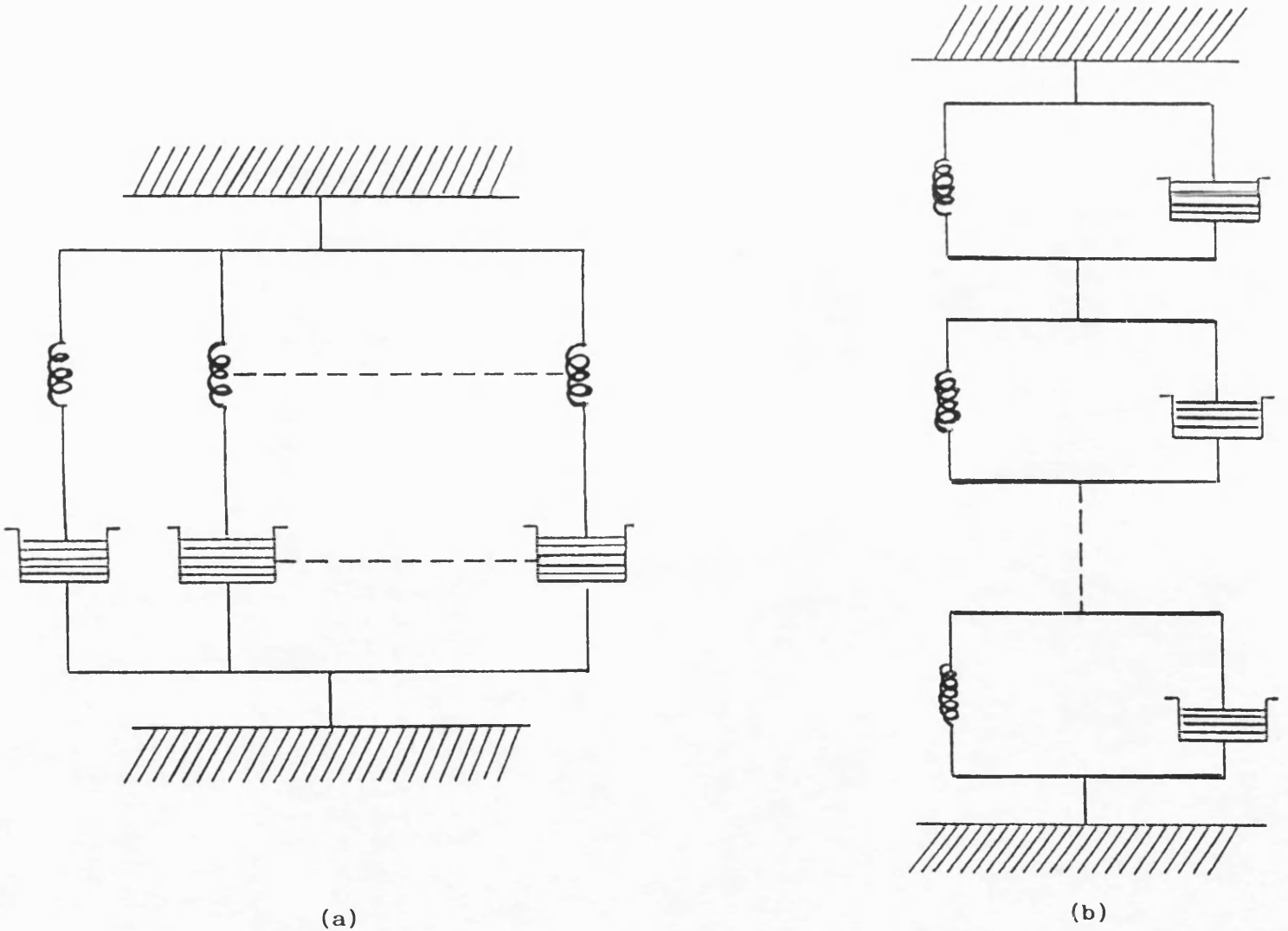

(a) (b)

FIG. 1.13 Mechanical models used to represent the viscoelastic behaviour of semisolids.

1.3.2 Analysis of Viscoelastic Behaviour

1.3.2.1 Stress Relaxation

One way of studying viscoelastic behaviour of particulate solids during compression is stress relaxation. During stress relaxation experiments the powder is compressed until a required peak force is reached. The punches are then held at this position and any decrease in punch force is monitored (Fig. 1.14). The porous compact is, therefore, restrained in a die under stress and constant strain conditions. As a result, time-dependent deformation of the material may continue from highly stressed areas into void spaces within the compact. As this process proceeds, the stress in the compact reduces and the driving force for further stress relaxation diminishes. The use of stress relaxation experiments to evaluate the compaction properties of materials, as well as attempts to linearise and analyse such data quantitatively are reported below.

Shlanta and Milosovich (1964) performed stress relaxation experiments using a hydraulic press in order to identify viscoelastic properties related to the time-dependent flow within a powder bed during compression. Their results were presented as plots of pressure against time; no attempt was made to analyse those data further. There was evidence that factors

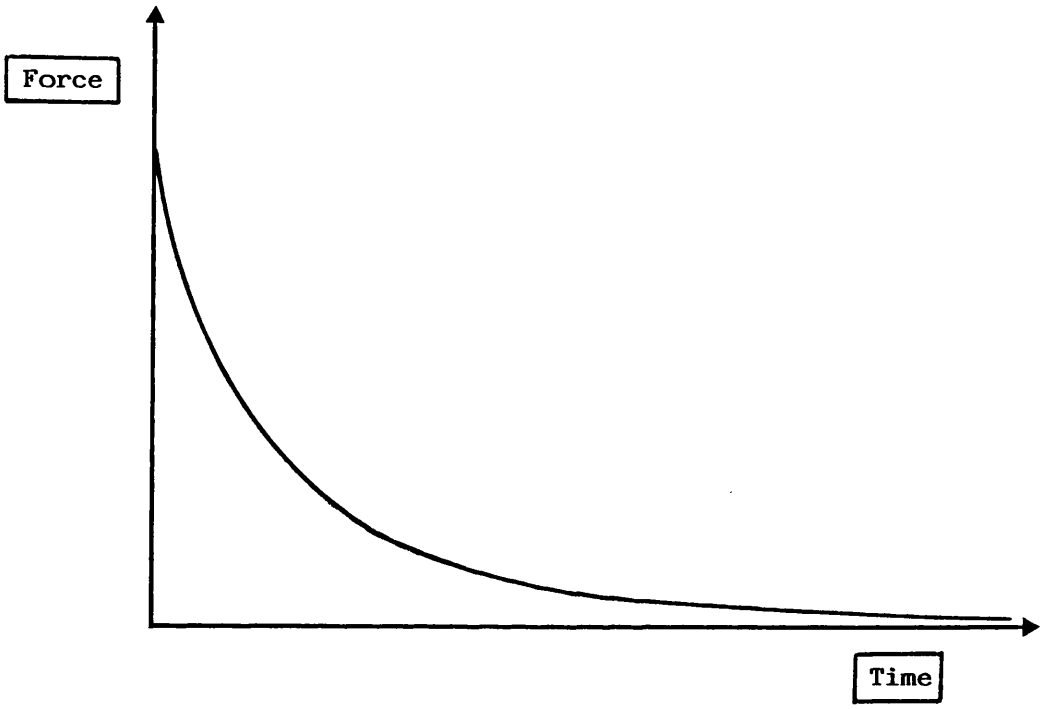

FIG. 1.14 Decrease in force with time during stress relaxation experiments.

known to affect tableting, such as particle size, particle size distribution, moisture content and loading rate, also affected stress relaxation data. They considered stress relaxation measurements to be valuable, since they provide information about the degree of plastic deformation the powders are likely to undergo during compaction. They concluded that, with the exception of aspirin, those materials which form good tablets by direct compression all showed intermediate stress relaxation.

The earliest reported attempt to quantify such data was made by Baba and Nagafuji (1965). They used an instrumented tableting machine and found an almost linear relationship between the relative stress, Sv, and log time, t, according to Eq. 1.34:

$$S_v = - k \cdot \log t + C \qquad \text{Eq. 1.34}$$

where,

$$S_v = S_t / S_e \qquad \text{Eq. 1.35}$$

S_t = stress at time t

S_e = stress at equilibrium

k = relaxation coefficient

C = constant

Cole et al (1975) used a compaction device, designed to simulate the compressive action of a rotary tableting machine (Rees et al, 1972), to study stress relaxation behaviour of inorganic chlorides, potassium citrate and lactose. The data were presented as the extent of stress relaxation monitored for two minutes. Baba and Nagafuji (1965) had, however, already

such curves to cross, resulting in changes in the rank order of materials at different times.

David and Augsburger (1977) treated plastic flow during stress relaxation mathematically, in terms of the Maxwell model under constant strain. Calculations led to Eq. 1.36:

$$\Delta F = \Delta F_o \cdot e^{-G \cdot t/\eta} \qquad \text{Eq. 1.36}$$

where,

ΔF = amount of the compressional force left in the viscoelastic region at time t

ΔF_o = total magnitude of this force at t=0

G = Young's modulus

η = viscosity coefficient

Thus, according to Eq. 1.36, the decay of compression force with time could be treated as a first order rate process:

$$\ln\Delta F = \ln\Delta F_o - k \cdot t \qquad \text{Eq. 1.37}$$

where,

$$k = G/\eta$$

They described k as the viscoelastic slope and stated that it may be expected to be greater for plastically deforming materials. Furthermore, ΔFo should also be greater for materials such as microcrystalline cellulose and compressible starch. Their results were in agreement with the Maxwell model, with the exception of compressible sugar for which a non-linear plot was obtained. They also concluded that the relaxation process was completed within ten seconds. According to them, such an

analysis could become a useful tool in explaining unusual shifts in tablet strength with time.

Rees and Rue (1978a) also used stress relaxation data in order to compare the time-dependent properties of materials. They used a single punch tableting machine, which was turned by hand and collected data for 360 seconds. They stated that none of the materials tested behaved as a Maxwell body. There was an initial curved section prior to the first order stress relaxation characteristic of a true Maxwell body. This was an indication of more than one relaxation time constant, the relaxation time being defined as the time required for the force to reach 1/e times the minimum force. They concluded that pseudo-equilibrium values for residual punch force obtained by David and Augsburger (1977) from a rotary tableting machine, must be the reason for the disagreement between the two experiments. In the rotary press concerned, stress relaxation would have taken place under virtually constant stress conditions because of the buffer effect of the powerful overload springs linked to the compression rolls. They also emphasised that a problem associated with stress relaxation measurements is that any plastic flow which occurs during the time required for initial force application, is not represented by stress relaxation curves, since they only represent flow occuring after the peak force is reached. The same workers (Rees and Rue, 1978b) used stress relaxation experiments to show differences in time-dependence between two batches of Elcema G250.

Another way of presenting stress relaxation data was reported by Hiestand et al (1977). They plotted relative pressure, P_v, against logt, where P_v is defined as:

$$P_v = P_t/P_o \qquad \text{Eq. 1.38}$$

where,

P_t = pressure at time t

P_o = pressure at t=0

These plots showed a change in slope after about 5 seconds. According to these authors, this suggests that some initially prominent mechanism soon becomes negligible. Their experiments also showed that entrapped air is not responsible for this effect.

The area under the stress relaxation curve up to a given time was proposed by Ho and Jones (1982) as a measure of the overall extent of stress relaxation exhibited by a material. However, this treatment does not account for differences in the shape of such curves which has been pointed out to be of great importance by Rees and Rue (1978b).

Malamataris et al (1984) presented their relaxation data (SR) as a percentage change in tablet thickness over 30 seconds:

$$SR = [(H_m-H_t)/H_t]\cdot 100 \qquad \text{Eq. 1.39}$$

where,

H_m = tablet thickness at maximum load

H_t = tablet thickness at t=30 s

A novel approach was reported by Shott (1983) based on earlier suggestions made by Schmid (1976). At the zero strain

rate that applies during stress relaxation, the creep strain which leads to a reduction in compact volume, must be balanced by an elastic strain tending to increase the volume. Thus, the overall strain remains constant, leading to the following relationship:

$$\ln(-d\sigma/dt) = \ln(G/B) + n \ln(\sigma) \qquad \text{Eq. 1.40}$$

where,

σ = stress

B, n = coefficients

G = Young's modulus

Therefore, a plot of $\ln(-d\sigma/dt)$ against $\ln(\sigma)$ produces a straight line of slope n and intercept $\ln(G/B)$. Shott (1983) reported that materials exhibiting large amounts of stress relaxation produced low values of slope n.

Huckle (1985) suggested that the stress relaxation characteristics of materials should be determined at a range of pressures and strain rates. This latter was confirmed by data published by Cook and Summers (1986) who stated that the rank order of materials changed at various relaxation times and pressures. They also concluded that for the materials tested, the relaxation of mixtures was more complex than an additive function of the properties of the individual components.

1.3.2.2 Creep Analysis

Another way to study viscoelastic behaviour, is by creep analysis. A stress is instantaneously applied to the material and then maintained constant. Strain response with time is recorded. Conventionally, compliance, J(t), is plotted against time, t, giving a curve similar to the one illustrated in Fig. 1.15a. Compliance values are calculated according to Eq. 1.41:

$$J(t) = \gamma/\sigma \qquad \text{Eq. 1.41}$$

where,

γ = strain

σ = stress

J(t) has the units 1/Pa.

A mechanical model which can be used to describe the creep results is illustrated in Fig. 1.15b (Barry, 1971). This model and the theory of linear viscoelasticity can be applied to creep data only if the strain is proportional to the applied stress, i.e. the material remains in the linear region of strain, obeying the Boltzmann principle (Ferry, 1970).

According to Sherman (1970), a typical creep curve (Fig. 1.15a) can be subdivided into three regions from which, several terms of Eq. 1.45 can be derived:

1. AB is the region of instantaneous compliance and can be represented by the elastic stretching of a spring:

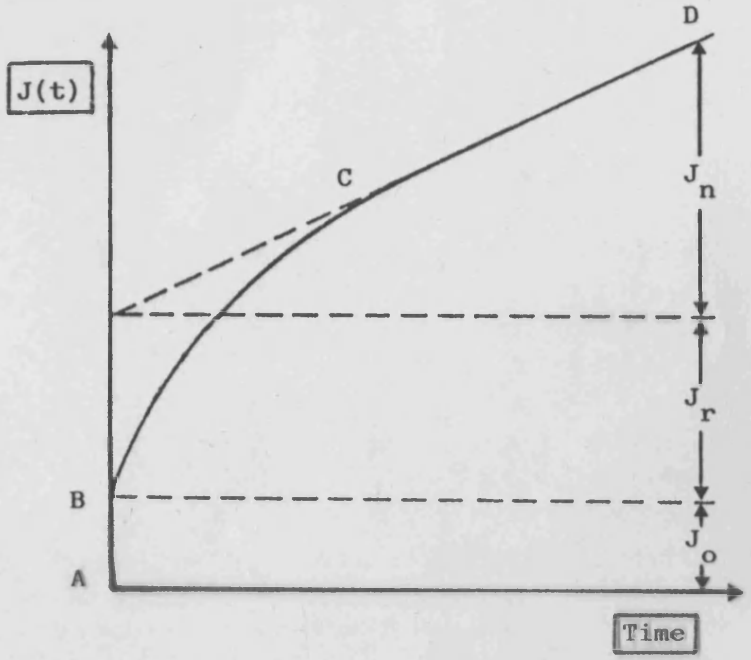

(a)

FIG.1.15 A typical creep curve annotated to show discrete deformation mechanisms (a) and

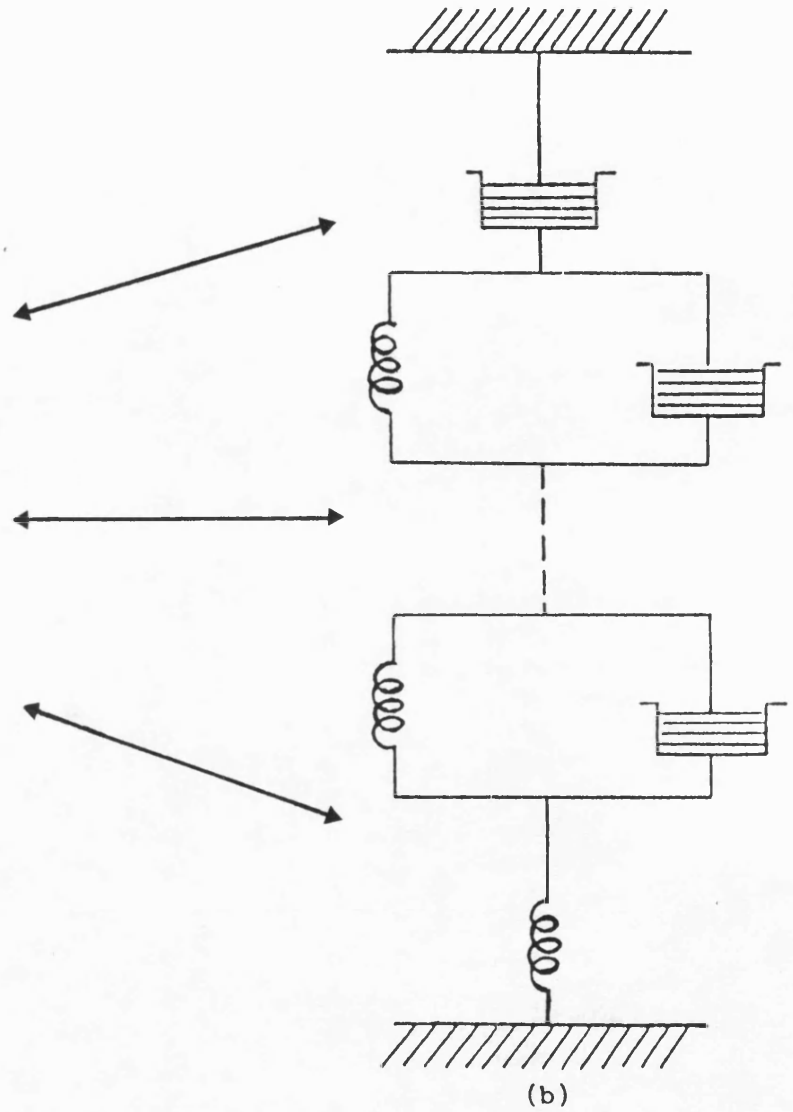

a mechanical model (b) used to describe creep behaviour.

It can be said, therefore,

$$J_o = 1/G = \gamma_o(t)/\sigma \qquad \text{Eq. 1.42}$$

where,

G = elastic modulus

γ_o = instantaneous elastic strain

σ = constant stress

2. BC is the time-dependent retarded elastic region with a compliance J_r. It can be represented by the stretching of a spring retarded by a dashpot connected to it in parallel. For a number of Voigt units:

$$J_r = \sum_{m=1}^{m} J_m \cdot (1-e^{-t/T_m}) = \gamma_r(t)/\sigma \qquad \text{Eq. 1.43}$$

where,

J_m = compliance of each Voigt element

T_m = retardation time of each Voigt element

γ_r = strain in the viscoelastic region

σ = constant stress

3. CD is the linear region of Newtonian compliance, J_n. It is modelled by the viscous flow of liquid in a dashpot:

$$J_n = t/\eta = \gamma_n(t)/\sigma \qquad \text{Eq. 1.44}$$

where,

η = shear viscosity of the liquid

γ_n = strain in the viscous region

σ = constant stress

J_n can be obtained from experimental data and η can be

calculated from the slope of the linear part of the curve.

According to Warburton and Barry (1968), Eq. 1.45 describes such a model's compliance to a constant stress:

$$J(t) = J_o + \sum_{m=1}^{m} J_m (1 - e^{-t/T_m}) + t/n \qquad \text{Eq. 1.45}$$

An interesting analysis of the process of dynamic compression was made by Morii et al (1973), by drawing curves corresponding to a normal creep curve in the static compression process. Stress-strain curves for different punch velocities were plotted and from each curve the strain under a certain value of stress was obtained. When these strain values were plotted against compression time, a group of curves corresponding to each stress level was obtained. They concluded that by this method it is possible to find the most suitable compression velocity for each material, as well as how far the change of the packing structure during dynamic compression can be attributed to plastic and viscoelastic deformation. It must be emphasised that although the curves obtained by these workers show the strain response of a powder versus time under a constant stress, they are derived from a dynamic compression process. They cannot be regarded as the same as the ones obtained from a static compression process. Their significance and interpretation needs caution and further investigation.

It is clear that there is a demand for a fundamental test performed at various stages of the manufacturing process, which

will assess the rheological properties of the materials. According to Barry (1974), a creep test would be suitable as an on-line quality control procedure. However, he advised that caution is necessary, the limits of linearity must be determined, and no internal stresses must be present in the sample before the constant stress is applied. The system must be in a completely relaxed state before a creep run is attempted.

Several investigators have already used Eq. 1.45 in order to study the viscoelastic properties of semisolids. Barry (1970) used creep data to explain changes in stability of emulsions of liquid paraffin in water employing different emulsifiers. A higher creep compliance curve indicated a looser nature of the viscoelastic network. Barry and Grace (1971a) described the effect of temperature on the consistency and behaviour of white soft paraffin. Work softening which may occur during a manufacturing process can also be investigated with the use of creep curves, according to Barry and Grace (1971b). Higher compliance curves showed a fractured network structure.

Limited reports of creep results for viscoelastic particulate solids have also appeared in the literature. Travers et al (1983) examined strain movements within the die of compacts maintained at constant stress and elastic recovery on sudden release after a range of holding times was recorded. They concluded that such tests can be used to predict the behaviour of materials at high compression rates. Following the same concept, Celik and Travers (1985) proposed an Elastic Recovery

Index (ERI) to predict the compressional behaviour of materials. Mashadi (1984) studied the creep behabiour of lactose microgranulates containing different proportions of Starch 1500 as a binding agent. Patel (1986) related the creep behaviour of particulate solids to the compactibility of the powders.

Clearly, more work needs to be devoted to the application of the creep test on the study of viscoelastic behaviour of pharmaceutical powders and the use of this testing method in the prediction of powder behaviour under load.

1.4 HIGH SPEED COMPACTION SIMULATOR

The instrumentation of a single punch reciprocating tableting machine has been developed substantially since Higuchi et al (1954) reported the use of strain gauges attached to a tablet press. This has enabled the detailed study of the physics of compression. However, a correlation between the behaviour of materials during a single compression event and their performance on the high speed rotary machine used in a production situation was not always straightforward.

Instrumentation of high speed rotary machines has not provided the solution. The numerous efforts (Shotton et al, 1963; Knoechel et al, 1967a and b) were often found to be difficult, expensive and sometimes inaccurate. Furthermore, use of a rotary press would involve relatively large quantities of material, not always available at the early stage of formulation studies. In an attempt to overcome such problems, a simulation device was developed by Rees et al (1972), using a universal mechanical testing instrument (Model TTDM, Instron Corp., Canton, Mass., U.S.A.). The double-acting compression was achieved by controlled downward movement of the die at a slower rate than the simultaneous downward movement of the upper punch. Control of the rate of loading, relative movement of the die and upper punch, time when movement of the die commenced, depth of compression and precompression of the powder bed, permitted

simulation of a range of machine settings for different types of rotary press. The use of the above-proposed simulation device was limited by its relatively low loading rates.

Hunter et al (1976) presented the details of the first high speed compaction simulator. The basic structure of all the hydraulic simulators constructed since then, is the same. The computer generates a displacement-time profile similar to the one performed by the upper and lower punch of the tableting machine to be simulated. The output is finally fed to the control valve situated on the load frame. The signal determines the flow of the hydraulic fluid from the power pack, through the valves to the actuators. The flow of this fluid causes movement of the actuators according to the intended profile. For each compression event, force and displacement data are obtained from upper and lower load cells and LVDTs. Compression rates of the same order as those achieved by conventional rotary machines make such devices ideal tools for fundamental research, formulation development and trouble shooting during production.

Several studies have been reported where such devices were used in the study of the compaction behaviour of materials and especially on the effect of compaction speed on the mechanical properties of tablets.

A comparative study (Bateman et al, 1987) was performed in order to investigate the equivalence of data produced by a number of compaction simulators in use by different research groups in the U.K. and U.S.A. Differences in the parameters

obtained for Tablettose samples obtained from the same original batch, such as the yield pressure for example, were attributed to errors in the correction for the elastic distortion and differences in the loading characteristics of the hydraulic systems. A certain degree of caution should, therefore, be exercised when comparing data produced by different research groups.

CHAPTER TWO

MATERIALS AND METHODS

2.1 MATERIALS

2.1.1 List of Powders

The materials used in this study together with the source of supply, are listed below alphabetically; B.N. defines the batch number:

- Amylose (practical grade)
  Sigma Chemical Co. Ltd., Poole, U.K., B.N. 96F-0489
- Amylopectin
  Sigma Chemical Co. Ltd., Poole, U.K., B.N. 25F-0608
- Avicel PH102 (microcrystalline cellulose)
  F.M.C. Co., Philadelphia, U.S.A., B.N. 7242
- Emcocel 90M (microcrystalline cellulose)

Edward Mendell Co. Inc., Carmel, N.York, U.S.A., B.N. 7019

- Emcompress (dicalcium phosphate dihydrate)

  Edward Mendell Co. Inc., Carmel, N.York, U.S.A., B.N. 5209 921

- Lactose (anhydrous)

  Humco Sheffield Chemical Corporation, Lyndhurst, N. Jersey, U.S.A., B.N. 2NL 15 31

- Magnesium stearate (technical grade)

  B.D.H Chemicals, Poole, U.K.

- National 1551 (fully pregelatinised corn starch)

  Laing National Ltd., Manchester, U.K., B.N. 11503

- Sodium bicarbonate (analytical grade)

  F.S.A. Lab. Supplies, Loughborough, U.K., B.N. 109

- Sodium chloride, B.P.

  Evans, U.K., B.N. 50183HA

- Starch 1500 (partially pregelatinised corn starch)

  Colorcon Ltd., Orpington, Kent, U.K., B.No's 611002, 811024, 801035, 903025, 807010, 306015 and Batch F

- Tablettose (lactose, α-monohydrate)

  Meggle Milchindustrie GmbH, West Germany, Lot 816

2.1.2 Characterisation of Particulate Solids

2.1.2.1 Bulk Density

The bulk density, d_b, of a powder is determined by dividing the mass of a certain amount of the material by its bulk volume. This latter value includes the volume occupied by solid and the volume of pores and void spaces between the particles:

$$d_b = m/V_b \qquad \text{Eq. 2.1}$$

where,

m = powder mass

V_b = volume the poured powder occupies

Bulk density determination can be affected by the dimensions of the container in which the measurements are made. Therefore, in order to simulate the packing conditions in a 12.7mm die, a 10ml glass measuring cylinder with an internal diameter of 12mm was used in this work. The powder was poured through a funnel of suitable orifice size. Three measurements were made for each material. The results are shown in Table 2.1.

2.1.2.2 Tapped Density

The reduction in volume of a particulate solid following a number of taps is a measure of the powder's rearrangement

TABLE 2.1 Density measurements for the materials tested.

Material	Particle Density (Kg/l)	Bulk Density (Kg/l)	Tapped Density (Kg/l)	% Compressibility	Flow
AMYLOPECTIN	1.54	0.47	0.70	32.86	very poor
AMYLOSE	1.50	0.43	0.62	30.64	poor
ANH. LACTOSE	1.53	0.57	0.72	20.83	passable
AVICEL PH102	1.57	0.28	0.40	30.00	poor
EMCOCEL 90M	1.57	0.29	0.40	27.50	poor
EMCOMPRESS	2.30	0.78	0.92	15.22	good
NAT. 1551	1.51	0.49	0.63	22.22	passable
SODIUM BICARBONATE	2.16	0.99	1.20	17.50	fair to good
SODIUM CHLORIDE	2.17	1.21	1.33	9.02	excellent
STARCH 1500 (0% R.H.)	1.51	0.66	0.90	26.67	poor
STARCH 1500 (22% R.H.)	1.51	0.65	0.87	25.29	poor
STARCH 1500 (53% R.H.)	1.51	0.62	0.78	20.51	passable
STARCH 1500 (80% R.H.)	1.51	0.57	0.72	20.83	passable
STARCH 1500 (94% R.H.)	1.51	0.53	0.69	23.19	passable
STARCH 1500 (<125um)	1.51	0.57	0.74	22.97	passable
STARCH 1500 (125-180um)	1.51	0.62	0.78	20.51	passable
STARCH 1500 (>180um)	1.51	0.60	0.74	18.92	fair to good
STARCH 1500 (>710um)	1.51	0.53	0.58	8.62	excellent
STARCH 1500 (>1680um)	1.51	0.51	0.53	3.77	excellent
TABLETTOSE	1.54	0.55	0.70	21.43	passable

ability; this is mainly dependent on particle size, shape and surface irregularity. The test was performed in a 10ml glass measuring cylinder which was tapped using a jolting volumeter (Model Stav 2003, Engelsmann A.-G, West Germany) and the powder volume was recorded after each "tap interval", until continuing taps had no more effect on the volume.

Tapped density, d_t, is, therefore, calculated according to Eq. 2.2:

$$d_t = m/V_t \qquad \text{Eq. 2.2}$$

where,

V_t = final volume of the powder, including the volume of the particles and remaining voids.

Three determinations were performed for each material. The results are presented in Table 2.1.

From bulk and tapped density values, the percentage compressibility (Carr, 1970) could be calculated according to Eq. 2.3:

$$\% \text{ compressibility} = (d_t - d_b)/d_b \cdot 100 \qquad \text{Eq. 2.3}$$

According to Carr (1970), high values are indicative of a powder reducing its volume substantially when subjected to tapping and thus, of one with poor flow properties. The % compressibility values of the materials studied in this work are listed in Table 2.1.

2.1.2.3 Particle Density

Particle density, d_p, of a powder is defined as the density of the material excluding accessible void and pore spaces:

$$d_p = m/V_p \qquad \text{Eq. 2.4}$$

where,

V_p = volume of the powder particles measured by gas displacement excluding accessible void and pore volume.

A helium-air pycnometer (Model 1302, Micromeritics Instr. Corp., Georgia, U.S.A.) was used for the true density determinations. Its basic principle is the change in pressure following a change in volume in an enclosed vessel. The instrument is very sensitive to temperature changes; therefore, it was allowed to equilibrate with the surrounding physical environment before each test and contact with it was minimised throughout the test. Greatest accuracy was achieved when the sample cup was kept as full as possible. The powders were dried for 2 hours at 60C and allowed to cool under vacuum. The samples were weighed after the volume determinations. For each material three different samples were tested and the mean particle density was calculated. The results for the materials tested are shown in Table 2.1.

2.1.2.4 Particle Size Analysis

As mentioned in 1.2.1.3, an important advance in the field of powder technology was the realisation that particle size, and hence surface area, have a significant effect on the compaction properties of particulate materials.

There are many methods available for determining particle size. Microscopy, sedimentation, and sieving are the ones most widely used. None of these methods, however, provides a truly direct measurement of size. Optical and electron microscopes allow the observer to view the actual particles, but the results obtained are not considered to be more direct than those of other methods, as only two of the three dimensions of each particle are taken into account. The sedimentation methods are based on Stoke's law according to which, the rate at which particles sediment through a suspending medium is directly related to their diameter. The use of stream counting devices, such as the Coulter counter, allows the measurement of particle volume by recording changes in resistance between two electrodes and, therefore, the calculation of equivalent volume diameter. The exact shape of the particles cannot, however, be determined. Finally, sieving involves the flow of the material through a series of standard calibrated sieves of decreasing aperture size. The material retained on each sieve represents the amount of powder with certain dimensions greater than the sieve

aperture size.

Since the range of particle size of most powders used in this study is 40-800μm approximately, sieving was chosen as the most appropriate technique. The test was applied according to British Standard (B.S. 410/1976). A series of sieves (B.S. 410/1969, Endecotts Ltd, U.K.) which complied with international recommendations for nominal aperture size 710, 500, 355, 250, 180, 125, 90, 63 and 45μm were used.

The sieves were assembled on a mechanical sieve shaker (Type 03.502, Fritch, supplied by Christison Ltd, U.K.) which provided a three-dimensional controlled motion and produced a continuous movement of the particles around the screen. The size of the sample for test sieving is largely governed by the density and size distribution of the materials, but there are other factors to consider. Very small and very large samples are associated with errors in weighing and difficulty in handling, respectively. Flaky materials are difficult to sieve and, therefore, sample weight should be reduced. Each sample was placed on the top sieve and shaken until the "end-point" was reached. This was determined for each material according to the following procedure (B.S. 410/1976): The whole sample was initially sieved for a period of 5 minutes. The weight of the material remaining on each sieve was recorded. Each sieve was then shaken separately and repeatedly for a period of 2 minutes until the weight of the material passing through in that time interval was less than 0.2% of the original test sample. Only

then, was the sample considered to have been completely separated regarding particle size. A 30-minutes shaking period was selected as a result of the above preliminary tests for the materials tested. The fraction quantities were measured with a precision of $\pm$ 0.2% of the original sample weight.

The percentage weight of particles on each sieve formed the basis of the analysis. The cumulative percentages of undersize (total percentage by weight passing each of a set of sieves of descending aperture size) and oversize (total percentage by weight retained on each of a set of sieves of descending aperture size) material were also calculated. The results are shown in Tables 2.2-2.4.

TABLE 2.2 Particle size analysis of Avicel PH102, Emcocel 90M, Starch 1500 and National 1551.

Sieve aperture (μm)	%	% Cumul. oversize	% Cumul. undersize	%	% Cumul. oversize	% Cumul. undersize
	AVICEL PH102			EMCOCEL 90M		
250	3.59	3.59	96.41	2.47	2.47	97.53
180	12.11	15.70	84.30	9.53	12.00	88.00
125	16.22	31.92	68.08	19.81	31.81	68.19
90	13.58	45.50	54.50	13.48	45.29	54.71
63	18.64	64.14	35.86	20.51	65.80	34.20
45	14.49	78.63	21.37	21.68	87.48	12.52
<45	21.37	100.00	0.00	12.52	100.00	0.00
	STARCH 1500 (B.N. 611002)			NATIONAL 1551		
250	2.78	2.78	97.22	0.33	0.33	99.67
180	1.75	4.53	95.47	4.26	4.59	95.41
125	16.49	21.02	78.98	21.18	25.77	74.23
90	29.73	50.75	49.25	26.09	51.86	48.14
63	31.53	82.28	17.72	25.42	77.28	22.72
45	14.17	96.45	3.55	11.31	88.59	11.41
<45	3.55	100.00	0.00	11.41	100.00	0.00

TABLE 2.3 Particle size analysis of sodium chloride, sodium bicarbonate, anhydrous lactose and Emcompress.

Sieve aperture (μm)	%	% Cumul. oversize	% Cumul. undersize		%	% Cumul. oversize	% Cumul. undersize
	SODIUM CHLORIDE				SODIUM BICARBONATE		
710	0.26	0.26	99.74	250	0.13	0.13	99.87
500	3.25	3.51	96.49	180	0.45	0.58	99.42
355	30.47	33.98	66.02	125	69.85	70.43	29.57
250	51.47	85.45	14.55	90	19.46	89.89	10.11
125	14.27	99.72	0.28	63	7.52	97.41	2.59
90	0.19	99.91	0.09	45	2.24	99.65	0.35
<90	0.09	100.00	0.00	<45	0.35	100.00	0.00
	EMCOMPRESS				ANHYDROUS LACTOSE		
250	7.75	7.75	92.25		15.73	15.73	84.37
180	40.67	48.42	51.58		19.00	34.73	65.27
125	29.25	77.67	22.33		19.80	54.53	45.47
90	12.82	90.49	9.51		21.40	75.93	24.07
63	7.92	98.41	1.59		15.94	91.87	8.13
45	1.34	99.75	0.25		4.98	96.85	3.15
<45	0.25	100.00	0.00		3.15	100.00	0.00

TABLE 2.4 Particle size analysis of amylose, amylopectin and batches of Starch 1500 containing different proportions of cold water solubles.

Sieve aperture (μm)	%	% Cumul. oversize	% Cumul. undersize	%	% Cumul. oversize	% Cumul. undersize
		AMYLOSE			**AMYLOPECTIN**	
250	2.01	2.01	97.99	1.37	1.37	98.63
180	2.96	4.97	95.03	1.84	3.21	96.79
125	6.39	11.36	88.64	2.35	5.56	94.44
90	0.09	11.45	88.55	0.55	6.11	93.89
63	37.85	49.30	50.70	44.16	50.27	49.73
45	21.26	70.56	29.44	33.72	83.99	16.01
<45	29.44	99.99	0.00	16.01	100.00	0.00
		B.N. 807010			**B.N. 811024**	
250	2.19	2.19	97.81	1.64	1.64	98.36
180	4.12	6.31	93.69	2.60	4.24	95.76
125	52.93	59.24	40.76	12.75	16.99	83.01
90	0.89	60.13	39.87	0.49	17.48	82.52
63	34.31	94.44	5.56	56.82	74.30	25.70
45	2.09	96.53	3.47	16.08	90.38	9.62
<45	3.47	100.00	0.00	9.62	100.00	0.00
		B.N. 801035			**B.N. 903025**	
250	1.05	1.05	98.95	2.03	2.03	97.97
180	2.37	3.42	96.58	2.48	4.51	95.49
125	18.56	21.98	78.02	28.83	33.34	66.66
90	0.57	22.55	77.45	0.58	33.92	66.08
63	54.34	76.89	23.11	52.24	86.16	13.84
45	14.88	91.77	8.23	4.50	90.66	9.34
<45	8.23	100.00	0.00	9.34	100.00	0.00

2.1.2.5 Moisture Content

The moisture content of a powder can be determined by measuring the loss in weight of a sample after a drying process.

$$\% \text{ moisture content} = [(W_o - W_s)/W_s] \cdot 100 \qquad \text{Eq. 2.5}$$

where,

W_o = original weight of the sample

W_s = weight of the sample after it has been dried to constant weight.

In this study, the materials were dried at 105C, over silica gel and under vacuum for 24 hours. The weight of the sample before and after the drying process was used to calculate the % moisture content according to Eq. 2.5. Three replicates were used for each material. The results for the materials tested are shown in Table 2.5.

2.1.2.6 Conditioning of Powders

In order to standardise powder conditioning, the materials were initially dried at 60C in an oven (Model OVL 570 010J, Gallenkamp, U.K.) over silica gel and under vacuum (High Vacuum Pump, Model E2M2, Edwards High Vacuum, U.K.), and subsequently stored at 25C and 53% relative humidity for a week. The samples were then weighed individually to + 0.5mg. After compaction, the tablets were also stored at 25C and 53% relative humidity for one week before they were subjected to any kind of testing.

TABLE 2.5 Moisture content of materials equilibrated at 53% relative humidity.

Material	% Moisture content
AMYLOPECTIN	9.6
AMYLOSE	9.8
ANHYDROUS LACTOSE	0.7
AVICEL PH102	5.4
EMCOCEL 90M	5.4
EMCOMPRESS	0.6
NATIONAL 1551	11.6
SODIUM BICARBONATE	0.8
SODIUM CHLORIDE	0.1
STARCH 1500	10.6
TABLETTOSE	5.2

The effect of storage conditions on the physico-mechanical properties of some materials was studied by storing the materials to be tested at a range of humidities. The materials were first dried at 105C over silica gel and under vacuum and then kept in desiccators, ensuring a range of relative humidity conditions, inside an incubator (Model IH-150, Gallenkamp, U.K.) set at 25C, for at least a week. A list of the saturated salt solutions used, as well as the associated relative humidities (Nyqvist, 1983), is given in Table 2.6.

TABLE 2.6 Substances used to provide a range of relative humidities at 25C.

Material	% Relative humidity
Silica gel	0
Potassium acetate (satur. solut.)	22
Magnesium nitrate (satur. solut.)	53
Ammonium chloride (satur. solut.)	80
Potassium nitrate (satur. solut.)	94

2.2 METHODS

2.2.1 Tablet Compression

The materials were compressed in a 12.7mm diameter die, between two flat-faced punches of an instrumented single station reciprocating tableting machine (Type E2, Manesty Ltd., Speke, Liverpool, U.K.) shown in Fig. 2.1. For all the powders, sufficient material to produce a 2.21mm thick tablet at zero theoretical porosity was used. The above mentioned thickness was chosen so that the sample weight of each material, calculated individually according to Eq. 2.6, would fit in the die without any precompression being required.

$$W = V \cdot d_p = \pi \cdot r_t^2 h_t \cdot d_p \qquad \text{Eq. 2.6}$$

where,

W = sample weight

V = sample volume

π = 3.1415927

d_p = powder's true (particle) density

h_t = tablet thickness

r_t = tablet radius (12.7/2mm)

The sample weights of all the materials tested are shown in Table 2.7. Twenty samples of each material were compressed at a range of compaction forces (6, 12 and 18kN). Each sample

FIG. 2.1 Instrumented E2 Manesty tableting machine with associated data acquisition and processing system.

TABLE 2.7 Weights of the materials used in experiments.

Material	W (mg)
AMYLOPECTIN	431
AMYLOSE	420
ANHYDROUS LACTOSE	428
AVICEL PH102	440
EMCOCEL 90M	440
EMCOMPRESS	644
NATIONAL 1551	423
SODIUM BICARBONATE	605
SODIUM CHLORIDE	607
STARCH 1500	423
TABLETTOSE	431

was fed into the die individually; accuracy in sample weight was therefore achieved. The fly-wheel of the tableting machine was turned manually. It was found, however, that it was impossible to maintain exactly the same contact time for replicates of each material or for different materials (Tables A.6 and A.7).

The die was lubricated before each compaction cycle by compressing a 50% w/w mixture of magnesium stearate and the material under test.

2.2.1.1 Data Acquisition and Manipulation

The force applied on the powder bed by the upper punch was monitored by a precalibrated load cell (Type 9021, Kistler Instr. Ltd., Hartley Wintney, U.K.). The upper punch holder was modified in order to hold the load cell as well as the load distribution washer so that the top end of the upper punch pressed directly against this washer. The punch was held loosely in position by a retaining screw so that its free movement would allow the force to be transmitted directly through the load distribution washer on to the load cell. The associated conditioning amplifier (Type 5054A, Kistler Instr. Ltd., Hartley Wintney, U.K.) converted changes in capacitance into changes in voltage.

The force transmitted to the lower punch was monitored by strain gauges (Welwyn Strain Measurement Ltd., Basingstoke, U.K.) bonded to the lower punch holder in such a way that the

same effect as above was obtained. The signals from the strain gauges were passed to a conditioning amplifier (Type 2120, Welwyn Strain Measurement Ltd., Basingstoke, U.K.) where changes in resistance were converted into changes in voltage. The load cell was used to calibrate the strain gauges in situ; the punches were brought in contact and the readings from both the load cell and the strain gauges were monitored (Fig. 2.2). The results are shown in Table 2.8. It was found that these results changed slightly with time; therefore, calibration of the strain gauges was performed before each set of experiments.

A 10mm linear variable displacement transducer (Type AG/10, Sangamo Instr. Ltd., Bognor Regis, U.K.) attached to the die table (Fig. 2.3) monitored the movement of the upper punch. The signals from the LVDT were fed into an amplifier card (Type CA2 series, Sangamo Instr. Ltd., Bognor Regis, U.K.) powered by a 15 Volt power supply. The LVDT was calibrated in-situ using a series of feeler gauges of known thicknesses (Fig. 2.4). The results are shown in Table 2.9.

Fig. 2.5 shows the new positioning of the LVDT on the die table. This was part of an effort to achieve accurate measurement of upper punch penetration during compaction, by reducing any effects due to deformation of the tableting machine above the upper punch holder. This was done by moving the arm further down the upper punch assembly, which necessitated the use of a longer arm for the transducer to bear on. The force applied by this latter on the arm is relatively small,

TABLE 2.8 Calibration data for the strain gauges.

Upper punch force (N)	Lower punch force (digital values)
492	880
1100	1808
2030	3152
4082	6128
6133	9168
7986	11856
10126	14912
12068	17664
14064	20464
16300	23424
18222	25936
20054	28416

Slope = 1.413

Intercept = 387.230

Corr. coefficient = 0.9998

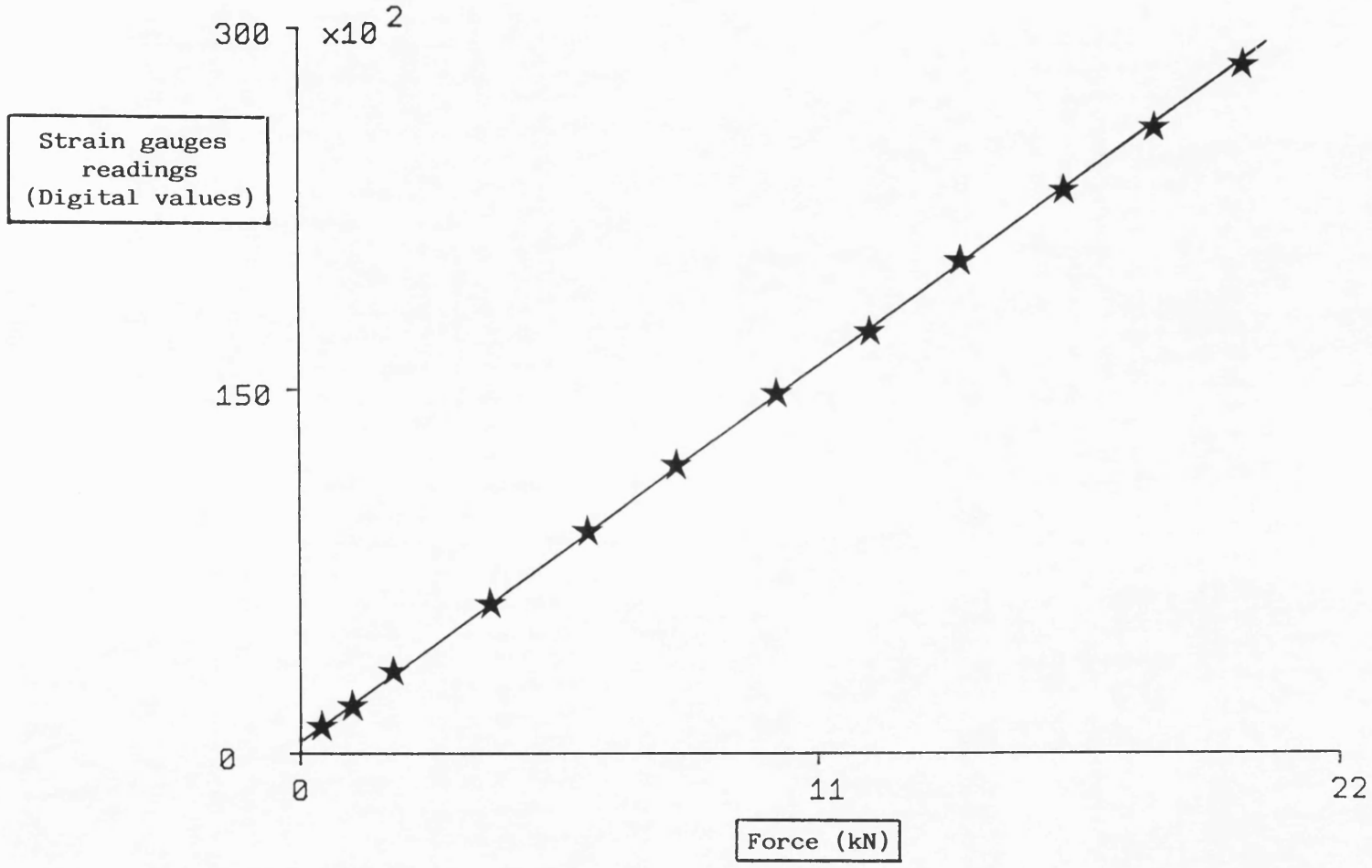

FIG. 2.2 Calibration curve for the strain gauges.

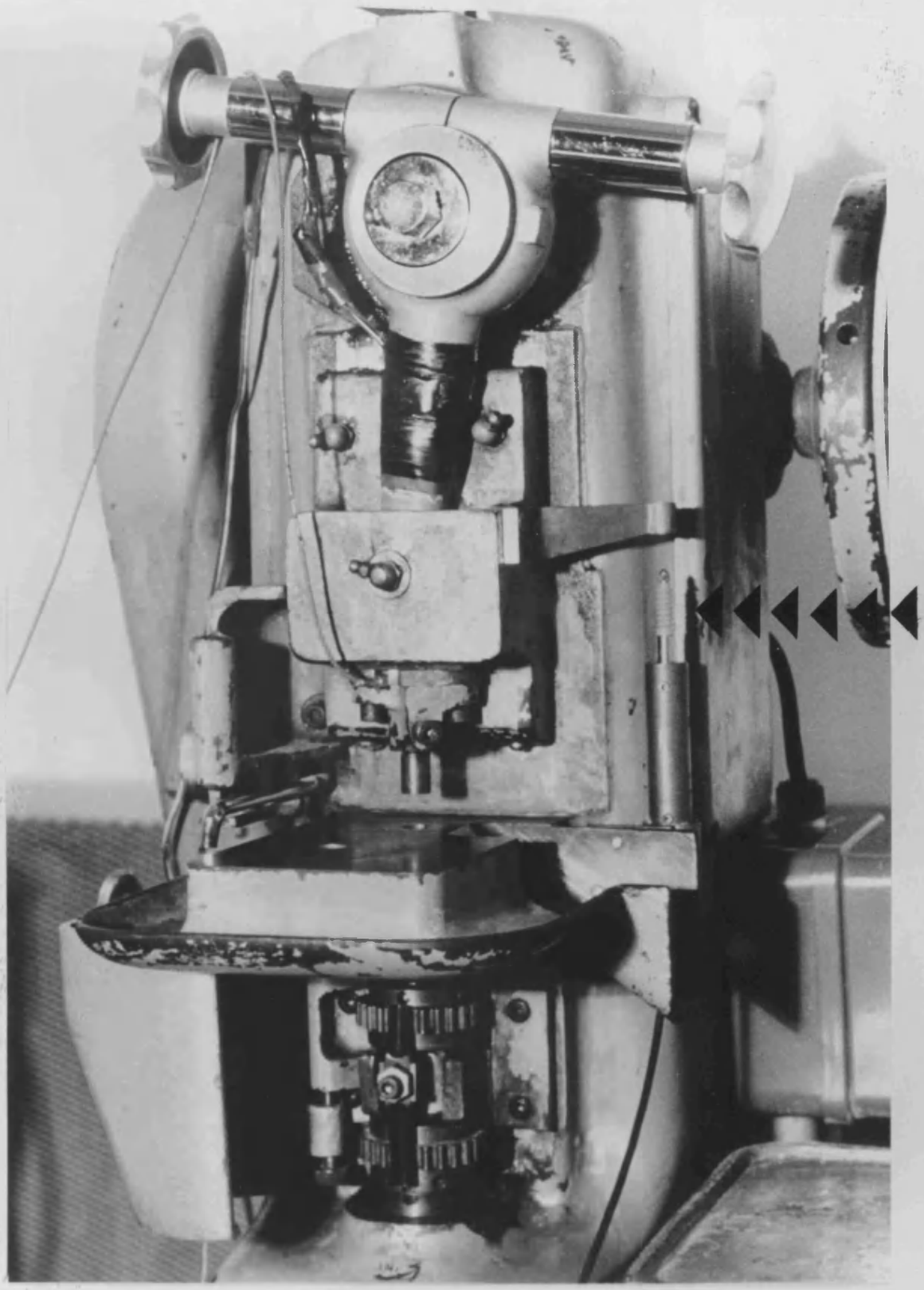

FIG. 2.3 Close-up of the tableting machine showing the position of the LVDT on the die table.

TABLE 2.9 Calibration data for 10mm LVDT (Type AG/10, Sangamo Instr. Ltd.).

Thickness (mm)	Displacement (digital values)
0.000	208
0.310	2064
0.632	4240
1.100	7632
2.472	15056
3.424	20944
5.028	29584
10.162	60688

Slope = 5911.580

Intercept = 461.622

Corr. coefficient = 0.99982

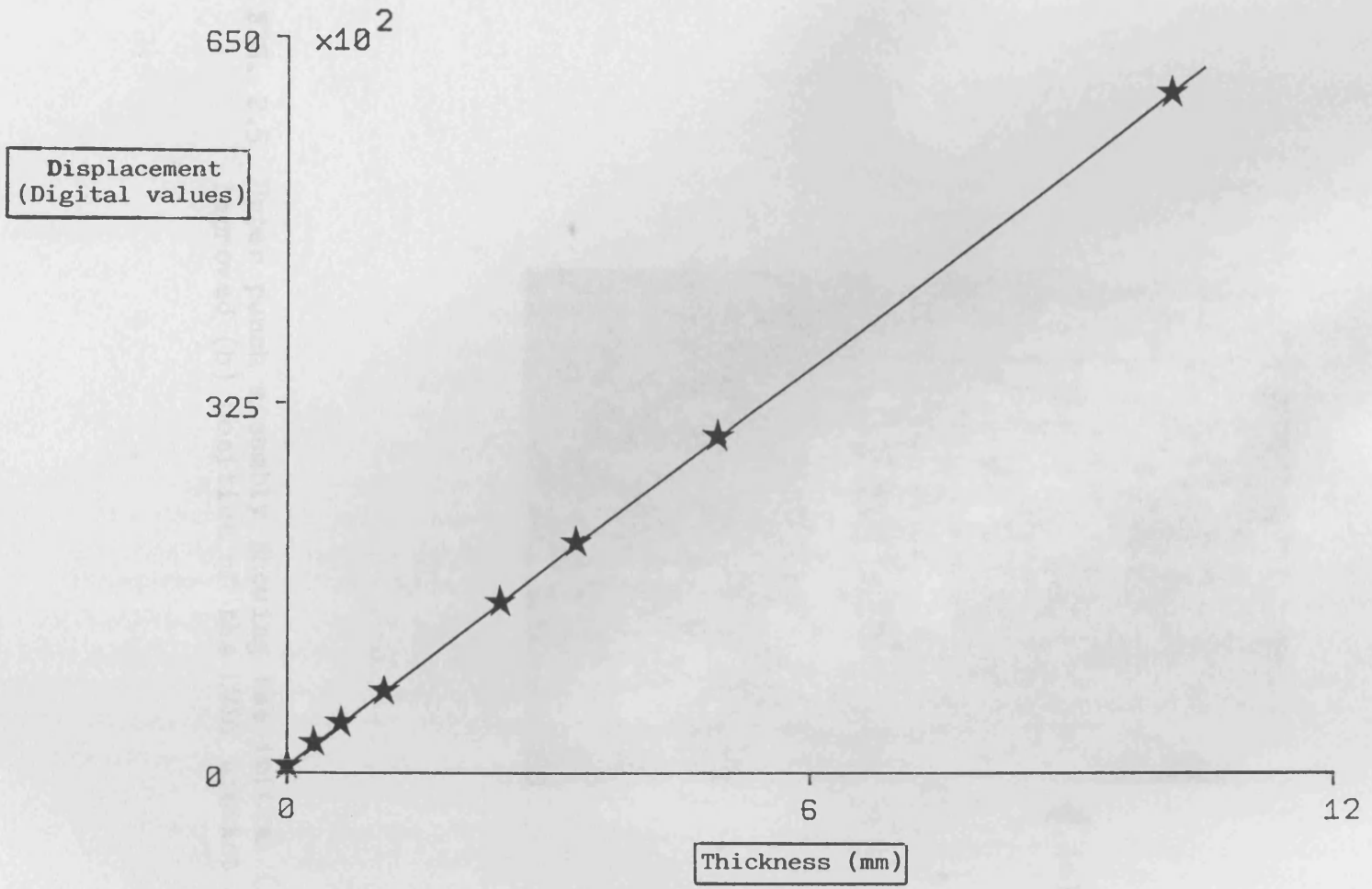

FIG. 2.4 Calibration curve for 10mm LVDT (Type AG/10, Sangamo Instr. Ltd.).

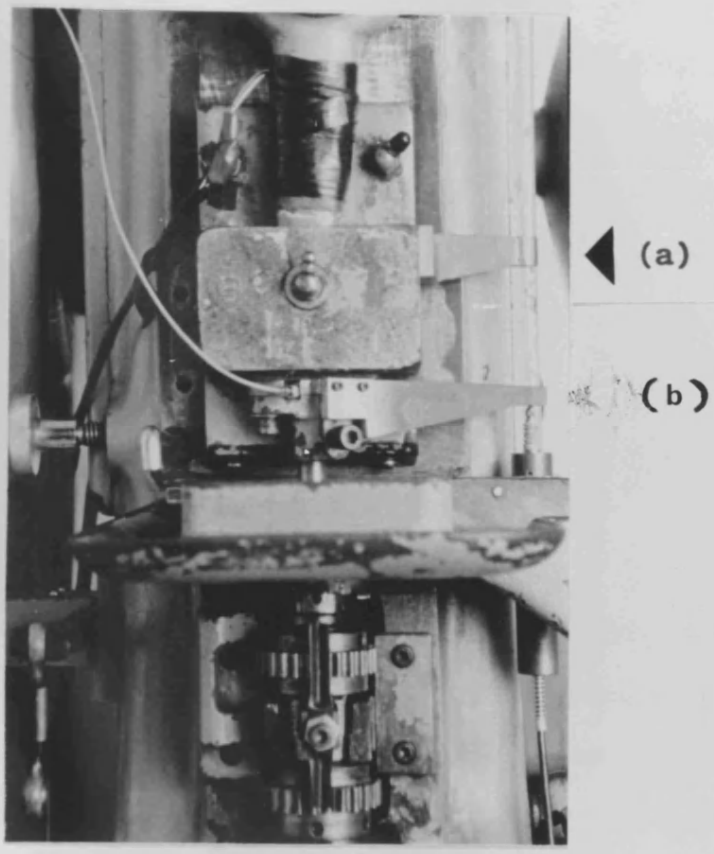

FIG. 2.5 Upper punch assembly showing the initial (a) and improved (b) position of the LVDT contact arm.

therefore, causing no measurable elastic distortion on the arm. This new setting was adopted for the rest of this study.

The analogue signals from force and displacement outputs were fed via an analogue-digital converter connected to the 1MHz Bus of a microcomputer (Master Series, British Broadcasting Co., U.K.). 500 digital values were obtained from each of the above mentioned measuring devices during one complete compression cycle. These values were stored in the memory of the microcomputer and processed at the end of each run. Twenty replicates were used to provide the mean values.

2.2.1.2 Elastic Distortion during Compression

Preliminary tests were performed in order to measure the elastic deformation of the punches under load. It was considered that since the expected volume changes of compacts under load were small, even small errors in displacement values would result in large errors in the calculated density values and therefore, in the term $\ln[1/(1-D)]$ of the Heckel equation.

A good approximation of the error involved can be achieved by pressing the punches against each other and monitoring changes in displacement with pressure. It should be noted that the top and bottom punch assemblies are distorted differently under the same applied pressure. When the two punches are pressed together, the recorded displacement is the total

displacement due to both the upper and lower punches deforming under the same load. When a compact is formed, however, the force applied by the upper punch is higher than that transmitted to the lower one. Therefore, the lower punch assembly will undergo less elastic deformation and the actual total distortion is more difficult to account for. It would not be unreasonable to argue that in practice, the lower punch distortion will not deviate substantially from the predicted amount, especially when the magnitude of the total distortion is considered. Preliminary tests showed, however, that even small deviations had a large effect on the parameters obtained. It can, therefore, be concluded that only if the exact deformation characteristics of both top and bottom punch assemblies are known, can one compensate accurately for each of their contributions to distortion under load.

For this purpose, a series of compressions was performed using the following experimental systems:

a) the punch holders equipped with flat-faced upper and lower punches as usual (Fig. 2.6a).

b) the punch holders equipped with only the lower punch plus an extra punch, placed on top of the lower punch and used to supply the length necessary for loading the lower punch without the presence of the upper punch (Fig. 2.6b).

c) the punch holders equipped with upper and lower punches as well as the extra punch mentioned in b) above, placed between them (Fig. 2.6c).

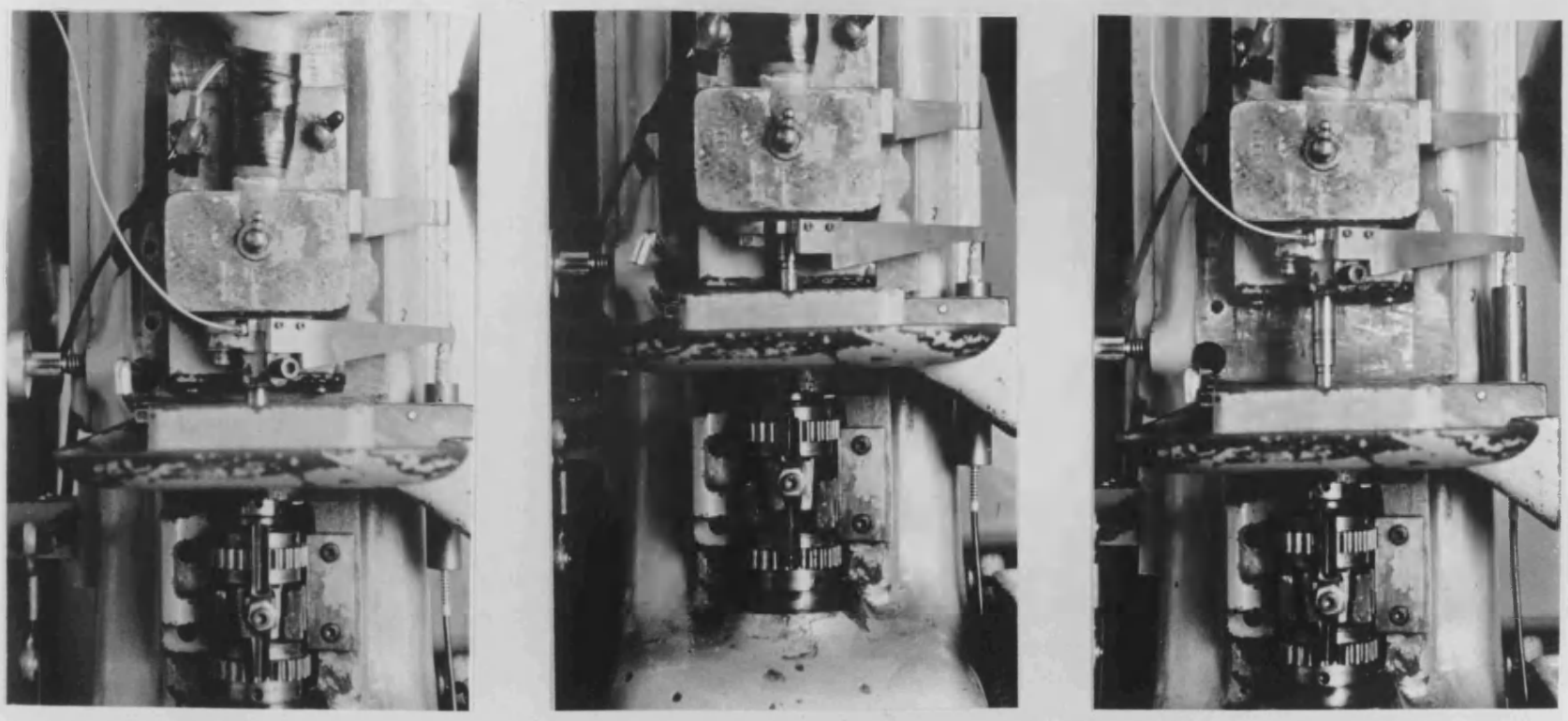

(a) (b) (c)

FIG. 2.6 Experimental systems used to determine the elastic distortion of the punch assemblies under load. For detail, see text.

Combination of the results obtained from each of the above settings allowed the calculation of the individual distortions due to the lower and upper punch assemblies (Fig. 2.7).

The experiment was performed in two ways. Firstly, by simply bringing the punch faces in contact and steadily increasing the applied force while recording the force-displacement values. Additionally, in order to simulate the compaction conditions, the same load was applied during a complete compression cycle. The results indicated no significant differences between the distortion characteristics of the system loaded in the two above-mentioned ways.

The relationship between force and punch distortion was non-linear, the data being described by a polynomial of the following form:

$$y = a + b \cdot x + c \cdot x^2 + d \cdot x^3 + e \cdot x^4 \qquad \text{Eq. 2.7}$$

where,

y = change in displacement with load

x = applied load

The equation parameters obtained during the above-mentioned experiments for the upper and lower punch assemblies respectively (Table 2.10), were built into the software which was used to manipulate the data. Thus, for each displacement value, a correction was made to account for the elastic deformation of each of the punch assemblies at that particular load. Therefore, changes in the dimensions of the compacts during compaction could be accurately calculated.

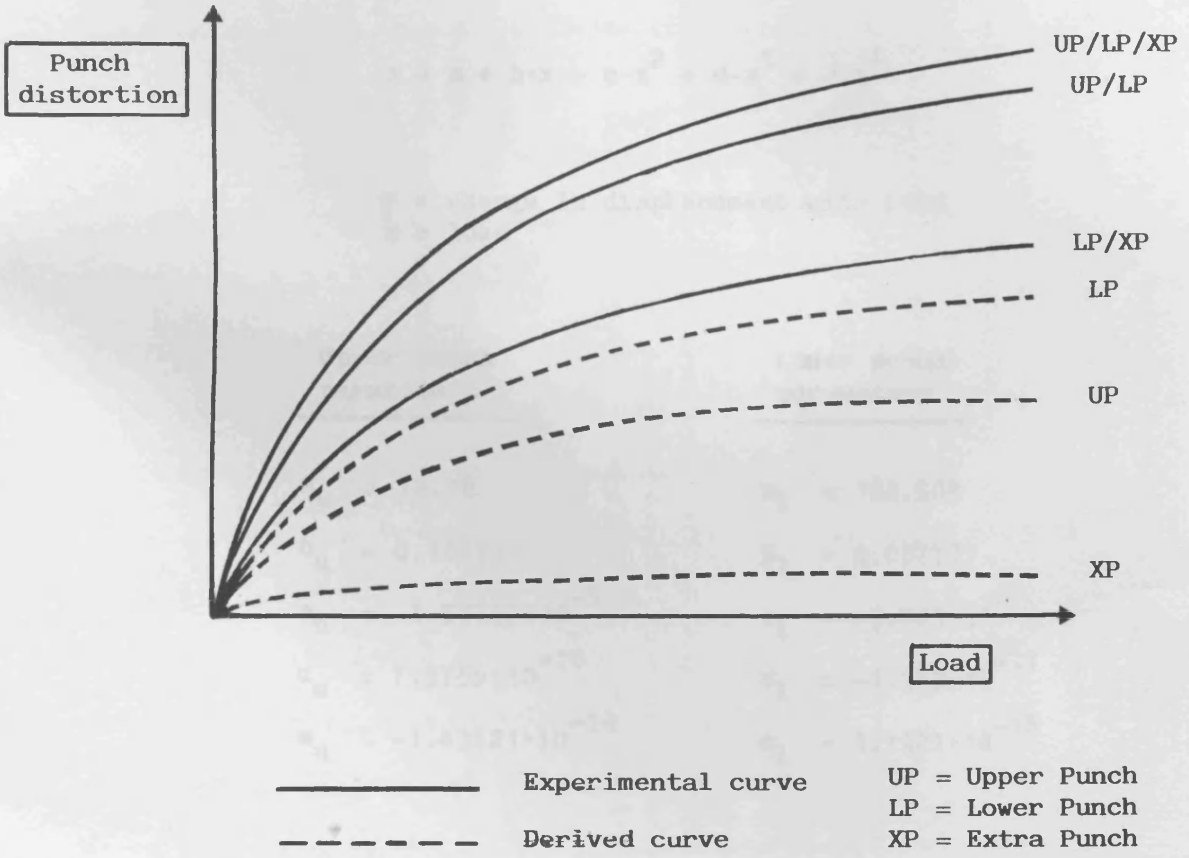

FIG. 2.7 Elastic distortion of the different systems used to calculate the individual distortions of the upper and lower punch assemblies during compaction.

TABLE 2.10 Correction applied for the elastic distortion of the punch assemblies of the tableting machine.

$$y = a + b \cdot x + c \cdot x^2 + d \cdot x^3 + e \cdot x^4$$

y = change in displacement with load
x = load

Upper punch parameters		Lower punch parameters	
a_u	= 12.78	a_l	= 182.509
b_u	= 0.184759	b_l	= 0.087771
c_u	$= -1.57797 \cdot 10^{-5}$	c_l	$= -3.003 \cdot 10^{-7}$
d_u	$= 7.5756 \cdot 10^{-10}$	d_l	$= -1.373 \cdot 10^{-11}$
e_u	$= -1.43621 \cdot 10^{-14}$	e_l	$= 1.1921 \cdot 10^{-15}$

In his study, Ho (1986) showed the importance of correct mounting of the LVDT for the accurate measurement of compact thickness. It should, however, be noted that he used a 25mm long stroke LVDT. The small sensitivity of that LVDT compared to the 10mm one used here could account for part of the inaccuracies he encountered. Furthermore, apart from the optimum LVDT positioning, it is also important to account correctly for the inaccuracies of the system, wherever they appear.

Software, developed in collaboration with Mrs. J.P. Hart, provided the following parameters for each tablet produced:

- peak upper punch force
- peak lower punch force
- upper punch displacement at peak force
- upper punch maximum displacement
- upper punch movement from peak force to peak displacement
- displacement at force removal
- tablet thickness at maximum load
- tablet thickness at maximum displacement
- tablet thickness at zero load
- work of compaction, done by the upper punch
- work of compaction, done on the lower punch
- expansion work, done during decompression
- "true" work of compaction, done by the upper punch
- "true" work of compaction, done on the lower punch
- total power of compaction, calculated from the work of

compaction and the contact time

- power during compression, calculated from the "true" work and the rise time
- power of expansion, calculated from the expansion work and the expansion time
- rate of expansion

Furthermore, force and displacement data were used to draw Heckel plots and calculate the relevant parameters. In addition to a typical Heckel plot, tablet dimensions and thus, ln[1/(1-D)] values were monitored not only up to peak force but also during force removal. The following values were recorded:

- tablet relative density at initial load application
- tablet relative density at maximum load
- tablet relative density at load removal
- linear regression of the rising force curve providing a correlation coefficient
- linear regression of the linear part of the rising force curve providing a slope and an intercept
- yield pressure
- slope of the linear part of the falling force curve
- intercept of the linear part on the ln[1/(1-D)] axis

The limits of linearity of the curves were assessed by calculating the second derivative of the plot and determining the points where it was zero.

Finally, the areas under the curves of such Heckel plots were calculated (Fig. 2.8) and presented as percentages of the

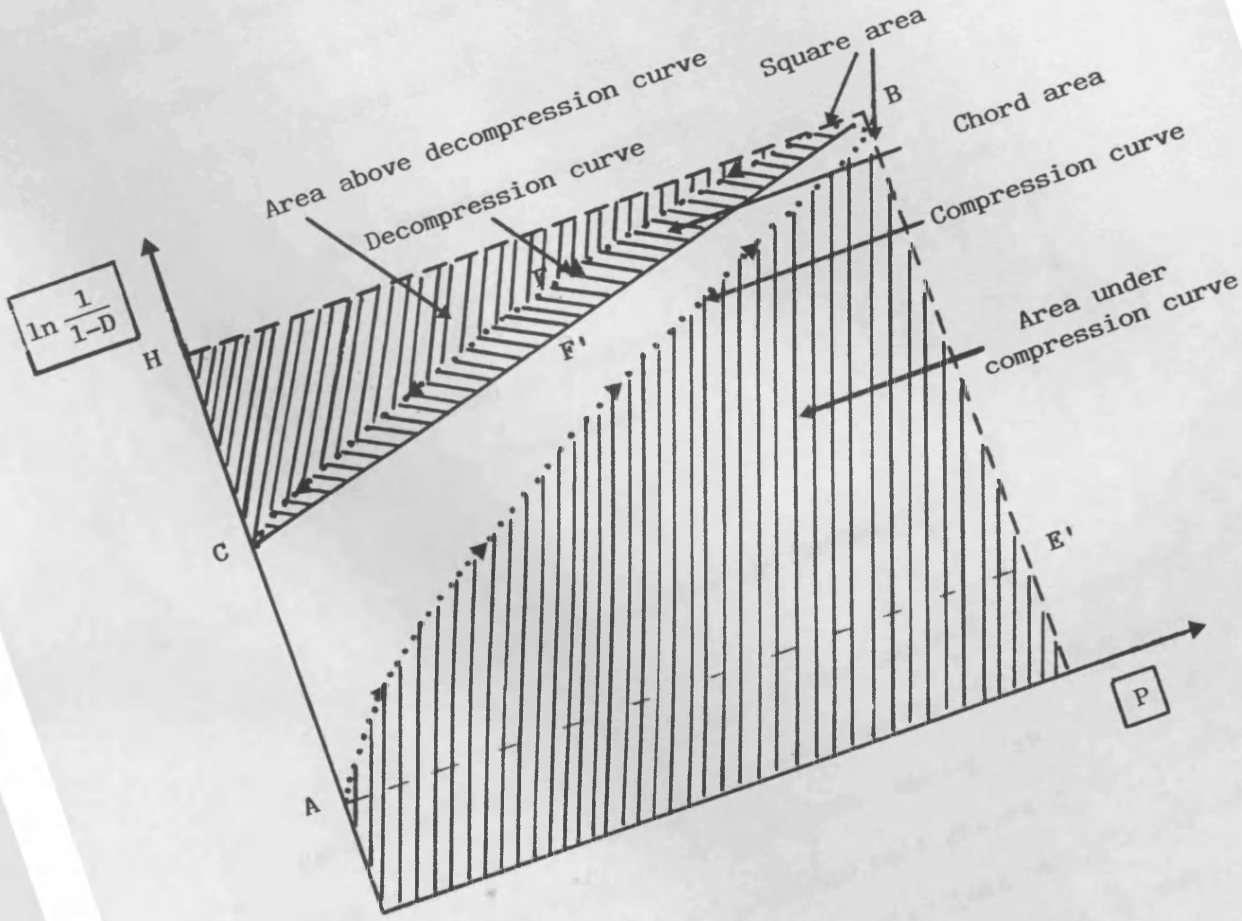

FIG. 2.8 Calculation of areas derived from extended Heckel plots.

square area AHBE':

- AHBE' area (square area)
- % ABE' area (area under the rising force curve)
- % CBH area (area above the falling force curve)
- % BFCF'B area (chord area)

2.2.2 Diametral Loading Test

A tensile tester (Type T22K, JJ Lloyd Instr., Ltd., Southampton, U.K.) was used in compression mode (Fig. 2.9) for the determination of the "toughness" of tablets as defined by Rees and Rue (1978c).

2.2.2.1 Data Acquisition and Manipulation

Before testing, the dimensions of the tablets were measured by means of the digital micrometer shown in Fig. 2.10. The force required to cause failure of a tablet during the diametral loading test was monitored by a load cell placed at the centre of the driven crosshead. The precalibrated load cells (JJ Instr. Ltd., Southampton, U.K.) were interchangeable and a number of them with different force ranges (100, 500 and 1000N) were used, depending on the strength of the tablets tested at the time. The crosshead speed was set at 2.2mm/min. Comparison with results previously generated under the same conditions was thus possible. Deformation of the tablets before failure was

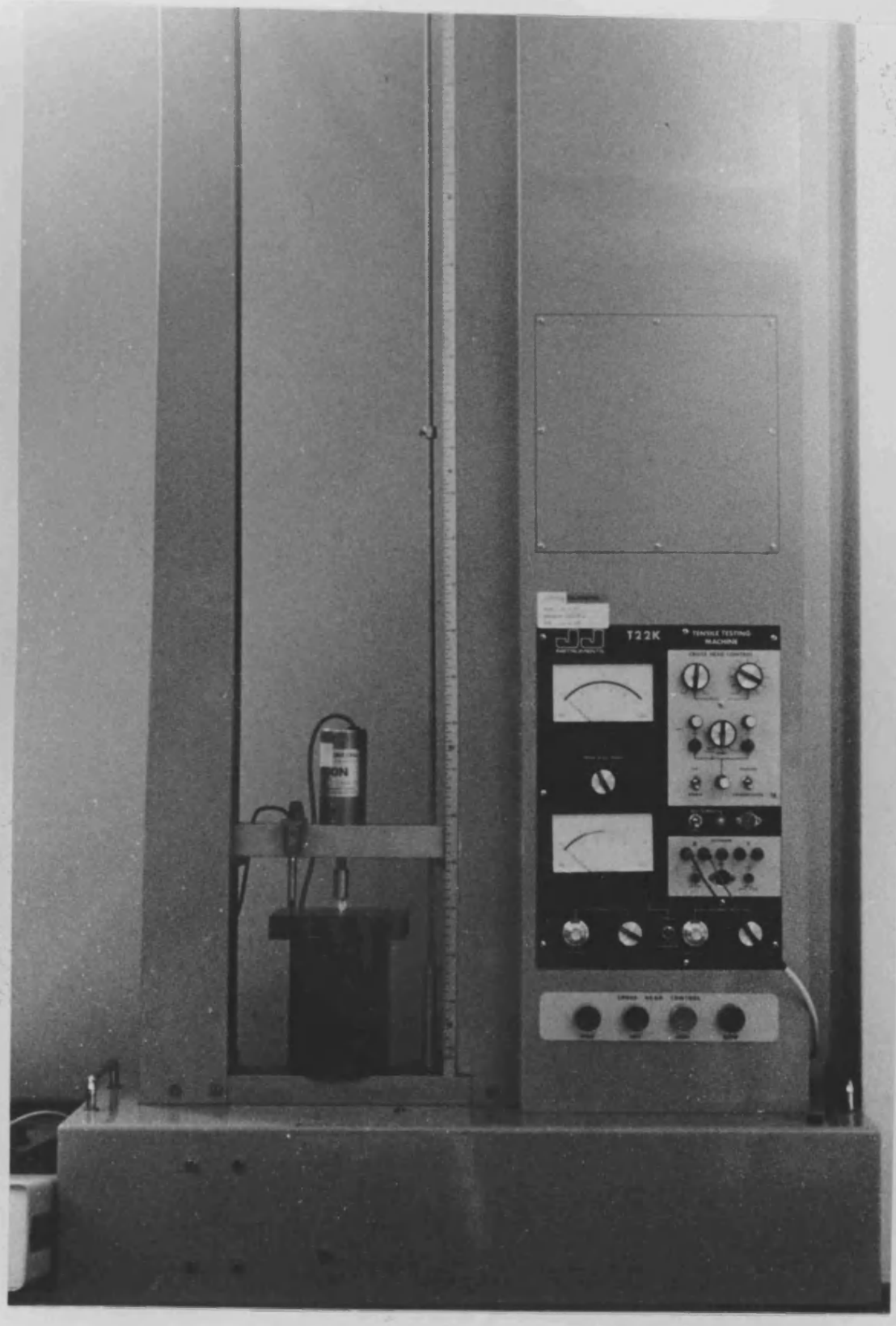

FIG. 2.9 Mechanical testing machine used to assess the mechanical properties of tablets.

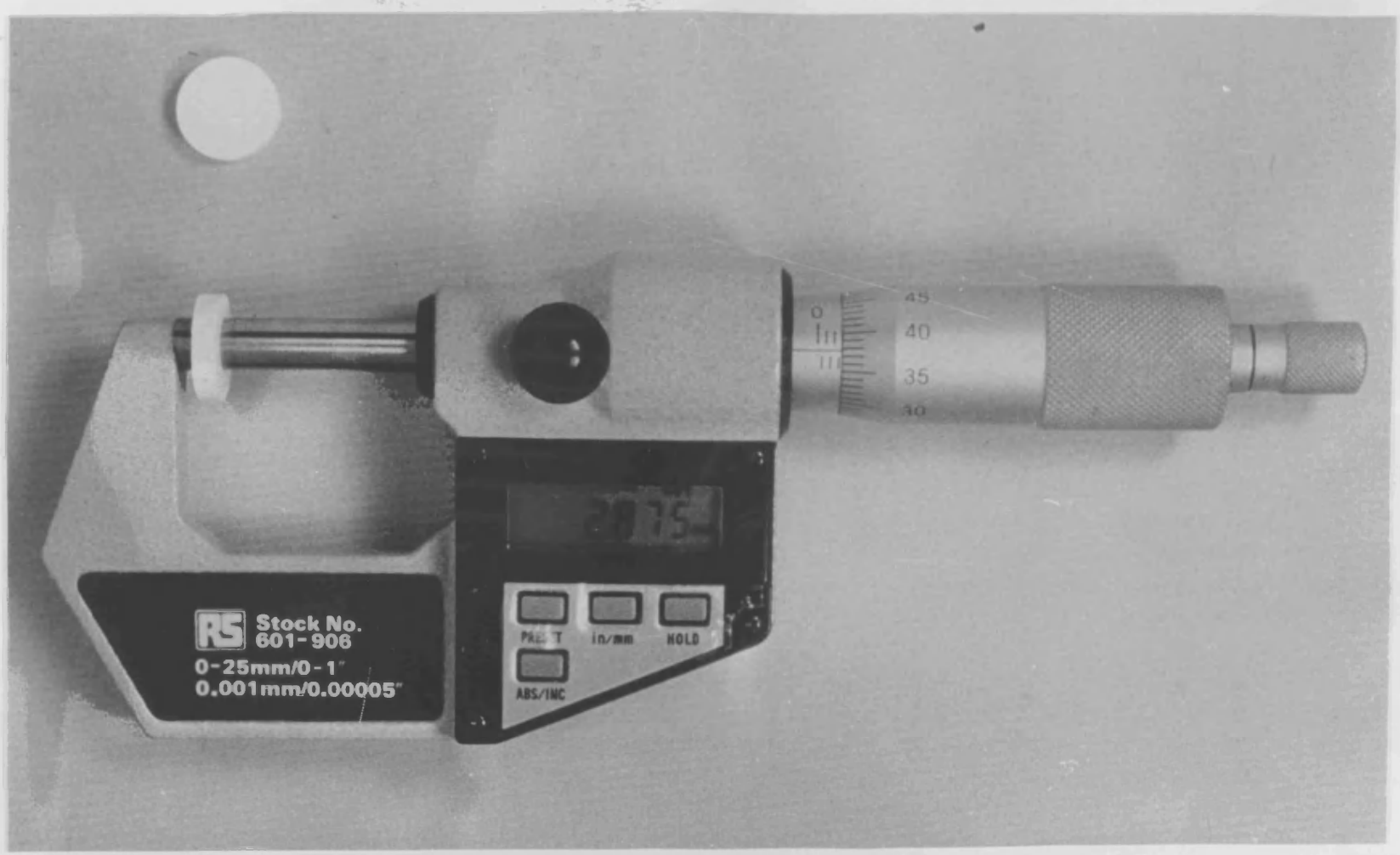

FIG. 2.10 Digital micrometer used to measure tablet dimensions.

monitored by a 5mm LVDT (Type AG/5, Sangamo Instr. Ltd., Bognor Regis, U.K.) attached to the moving crosshead (Fig. 2.11). An amplifier card (Type CA2 series. Sangamo Instr. Ltd., Bognor Regis, U.K.), powered by a 15 Volt power supply, was used to condition the signal from the LVDT. Calibration of the LVDT (Fig. 2.12) was carried out on the tensile tester using a set of feeler gauges. The results are shown in Table 2.11.

The analogue signals from force and displacement outputs (Fig. 2.13) were fed via an analogue-digital converter connected to the 1MHz Bus of the microcomputer mentioned in 2.2.1.1. The digital values, 500 for each output, were stored in the memory of the microcomputer and processed as required. Ten replicates were tested for each material.

Using the appropriate calculations, the following values were obtained for each tablet tested:

- peak force
- deformation undergone by the tablet before failure
- time required for the tablet to break
- work of failure
- corrected work of failure
- power of failure
- radial tensile strength
- apparent failure viscosity
- area-ratio

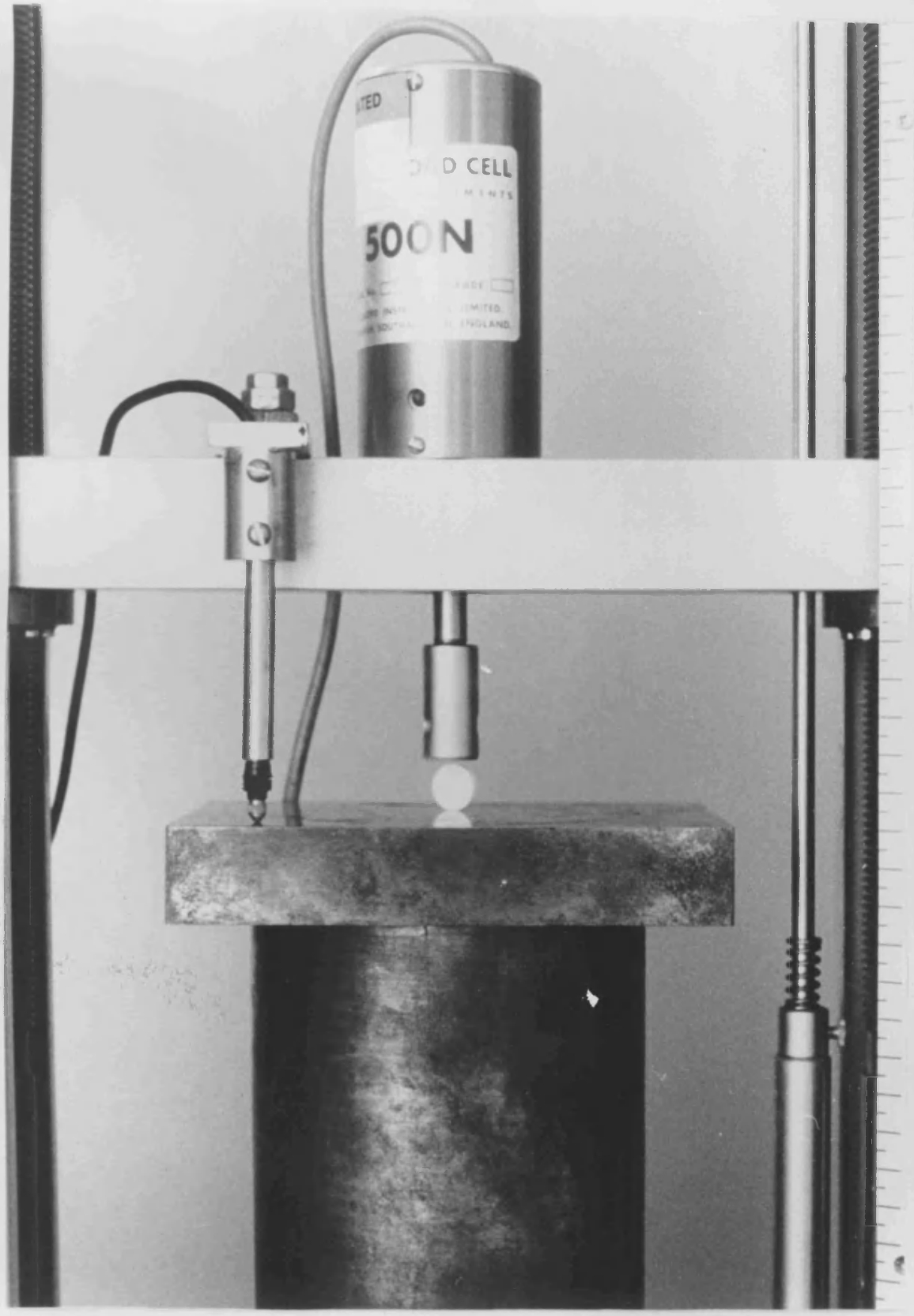

FIG. 2.11 Experimental system used for diametral loading of tablets, showing the position of the LVDT on the moving crosshead of the mechanical testing machine.

TABLE 2.11 Calibration data for 5mm LVDT (Type AG/5, Sangamo Instr. Ltd.).

Thickness (mm)	Displacement (digital values)
0.056	2592
0.079	3520
0.120	4224
0.160	5872
0.257	9152
0.310	10752
0.384	12992
0.634	20864
1.102	35698

Slope = 31661.456

Intercept = 828.018

Corr. coefficient = 0.9999

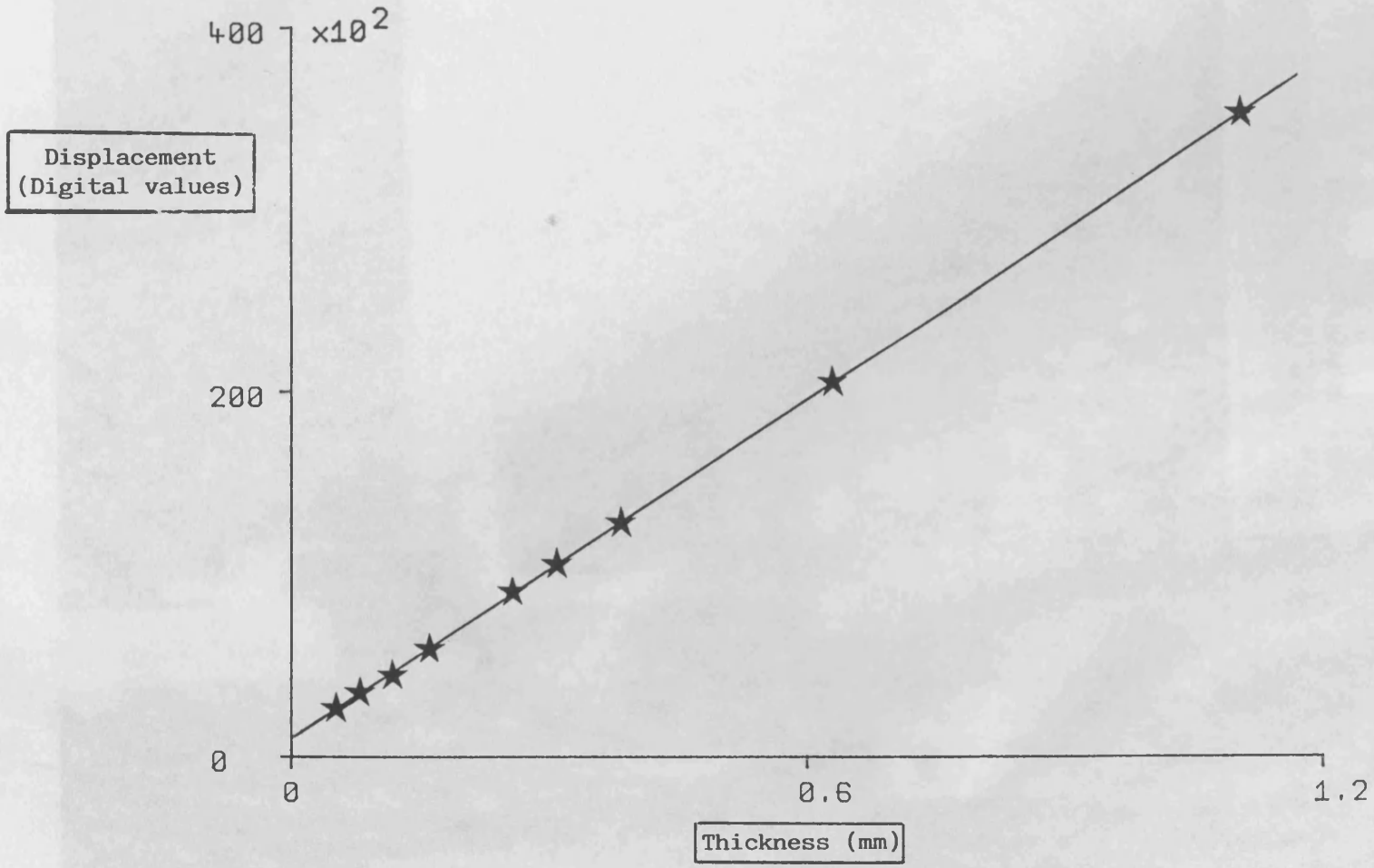

FIG. 2.12 Calibration curve for 5mm LVDT (AG/5, Sangamo Instr. Ltd.).

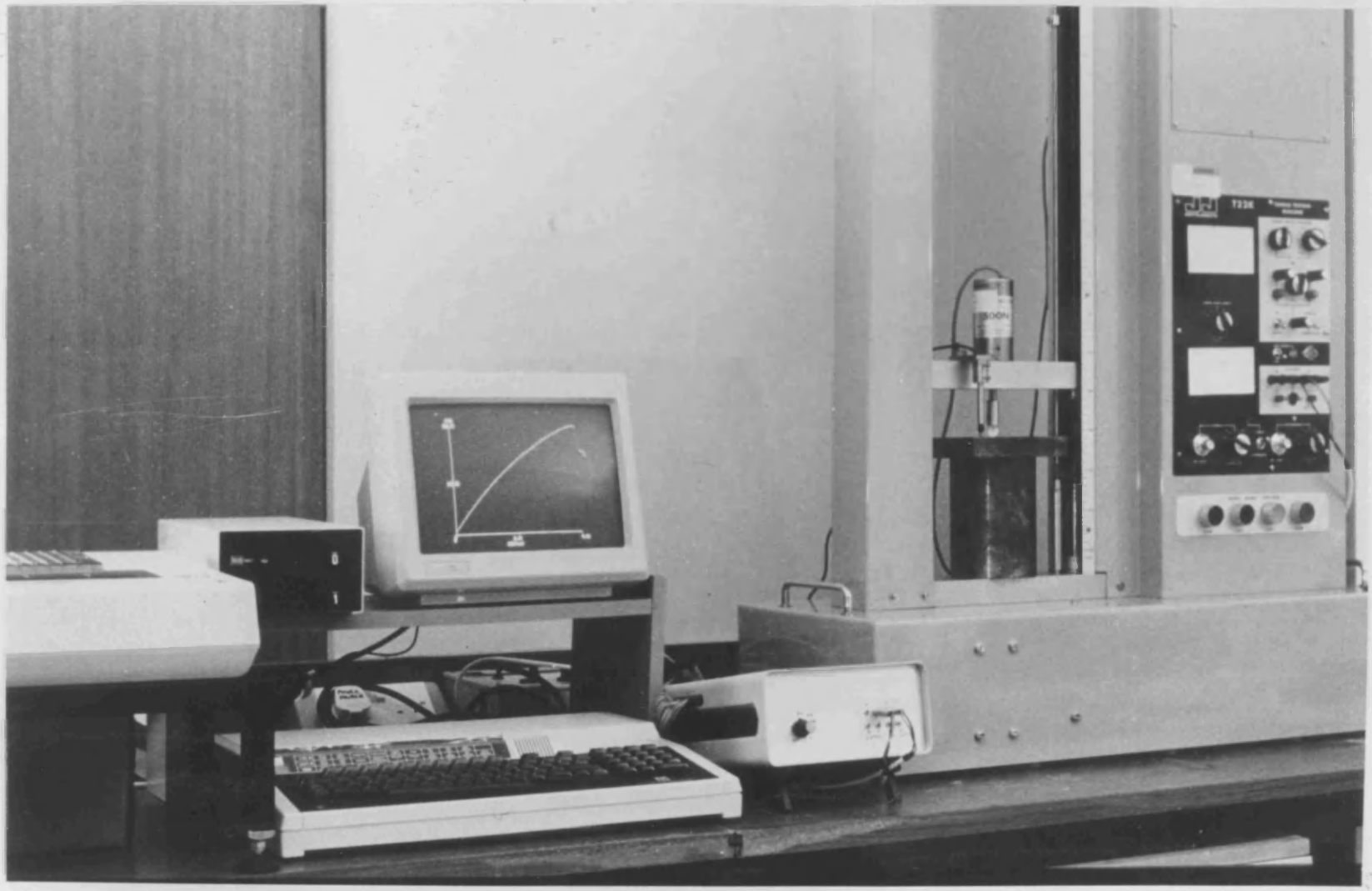

FIG. 2.13 Mechanical testing machine with associated data acquisition and processing system.

2.2.3 Direct Tension Test

The tensile tester (Type T22K, JJ Lloyd Instr. Ltd., Southampton, U.K.) mentioned in section 2.2.2, was used in tension mode for the direct tension testing of materials. A pair of holders was connected to the moving crosshead and the fixed base of the tester (Fig. 2.14). Cyanoacrylate adhesive (RS Components, Corby, Northants., U.K.) was used to attach the tablets between the two holders. The ball and socket structure of the upper holder enabled the alignment of the system without the introduction of shear stresses into the tablets tested (Fig. 2.15). The use of metal discs screwed on to the lower holder (Fig. 2.15) allowed the failed tablets to be examined using scanning electron microscopy (S.E.M.).

2.2.3.1 Data Acquisition and Manipulation

The data acquisition and manipulation during direct tension experiments were the same as in 2.2.2.1. However, in this case, axial tensile strength was calculated as mentioned in section 1.2.3.3. Other associated results were also determined.

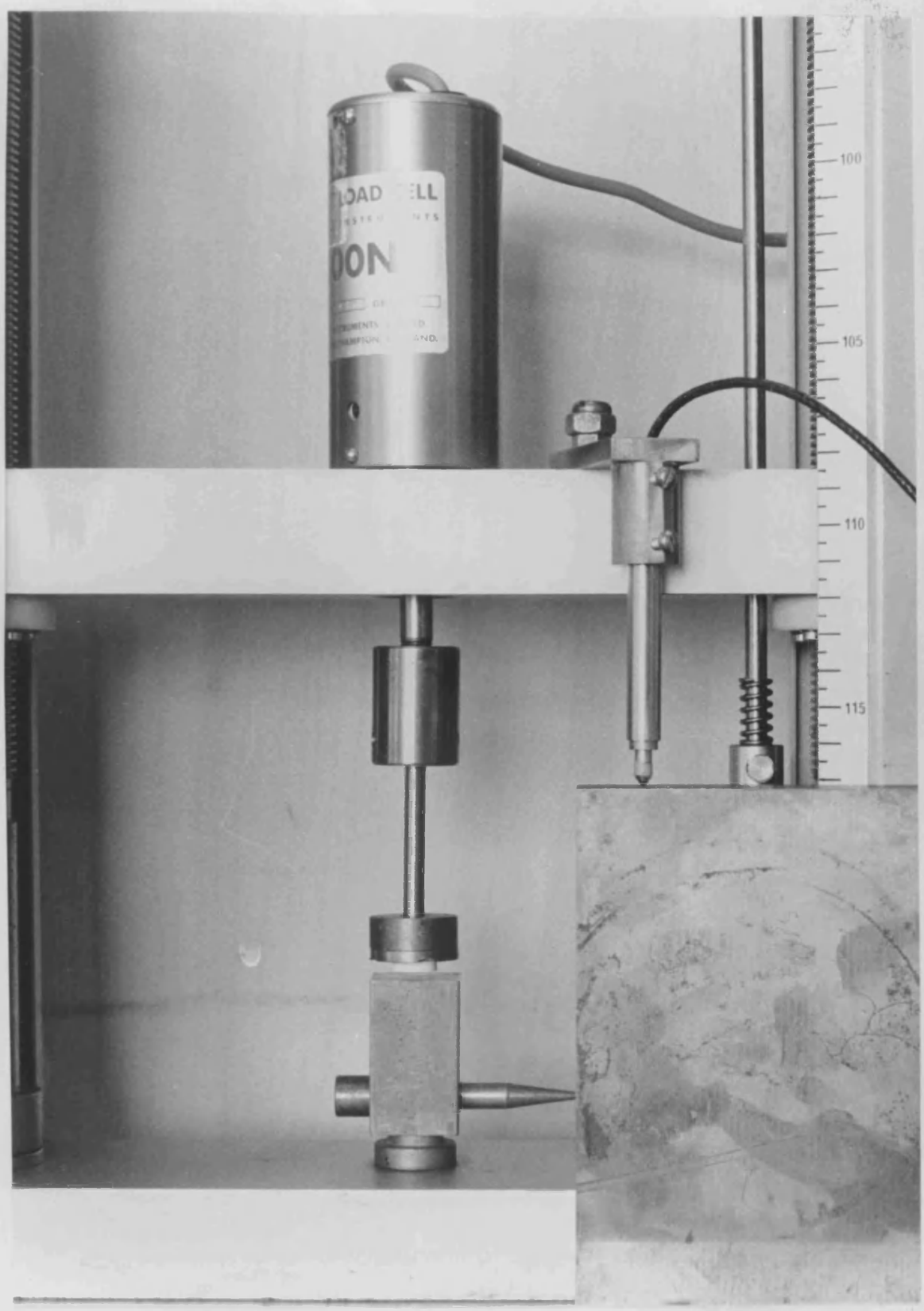

FIG. 2.14 Experimental system used for direct tension testing of tablets.

FIG. 2.15 Ball and socket assembly used during direct tension testing of tablets to ensure axial alignment.

2.2.4 Stress Relaxation

The tensile tester (Type T22K, JJ Lloyd Instr. Ltd., Southampton, U.K.) mentioned in section 2.2.2 was also used for the stress relaxation experiments (Fig. 2.16). Fitted to it, a compression cage allowed the application of compressional loads up to 20kN while the machine was operated in tensile mode. Interfaced to the drive mechanism of the rig, a constant stress module (Type T510 JJ Lloyd Instr. Ltd., Southampton, U.K.) allowed the load to be increased up to the required level. The drive mechanism of the rig was then stopped and thus the distance between the punches was maintained constant. The force decay was thereafter monitored for five minutes. A 12.7mm punch and die set were used (Fig. 2.17).

2.2.4.1 Data Acquisition and Manipulation

A precalibrated 20kN load cell (Grade B, JJ Lloyd Instr. Ltd., Southampton, U.K.) was used to monitor drop in force during the test. 500 values were obtained from each run, while six replicates were used for the calculation of the mean values. Finally, when the compression cage was loaded and held under the same constant strain conditions, no significant drop in force was observed.

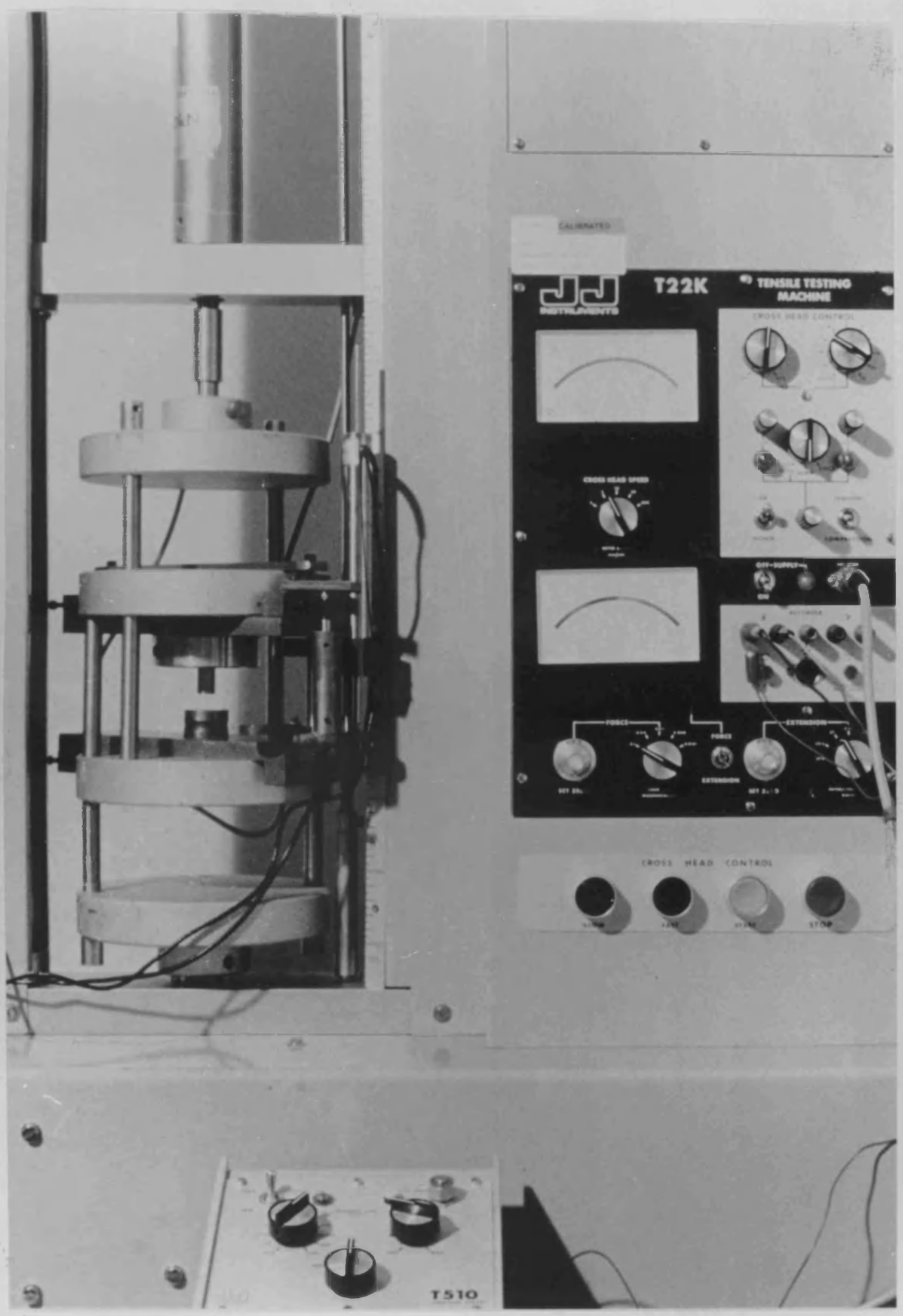

FIG. 2.16 Mechanical testing machine equipped with a compression cage and constant stress module.

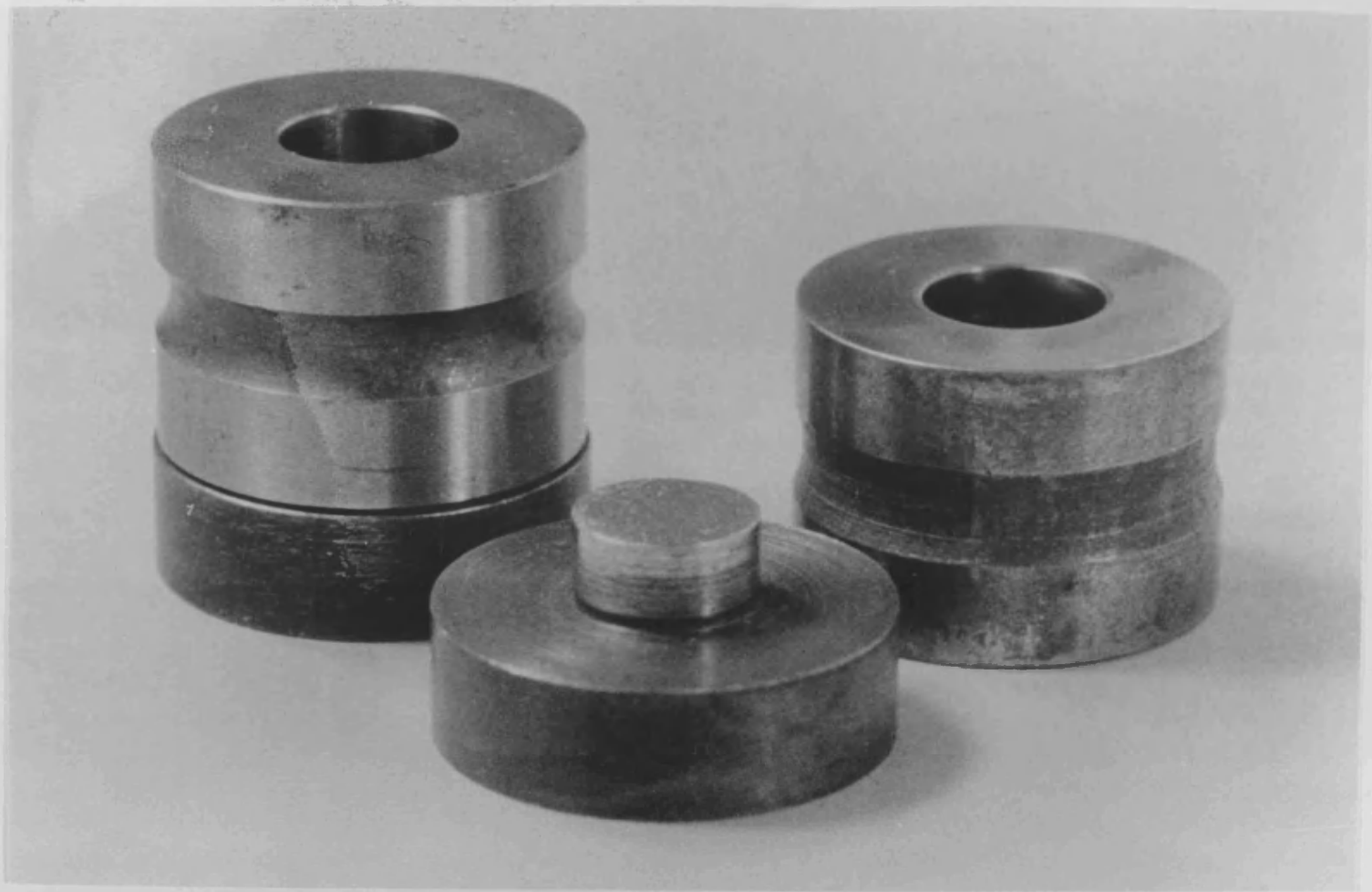

FIG. 2.17 Lower punch and die used with the compression cage.

2.2.5 Creep Test

The tensile tester (Type T22K, JJ Lloyd Instr. Ltd., Southampton, U.K.) equipped as mentioned in section 2.2.4 (Fig. 2.16), was also used for creep experiments. The constant stress module was employed to maintain the stress at the required constant value.

2.2.5.1 Data Acquisition and Manipulation

The 20kN load cell mentioned in 2.2.4.1 was used to monitor load during testing. Two LVDTs were attached to the cage (Fig. 2.18) so that any movement of the lower punch was monitored throughout the test. A 5mm LVDT (Type D5/500A, RDP Electronics Ltd., Wolverhampton, U.K.) was used to monitor coarse movement and calculate the thickness of the specimen at the beginning of the creep test (t=0). Calibration results (Fig. 2.19) are given in Table 2.12. A 5mm LVDT (Type AG/5, Sangamo Instr. Ltd., Bognor Regis, U.K.) was used to monitor the fine movement of the lower punch during the creep test. During one run, 257 digital values were obtained from each output, while ten replicates were used to calculate the mean values. Finally, preliminary tests showed that at the loads used in this study, the compression cage itself exhibited minimal creep behaviour.

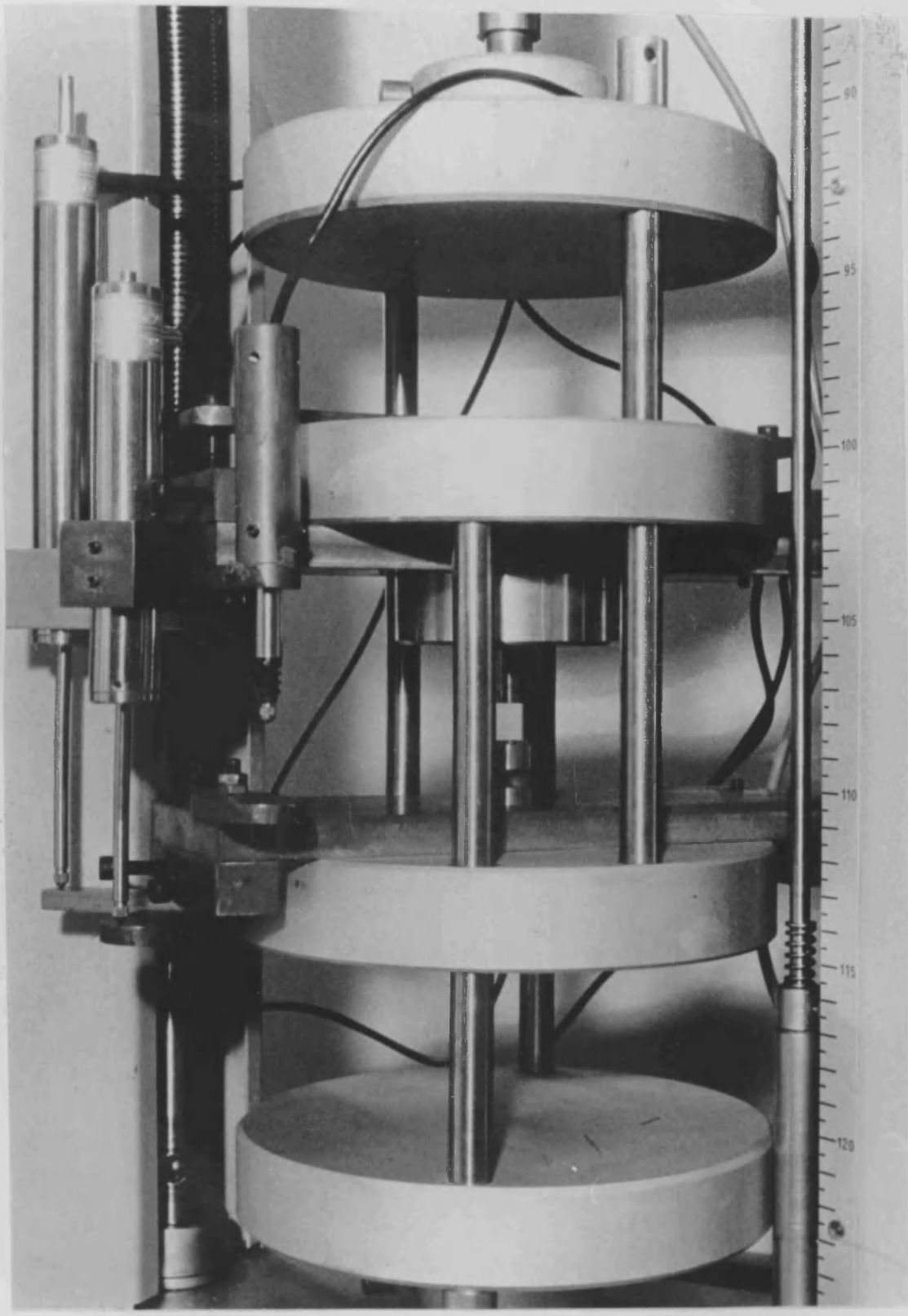

FIG. 2.18 The compression cage showing the position of the LVDTs during creep testing.

TABLE 2.12 Calibration data for 5mm LVDT (Type D5/500A, RDP Electr. Ltd.).

Thickness (mm)	Displacement (digital values)
0.160	2656
0.257	4080
0.310	4896
0.384	5888
0.639	9456
1.102	16032
2.480	35328
3.209	45536
3.431	48672
4.535	64160

Slope = 14042.128

Intercept = 491.059

Corr. coefficient = 0.9999

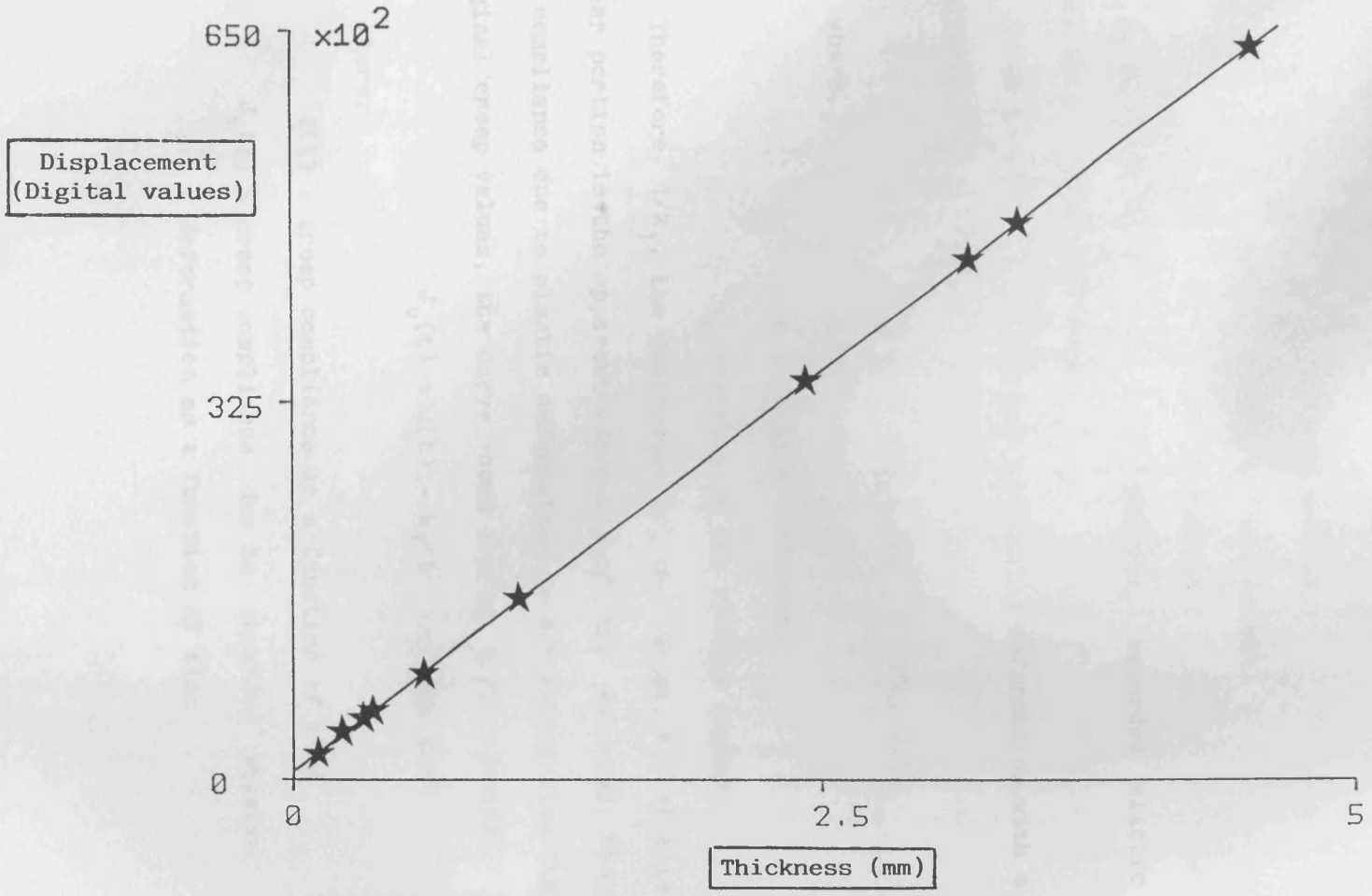

FIG. 2.19 Calibration curve for 5mm LVDT (D5/500A, RDP Electr. Ltd.).

As mentioned in section 1.3.2.2, a typical creep curve (Fig. 1.15) can be subdivided into three regions:

1. AB is the region of instantaneous compliance J_o:

$$J_o = 1/G = \gamma_o(t)/\sigma \qquad \text{Eq. 2.12}$$

where,

G = elastic modulus

γ_o = instantaneous strain

σ = constant stress

2. BC is the region of time-dependent, retarded elastic strain with a total compliance J_r.

3. CD is the linear region of plastic deformation with a compliance, J_n:

$$J_n = t/\eta = \gamma_n(t)/\sigma \qquad \text{Eq. 2.13}$$

where,

η = apparent viscosity

γ_n = strain in the viscous region

Therefore, $1/k_1$, the reciprocal of the slope, k_1, of this linear portion is the apparent viscosity of the material. When the compliance due to plastic deformation is subtracted from the original creep values, the curve shown in Fig. 2.20b results:

$$J_v(t) = J(t) - k_1 \cdot t \qquad \text{Eq. 2.14}$$

where,

J(t) = creep compliance as a function of time

$J_v(t)$ = creep compliance due to retarded elastic deformation as a function of time

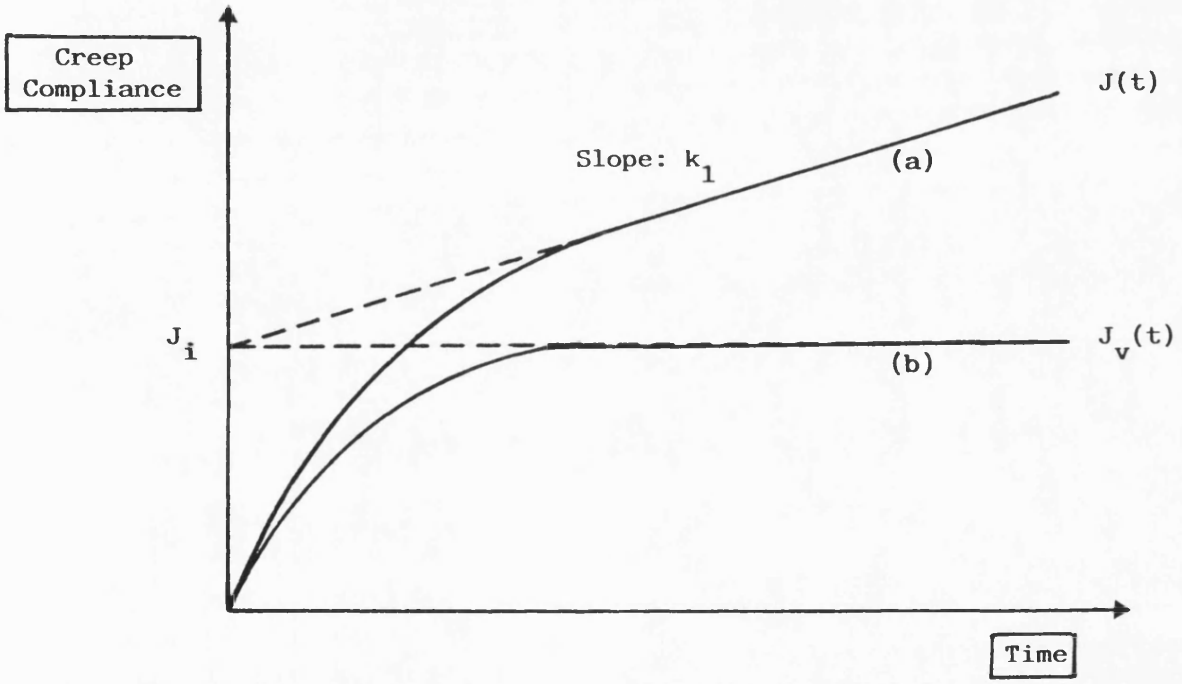

FIG. 2.20 Original creep curve (a) and the derived curve (b) describing compliance due to retarded elastic deformation as a function of time.

This new curve represents the compliance due to retarded elastic deformation of the material under constant stress and can be described by Eq. 2.15:

$$J_v(t) = J_i \cdot e^{-k_2/t} \qquad \text{Eq. 2.15}$$

J_i is the equilibrium value of compliance at infinite time as a result of retarded elastic deformation and, k_2 quantifies the retardation of the elastic strain in the viscoelastic region. A high k_2 value reflects a high degree of retardation, i.e. a low rate of retarded elastic deformation and is, therefore, indicative of a material with marked time-dependent characteristics. When the apparent viscosity and the k_2 value of a material are considered, its ability to undergo plastic deformation and relieve elastic strain can be fully assessed.

It must be emphasised that, the elastic compliance J_o was not measured directly, since instantaneous loading of the material in the die could not be achieved. This parameter was derived from a linear regression of the initial section of the creep curve over 5 seconds, and extrapolated back to zero time. As an estimated value, it will be expressed as J_o^* in the rest of this work. Therefore, although in principle in order to derive $J_v(t)$, the estimated value of J_o^* should be subtracted from the total creep compliance J(t) in Eq. 2.14, this was not done for the above-mentioned reason.

A statistical package (GLIM 3.77, Copyright Royal Statistical Society, London) was used in order to obtain the viscoelastic parameters discussed above.

CHAPTER THREE

BEHAVIOUR OF MATERIALS DURING COMPACTION

3.1 WORK DURING COMPACTION

One way to assess bond formation within a powder bed under load and, thereby to forsee the strength of the resulting compact, is to measure the energy involved in the compaction process. The energy responsible for bond formation during compaction can be expressed as the work done by the upper and/or on the lower punch, calculated as mentioned above in 1.2.2.1.

In order to assess the elastic deformation of the material during compression which can lead to bond rupture during decompression, the work performed during the elastic recovery of the compact may be measured. In this study, only part of this work was determined, since the measurement involved only the elastic recovery of the compact during decompression in the die after one single compression (De Blaey and Polderman, 1970).

Therefore, the true work of compaction could not be calculated from the difference between the expansion work and the total work done by either of the punches. Instead, values for the total work performed by the upper and on the lower punch were obtained, as well as the work due to the elastic expansion of the compact in the die during the normal short decompression time. This latter value was used for comparative purposes, as an indication of the elastic properties of each material. The work resulting from the subtraction of the expansion work from the work performed on the lower punch was also determined as the most useful means of evaluating energy utilisation in compaction and will be called "true" work of compaction for the rest of this study. As explained above, this will include a small error in that it ignores the work associated with further elastic recovery of a compact following decompression. The results obtained are shown in Tables A.1 and A.2.

In order to study the compaction behaviour of a model elastic material, a rubber plug of 12.7mm diameter and 7mm thickness was compressed under the same conditions. (Table A.3).

At all compaction forces, the highest values for upper punch displacement were obtained for the two microcrystalline celluloses. Therefore, the exceptionally high values for total work and "true" work (Fig. 3.1) done on the lower punch, were not unexpected. Similarly, Starch 1500 showed an increase in these values with compaction force. Although the other materials also deformed more as the pressure was increased, their values

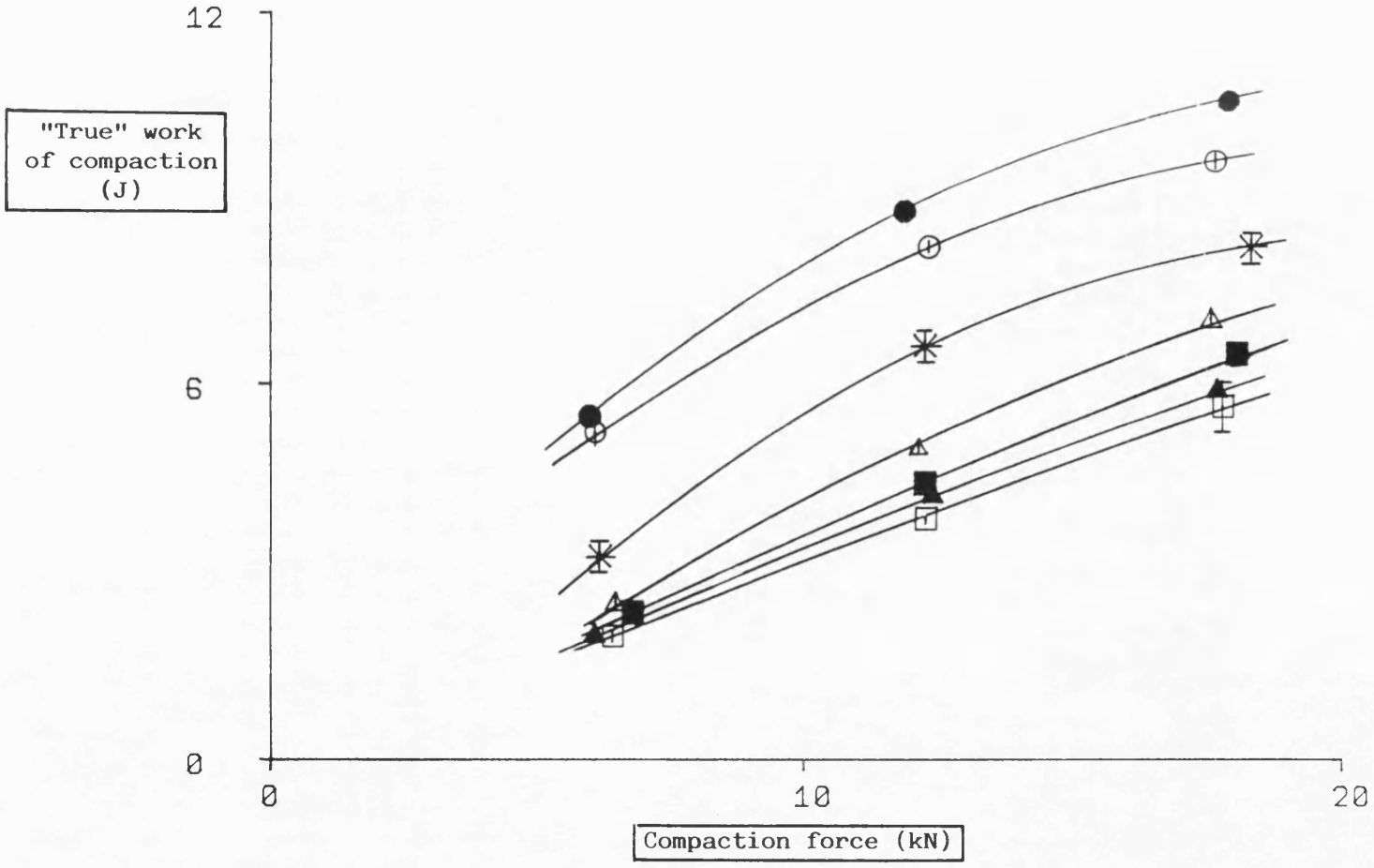

FIG. 3.1 "True" work done on the lower punch during compaction, at a range of compaction forces.

(Key: page xxiii)

were generally much lower. The order was as follows:

sodium chloride > anhydrous lactose > sodium bicarbonate > Emcompress

Power values, calculated from the "true" work of compaction and rise time (Fig. 3.2), minimised the above-mentioned differences. This is not surprising, since high work values were divided by high time values.

Expansion work values, calculated as explained in section 1.2.2.1, are given in Tables A.4 and A.5. It can be seen, that there is an increase in these values with compaction force for all materials (Fig. 3.3). Although values for Starch 1500 were generally the highest, they did not seem to demonstrate sufficiently its much higher degree of elasticity (David and Augsburger, 1977; Rees and Rue, 1978a; Paronen and Juslin, 1983). One possible explanation could be that the measurement involved only a portion of the total elastic recovery, due to the time-dependent nature of the material's anelastic recovery (Rees and Rue, 1978a). This effect, although present in most materials, is more pronounced in materials such as starches and microcrystalline celluloses. It must be noted, that Emcocel 90M and, in particular, Avicel PH102 showed interestingly high expansion work values at low load. This is in agreement with previous results for Avicel PH102 (Aulton et al, 1974). Sodium bicarbonate, Emcompress and anhydrous lactose followed, while sodium chloride showed the lowest values, suggesting a minimal amount of elastic deformation during compression.

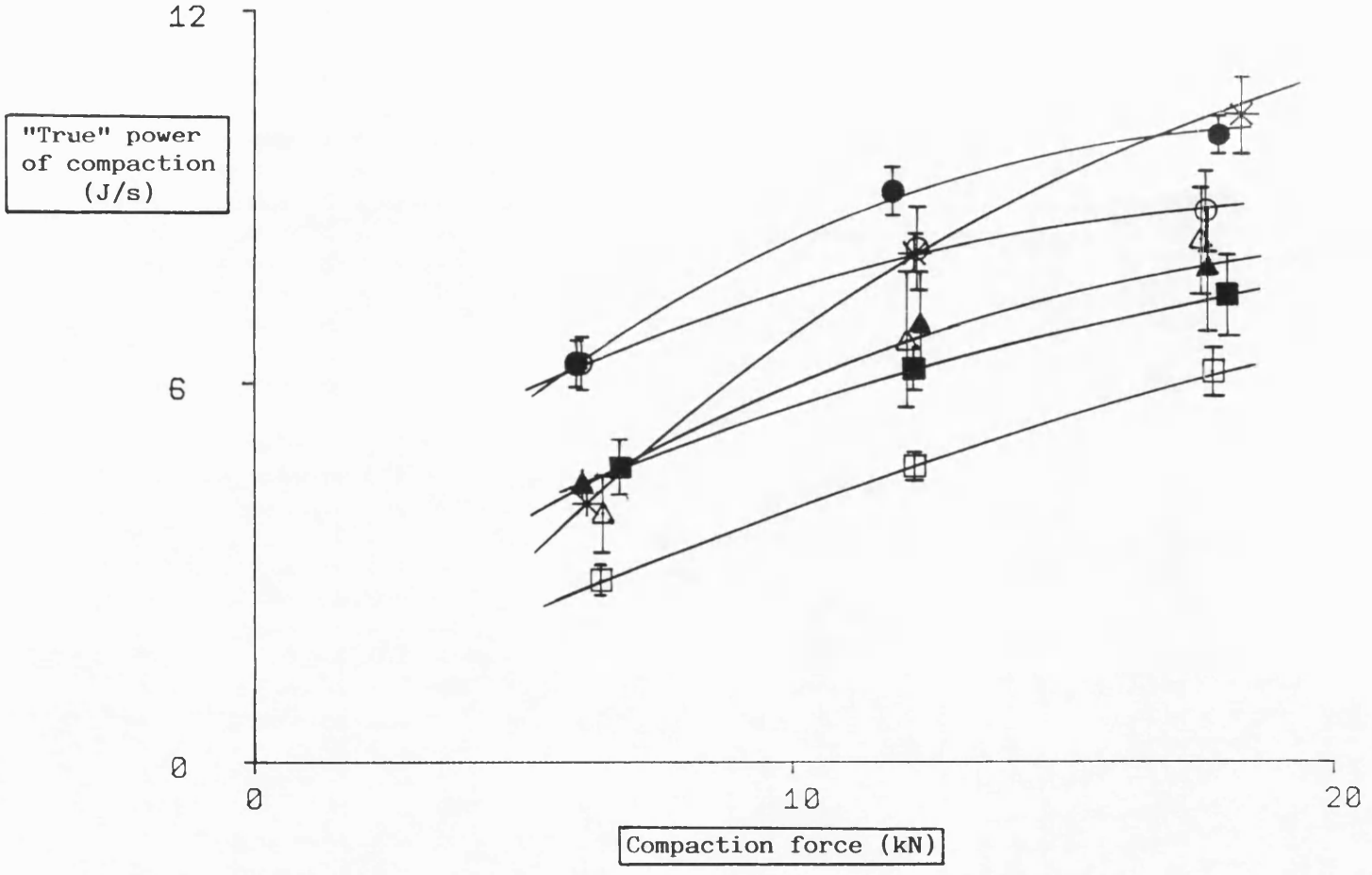

FIG. 3.2 "True" power of compaction, at a range of compaction forces.

(Key: page xxiii)

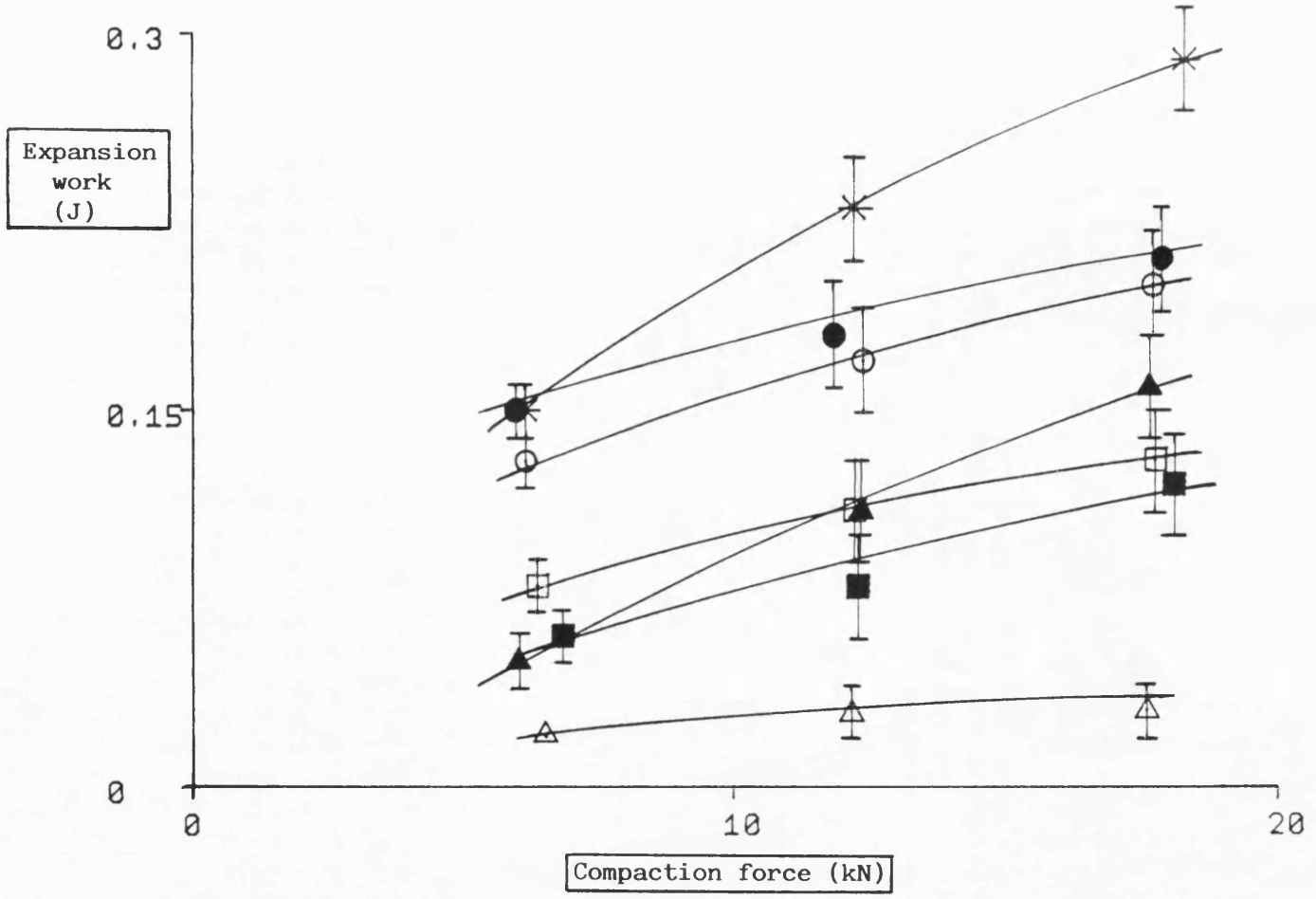

FIG. 3.3 Expansion work undergone by materials during decompression, at a range of compaction forces.

(Key: page xxiii)

An alternative way to study how efficiently energy is utilised during compaction, is to express "true" work of compaction as a percentage of the total work. Fig. 3.4 ranks the materials according to their ability to use work done during compaction to undergo non-recoverable deformation, leading to the creation of permanent bonds. This parameter is, therefore, suggested as a better means of assessing energy utilisation during compaction than "true" work or expansion work alone.

Fig. 3.5 shows how the rate of expansion decreased with compaction force for all materials. This is possibly due to the smaller in-die recovery they exhibited as force increased and the increasing number of bonds inhibited compact expansion. However, an increase in expansion time with force (Tables A.4 and A.5) contributed to this effect, too. Starch 1500 and the two microcrystalline celluloses were shown to have the highest expansion rate values throughout the whole range. The rest of the materials stood as follows:

sodium bicarbonate > anhydrous lactose > Emcompress > sodium chloride

On the other hand, power of expansion (Fig. 3.6) did not seem to offer any further information about the materials, as far as their elastic properties are concerned.

It has been reported (Ho, 1986) that rise time, i.e. the time interval between the initial force application and the point at which the peak force is reached, is in agreement with the ability of materials to form compacts. Contact time and rise

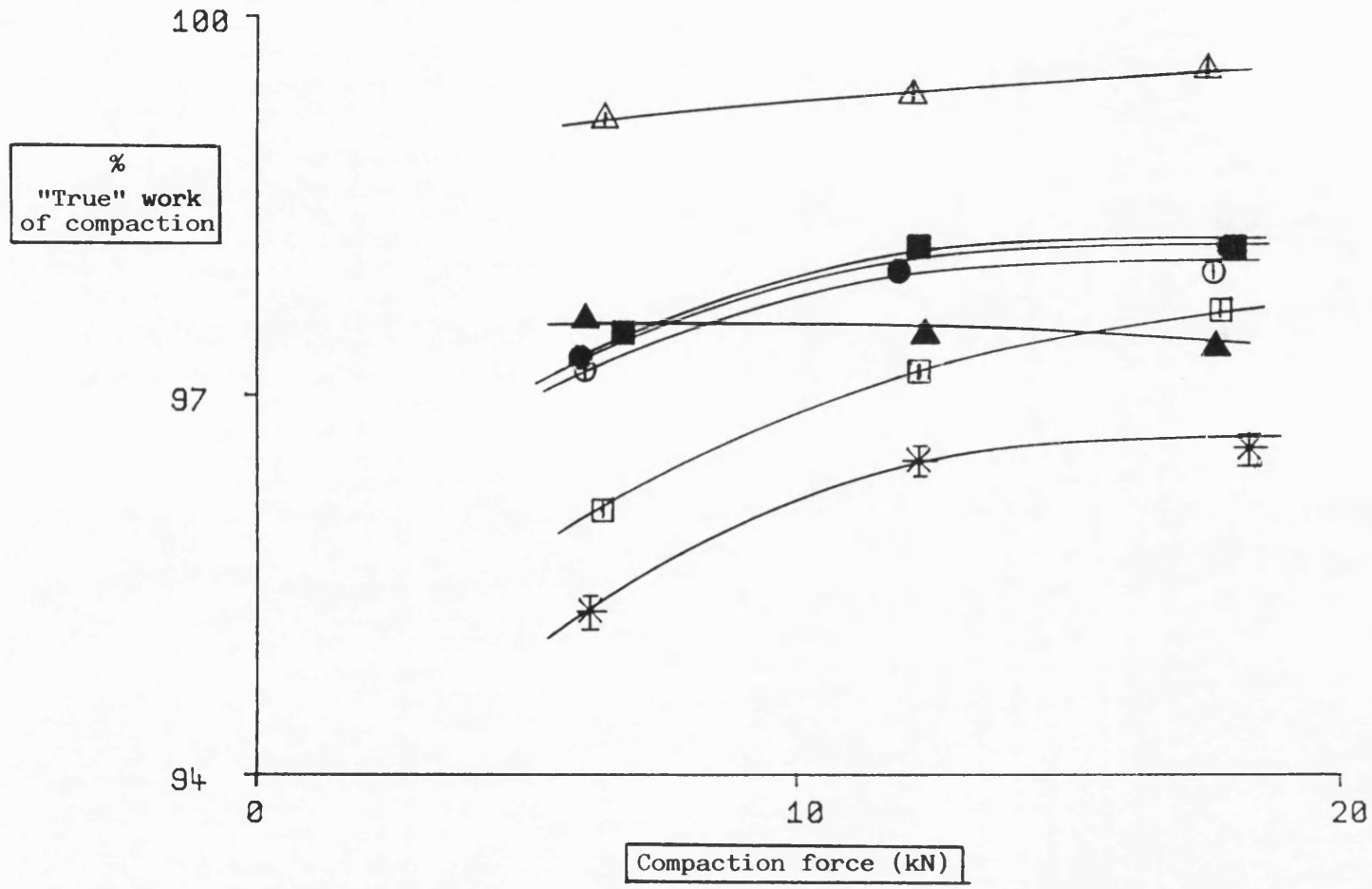

FIG. 3.4 "True" work of compaction as a percentage of the total work of compaction, at a range of compaction forces.

(Key: page xxiii)

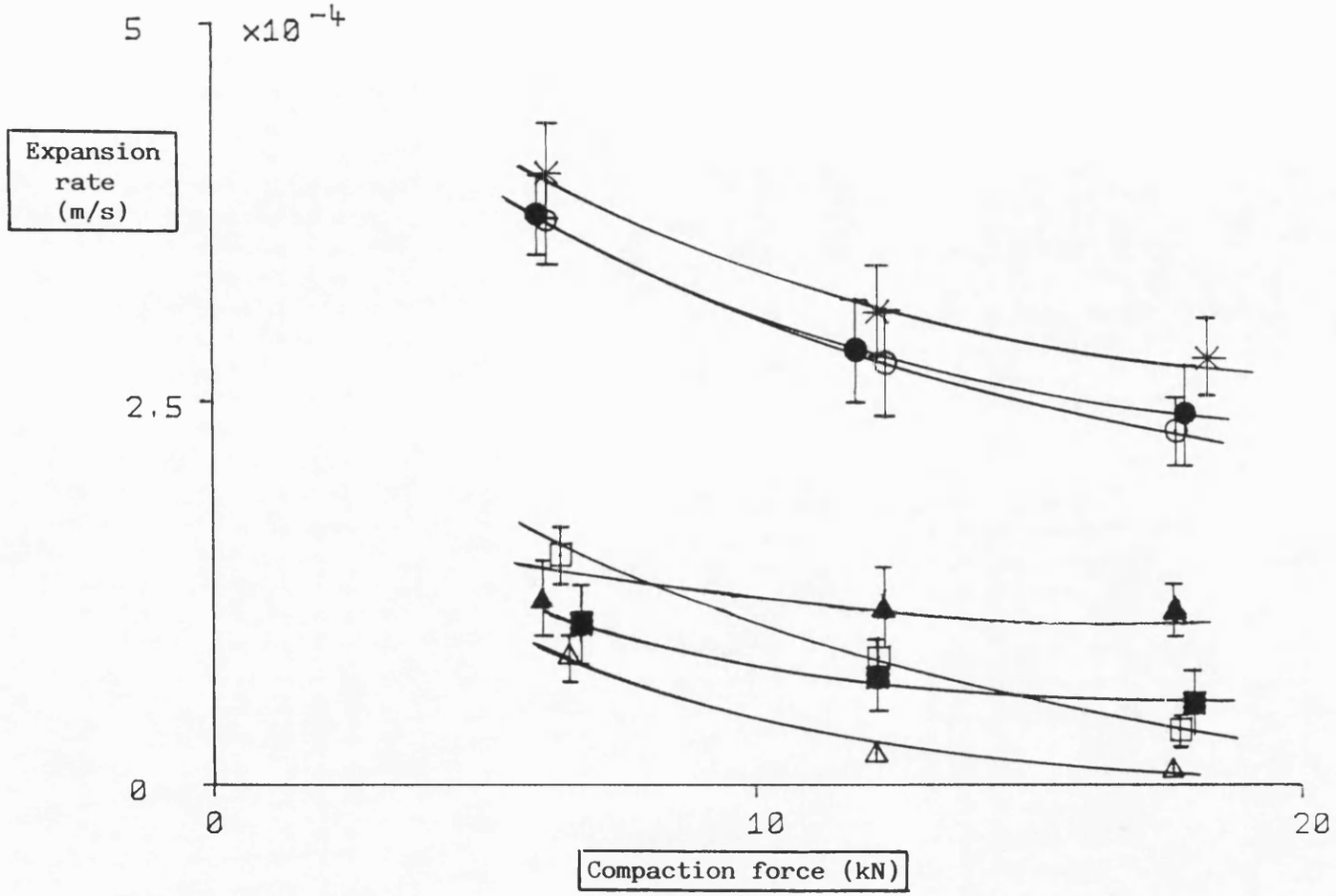

FIG. 3.5 Expansion rate of materials during decompression, at a range of compaction forces.

(Key: page xxiii)

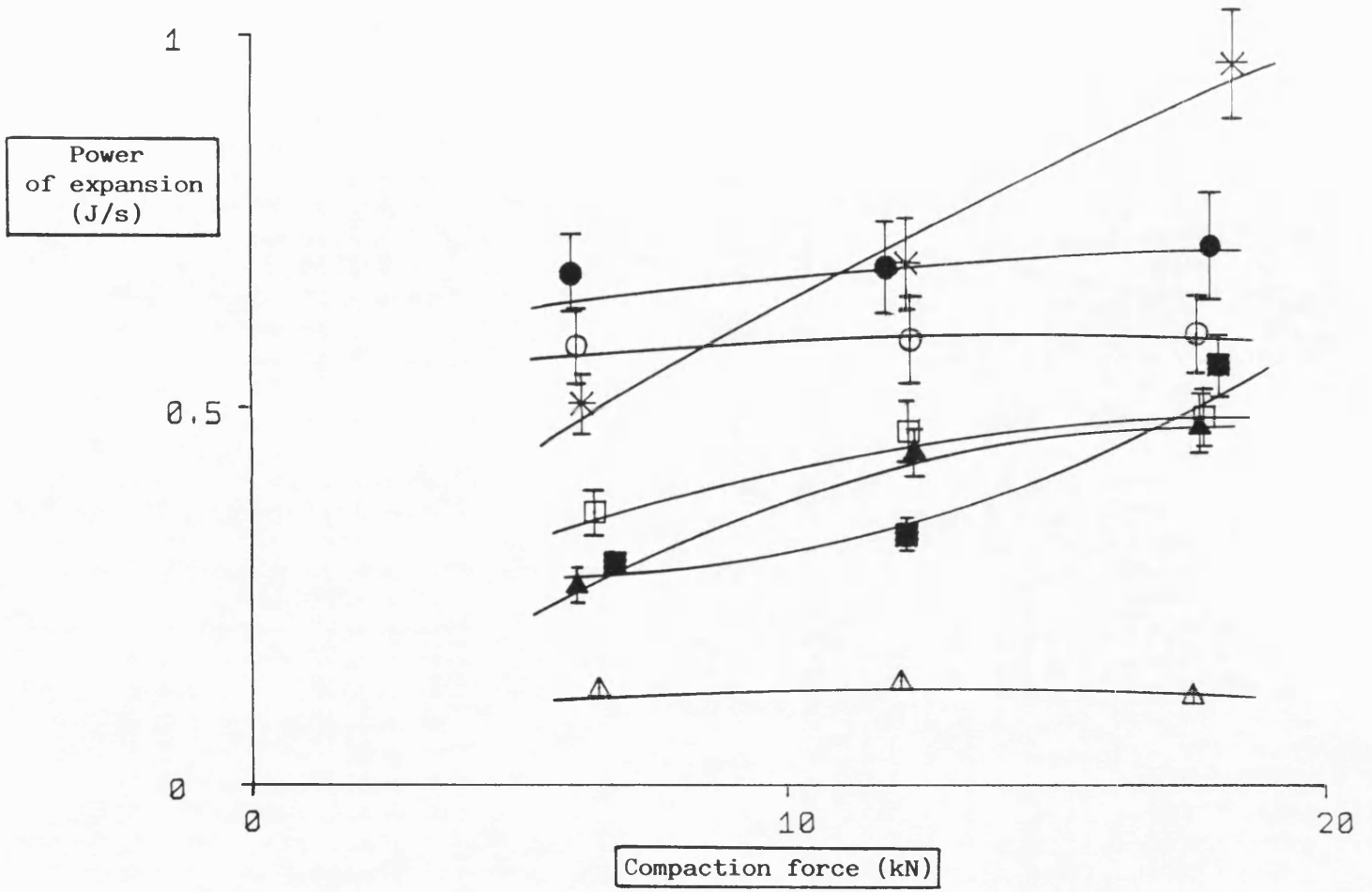

FIG. 3.6 Power of expansion of materials during decompression, at a range of compaction forces.

(Key: page xxiii)

time values are shown in Tables A.6 and A.7. Although the values of both parameters for the plastically deforming materials are generally higher than those for the brittle ones, the differences were too small compared to their compressional differences. It should be noted, that although every effort was made to maintain the same strain rate, some variation was inevitable since the fly-wheel of the tableting machine was turned manually. It is possible that differences between materials might increase under better controlled strain rate conditions.

Expansion time was calculated as the time taken by the compact to expand during decompression. The value obtained for the rubber plug is given in Table A.3. Rubber behaves as an elastic material and exhibits instantaneous recovery (Windheuser et al, 1963). Clearly, actual instantaneous elastic recovery did not take place, due to the restriction in movement caused by the presence of the upper punch. However, the expansion time for rubber represents the time during which the material was "allowed" to fully recover. It might be expected that materials with values close to those for rubber must behave in a similar way to that of an elastic body, with respect to their elastic component whereas, high values of expansion time must reflect a retarded elastic recovery. However, the values obtained for the particulate materials (Tables A.4 and A.5) were very similar, with the exception of Starch 1500, and were therefore, incapable of yielding more information about their elastic recovery.

The dimensions of the tablets were also measured after storage. The effect of compaction force on the relative density of the compacts produced can be seen in Fig. 3.7. Interestingly, the values for both Starch 1500, a plastically deforming material and Emcompress, a brittle material, were the lowest. This can be explained when the elastic recovery of the starch compacts is considered. On the other hand, sodium chloride, a material which undergoes plastic deformation and minimal elastic deformation, yielded the highest values. The two microcrystalline celluloses also showed relatively high density values, except at 6kN. This reflects the particularly high degree of elastic deformation these materials undergo at low loads, also demonstrated by high values of expansion work, mentioned earlier. Furthermore, sodium bicarbonate and anhydrous lactose showed slightly lower relative density values.

The nature of the plots in Fig. 3.7 shows that compaction force had a less marked effect on the relative density of brittle materials. This was expected, as it is known that particle fragmentation is believed to occur at relatively low pressures (Hersey et al, 1973; Cole et al, 1975; de Boer et al, 1978). Thereafter, any increase in load can only lead to a relatively small increase in density. The behaviour of sodium bicarbonate, a material thought to consolidate by plastic deformation (Alderborn et al, 1985) cannot, however, be explained unless brittle fracture is assumed to take place in this material, too.

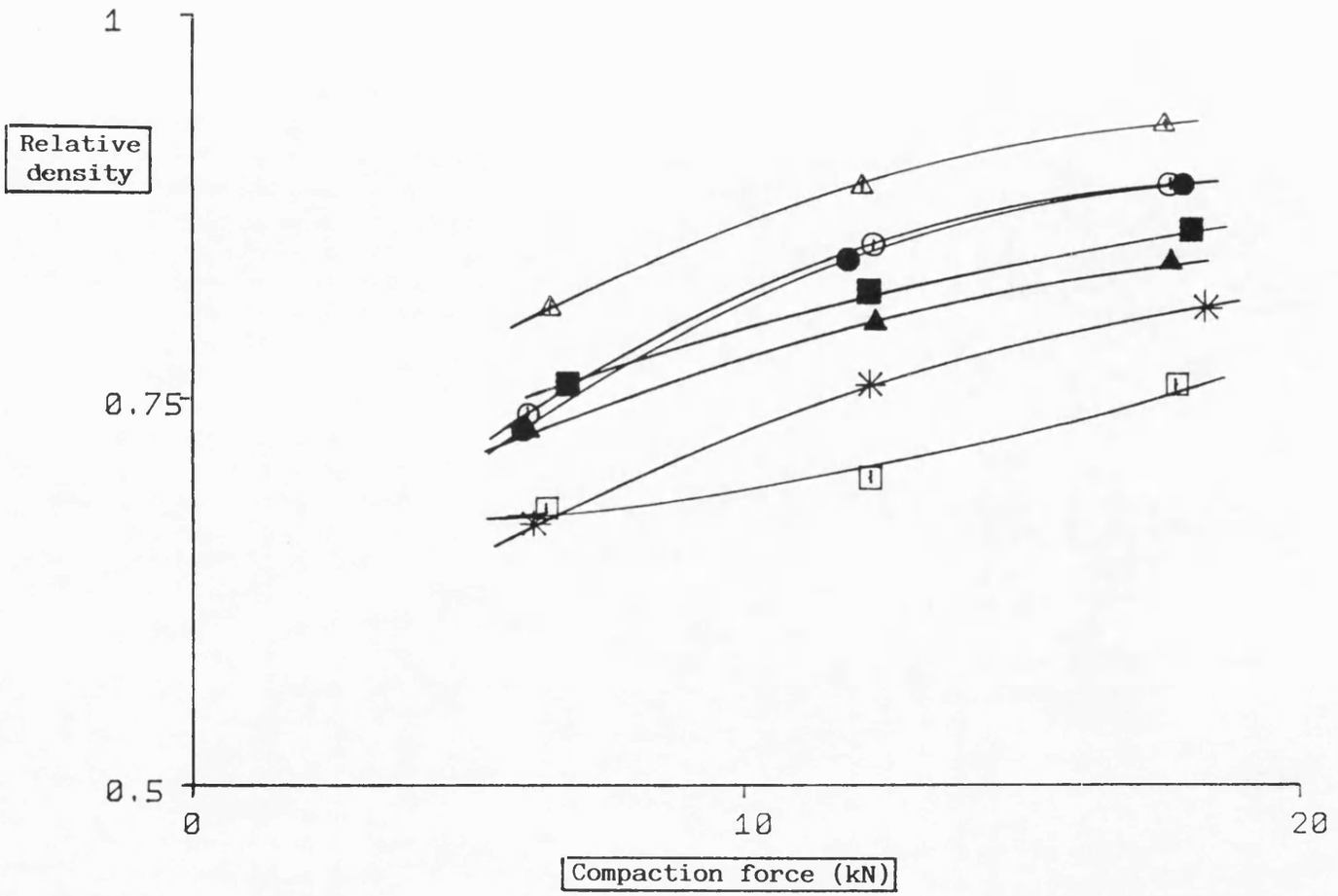

FIG. 3.7 Effect of compaction force on the relative density of the produced tablets.

(Key: page xxiii)

3.2 BEHAVIOUR OF MATERIALS AT PEAK LOAD

During compression of the materials into tablets, it was noticed that peak values for force and displacement were not obtained simultaneously. In most cases, there was a further increase in upper punch penetration after the peak force had been reached, concurrent with a decrease in the applied force.

The above-mentioned phenomenon is attributed to the time-dependent nature of materials. Deformation of particles and filling of the interparticle voids due to the applied force continues even after the peak force has been reached. This continuing flow and consolidation of the material decreases the force needed to further densify the compact. The same effect has been reported by Caspar and Muller (1983) who attributed it to compact stress relaxation. They also suggested the use of the time difference between peak force and peak displacement as an index describing the time-dependence of materials.

For a non-particulate elastic solid, such as a rubber plug, the value obtained for punch movement at peak load (Table A.3) was within the limits of accuracy of the displacement measurement system used ($\pm$ 0.0005mm). The case is different, however, for the particulate materials studied. The extent of this further punch movement (relaxation displacement), as well as the time elapsed between peak force and peak displacement (relaxation time), varied according to the materials (Tables A.6

and A.7). Those known to deform plastically, such as the two microcrystalline celluloses and Starch 1500, produced high values for both parameters. The results for sodium chloride and sodium bicarbonate confirm previous findings of their ability to deform plastically (Hardman and Lilley, 1970; Duberg and Nystrom, 1985). The decrease in these parameters with increasing compaction force seems to suggest a limit to a material's ability to deform plastically under the confined conditions of die compaction. In contrast, the values obtained for anhydrous lactose were relatively low, but increased as force increased. This is in agreement with the lower propensity of this material to undergo plastic deformation and, therefore, the higher force that is needed to cause particle deformation. The results confirm the proposed use of these parameters to describe the plasticity of materials. However, relaxation time seems to do that less effectively, since differences between materials are less apparent when this parameter is considered (Tables A.6 and A.7).

The dwell time, i.e. the time during which the peak force remains unchanged during compaction should provide information on a material's ability to relieve strain through plastic deformation. The results shown in Tables A.6 and A.7, however, fail to demonstrate any consistent ranking of the materials tested. This may be due to the turning of the fly-wheel of the tableting machine manually and, therefore, failing to maintain the same loading conditions.

3.3 EXTENDED HECKEL PLOTS

As mentioned in 2.2.1.2, in order to study the recovery behaviour of compacts, their dimensions and, therefore, their relative density and corresponding $\ln[1/(1-D)]$ values were calculated not only up to peak force, but also until the upper punch left the compact and the force was removed. Typical extended Heckel plots obtained for the materials at 18kN are shown in Figs. 3.8 and 3.9. The derived values are listed in Tables A.8 and A.9.

The dimensions of the tablets were also measured with a micrometer (Fig. 2.10) immediately after ejection, until recovery was complete. The eventual aim was to assess the dimensional changes occuring in materials following compression. For this purpose, three-dimensional profiles of $\ln[1/(1-D)]$ against pressure and time were drawn. The profiles for two extreme materials, Starch 1500 and Emcompress compressed at 18kN are shown in Figs. 3.10 and 3.11 respectively.

Different sections of extended Heckel plots can be considered separately:

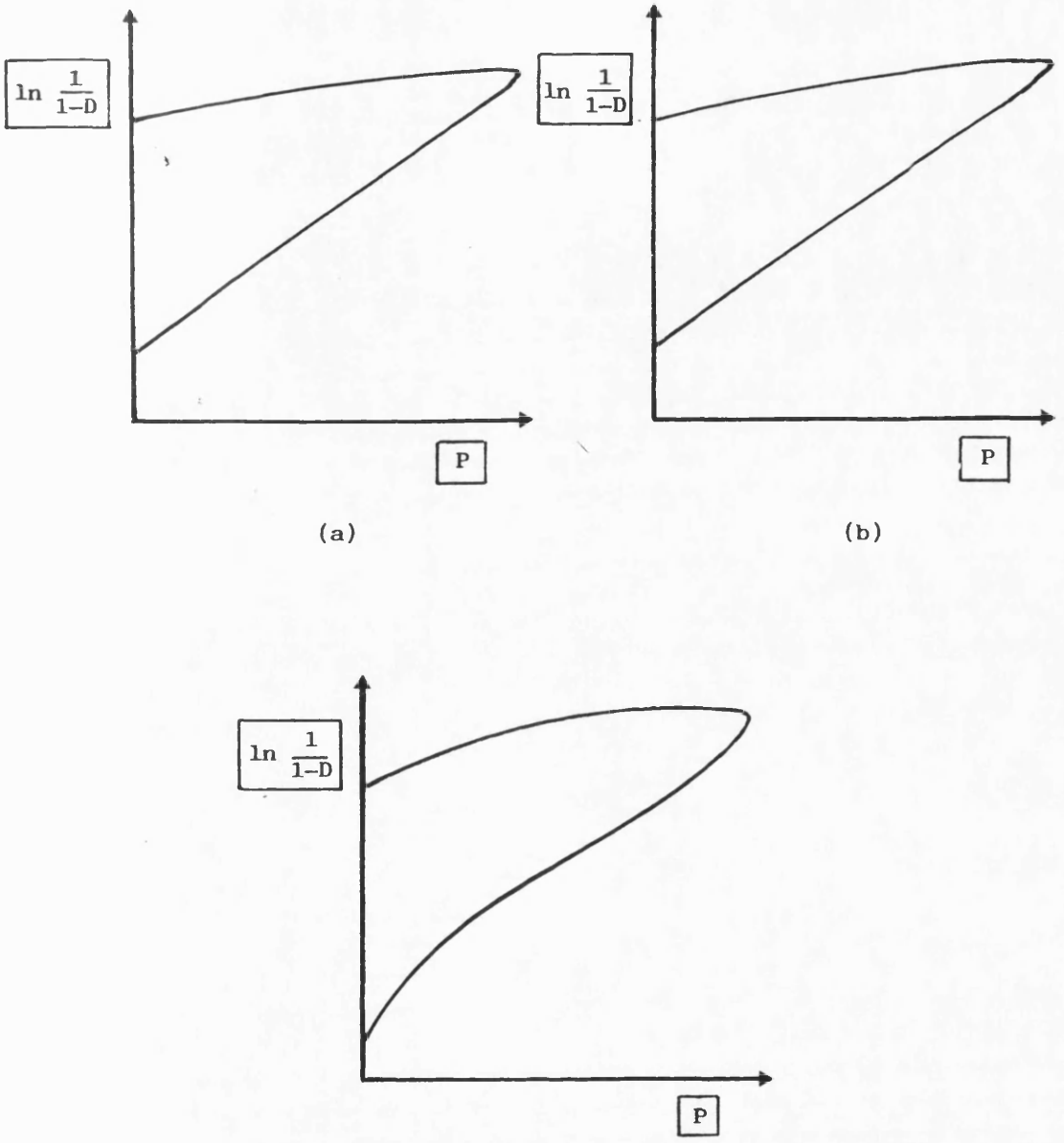

FIG. 3.8 Extended Heckel plots obtained for (a) Avicel PH102, (b) Emcocel 90M and (c) Starch 1500 at 18kN.

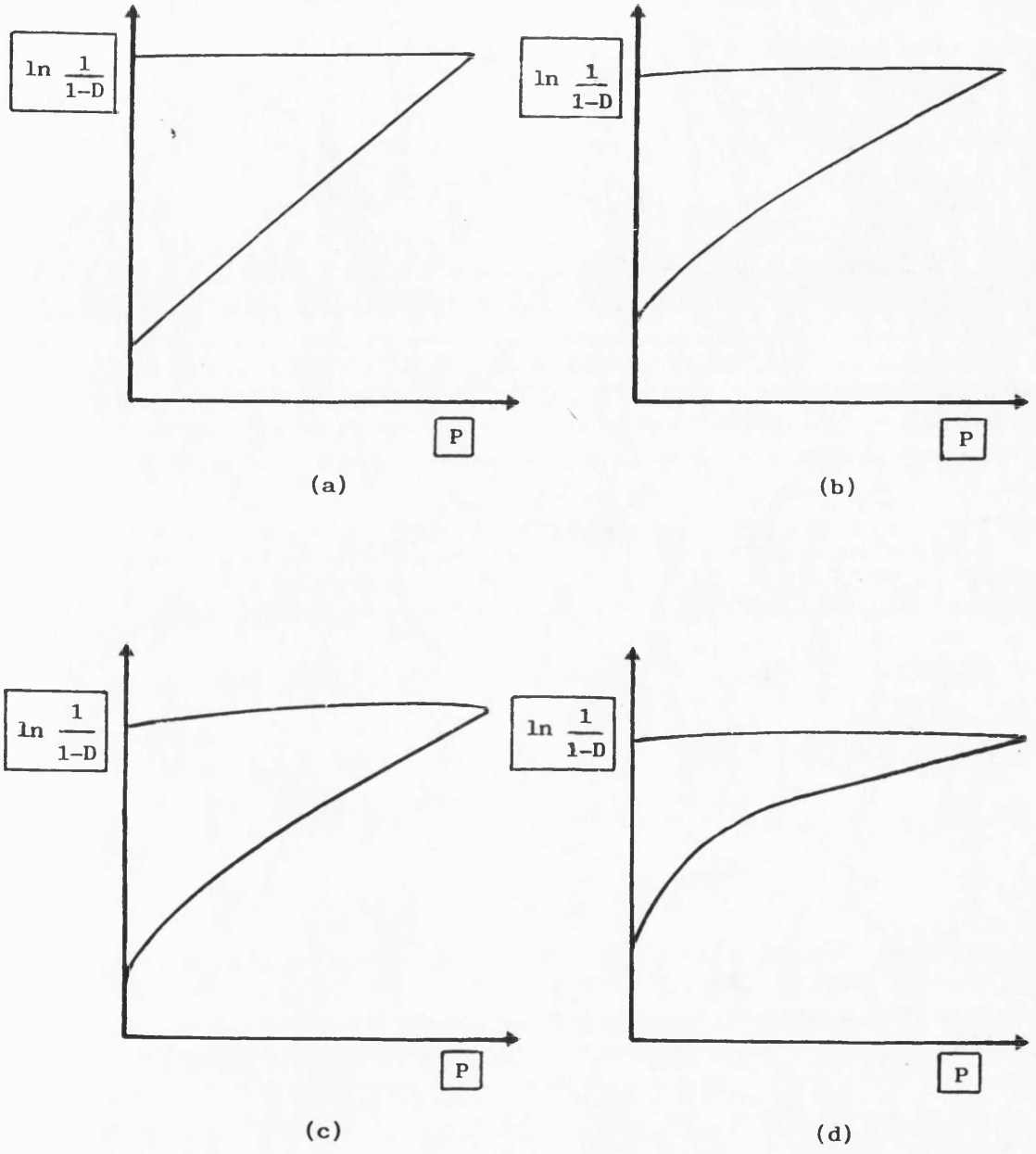

FIG. 3.9 Extended Heckel plots obtained for (a) sodium chloride, (b) sodium bicarbonate, (c) anhydrous lactose and (d) Emcompress at 18kN.

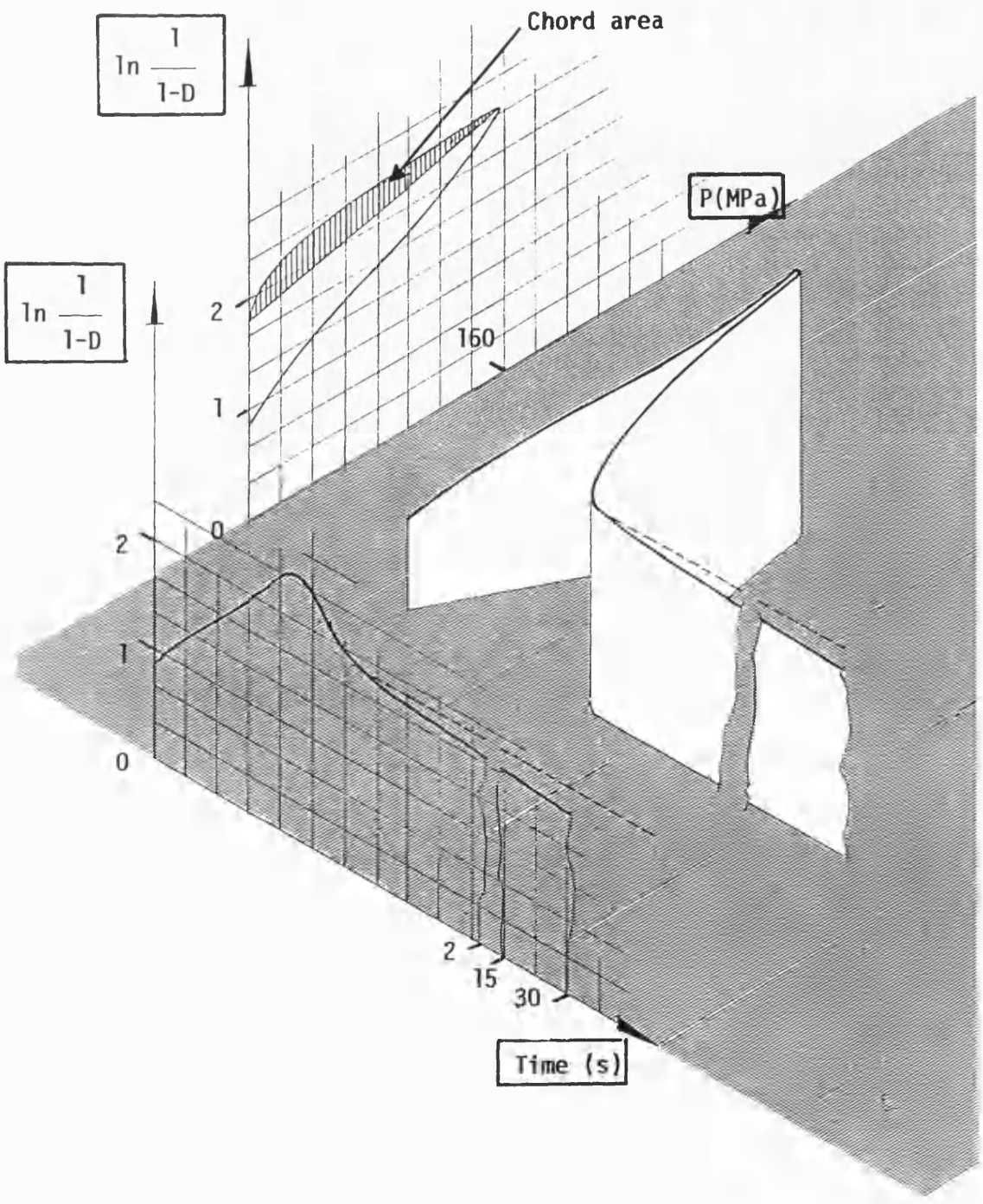

FIG. 3.10 Three-dimensional profile of ln[1/(1-D)], plotted against pressure and time for Starch 1500 at 18kN.

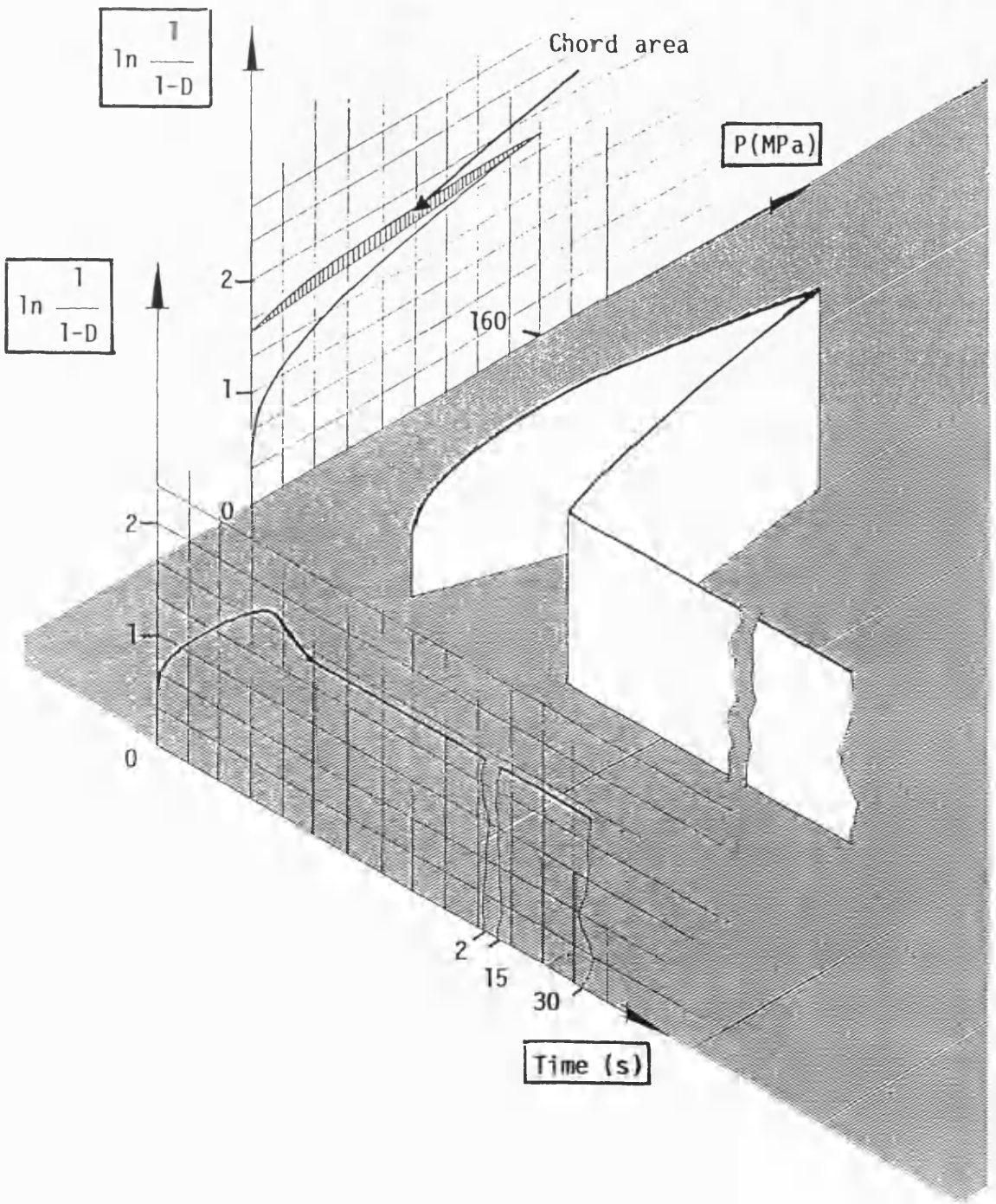

FIG. 3.11 Three-dimensional profile of ln[1/(1-D)], plotted against pressure and time for Emcompress at 18kN.

3.3.1 Low Pressures

The commonly reported deviation from linearity at low pressures for some materials, was also observed in this study (Fig. 3.9). The large increase in density with pressure at this stage is highly dependent upon the initial packing arrangements in the die, and the frictional properties of materials. Fragmentation also occurs during this phase, hence contributing to a considerable decrease in volume. Duberg and Nystrom (1982 and 1985) suggested a comparison of deviation from linearity in this region as an index of the fragmentation tendency of materials. From the correlation coefficients obtained from a linear regression analysis of the Heckel plots at low loads (6kN), it can be seen that their proposed statement is justified (Tables A.8 and A.9); the materials are ranked in an order which is in full agreement with their fragmentation tendencies demonstrated by other methods so far. Emcompress obtained the lowest values whereas, materials known to deform plastically gave correlation coefficient values close to one. Anhydrous lactose, on the other hand, held an intermediate position. However, such a treatment of the results does not take into account other events apart from particle fragmentation which also occur in this region at the same time, such as particle slippage and rearrangement. In addition, it does not describe the fragmentation which for some materials may take place at much higher pressures.

3.3.2 Linear Region

This section represents the part of the plot, where powder compaction can be considered analogous to a first order chemical reaction, as initially proposed by Heckel (1961a). The use of yield pressure as a means to characterise the plasticity of materials has been reported by several authors (Hersey et al, 1972; Duberg and Nystrom, 1985; Roberts and Rowe, 1985 and 1986b). For some materials, yield pressure values correlate fairly well with other parameters describing their plasticity (Hardman and Lilley, 1973). However, for other materials the results are less in agreement. It is suggested that this is due to the effect of several consolidation mechanisms taking place simultaneously. This means that the calculation of yield pressure is based on dimensional changes which include both plastic and elastic deformation of the tablet constrained in the die. This could lead to erroneous conclusions, in that a material with marked elastic properties might be assumed to deform plastically when evaluated with the aid of a yield pressure determined by the tablet-in-die method. Since the correlation coefficient for the earlier rising section of this curve reflects mainly the degree of fragmentation, whereas the inverse slope in the linear region represents the combination of both plastic and elastic deformation, an agreement between these

two may not always be obtained. On the other hand, the ejected tablet method (Hersey and Rees, 1971), where relative density values are measured following ejection and after recovery of the compacts, seems to be the method of choice when plastic deformation is examined (Paronen and Juslin, 1983).

Here, correlation coefficient values obtained at relatively low pressures (6kN) and yield pressure values calculated from the linear part of the Heckel plot (Tables A.8 and A.9), on the whole ranked the materials tested in the same order (Fig. 3.12). Starch 1500 gave the lowest values, indicating that it undergoes deformation under load to a greater extent than the other materials. As mentioned above, however, this mean yield pressure reflects the ability of a material to deform both plastically and elastically. The two microcrystalline celluloses gave slightly higher values of yield pressure, confirming previous reports regarding their plasticity (Hardman and Lilley, 1973). Similarly, the relatively low values obtained for sodium chloride are in agreement with previous reports regarding the ability of the material to undergo plastic deformtion during compaction (Hardman and Lilley, 1970). In contrast, the highest yield pressure values were obtained for Emcompress, indicating that this material consolidates by brittle fracture. On the other hand, sodium bicarbonate and anhydrous lactose held an intermediate position, suggesting that these materials undergo a certain amount of particle fragmentation under load.

Fig. 3.13 illustrates the values for the intercept A of the

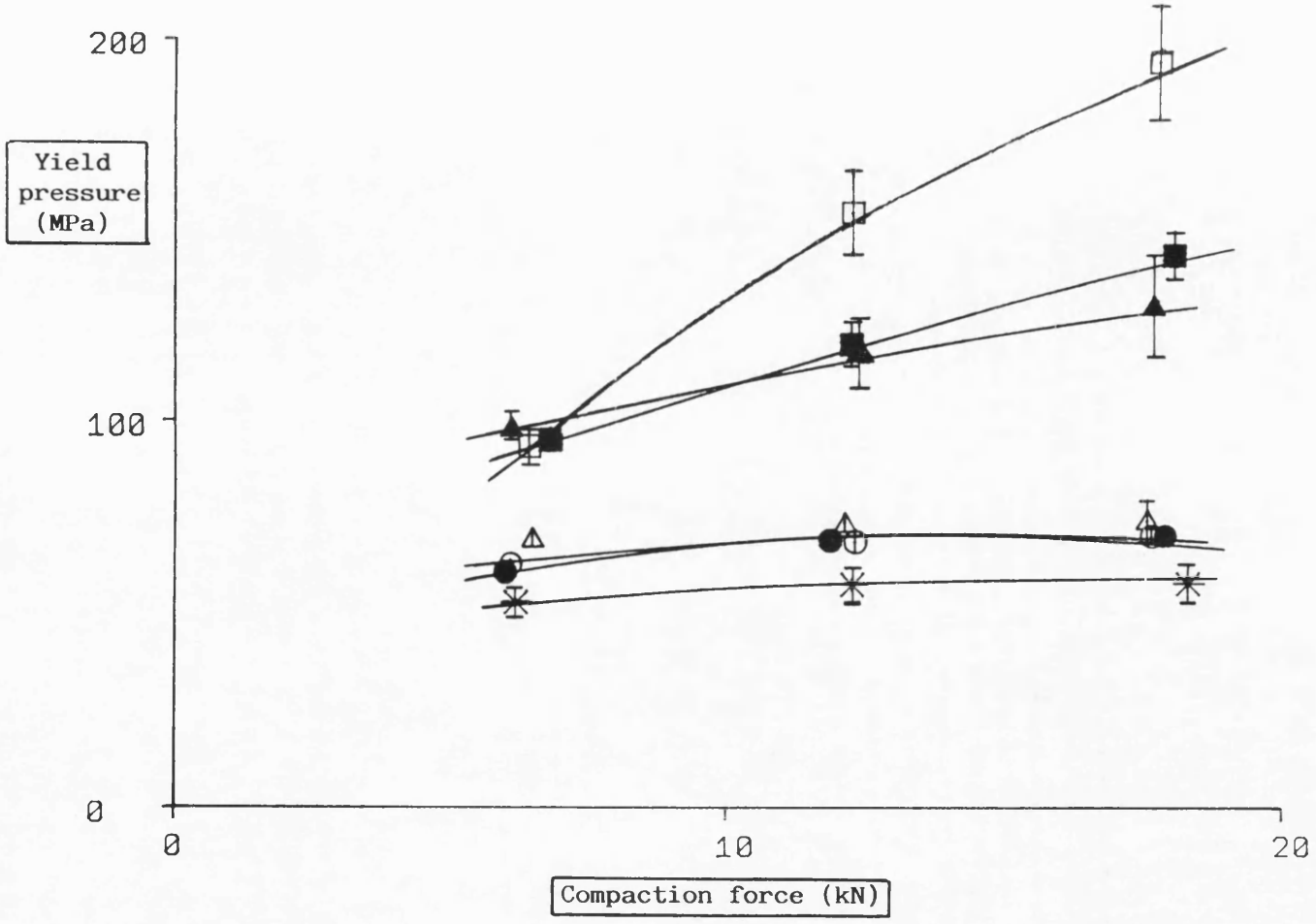

FIG. 3.12 Yield pressure values, at a range of compaction forces.

(Key: page xxiii)

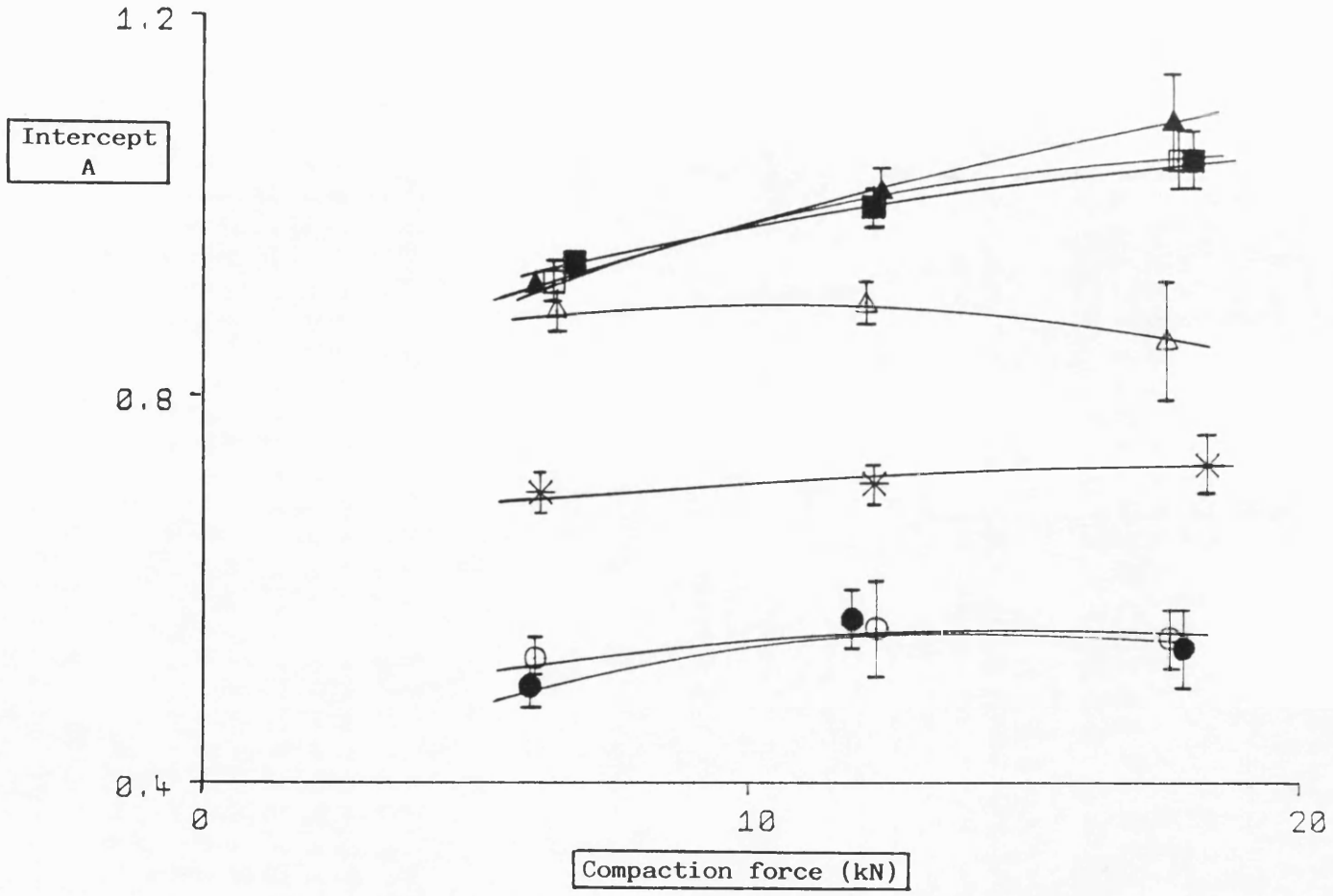

FIG. 3.13 Values for the intercept A of the Heckel equation, at a range of compaction forces.

(Key: page xxiii)

3.3.3 High Pressures

It has been shown, that for some materials linearity of their Heckel plots is lost again at high pressures (Hersey et al, 1972; Roberts and Rowe, 1985 and 1986b). This was considered to be a consequence of the limitation of the Heckel equation. Under the pressures used in this study, only Starch 1500 demonstrated such a behaviour, producing sigmoidal curves (Fig. 3.8c). It is likely that under such high pressures the material's actual structure of the polymeric chains changes, forcing molecules into closer proximity, thus increasing the density of the particles, so that the true density measured on the powdered material no longer represents the material under load. This might be responsible for the curvatures observed. Unfortunately, no evidence can so far be produced to support this hypothesis.

3.3.4 Decompression Curve

The decompression curve of an extended Heckel plot represents changes in porosity due to a combination of events. Instantaneous and retarded elastic recovery are being opposed by continuing densification of the material while still under pressure during the removal of the applied load.

Linear regression of the decompression curves can be used to assess the elastic recovery of materials during the decompression stage. A high value for the slope of this curve reflects a relatively large increase in compact volume and, therefore, elastic recovery of the material. In contrast, a low value is obtained for materials undergoing limited elastic recovery during decompression. Although such data should provide some information about the recovery behaviour of compacts, caution would be necessary when interpreting such results. The non-linearity of these curves for some materials may be the cause for wrong conclusions.

When a rubber plug was compressed under the same conditions, it underwent almost ideal elastic recovery. The decompression curve obtained in this case showed only a minimal deviation from linearity (Fig. 3.14). The linear regression results indicated that for a material that exhibits pure elastic deformation, the recovery curve is characterised by a high correlation coefficient (0.9999). In contrast, this is not the case for materials that also deform by other mechanisms. Depending on the material, the decompression curves deviated from linearity by varying extents (Figs. 3.8 and 3.9).

In order to quantify this curvature, the chord area shown in Fig. 2.8 was calculated. This area is attributed to the combined effect of instantaneous elastic recovery and the viscous retardation of the elastic recovery. In the case of a time-dependent material, as the applied load began to fall, the

Linear regression of the decompression curves can be used to assess the elastic recovery of materials during the decompression stage. A high value for the slope of this curve reflects a relatively large increase in compact volume and, therefore, elastic recovery of the material. In contrast, a low value is obtained for materials undergoing limited elastic recovery during decompression. Although such data should provide some information about the recovery behaviour of compacts, caution would be necessary when interpreting such results. The non-linearity of these curves for some materials may be the cause for wrong conclusions.

When a rubber plug was compressed under the same conditions, it underwent almost ideal elastic recovery. The decompression curve obtained in this case showed only a minimal deviation from linearity (Fig. 3.14). The linear regression results indicated that for a material that exhibits pure elastic deformation, the recovery curve is characterised by a high correlation coefficient (0.9999). In contrast, this is not the case for materials that also deform by other mechanisms. Depending on the material, the decompression curves deviated from linearity by varying extents.

In order to quantify this curvature, the chord area shown in Fig. 2.8 was calculated. This area is attributed to the combined effect of instantaneous elastic recovery and the viscous retardation of the elastic recovery. In the case of a time-dependent material, as the applied load began to fall, the

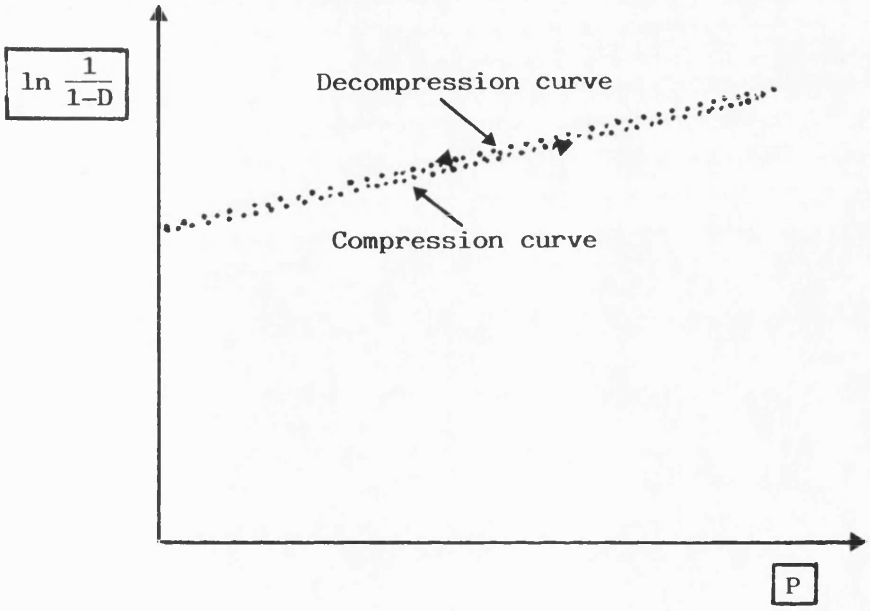

FIG. 3.14 Extended Heckel plot obtained for a rubber plug at 18kN.

consolidation term $\ln[1/(1-D)]$ increased further momentarily because of the continuing time-dependent deformation of the material under a finite load. Thereafter, this term decreased due to compact expansion. The two above-mentioned effects resulted in the formation of the chord area. Therefore, it may not be unreasonable to assume, that any deviation from linearity would be an indication of time-dependent plastic deformation, continuing to take place even during decompression.

The values for materials exhibiting time-dependent deformation were considerably higher than those for the brittle materials which showed consistently low values at all compaction forces (Tables A.8 and A.9). This can be seen from a plot of chord area, expressed as a percentage of the square area, against compaction force for the materials tested (Fig. 3.15). Starch 1500, in particular, gave the highest values followed by the two celluloses (Table A.8). In other cases, the combined effect of continuing plastic deformation and elastic recovery resulted in an initial, almost level part, after which, depending on the material, the consolidation term decayed at an increasing rate as the load was removed. Of all the materials, sodium chloride, anhydrous lactose and Emcompress showed the closest approximation to a linear recovery curve and, therefore, the minimum chord area values (Table A.9).

It may, therefore, be concluded that this new parameter obtained from extended Heckel plots is useful in quantifying time-dependent characteristics of materials. Such information

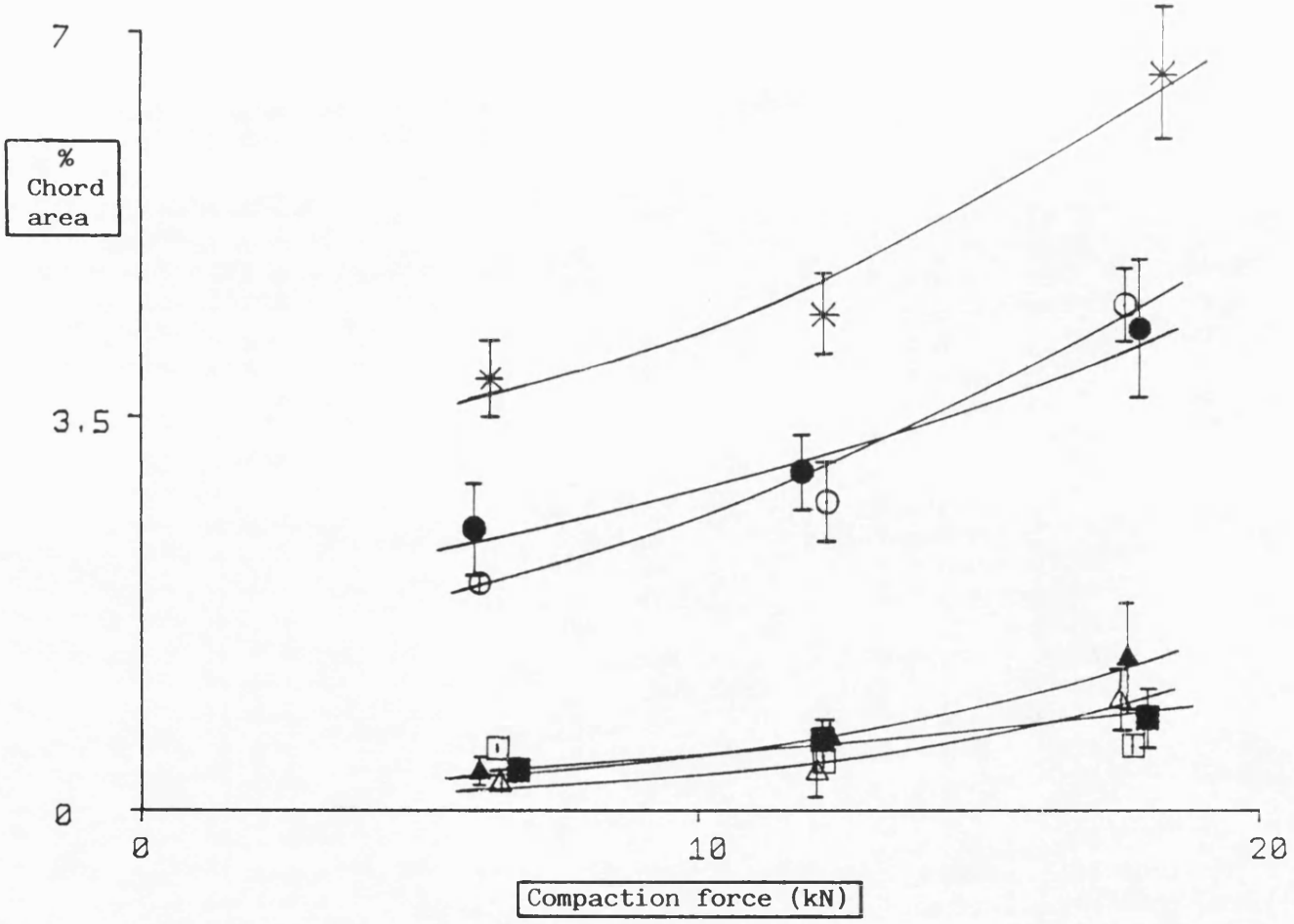

FIG. 3.15 Chord area values expressed as a percentage of the square area, at a range of compaction forces.

(Key: page xxiii)

when added to data from conventional Heckel plots, contributes to a fuller understanding of the tableting behaviour of a material.

3.3.5 Other Areas Derived from Extended Heckel Plots

Other areas under extended Heckel plots expressed as a percentage of the square area (Fig. 2.8) are also listed in Tables A.8 and A.9. The square area reflects the overall extent of densification occuring during compression with respect to the applied pressure. As expected, plastic and elastic materials gave higher values than the brittle ones.

The area under the compression curve, i.e. the rising force curve, represents the densification of the material due to elastic and plastic deformation and/or brittle fracture. As a percentage of the square area, it provides a measure of the curvature of the rising curve. The difficulty, in this case, is that interpretation of the results has to take into account not only particle fragmentation, but also rearrangement at low pressures and loss of linearity at high pressures, as mentioned earlier. In general, the lowest values were observed for the plastic materials, being close to 50% or so (Tables A.8 and A.9). This was not unexpected because of the linearity of their curves. On the other hand, brittle materials gave values around 75-80% due to the curved nature of the initial part of their

Heckel plots. Apart, however, from the use of this parameter as a means of assessing the linearity of Heckel plots, such results do not provide any more information regarding the consolidation behaviour of materials.

The area above the decompression curve, i.e. the falling force curve, reflects the amount of elastic recovery and bond rupture during decompression, and can, therefore, be used to assess the extent of this process for each material. Not surprisingly, Starch 1500 gave the highest values (Fig. 3.16). The two microcrystalline celluloses showed similar values except at 18kN, where Starch 1500 compacts showed a more pronounced elastic recovery. The values obtained for the other materials were particularly low, but did not allow the differences in their elastic properties to be demonstrated (Fig. 3.19).

In conclusion, extended Heckel plots are useful in studying the consolidation behaviour of materials during compression and decompression. The chord area, in particular, provides a means of assessing the time-dependent tendencies of materials and can, therefore, be used to predict potential problems during tablet manufacture.

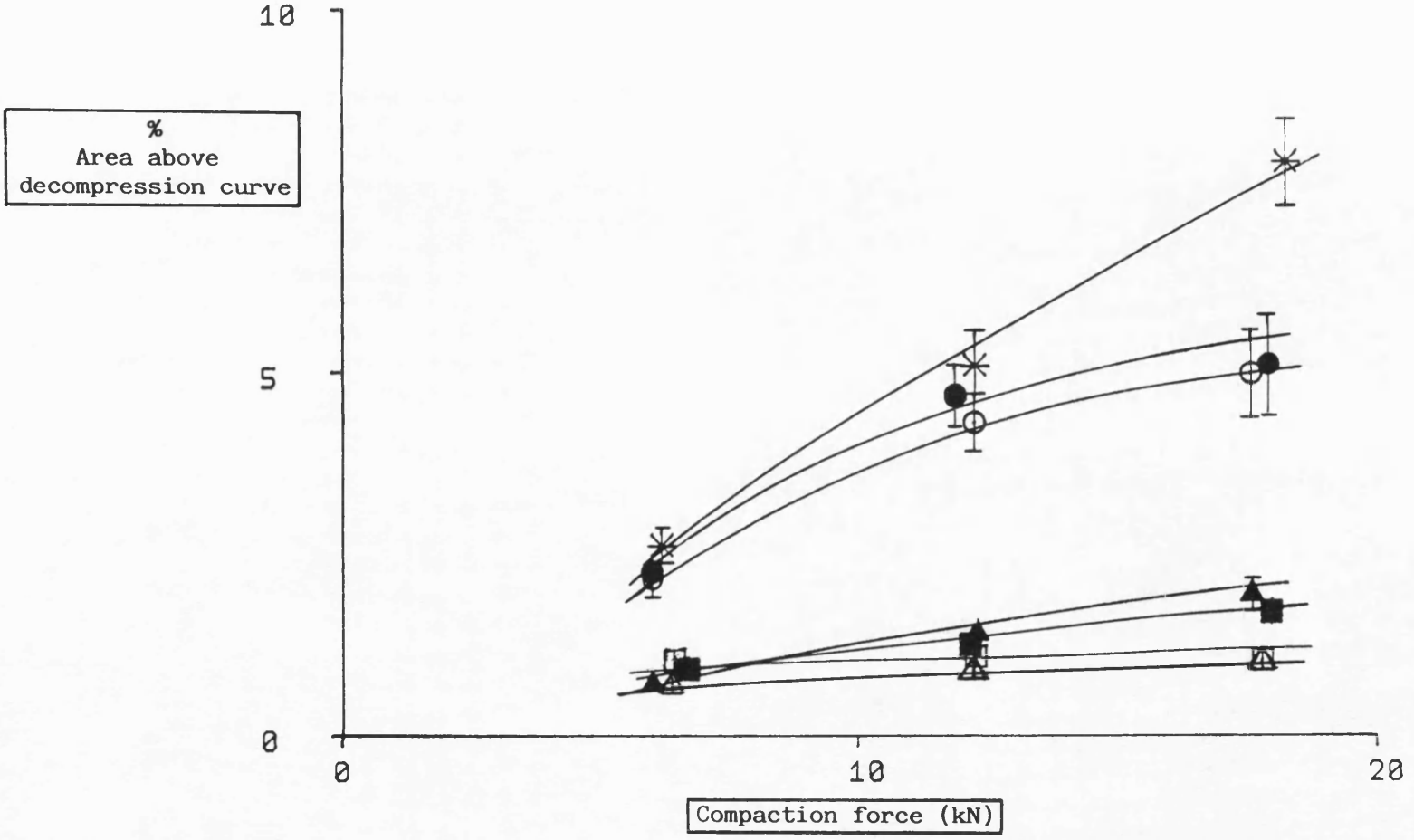

FIG. 3.16 Values of the area above the decompression curve expressed as a percentage of the square area, at a range of compaction forces.
(Key: page xxiii)

CHAPTER FOUR

ASSESSMENT OF THE MECHANICAL STRENGTH OF TABLETS

4.1 DIAMETRAL LOADING TEST

4.1.1 Diametral Loading of Compacts

The results obtained from the diametral loading test on tablets (section 2.2.2.1), are listed in Tables B.1-B.3. The radial tensile strength against compaction force profiles are shown in Fig. 4.1. The two microcrystalline celluloses gave the highest values at all compaction forces and showed a large increase in tensile strength with compaction force. This effect was more pronounced for Emcocel 90M which showed slightly higher values throughout the force range. These results confirm that plastic flow is an important factor affecting the ability of a material to form strong compacts (David and Augsburger, 1977).

For Starch 1500, however, radial tensile strength values were considerably lower, ranked below those of anhydrous lactose and sodium chloride (Fig. 4.1). This confirms that plastic

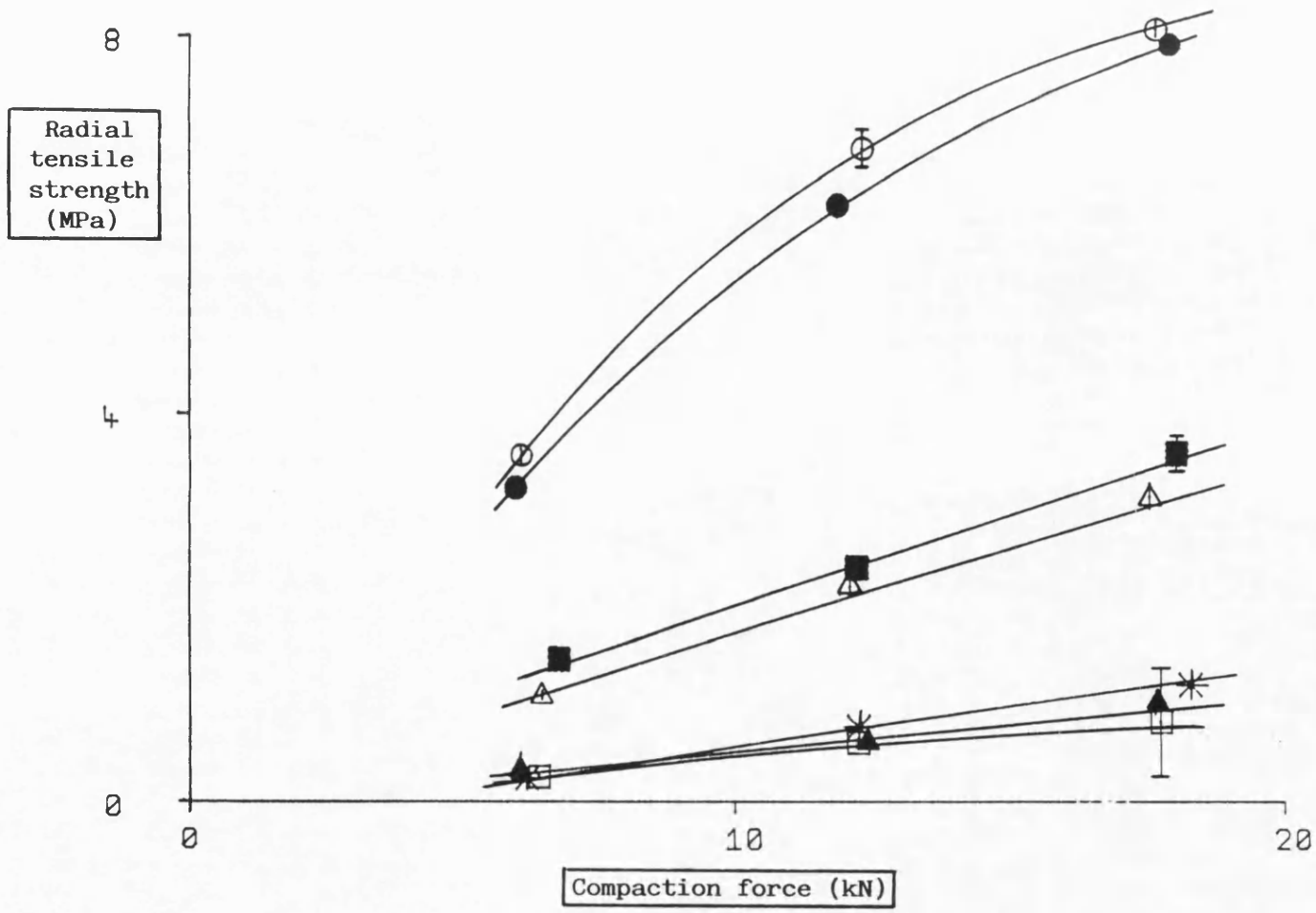

Fig. 4.1 Radial tensile strength values at a range of compaction forces.
(Key: page xxiii)

deformation alone is not enough to ensure the formation of strong tablets. Plastic deformation for Starch 1500 may occur too slowly to produce extensive interparticle bonding during compression. Furthermore, bonding is dependent on the extent of both plastic and elastic deformation undergone by the material during the compression-decompression cycle. For Starch 1500, a large proportion of the total deformation is elastic (Fig. 3.5) and recovers during decompression and after ejection. Bonds are ruptured and the area of interparticle bonding is reduced. The greater elasticity of Starch 1500 was largely evidenced by results obtained during compaction (sections 3.1 and 3.3).

Sodium chloride and anhydrous lactose held an intermediate position in Fig. 4.1. Values of radial tensile strength for these materials indicate a fair amount of bonding within the compacts. In contrast, sodium bicarbonate gave relatively low values. It has been reported that, although this material undergoes plastic deformation, the extent of bonding in terms of either bonding surface area or bond strength is not sufficient to form strong tablets (Duberg and Nystrom, 1985). In this work, intermediate yield pressure values coupled with low radial tensile strength values also seem to suggest lack of sufficient bonding. Emcompress values of tablet strength were relatively low, confirming that particle fragmentation does not necessarily increase the true area of contact between particles.

Schubert et al (1975) stated, that although the tensile strength of materials may be identical, their fracture strain

may be different. Therefore, deformation before failure is another parameter that contributes to a better understanding of the mechanical properties of compacts (Rees and Rue, 1978c). The platen displacement against compaction force profiles are shown in Fig. 4.2. The materials are ranked as follows:

Emcocel 90M > Avicel PH102 > Starch 1500 > sodium bicarbonate > anhydrous lactose > Emcompress > sodium chloride

As reported by Rees and Rue (1978c), sodium chloride gave surprisingly low values. It is a material consolidating by plastic deformation (Hardman and Lilley, 1970) and a higher degree of deformation before failure might be expected. The results, however, can be explained when work hardening is considered. It has been suggested (Rees and Rue, 1978c; Rosenberg, 1984) that such a phenomenon is predominant in sodium chloride crystals. It is possible that work hardening during compaction is the cause for the observed limited deformation of sodium chloride compacts before they fail in diametral loading.

Radial work of failure values, calculated as described in section 1.2.3.2, are illustrated in Fig. 4.3. Differences between materials increased due to the combined effect of radial tensile strength and deformation before failure values. Therefore, the materials were ranked according to their ability to undergo deformation both during the compaction event and before failure in the diametral loading test. It is thought, that this parameter characterises compacts more fully than tensile strength or deformation before failure alone.

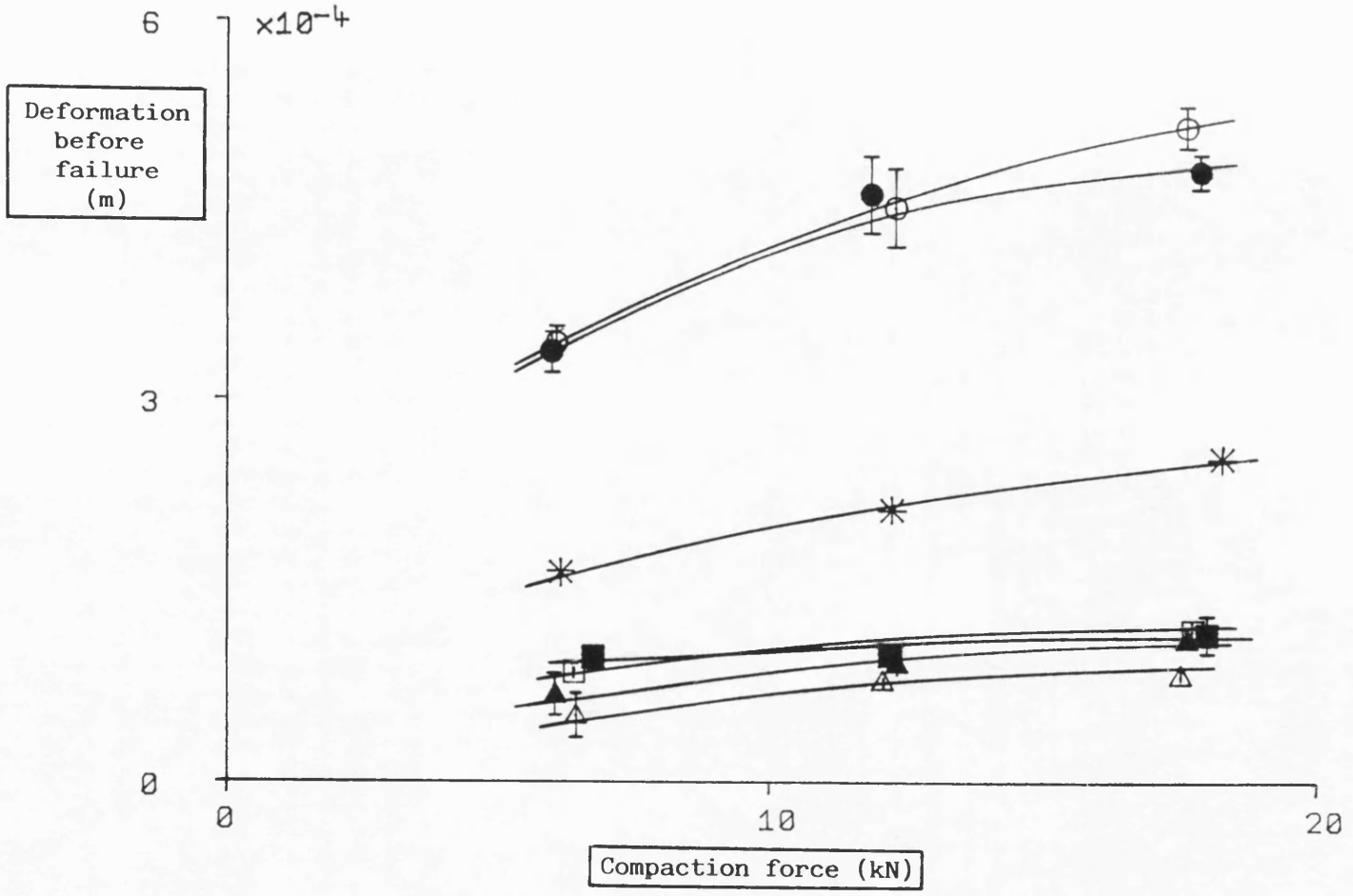

Fig. 4.2 Deformation before failure during diametral loading of tablets at a range of compaction forces.

(Key: page xxiii)

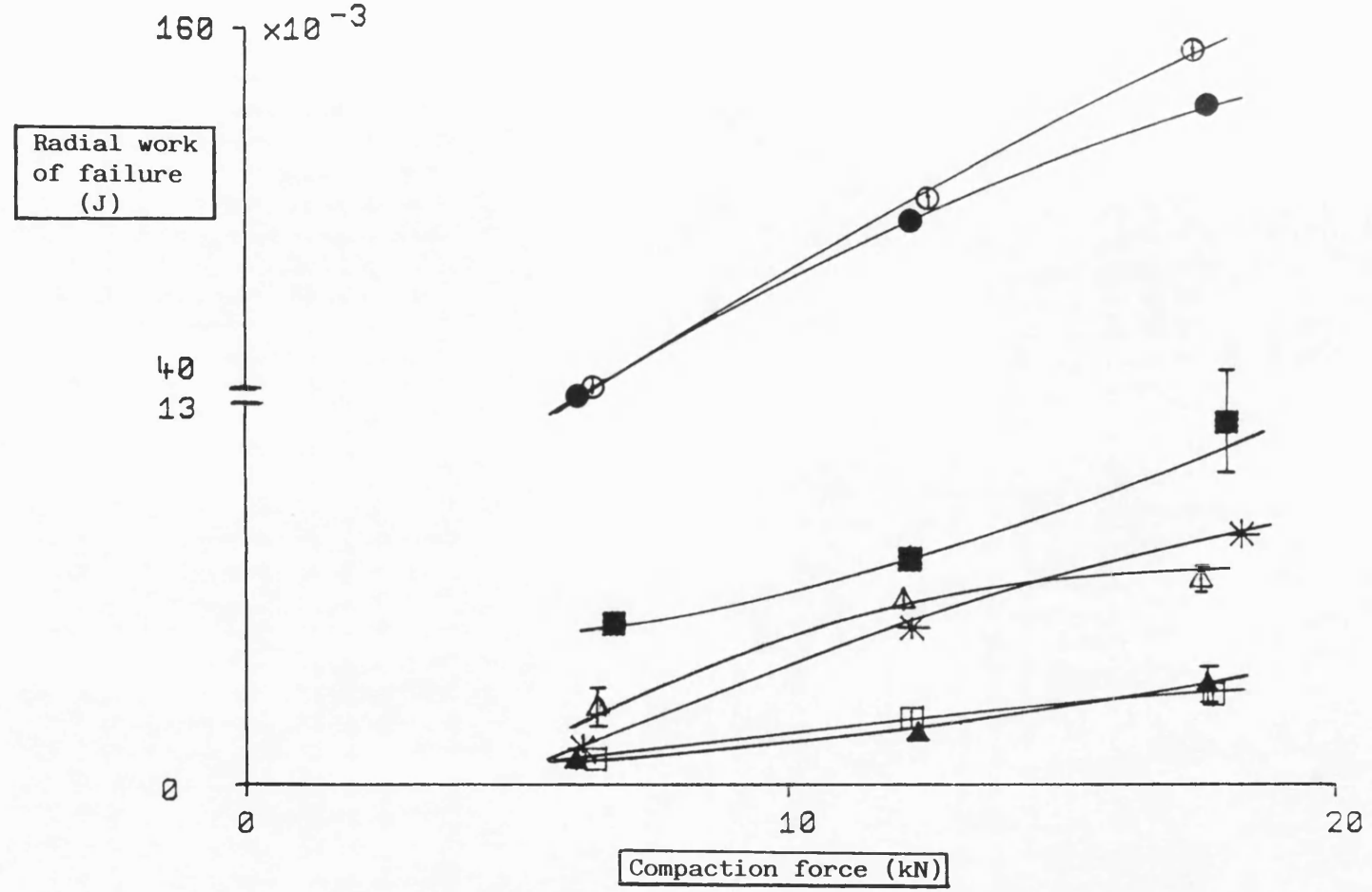

Fig. 4.3 Radial work of failure values at a range of compaction forces.
(Key: page xxiii)

The materials are generally ranked as in Fig. 4.1. The only difference is the intersection of Starch 1500 and sodium chloride curves. Despite their low radial tensile strength, Starch 1500 compacts showed a higher increase in radial work of failure values due to their more extensive deformation before failure compared with sodium chloride compacts.

In order to take into account tablet dimensions, corrected work of failure values were calculated as mentioned in section 1.2.3.2, and plotted against compaction force (Fig. 4.4). It is clear, that the materials are again ranked as in Fig. 4.3. This was expected, since in this work, both compact thickness and diameter were similar for all materials. Corrected work of failure should, however, prove useful when compacts of different dimensions need to be compared.

Time-to-failure values were used to calculate power of failure values. This parameter, however, does not offer any more information about the mechanical properties of tablets. This is attributed to the division of a parameter which involves displacement measurements by another which, in effect, also describes the ability of the compacts to deform before failure.

The differences between materials are also demonstrated when apparent failure viscosity values, calculated as described in section 1.2.3.2, are plotted against compaction force (Fig. 4.5). The profiles obtained for the materials are similar to those of work of failure and corrected work of failure plotted against compaction force. This was not unexpected, as apparent

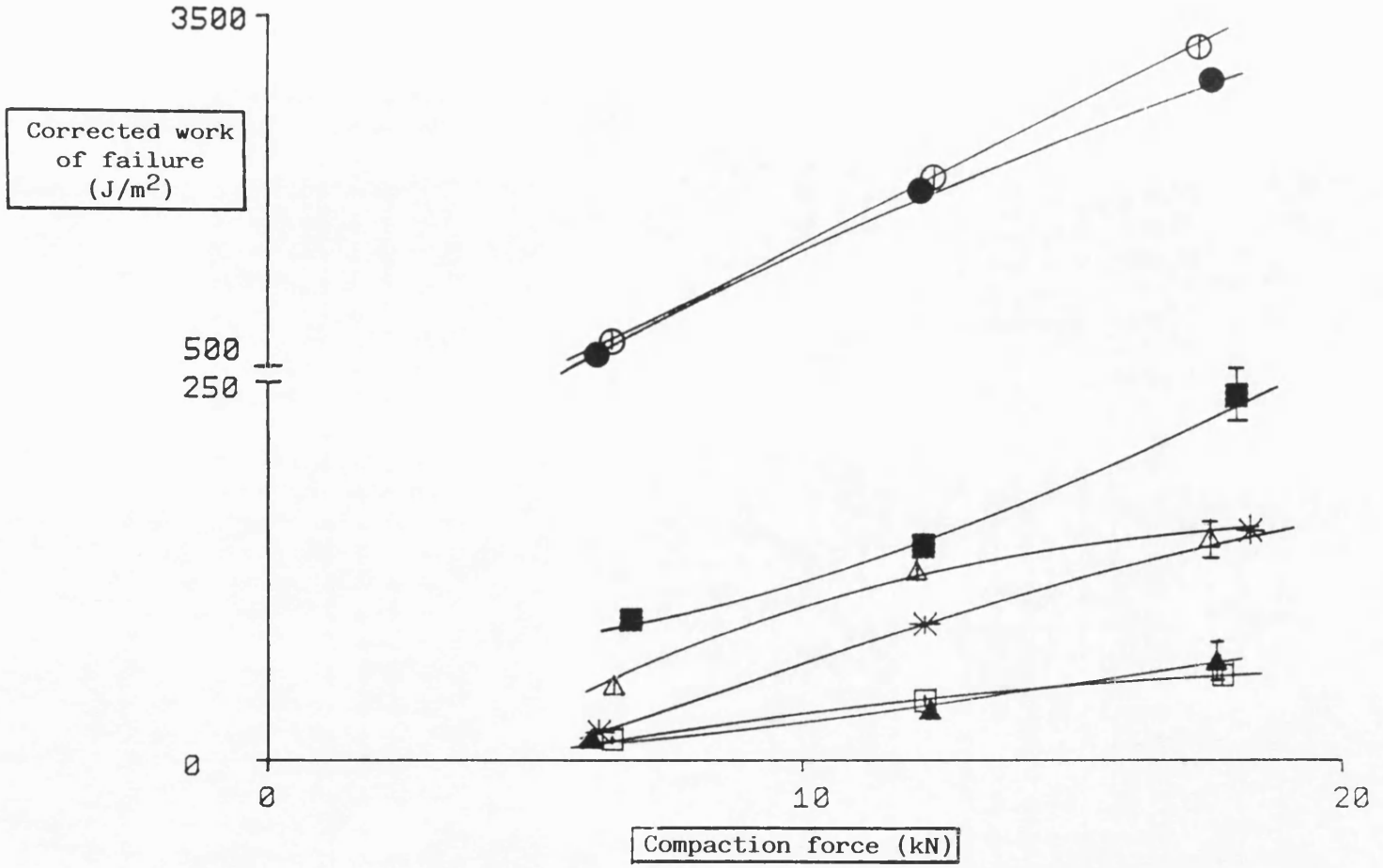

Fig. 4.4 Corrected work of failure during diametral loading of tablets at a range of compaction forces.

(Key: page xxiii)

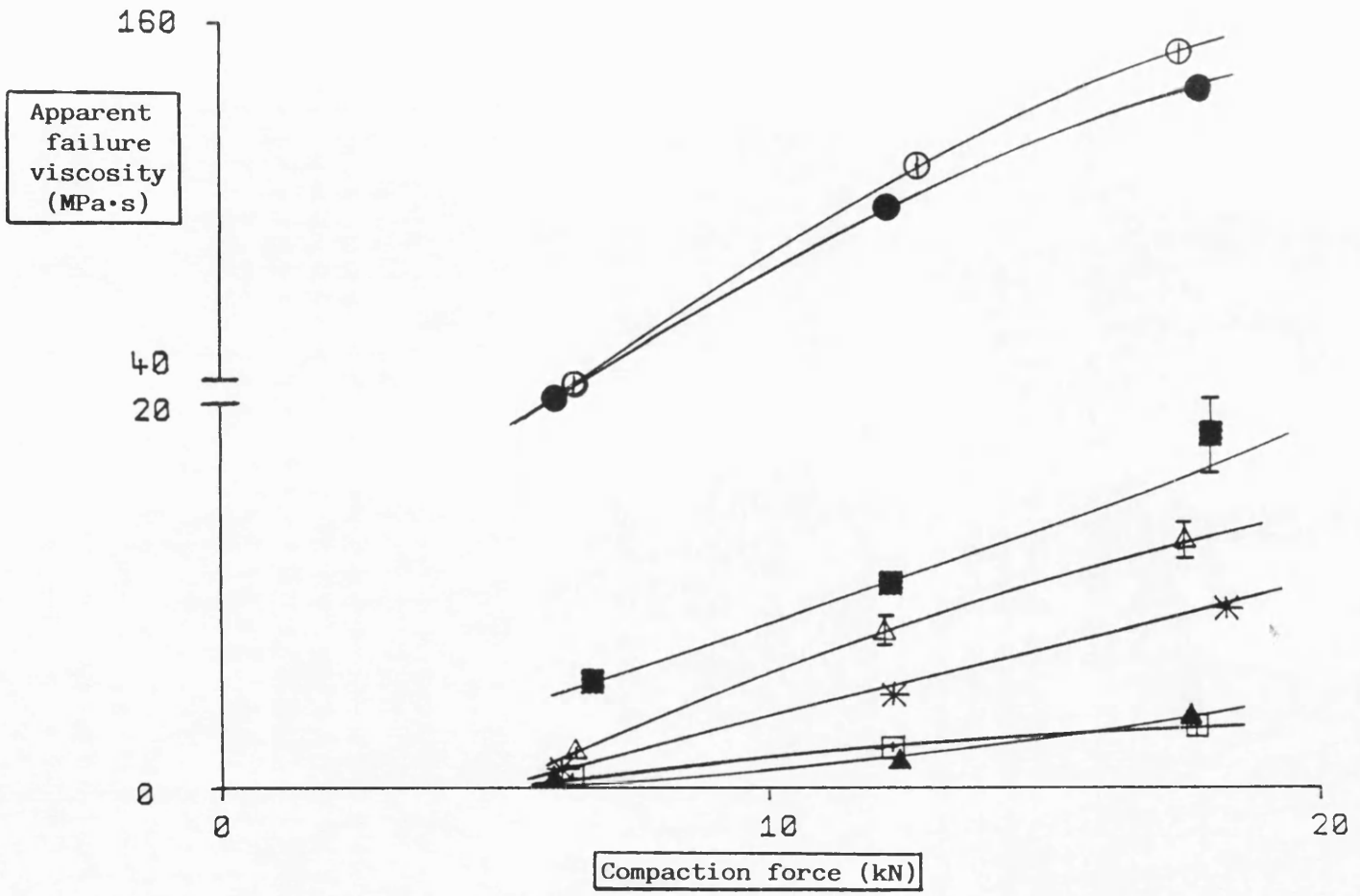

Fig. 4.5 Apparent failure viscosity values obtained during diametral loading of tablets, at a range of compaction forces.
(Key: page xxiii)

failure viscosity values are dependent on tensile strength and time-to-failure values, an indirect measure of the deformation of the material before failure. It seems, therefore, justifiable to use apparent failure viscosity values as a means to characterise the physico-mechanical properties of compacts.

Finally, the area-ratio (Moschos, 1985) was calculated in order to assess the resistance of materials to deformation during the diametral loading test (Fig. 1.10). The values obtained are given in Tables B.1-B.3. The values obtained for the two microcrystalline celluloses suggest that those materials resist deformation at the beginning of the test and, therefore, contradict those of Moschos (1985). This may be because extensive bonding created during compaction opposes further deformation of the material. The rest of the materials gave very similar profiles and, therefore, similar values of the area-ratio. Sodium chloride gave particularly low values, confirming resistance to deformation, attributed to work hardening during compaction. Starch 1500, on the other hand, was less resistant to deformation at the beginning of the test, producing area-ratio values closer to 1. On the whole, although this parameter offers some information regarding resistance of materials to deformation during a diametral loading test, it does not seem able to characterise the large differences between such extreme materials.

4.1.2 Effect of Platen Rate on the Diametral Loading Results Obtained for Avicel PH102 Compacts

This work was a repetition of a study performed earlier by Moschos (1985) who reported that Avicel PH102 tablets showed a sudden decrease in work of failure values at platen rates above 16mm/min. The effect was greater for tablets made at compaction forces above 10kN and was attributed to a latent brittleness of the material.

Avicel PH102 tablets were produced at 4, 10, 15, 20 and 25kN (section 2.2.1). The tablets were subjected to a diametral loading test and the platen rate was varied (1-45mm/min). The results (Tables B.4 and B.5) showed no significant decrease in radial tensile strength or work of failure values when the platen rate was increased (Figs. 4.6 and 4.7). On the contrary, these parameters showed a slight increase with platen rate. This may be caused by an increasing resistance to deformation before failure, due to the material's time-dependent nature. When Avicel PH102 compacts are loaded at low rates, they undergo considerable deformation, and an obvious flattening at the contact points. This leads to a large distortion of the tablet structure and lower loads are required to cause tablet failure than for compacts loaded at higher platen rates. It is suggested, that higher platen rates than the ones used here should be studied to detect the effect of loading rate on the mechanical properties of materials.

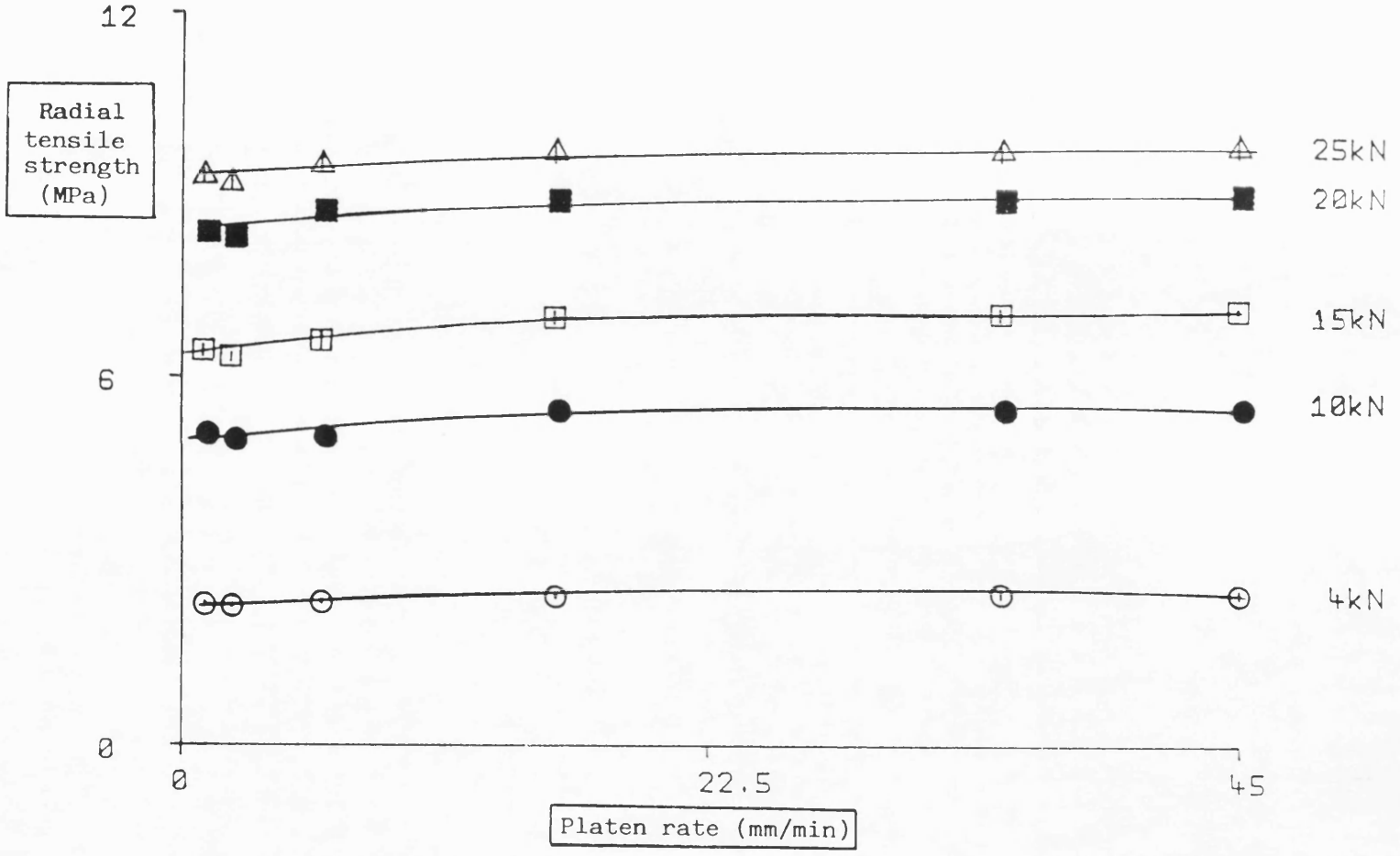

Fig. 4.6 Effect of loading rate on the tensile strength of Avicel PH102 tablets at a range of compaction forces.

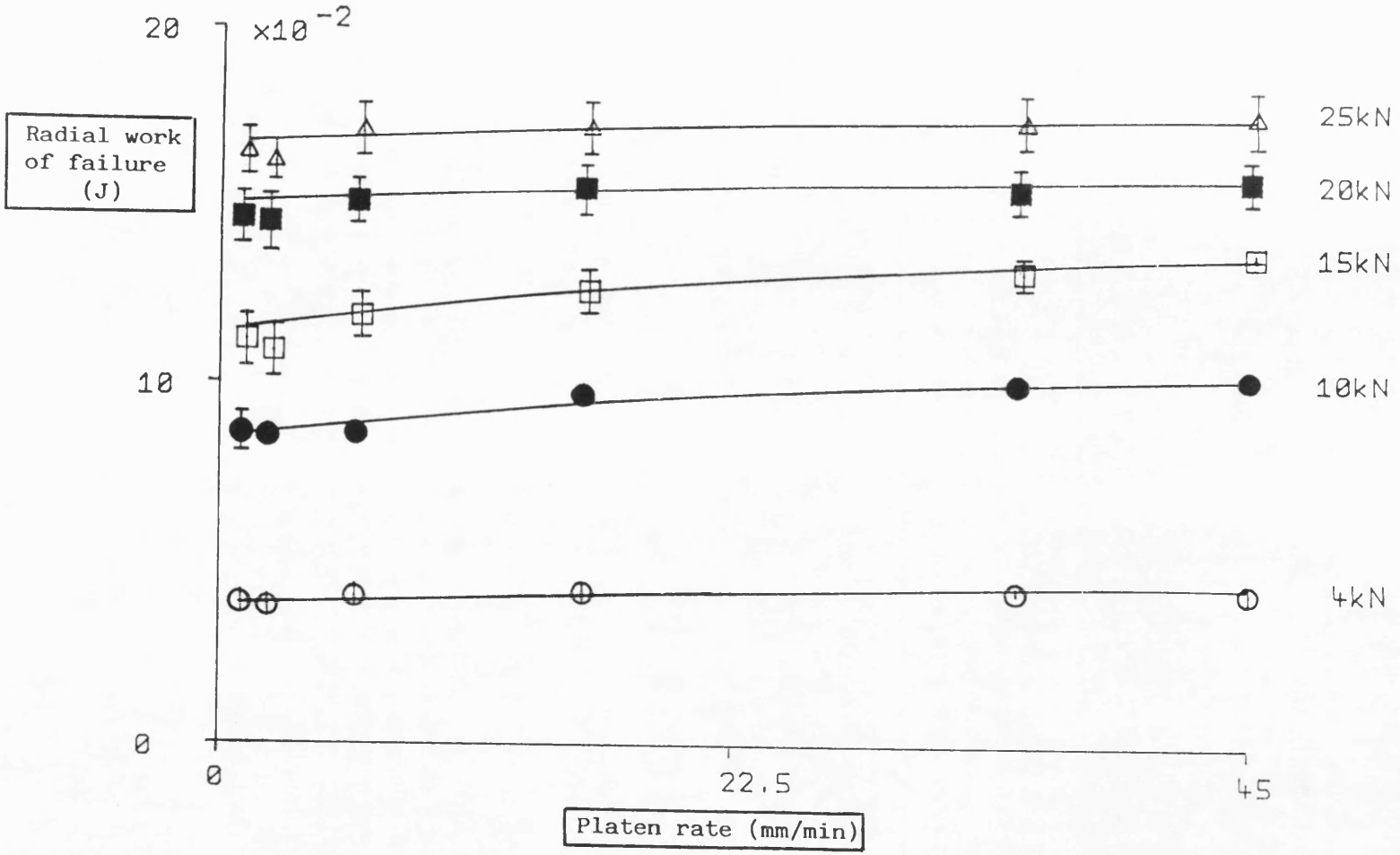

Fig. 4.7 Effect of loading rate on the radial work of failure of Avicel PH102 tablets at a range of compaction forces.

4.2 DIRECT TENSION TEST

To complement the data obtained from the diametral loading test (section 4.1), tablets were also subjected to a direct tension test, as mentioned in 2.2.3. The results are given in Tables B.6-B.8. The profiles of axial tensile strength against compaction force for the materials tested are shown in Fig. 4.8. Again, the two microcrystalline celluloses gave the highest values at all compaction forces. However, differences between these materials and the rest were not as pronounced as in the case of the diametral loading test. Other materials that deform by plastic deformation during compaction, such as Starch 1500 and sodium chloride, also showed lower tensile strength values compared to the ones demonstrated during the diametral loading test (Tables B.1-B.3). In contrast, radial and axial tensile strength values obtained for Emcompress were approximately equal. For anhydrous lactose, axial strength values were slightly lower than the radial ones. Finally, sodium bicarbonate yielded the lowest values, which were even lower than the ones obtained from the diametral loading test.

These results are in agreement with previous reports of differences in strength values obtained when the materials were subjected to a direct and an indirect tension test (Nystrom et al, 1977 and 1978; Duberg and Nystrom, 1985). According to Train

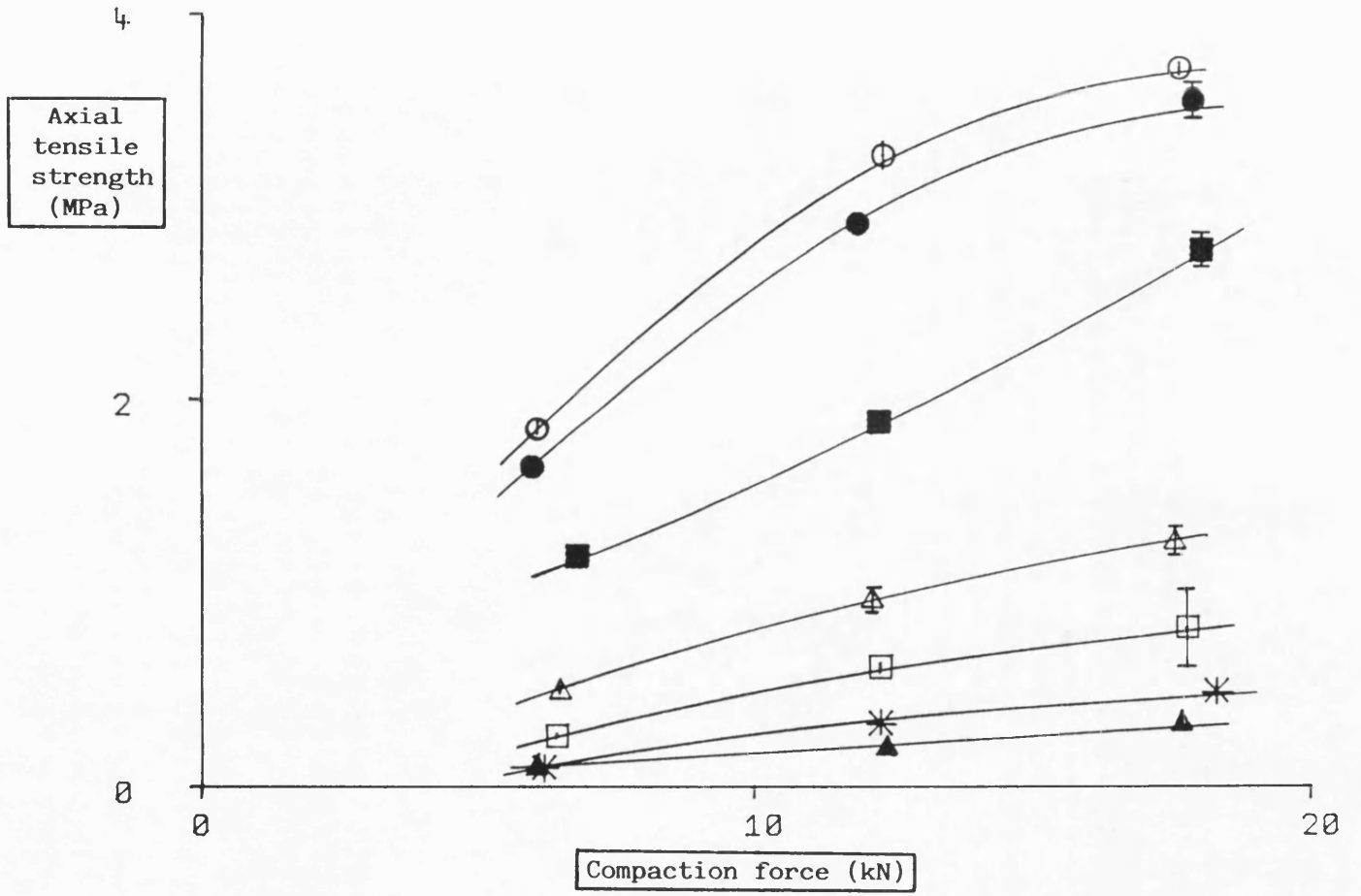

Fig. 4.8 Axial tensile strength values at a range of compaction forces.

(Key: page xxiii)

(1957), uniaxial compaction of powders results in heterogeneous compacts with regard to porosity and stress distribution. It has also been suggested that powder consolidation through plastic deformation results in more heterogeneous compacts than when particle fragmentation occurs (Duberg and Nystrom, 1982). Fragmentation in materials reduces the internal stresses more efficiently than plastic deformation normally would. This could be due to either fragmentation resulting in better particle packing or to the increased number of contact points and a decreased local pressure at each point, or both. Strength measurements in the axial direction indicate the weakest plane of an heterogeneous tablet, whereas the radial tensile strength is more a description of the mean strength of the tablet.

According to Nystrom et al (1978), the ratio between axial and radial strength expresses the strength isotropy in a tablet. This ratio is close to unity for a homogeneous body, decreasing to zero when the axial strength diverges from the radial one. It is not unreasonable, therefore, to assume that the strength isotropy ratio (SIR) reflects the amount of particle fragmentation during compaction. Compacts made from brittle materials are more homogeneous and, according to the above, will give higher ratios. Ratios close to unity imply that the material consolidates mainly by brittle fracture, while low ratios can be due to either plastic deformation or capping tendency.

The results obtained here (Tables B.6-B.8) for various materials show that although the axial strength of materials undergoing brittle fracture during compaction, such as Emcompress and anhydrous lactose, was lower than the radial one, they gave the highest SIR values (Table B.9) throughout the compaction force range (Fig. 4.9). A more dramatic decrease in tensile strength in the axial direction and, therefore, in the strength isotropy ratio was observed for materials consolidating by plastic deformation. The lowest SIR values were obtained for sodium bicarbonate, a material which is reported to form relatively weak bonds (Duberg and Nystrom, 1985). The two microcrystalline celluloses, Starch 1500 and sodium chloride also showed low SIR values and held an intermediate position in the graph (Fig. 4.9).

Tablet deformation before failure during the direct tension test was monitored as mentioned in section 2.2.3. Work of failure and associated parameters were, therefore, obtained and are presented in Tables B.6-B.8. Fig. 4.10 illustrates axial work of failure values plotted against compaction force for the materials tested. It can be seen, that axial work of failure values for materials undergoing plastic deformation during compaction were considerably lower than the radial ones. As in the case of axial tensile strength values, however, a less dramatic difference was obtained for the brittle materials.

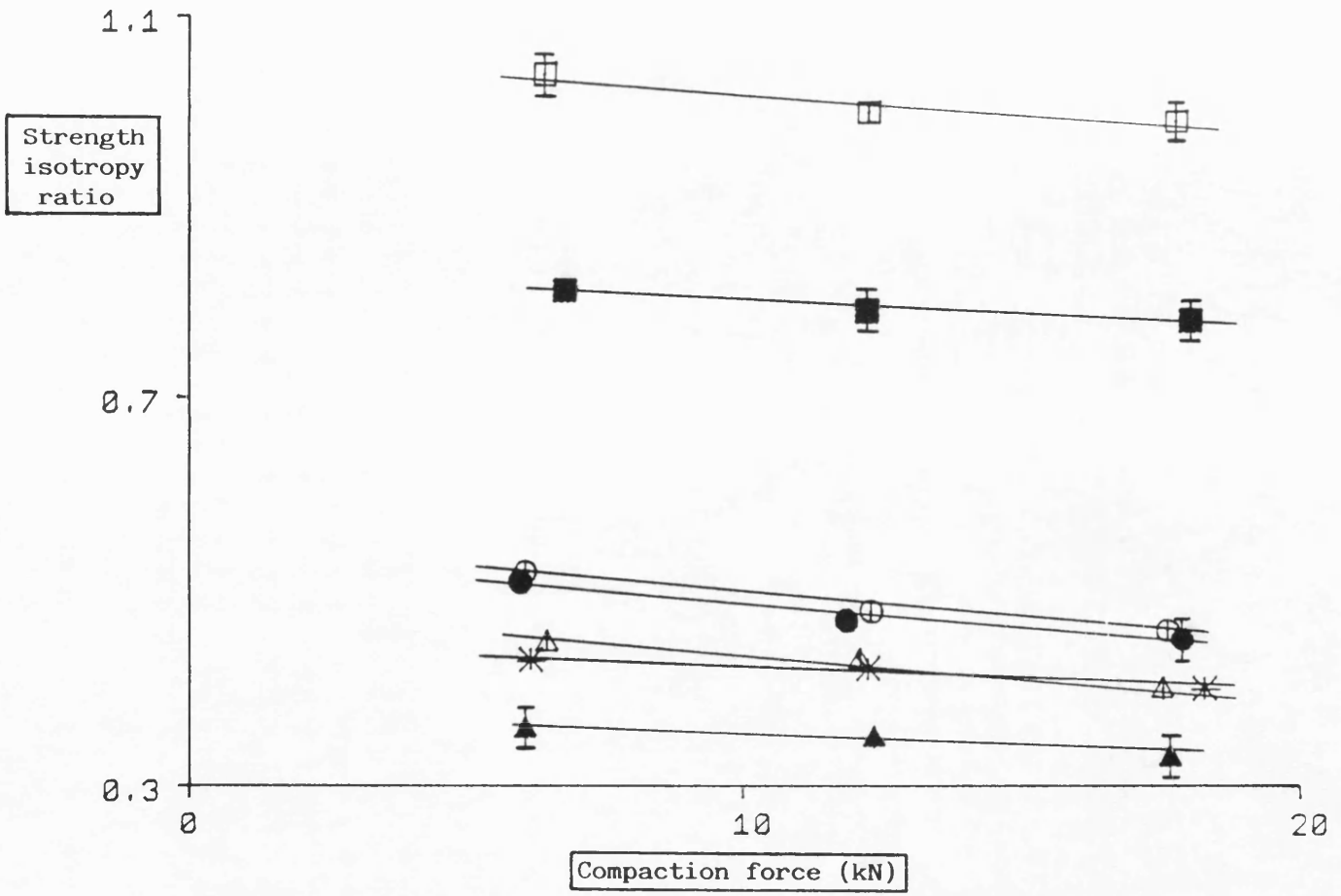

Fig. 4.9 Strength isotropy ratio values at a range of compaction forces.

(Key: page xxiii)

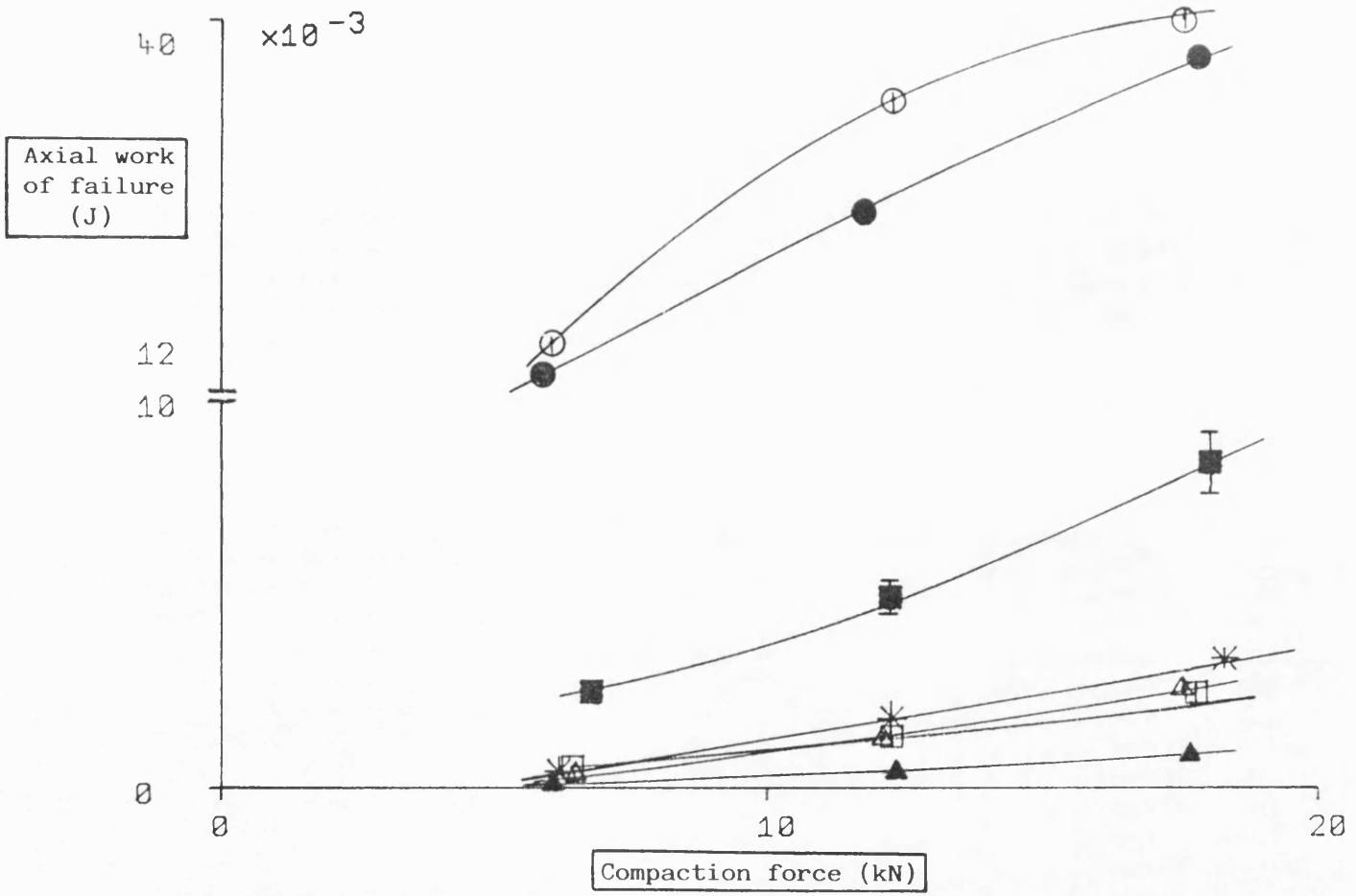

Fig. 4.10 Work of failure during direct tension testing of tablets at a range of compaction forces.

(Key: page xxiii)

Lower axial work of failure values compared with the radial values were also obtained by Jarosz and Parrott (1982), who studied the effect of lubricants on the mechanical properties of tablets by subjecting them to a direct tension test and a diametral loading test. These workers found that, an increase in the concentration of the lubricants they studied, resulted in a decrease in the work needed to cause tablet failure. This effect was especially marked in the axial plane which was considered to be the weakest plane in a tablet.

The results presented here demonstrate the difficulty in predicting tablet strength from a knowledge of the consolidation mechanism only. Plastic deformation does not necessarily lead to compacts of adequate mechanical properties. The surface area over which bonding occurs is also a primary parameter that needs to be considered. Comparison of data obtained from axial and radial failure of tablets provides information regarding strength isotropy in tablets and potential capping tendency (Duberg and Nystrom, 1985). Therefore, studies on tablet strength should be performed in both the axial and radial planes over a wide range of compaction forces in order to have a better understanding of the bond distribution within the tablets and to facilitate prediction of potential problems during compaction.

4.3 SCANNING ELECTRON MICROSCOPY

The samples to be tested were all stored under the same conditions (53% relative humidity and 25C). They were placed on an aluminium planchette using a film of double-sided adhesive tape. The specimens were coated below a gold film in the chamber of a sputter coater (Type S150B, Edwards High Vacuum, Crawley, U.K.). They were then mounted on the specimen stage with the use of a conducting paint and introduced into the column of the scanning electron microscope (Type T330, JEOL, Japan). The chamber was evacuated and the appropriate accelerating voltage, usually 5kV, was selected depending on the sensitivity of the specimen tested at the time.

Each material was initially examined as a powder. In this case, a small representative sample was removed from the material and studied regarding its particle morphology. The surface of the tablets before and after failure during a direct or an indirect tension test was also examined. The size and shape of particles before and after compression were compared and this revealed useful information regarding the deformation mechanism of materials, as discussed below.

Fig. C.1 illustrates the surface morphology of Avicel PH102 and Emcocel 90M powders prior to compaction. Their fibrous nature can be seen but there are no obvious differences between them. Starch 1500 (Fig. C.2) seems to consist of smooth round

particles of a wide size distribution. The cubic crystals of sodium chloride (Fig. C.7) clearly distinguish themselves from the other materials. Sodium bicarbonate particles (Fig. C.8), in turn, show relatively smooth surfaces, the overall structure being planar. Numerous surface irregularities can be observed in anhydrous lactose particles (Fig. C.8). Similarly, Emcompress consists of relatively large particles with many surface projections and indentations (Fig. C.9).

Figs. C.1-C.9 also show the surfaces revealed after the failure of the tablets during diametral loading and allow their consolidation pattern to be assessed. Plastic deformation undergone by materials such as the microcrystalline celluloses and Starch 1500 is obvious; primary particles with approximately the same size as before compaction can be observed. Similarly, particle fragmentation was not observed in sodium chloride tablets. Sodium bicarbonate, however, showed a certain degree of fragmentation. In comparison, substantial particle size reduction seems to have occured in Emcompress and anhydrous lactose compacts.

CHAPTER FIVE

STRESS RELAXATION

5.1 STRESS RELAXATION BEHAVIOUR OF MATERIALS

Stress relaxation experiments were performed on a range of materials known to consolidate by different mechanisms: Avicel PH102, Starch 1500, anhydrous lactose and Emcompress. As explained in section 2.2.4, the materials were loaded up to the peak force and then the strain was held constant while the drop in force was monitored for 5 minutes. The peak loads selected in this study were 2 and 6kN.

Force decay with respect to time for the materials that had been loaded to 2kN at 10mm/min, are shown in Fig. 5.1. It can be seen that the curves approach an asymptotic value of force. The results derived from such plots are given in Table D.1.

The high values for total force drop shown by Starch 1500 indicate that this material is capable of extensive stress relaxation. Relative force drop, calculated as the total force drop divided by the peak force, enables the amount of stress relaxation undergone by different materials to be compared (Fig.

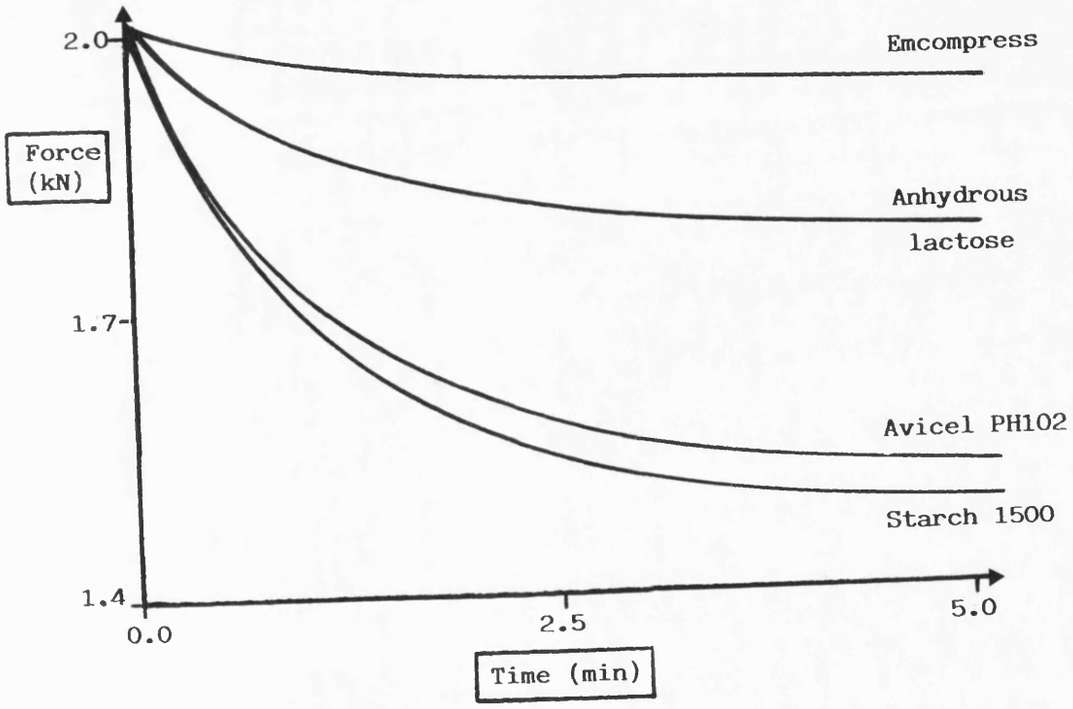

Fig. 5.1 Stress relaxation curves for the materials loaded to 2kN at 10mm/min.

5.2a). Again, Starch 1500 gave the highest values, indicating a greater degree of time-dependent deformation. On the other hand, Emcompress did not exhibit much stress relaxation and produced the lowest values for total and relative force drop. The materials were ranked as follows:

Starch 1500 > Avicel PH102 > anhydrous lactose > Emcompress

The rate of force decay to half force drop provides a measure of a material's time-dependent deformation. A high value represents a material which can undergo rapid deformation during the early stages of stress relaxation. Again, the materials were ranked as above (Fig. 5.2b).

The effect of strain rate, during the initial loading of materials, on their subsequent stress relaxation behaviour was assessed by raising the powders to peak force during the loading stage, at 10 and 50mm/min. As strain rate is increased, it would be expected that less plastic deformation can take place during compaction. There is, therefore, more potential for time-dependent deformation when the material is held under constant bulk strain. The effect of strain rate on the total force drop was much greater in the case of the plastically deforming materials. In contrast, anhydrous lactose showed a small, and Emcompress no strain rate dependence (Figs. 5.2a and 5.2b), when assessed by either total force drop or rate of force decay to half force drop (Table D.1).

(Key: page xxiii)

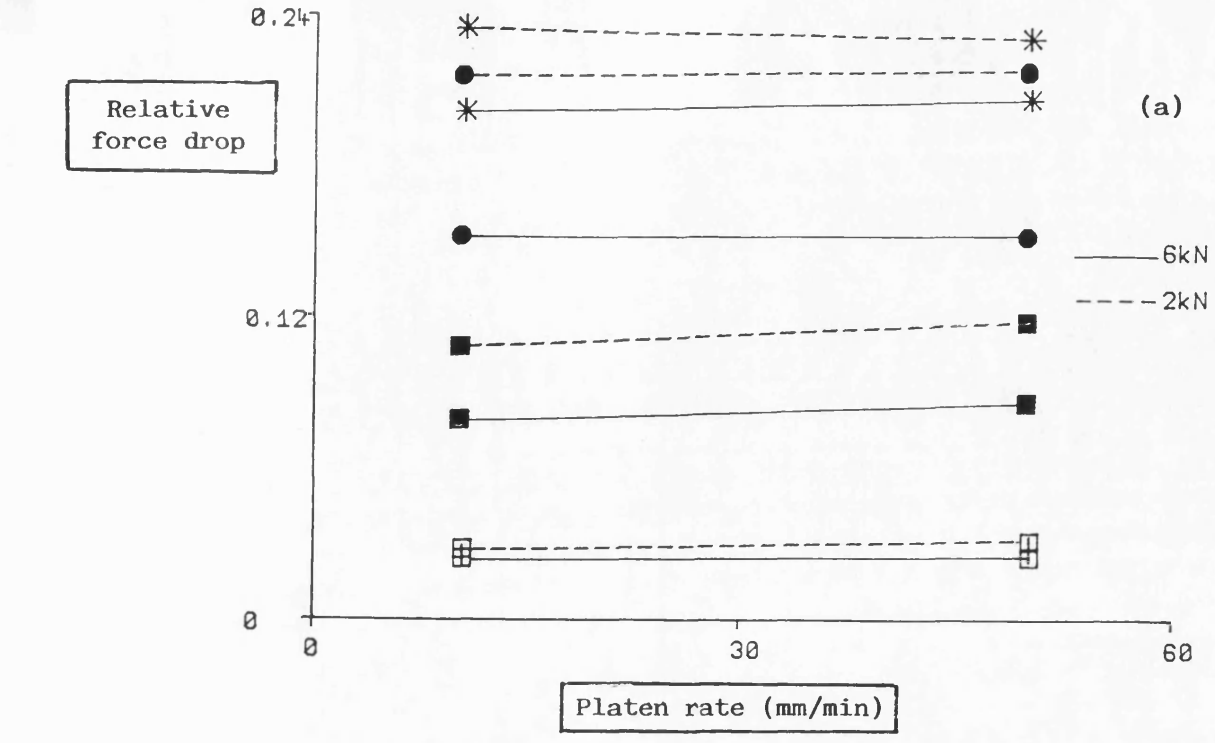

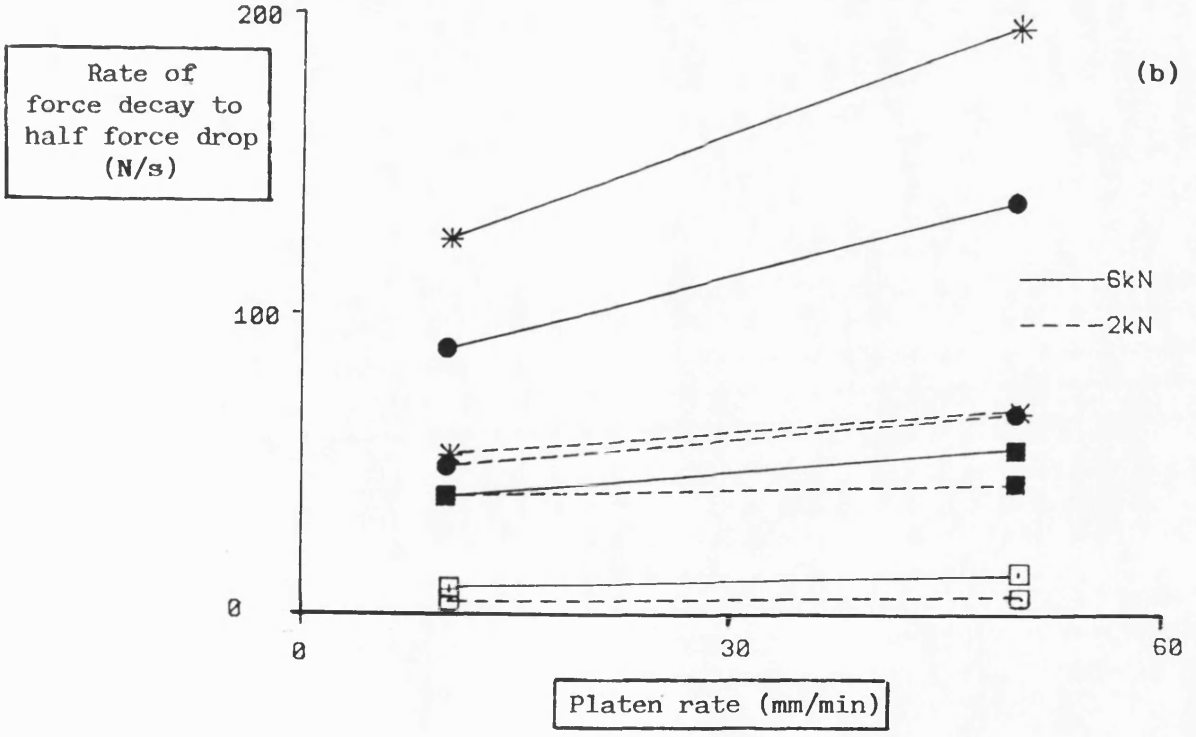

Fig. 5.2 Relative force drop (a) and rate of force decay to half force drop (b) during stress relaxation experiments.

5.2 LINEARISATION OF STRESS RELAXATION DATA

Previous attempts to linearise stress relaxation data have been discussed in 1.3.2.1. In this study, F_t/F_{min} was plotted as a function of the natural logarithm of time, t, as proposed by Baba and Nagafuji (1965):

where,

F_t = force at time t

F_{min} = force at the end of a stress relaxation experiment

A typical plot is illustrated in Fig. 5.3. It can be seen, that there is a continuous small change in slope, suggesting that some mechanism or mechanisms taking place initially, gradually become negligible. Despite this slight deviation from linearity, high values for the correlation coefficient were derived from a linear regression of these plots (Table D.2), especially for the plastically deforming materials. The values for the slope and the intercept on the force axis are shown in Table D.2.

The slope provides a measure of a material's ability to undergo deformation as a function of time, under the particular constant strain conditions. High values reflect a high rate of deformation relieving elastic strain, whereas low values are indicative of more gradual stress relaxation. The materials were ranked as follows (Fig. 5.4a):

Starch 1500 > Avicel PH102 > anhydrous lactose > Emcompress

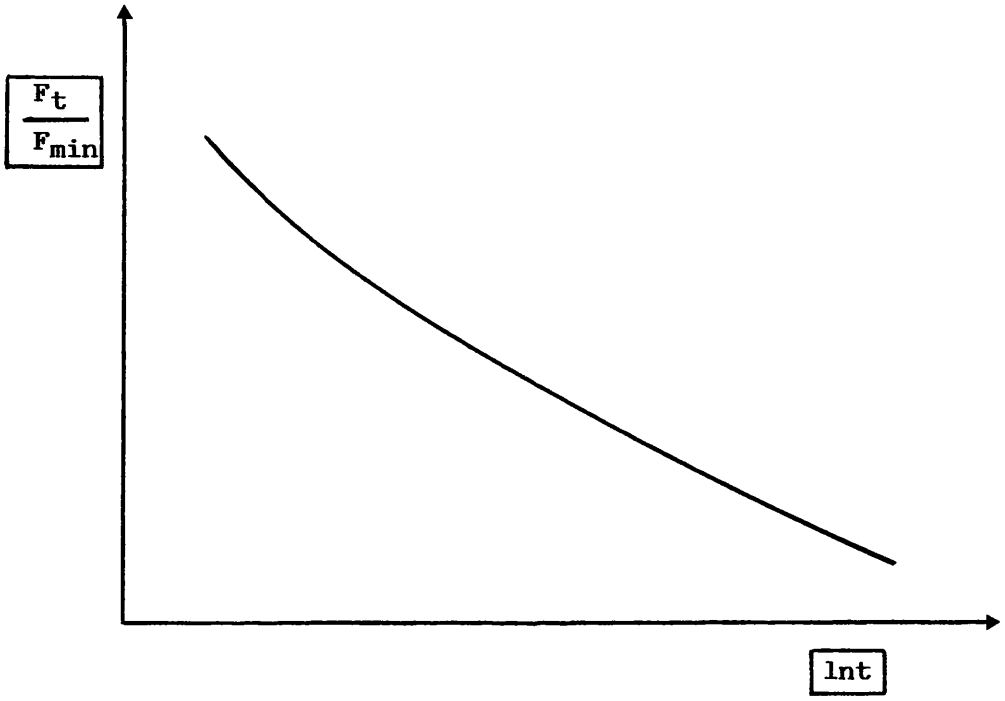

Fig. 5.3 Stress relaxation data plotted as F_t/F_{min} against lnt.

(Key: page xxiii)

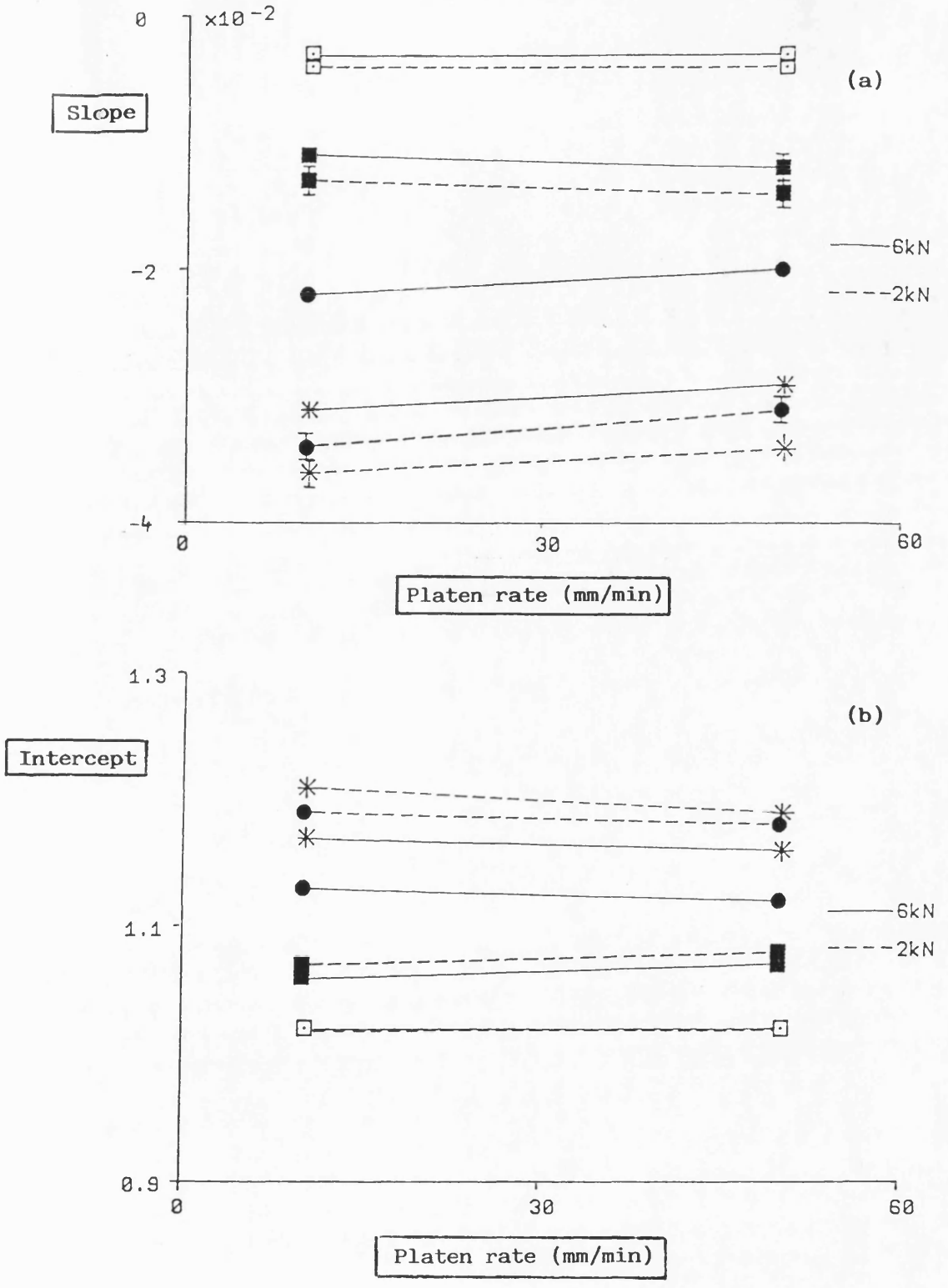

Fig. 5.4 Slope (a) and intercept (b) values obtained from a plot of F_t/F_{min} against lnt.

The intercept on the F_t/F_{min} axis provides a measure of the magnitude of stress relaxation undergone by the material as a function of the applied stress. Again, the materials were ranked as above (Fig. 5.4b).

Since incomplete linearisation was achieved using the approach mentioned above, an alternative mathematical treatment was investigated. Plots such as those illustrated in Fig. 5.5a, in which the curve passes through the origin, and the dependent variable, Y, approaches an asymptotic value as the independent variable, X, increases, are often described by a hyperbolic equation of the form:

$$Y = a \cdot b \cdot X/(1 + b \cdot X) \qquad \text{Eq. 5.1}$$

where,

a, b = constants

If this type of equation fits the experimental data, then a plot of X/Y against X should be a straight line with a slope and an intercept, equal to 1/a and 1/(a·b) respectively (Fig. 5.5b):

$$X/Y = (1/a)\ X + 1/(a \cdot b) \qquad \text{Eq. 5.2}$$

And, therefore,

a = 1/slope, which represents the asymptotic value of Y

The constant a, therefore, has units of Y.

The second constant, b, can be calculated from the slope and the intercept obtained from a linear regression of the plot of X/Y versus X, according to Eq. 5.3:

$$b = \text{slope/intercept} = (1/a)/(1/a \cdot b) \qquad \text{Eq. 5.3}$$

The constant b has the units 1/X.

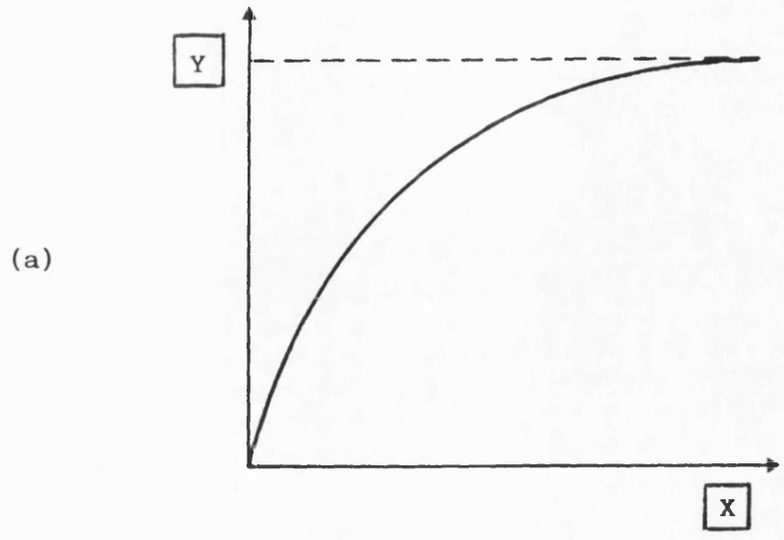

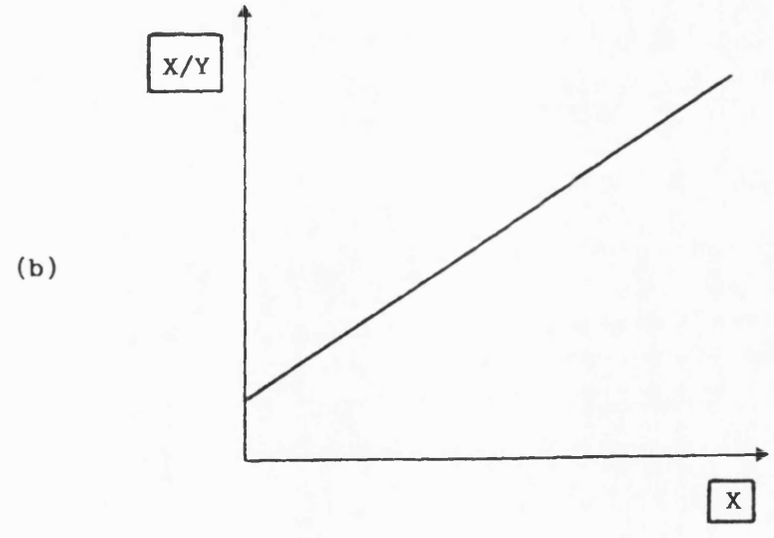

Fig. 5.5 Hyperbola (a) and its linear transformation (b).

In the case of stress relaxation data,

$$(F_{max}-F_t) = a \cdot b \cdot t/(1 + b \cdot t) \qquad \text{Eq. 5.4}$$

where,

F_{max} = force at t=0

F_t = force at time t

t = time

One benefit of this treatment, compared with that of Baba and Nagafuji (1965) for example, is that no estimate of the equilibrium value F_{min} is required. The inverse of the gradient of such a plot, a, represents the total force drop at equilibrium, i.e. equals the total stress relaxation undergone by the material and, therefore, reflects a material's ability to relieve elastic strain. Furthermore, the constant b, calculated from Eq. 5.3 as above, is a measure of the rate at which a material undergoes time-dependent deformation during stress relaxation. As time approaches zero, the term $(1 + b \cdot t)$ approaches unity, i.e.:

when $t \rightarrow 0$, then $(1 + b\ t) \rightarrow 1$

And, therefore,

$$F_{max}-F_t \rightarrow a \cdot b \cdot t$$

In other words, at short times there is a linear relationship between the force drop and time. This latter can be extremely useful, since stress relaxation undergone by a material in the early stages of an experiment is of particular interest as far as its time-dependent compaction behaviour is concerned.

The results for linear regressions of plots of $t/(F_{max}-F_t)$ against t for the four materials (Fig. 5.6) are given in Table D.2. Clearly, the correlation coefficients obtained in this case are closer to unity than those for the Baba and Nagafuji (1965) treatment (Table D.2).

The differences between the materials were not so apparent as in the linearisation treatment mentioned in the first part of this section (Figs. 5.4a and 5.4b) when the slope and the intercept from the linear regressions were plotted for the four materials (Figs. 5.7a and 5.7b). The results for Emcompress, however, were separated from the others, due to particularly high values for the gradients and the intercepts on the $t/(F_{max}-F_t)$ axis. A similar plot was obtained where values of the constant b were presented for the materials (Fig. 5.8b).

The differences in the stress relaxation behaviour of materials are demonstrated when the constant a of Eq. 5.4 is plotted in Fig. 5.8a. As explained above, this parameter represents the total force drop at equilibrium and, therefore, provides a measure of the full extent of stress relaxation the material is able to undergo when loaded at a certain force. The materials were ranked as follows:

Starch 1500 > Avicel PH102 > anhydrous lactose > Emcompress

Finally, Fig. 5.9 shows the values obtained for the product a·b, i.e. the rate of force drop at times close to zero. This parameter is of particular interest, since it provides information regarding the stress relaxation behaviour of

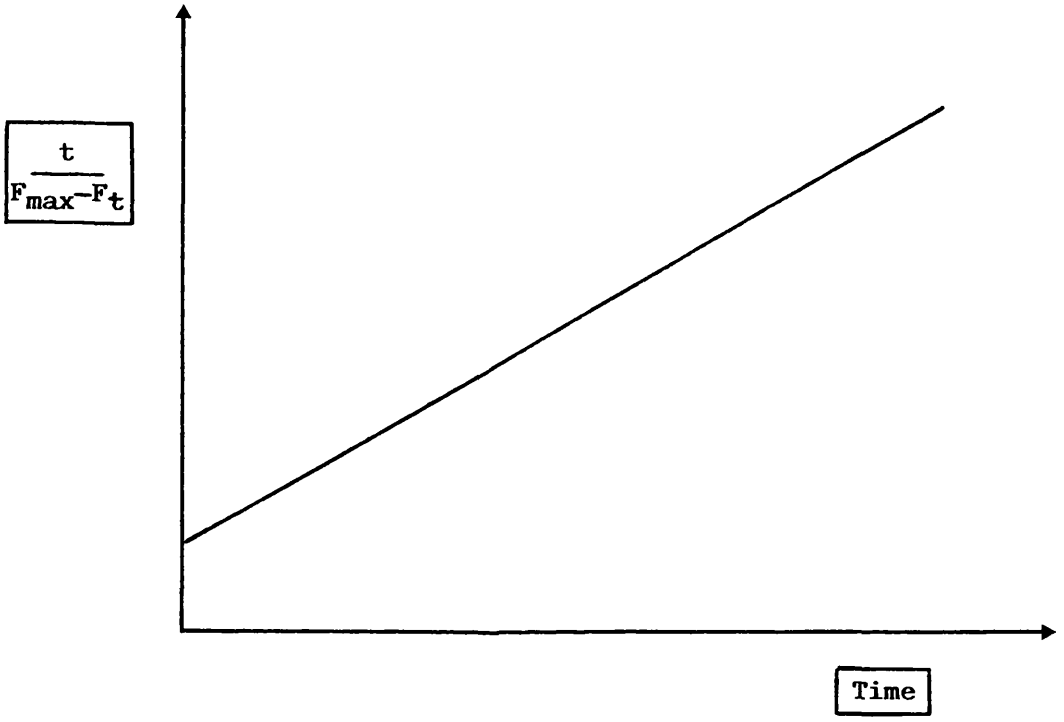

Fig. 5.6 Stress relaxation data plotted as $t/(F_{max}-F_t)$ against t.

(Key: page xxiii)

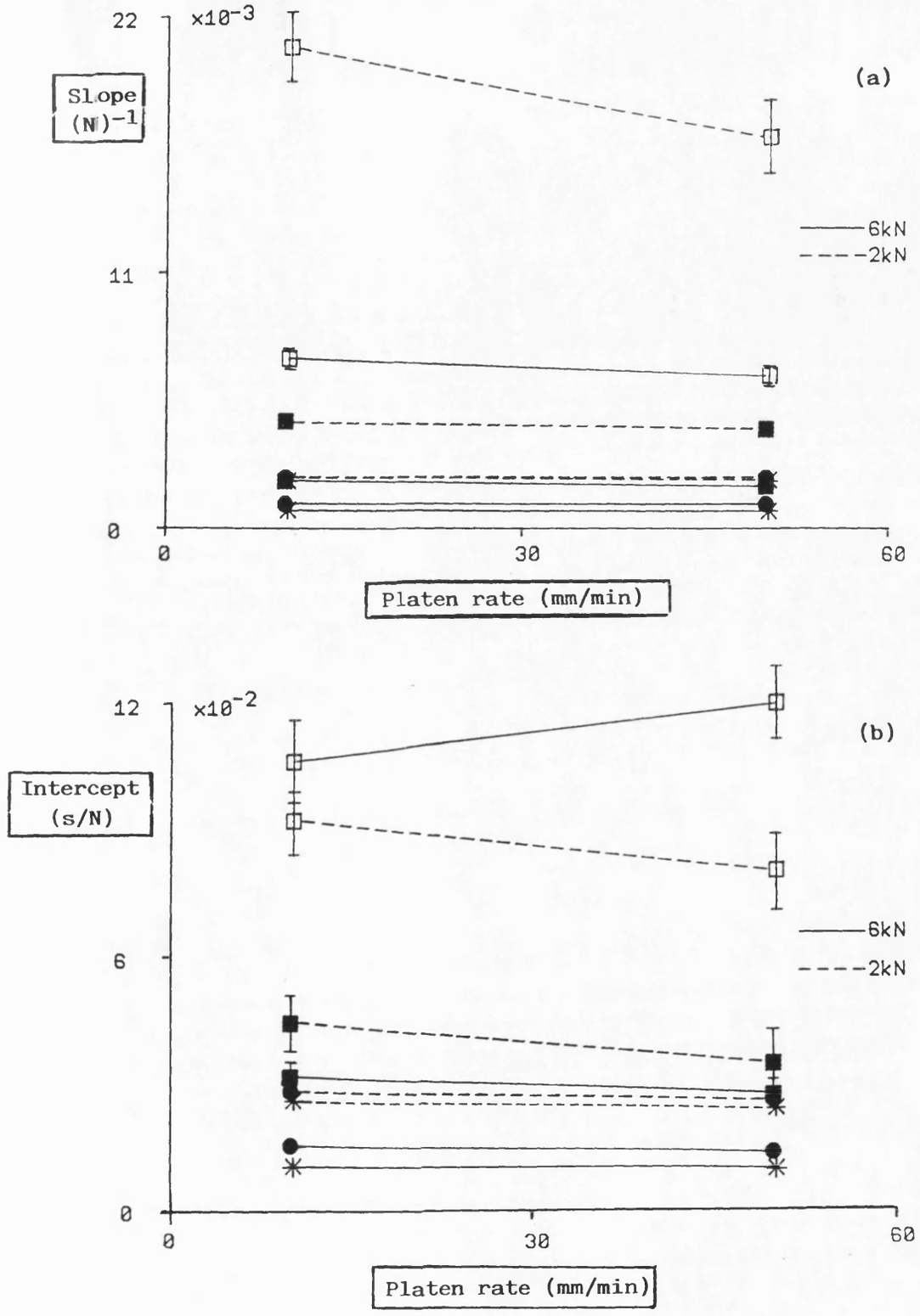

Fig. 5.7 Slope (a) and intercept (b) values obtained from a plot of $t/(F_{max}-F_t)$ against t.

(Key: page xxiii)

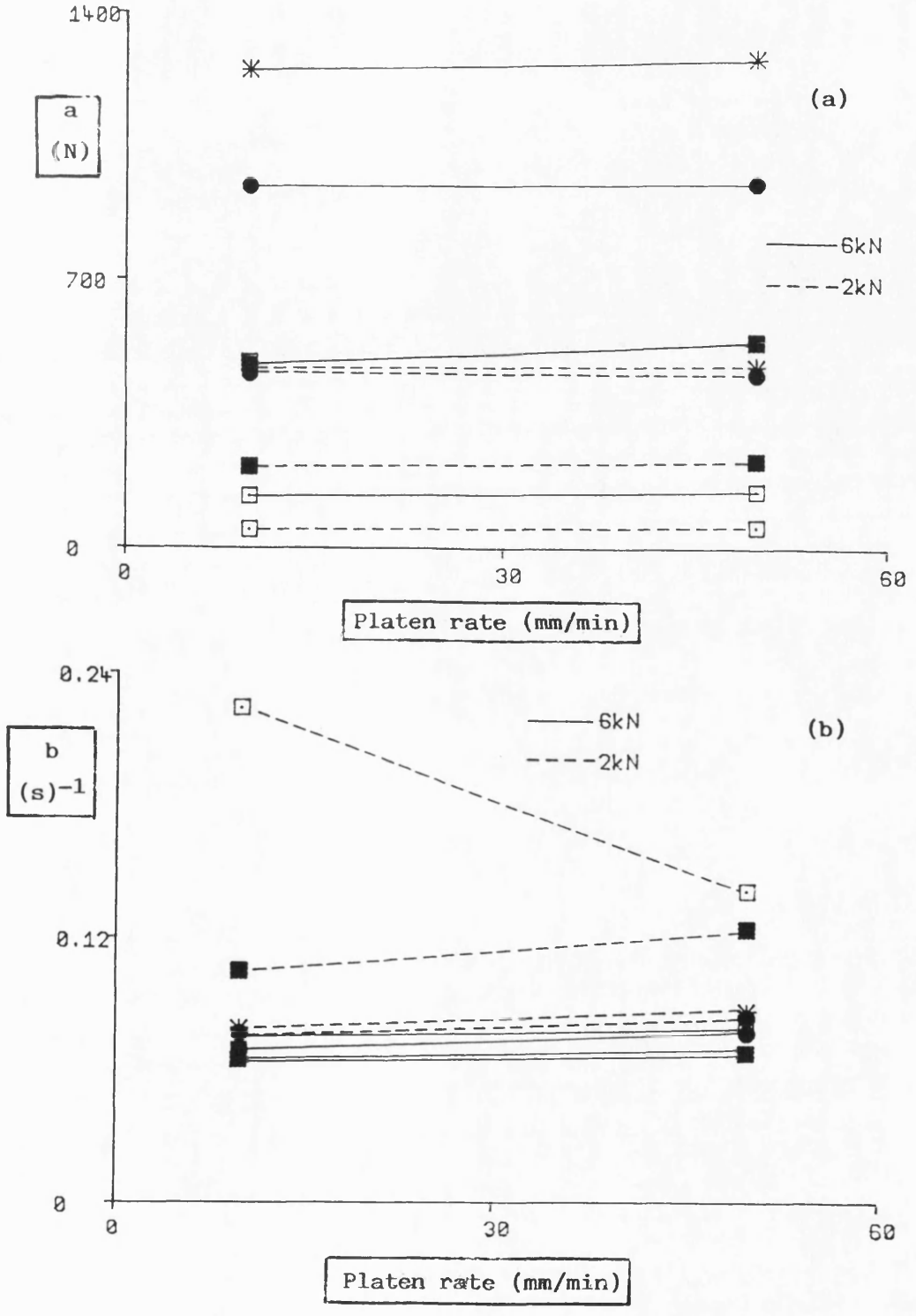

Fig. 5.8 Values for the parameters a (a) and b (b) of the hyperbolic equation used to describe stress relaxation data.

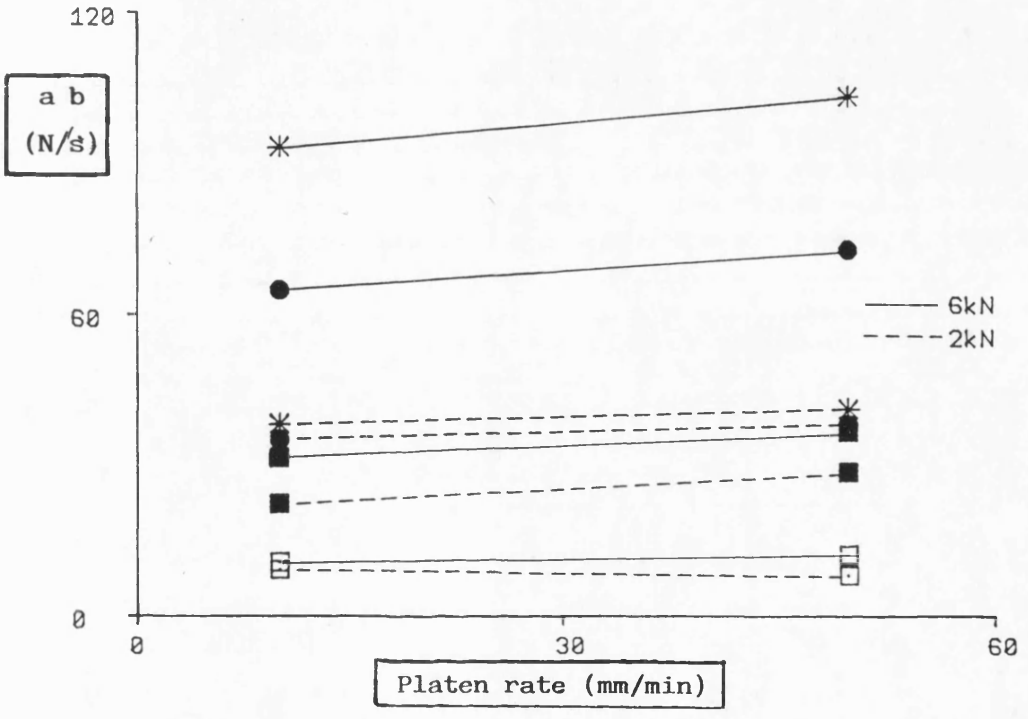

Fig. 5.9 Values for the product a.b of the parameters a and b of the hyperbolic equation.

materials during short time intervals following compaction, and may be related to contact time effects during compaction.

It must be noted, that the parameters obtained from stress relaxation experiments do not offer any detailed information regarding the viscous properties of the materials alone, since the results depend on both their viscous and viscoelastic behaviour. Furthermore, such parameters disregard any deformation undergone during the initial loading of the materials and cannot, therefore, be used to predict powder consolidation during compaction.

However, stress relaxation data were found to be well described by a hyperbolic relationship of the form of Eq. 5.1. Two constants, a and b, can be obtained, which define the extent and rate of stress relaxation of a material, respectively. These parameters can be extremely useful in ranking materials according to their time-dependent tendencies. In particular, the product a·b, which characterises stress relaxation behaviour of a material at short times may well prove to be an easy and realistic method of characterising time-dependent consolidation.

CHAPTER SIX

CREEP ANALYSIS

Prior to testing different materials, it was necessary to undertake a series of initial experiments in order to validate the method used and to select the optimum experimental conditions. The effect of several factors was studied, such as the applied load, the duration of the creep test, the weight of powder used and the loading rate. An assessment was also made of the benefits of applying the creep test to preformed compacts in comparison with applying the load directly to a loose powder. The creep behaviour of different materials could be compared on the basis of changes occuring either at identical constant stress or equal relative density. The relative merits of these two approaches were evaluated. Furthermore, the effect of shape and dimensions of dies and punches on creep data was also studied.

6.1 PARAMETERS AFFECTING CREEP EXPERIMENTS

6.1.1 Effect of Applied Load and Test Duration

Clearly, one variable that affects the parameters obtained from the creep test, is the load applied to the powder bed. Preliminary tests showed that creep results depended on the load and, therefore, on the porosity of the compact under test. Thus, the different materials could be compared either on the basis of identical constant stress or of equivalent relative density. It was concluded, that since the stress applied was accounted for in the calculation of creep compliance values, and since creep parameters are dependent on the void space in the compact, comparison of the creep behaviour of materials with respect to their relative density was more meaningful.

Furthermore, creep tests were performed for a range of lengths of time in order to assess the effect of time on the parameters obtained. In theory, a material loaded at constant stress, in an unconstrained condition, would flow in a viscous manner described by the viscosity coefficient, $1/k_1$. However, in the case of a particulate solid constrained in a die, viscous flow of the material into the void space will lead to a decrease in porosity with time, affecting the ability of the material to flow further. This will be reflected by a gradual decrease in slope k_1 and an increase in the viscosity coefficient.

Samples of materials known to exhibit different consolidation behaviour, i.e. Starch 1500 and Emcompress, were loaded at 3 and 8kN respectively and creep compliance was monitored for 60, 90, 120, 300 and 600 seconds. The results can be seen in Table E.1. The experiments which ran for 60s gave an insufficient linear portion for a meaningful linear regression to be performed. On the other hand, 120, 300 and 600 seconds experiments showed no significant improvement in the values of the correlation coefficient obtained from a linear regression analysis of the linear part of the creep curves. Although there was a tendency for the viscosity coefficient values obtained for Starch 1500 to increase with time, no significant changes were observed. Based on the above results, 90 seconds was the time interval chosen for the creep experiments that followed.

6.1.2 Creep Testing of Powder and Preformed Compacts

A creep test can be performed on either a loose powder or a compact. The purpose of this work was to study the effect of the state of the material prior to applying the constant stress. Creep analysis was, therefore, performed on powders as well as on preformed compacts of relative density 0.6 and 0.8. The materials tested were Avicel PH102, Starch 1500, anhydrous lactose and Emcompress. Preliminary tests were performed to determine the load required to produce compacts of the above

mentioned densities for each material. The compacts were allowed to recover fully in the die at 25C and 53% relative humidity for 48 hours. The samples were then loaded at a range of loads and their creep compliance monitored as a function of time.

It was concluded that there was no significant effect of the initial state of the material on its subsequent creep behaviour under constant stress, provided the applied load was sufficient to cause further densification when a compact was employed. More reproducibile results were achieved when preformed compacts, especially those of relative density 0.8, were used. Because, however, of the additional procedure involved in the compact formation, it was preferred to use powder samples and increase the number of replicates to be tested instead. Furthermore, the use of powder samples allowed the creep behaviour of the materials to be assessed over a larger range of relative density, i.e. from 0.5 upwards.

6.1.3 Effect of Powder Mass

Part of the procedure for validating the experimental technique used in creep analysis was a study of the effect, on the creep parameters, of varying the mass of powder tested. Starch 1500 and Emcompress were chosen as materials exhibiting extreme densification behaviour.

Powder samples equivalent to 25, 50, 100 and 150 percent of

the mass used for each material in previous sections of this work (Table 2.7) were loaded under the same conditions. The lowest amount of powder used was chosen so that at least a thin layer of material covered the lower punch. The maximum amount was limited by the depth of free space in the die and by the amount of powder which could be poured into it without the need for tapping or precompression. The load applied was 3kN in the case of Starch 1500 and 8kN for Emcompress. This was chosen so that their compacts had the same relative density at the beginning of the creep test.

The creep data (Table E.2) showed that under the conditions used, there was no significant effect of powder mass on any of the creep parameters for either Starch 1500 or Emcompress. Although reproducibility of the results improved slightly as powder mass increased, it was decided, for comparative purposes, to use the same powder weights as those used in other parts of this work (Table 2.7).

6.1.4 Effect of Loading Rate

The effect of loading rate on the deformation of materials has been an issue well reported (Seitz and Flessland, 1965; Baba and Nagafuji, 1965; Hiestand et al, 1977). Creep testing involves the progressive deformation of materials under constant stress and is, therefore, dependent on their ability to deform

under such conditions.

As already mentioned, the technique used in this study did not allow the instantaneous loading of the material up to the desired constant stress. A time interval, which varied for different materials, elapsed before the load reached the set value. The rate at which this loading occurred, had an important effect on the physico-mechanical properties of the compact at the point when the set stress value was reached and the creep test began.

It was decided, therefore, that since loading rate was an important variable, a detailed study of its effect on the creep parameters was needed. Avicel PH102, Starch 1500 and Emcompress were chosen for comparative purposes. The materials were loaded at 5, 3 and 8kN respectively, so that their relative densities at the beginning of the test were as similar as possible. The crosshead speed was set at a range of levels, i.e. 2.5, 5, 10, 25 and 50mm/min. Although attempted, it was not possible to use higher rates due to the increasing difficulty of stopping the drive mechanism before the load exceeded the required value. For the same reason, it was also found that at the high rates used, it was necessary to adjust the setting of the constant stress module below the required stress. Preliminary tests allowed this lower setting to be determined. When the set constant stress was reached, the setting was quickly returned to the correct value and the test performed as normal.

Although statistically insignificant, there was a tendency

for the relative density of Avicel PH102 and Starch 1500 compacts at the start of the creep test to decrease as the loading rate increased. Such an effect might be expected since deformation of these materials is known to be time-dependent.

The viscosity coefficient values obtained for these two materials showed an increase with loading rate (Fig. 6.1a). This suggests that the initial rate of load application and, therefore, the resulting structure within the materials reduces their ability to deform plastically under constant stress. Furthermore, J_i values, estimated as mentioned in section 2.2.5.1, showed an increase with loading rate for these two materials (Fig. 6.1b). This indicates a larger potential for retarded elastic deformation, possibly due to the relatively large amount of energy stored in the elastic region and the increased viscosity of the materials when high rates are used.

It is interesting, that when the stress relaxation behaviour of these materials was studied (sections 5.1 and 5.2), an increase in loading rate resulted in an increase in the relative force drop and in the rate of force decay to half force. This was attributed to the material exploiting its potential for time-dependent deformation, that was not utilised during the initial load application. These creep results suggest that high loading rates reduced their ability to deform plastically, while the potential for time-dependent viscoelastic deformation was increased. The changes monitored during the stress relaxation experiments may, therefore, be a result of a

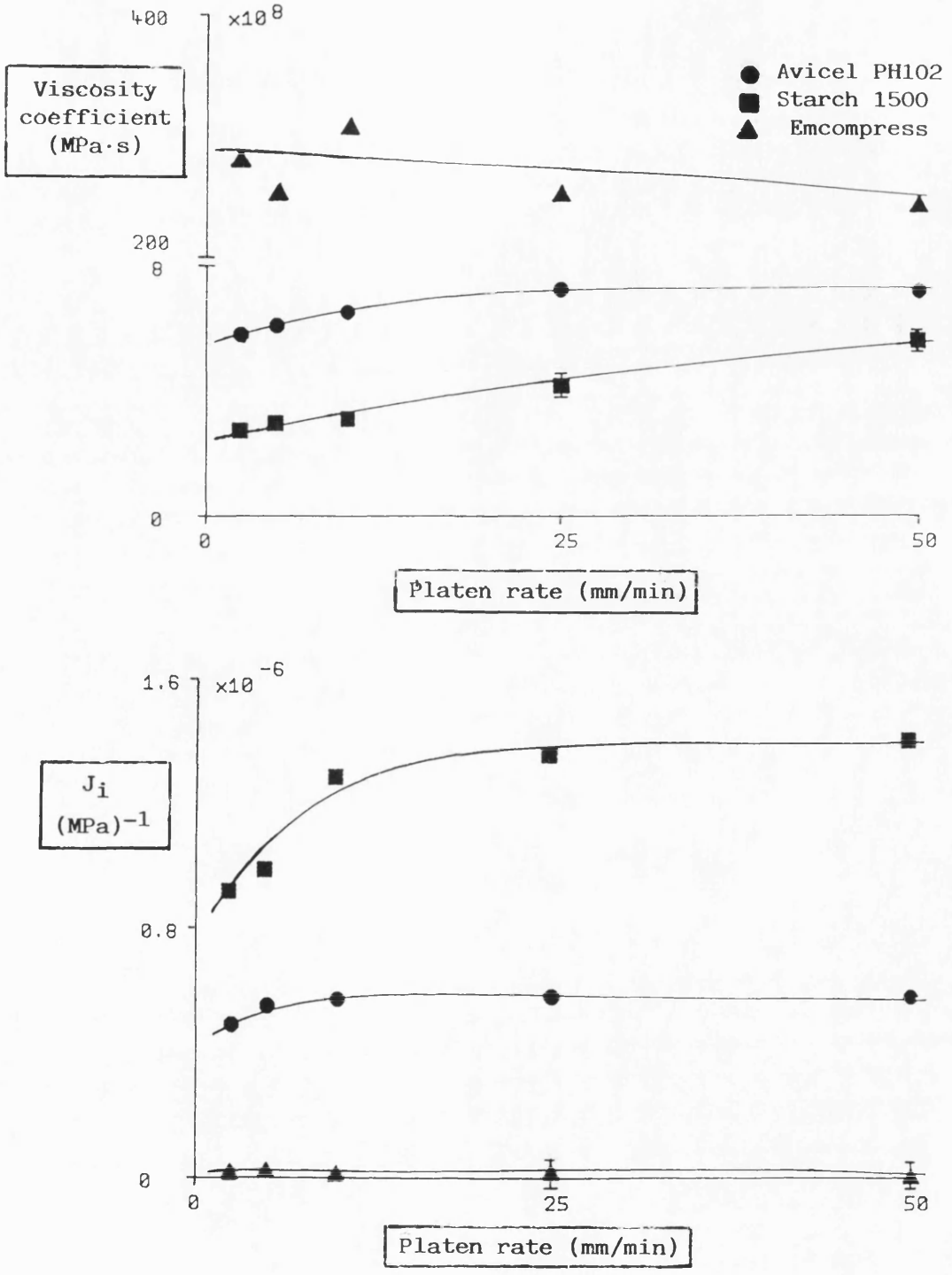

Fig. 6.1 Effect of initial loading rate on the viscosity coefficient and J_i values of Avicel PH102, Starch 1500 and Emcompress.

higher degree of viscoelastic deformation of the materials.

Finally, none of the creep parameters obtained for Emcompress was affected by the loading rate (Fig. 6.1). This was not unexpected since brittle fracture is known to be rate independent.

6.1.5 Effect of Tooling Dimensions

Creep analysis involves the application of a constant bulk stress to a material. In a non-isotropic system, the resulting elastic, viscous and viscoelastic deformation will depend on the magnitude of the stresses developed locally within the material. Since punch geometry affects the stress distribution within a powder bed (Sixsmith, 1980), the effect of punch diameter and concavity on creep compliance was studied using two materials, Starch 1500 and Emcompress, which represent extremes in terms of their consolidation behaviour. The effect of punch diameter was evaluated using a series of flat-faced punches of different diameter (7.9, 10.0, 12.7 and 14.2mm). In addition, to study the effect of punch concavity, creep behaviour of each material was monitored between a flat-faced lower punch of 12.7mm diameter and a range of upper punches of different radii of concavity: 6.3, 8.0 and 16.5mm. In the latter case, tablet volume was calculated from the radius and depth of curvature and thickness and diameter of the cylindrical portion of the tablet. The

results are shown in Tables E.3 and E.4.

Concavity did not affect any of the creep parameters obtained for either material (Table E.3). Punch curvature is most likely to affect the stress distribution of the material within the convex segment. The results imply, that there is no apparent effect in the cylindrical portion and that the axially applied pressure, which remained effectively unchanged, is the main factor influencing the creep behaviour of the compact.

During compaction of particulate materials in a die, the pressure transmitted to the lower punch is lower than the pressure applied by the upper punch. The difference between these two pressures is smaller when the die diameter is increased and compact thickness is decreased at constant volume. Consequently, average compact porosity is reduced for larger diameter punches. This produces less available void space into which the material can deform. This was evidenced by the relative density values for Starch 1500 (Table E.4) and may explain the increase in viscosity coefficient and elastic modulus values, reflecting the reduced ability of the material to deform into the smaller void space.

Brittle materials, such as Emcompress, have a more uniform stress distribution, due to their ability to relieve elastic strain through particle fragmentation. This would explain the absence of any apparent effect of the thickness/diameter ratio on the consolidation behaviour of Emcompress.

6.2 CREEP BEHAVIOUR OF MATERIALS

Fig. 6.2 shows the creep curves obtained at a relative density of approximately 0.7 for the materials. Creep compliance values J_o^*, J_r and J_n for the elastic, viscoelastic and viscous regions are given in Tables E.5 and E.6. In Figs. 6.3-6.5 these values are plotted against the relative density of the compacts at the beginning of the creep test. Fig. 6.3 ranks the materials according to their ability to deform elastically. The well-reported elastic properties of Starch 1500 are confirmed by the particularly high J_o^* values obtained for this material.

In Fig. 6.4, the extent of viscoelastic deformation undergone by the materials under constant stress is illustrated by the compliance J_r. Starch 1500 showed the highest values followed by the two microcrystalline celluloses. As expected, the brittle materials, anhydrous lactose and Emcompress gave the lowest values. A similar graph is obtained when J_n values are plotted against relative density (Fig. 6.5). These values reflect the amount of densification due to plastic deformation of the materials during the 90 seconds of the creep test. Again, the brittle materials showed the lowest values.

In an effort to use creep data to predict the mechanical properties of compacts, the ratio $J_n/(J_o^* + J_r)$, analogous to the plasto-elasticity ratio proposed by Malamataris and Pilpel (1984), was calculated. This compares the amount of recoverable

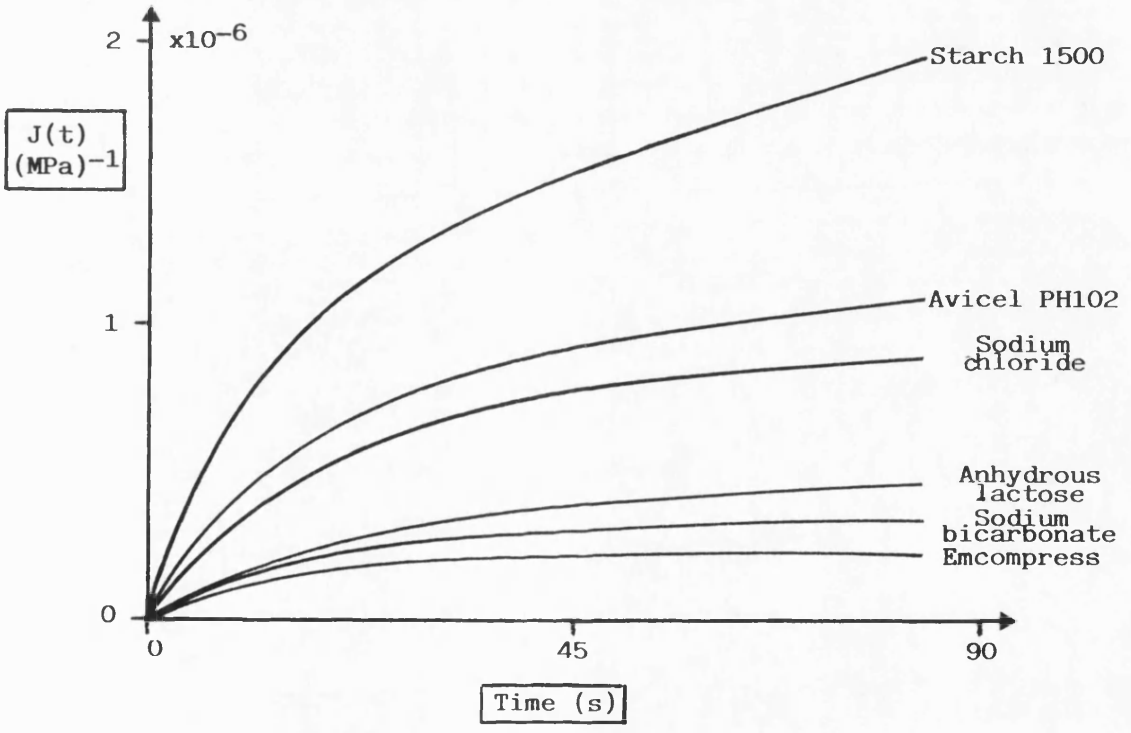

Fig. 6.2 Creep curves for the materials at approximately 0.7 porosity.

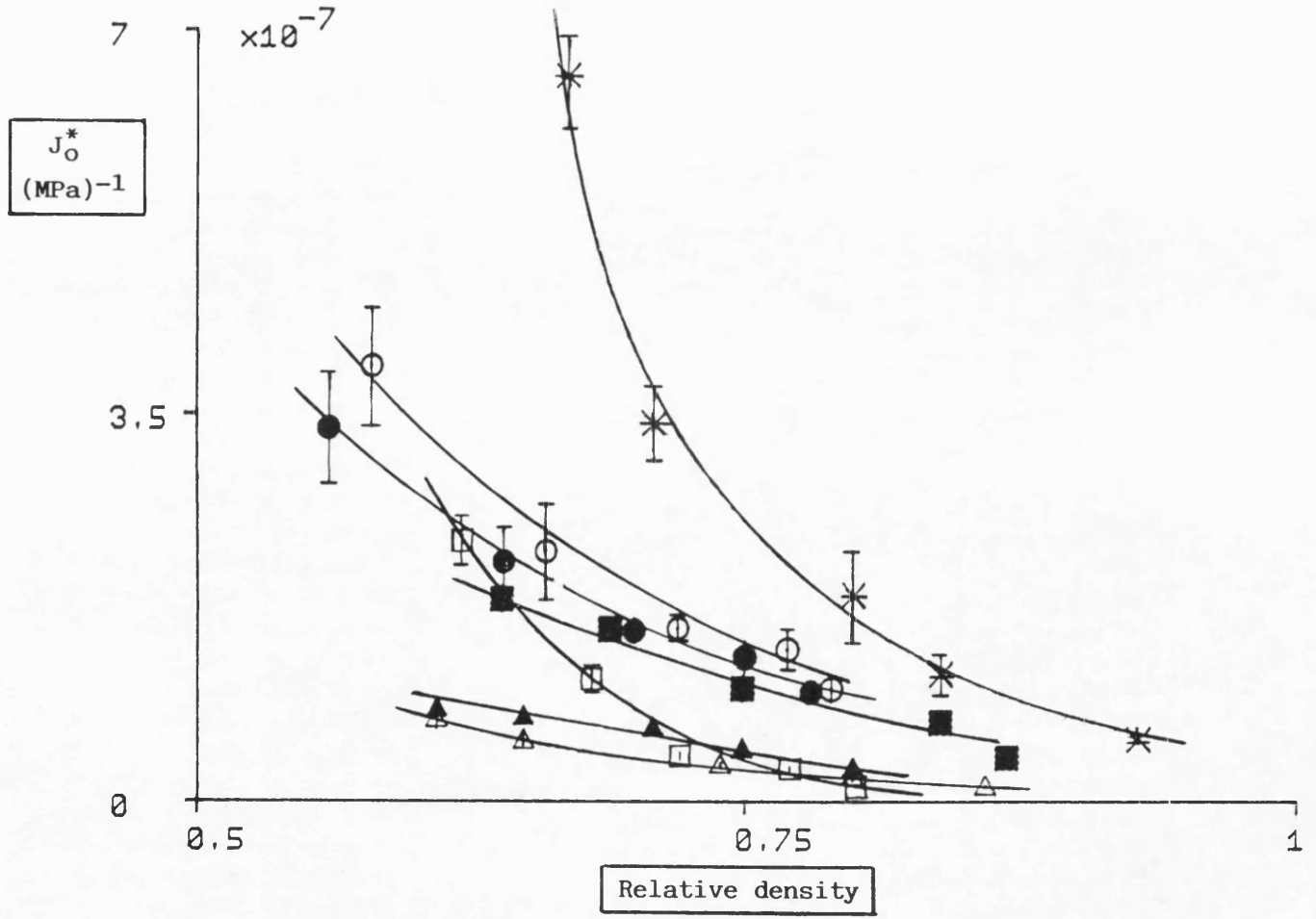

Fig. 6.3 J_o^* values for the materials at a range of relative densities.

(Key: page xxiii)

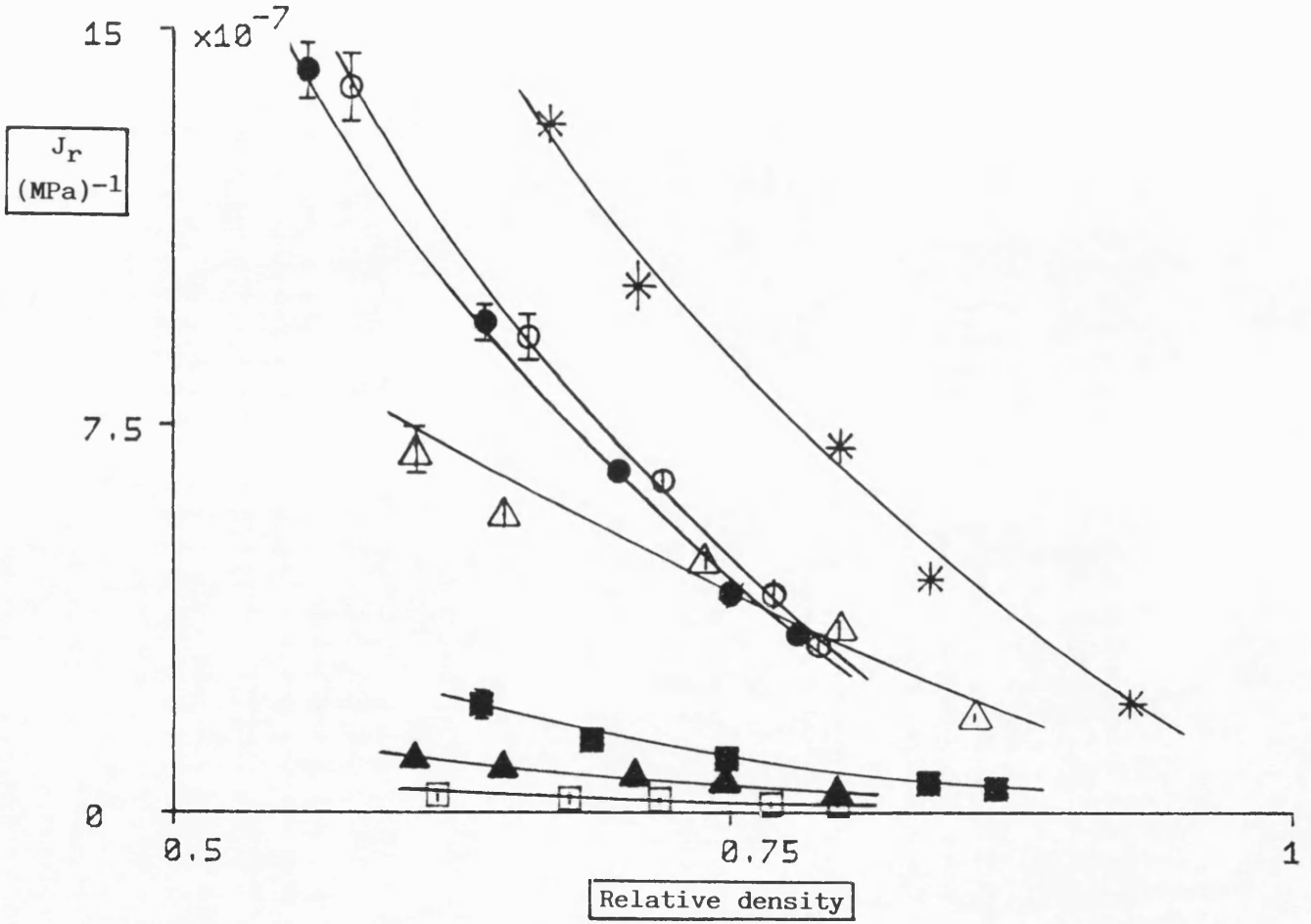

Fig. 6.4 J_r values for the materials at a range of relative densities.
(Key: page xxiii)

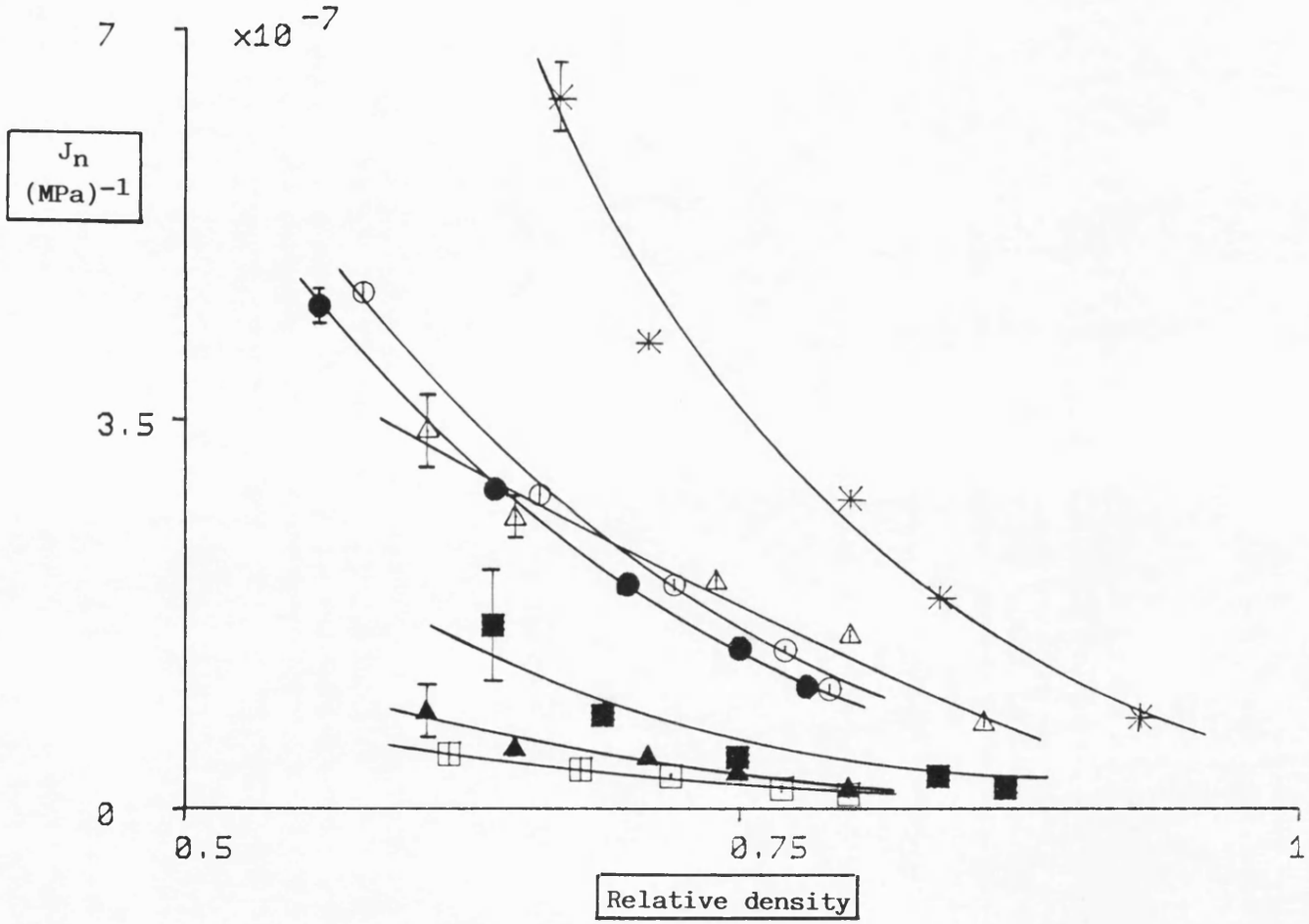

Fig. 6.5 J_n values for the materials at a range of relative densities.

(Key: page xxiii)

($J_o^* + J_r$) and non-recoverable deformation (J_n) of a material under given conditions, thus reflecting its abilty to undergo deformation leading to permanent bond formation. High values of this ratio should indicate a material that undergoes a relatively high degree of non-recoverable deformation, whereas low values should reflect a high proportion of elastic and viscoelastic deformation under load. The values obtained for the materials studied are presented in Tables E.5 and E.6.

It must be noted that, although in theory, viscoelastic deformation of viscoelastic liquids is completely recoverable, this may not necessarily be the case for particulate solids. Here, viscoelastic deformation may not be fully recoverable and may, therefore, contribute to the material's permanent consolidation and bond formation. This may explain why the two celluloses gave the lowest values of this ratio, although they form particularly strong compacts. These values were not greatly different from those obtained for Starch 1500, a material which forms compacts that are mechanically inferior to those of celluloses. Similarly, the values of the $J_n/(J_o^* + J_r)$ ratio obtained for the other materials (Table E.6) could not be used to predict the mechanical properties of their compacts, results for which are presented earlier (sections 4.1 and 4.2).

Tables E.7 and E.8 list the other parameters derived from the creep data. In Fig. 6.6, the viscosity coefficient values, calculated as in 2.2.5.1 are plotted against relative density. This parameter, as opposed to others such as the yield pressure

for example, reflects solely the ability of a material to undergo plastic deformation. From the calculations involved, it becomes obvious that this parameter is independent of other mechanisms such as elastic or anelastic deformation. Starch 1500 gave the lowest values, indicating that its ability to deform plastically is greater than the rest of the materials. Interestingly, the two microcrystalline celluloses gave slightly higher values. These results suggest that the problem with Starch 1500 is not a lack of ability to undergo plastic deformation. If anything, its potential for plastic deformation seems here to be greater than that of the two celluloses. The reason this material does not form compacts of adequate strength is probably its particularly high degree of elasticity, as indicated by the high values of J_o^*.

As expected, values of the viscosity coefficient for sodium chloride were fairly low. This material has also been reported to deform by plastic deformation (Hardman and Lilley, 1970) and these results are, therefore, in agreement with such reports. Lactose values were next in order followed by sodium bicarbonate. The results for sodium bicarbonate confirm conclusions drawn in section 3.3.2, based on its relatively high yield pressure values. These are in conflict with previous reports regarding the ability of sodium bicarbonate to undergo a fair amount of plastic deformation (Duberg and Nystrom, 1982 and 1985). Emcompress gave the highest values of viscosity coefficient confirming its low degree of plasticity.

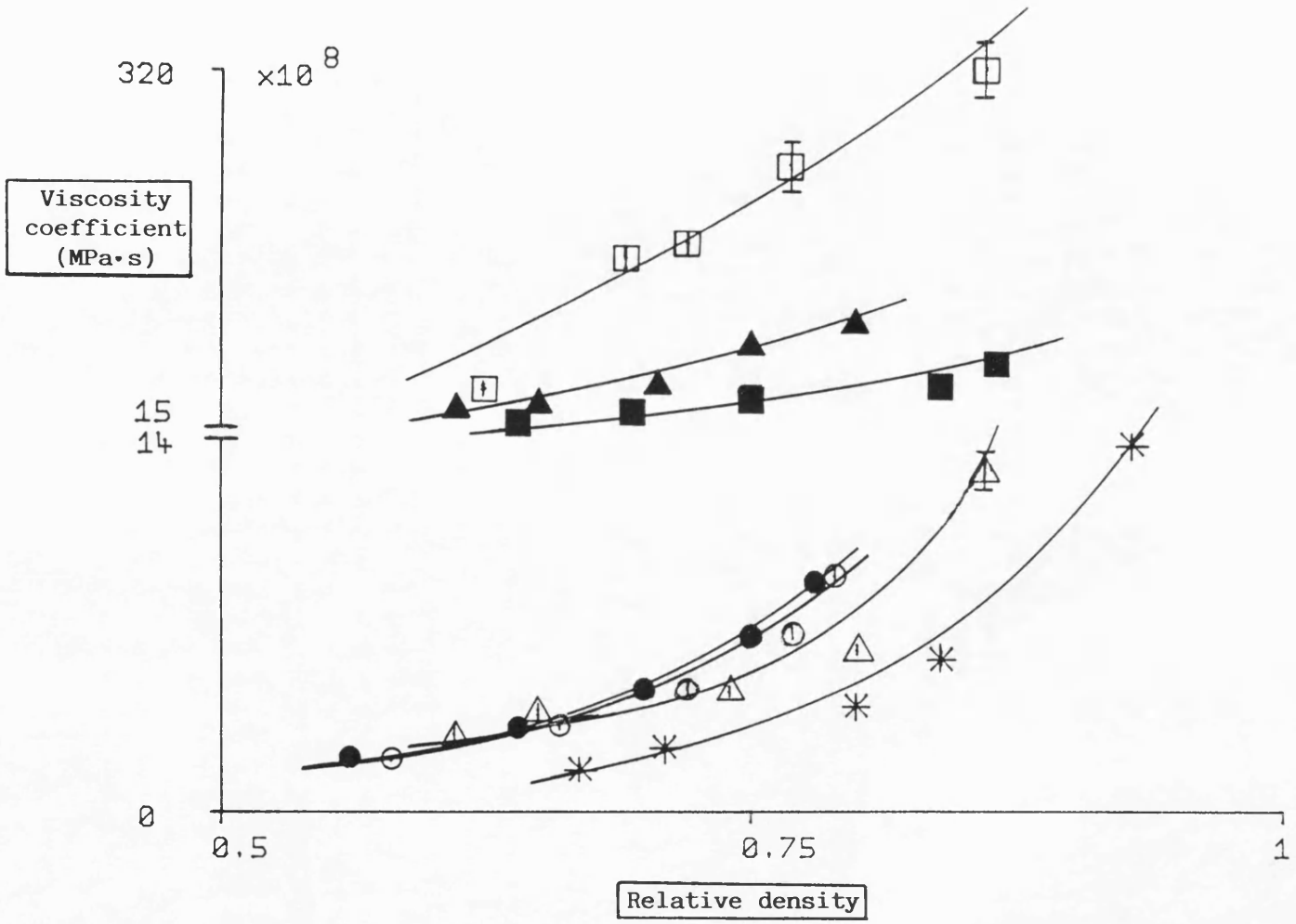

Fig. 6.6 Viscosity coefficient values for the materials at a range of relative densities.

(Key: page xxiii)

It should be noted that the viscosity coefficient values for all the materials showed an increase with increasing relative density. The reason for this is that the viscosity coefficient inversely reflects the ability of the materials to undergo plastic deformation under constrained conditions of bulk volume. As porosity decreases, higher values of viscosity coefficient reflect the increasing difficulty of the materials intruding into the remaining void space. Therefore, the change in this parameter with porosity provides useful information relating to the compaction behaviour of materials.

In Fig. 6.7, elastic modulus values, G^*, are plotted against relative density. It has been emphasised that the values obtained are only estimates of the real values since instantaneous elastic compliance could not be measured (section 2.2.5.1). Nevertheless, the results still enable a ranking of the elastic characteristics of the materials. Starch 1500 gave the lowest values of G^* confirming that it undergoes extensive elastic deformation. Values for Avicel PH102 and Emcocel 90M were also relatively low, particularly at low relative density values. This is in agreement with the relatively high expansion work values obtained for these materials after they were compressed at low loads (section 3.1). Anhydrous lactose and sodium bicarbonate were followed by Emcompress and sodium chloride which gave the highest values of G^*.

Again, the results for G^* depend on the porosity of a compact, increasing as the porosity diminishes at higher loads.

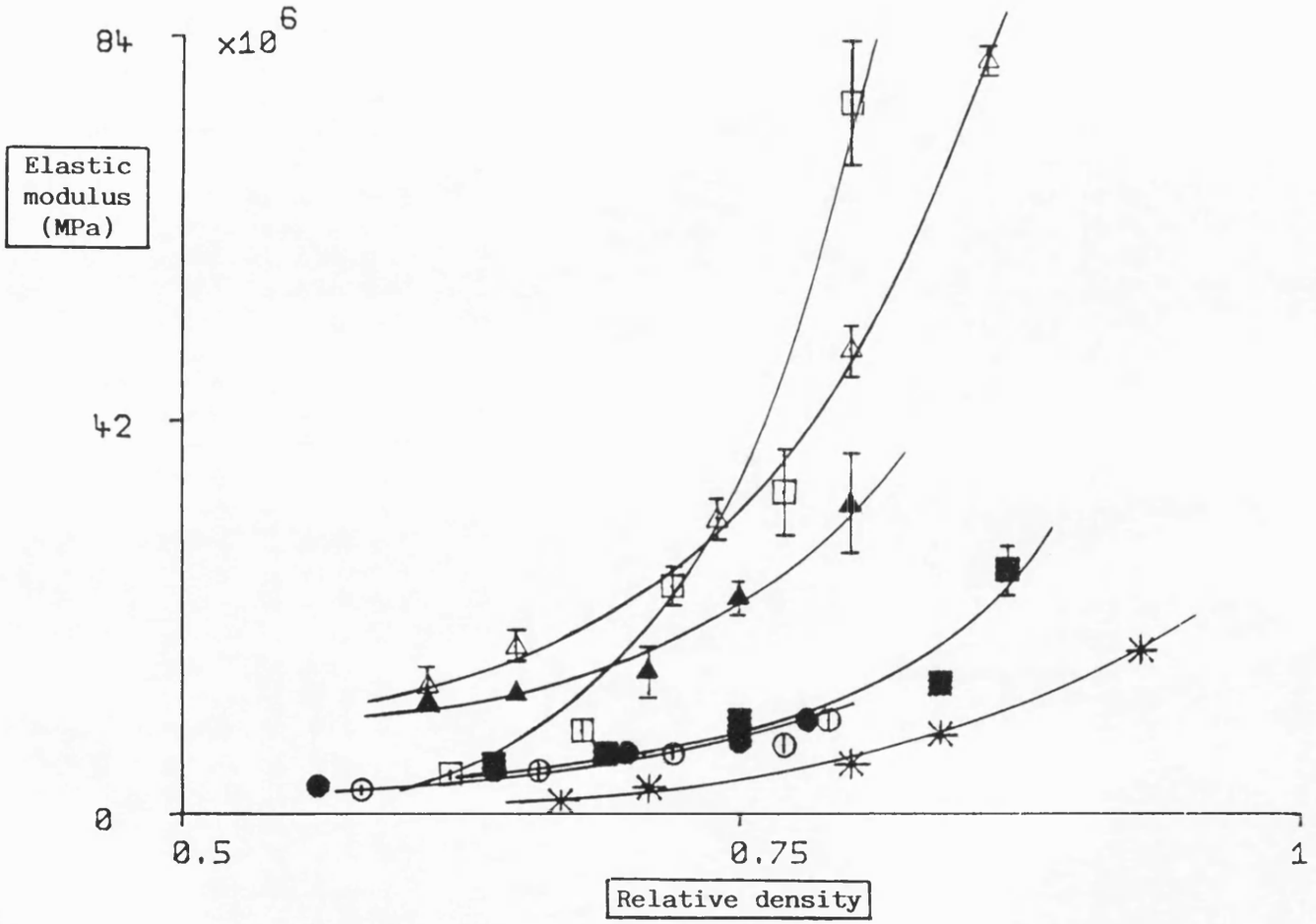

Fig. 6.7 Elastic modulus values for the materials at a range of relative densities.

(Key: page xxiii)

It is logical to expect that, while restrained in a die, the ability of a particulate solidto deform in an elastic manner will reduce as the void space within the powder bed reduces. This effect will depend not simply on the total pore volume, but also on the size and size distribution of the constituent pores.

A number of expressions have been proposed, relating properties of solids to their porosity (Mackenzie, 1950; Gatto, 1950). However, many of these equations have been found to be unsatisfactory for analysing sets of data, possibly because the required conditions, relating to size, shape and distribution of pores within the material for example, were not always met. In 1961, Spriggs proposed an empirical exponential equation. This equation had been suggested by Knudsen (1959) and Duckworth (1953), relating porosity and strength results obtained earlier by Ryshkewitch (1953). According to Spriggs (1961):

$$G = G_o \cdot e^{-r \cdot \varepsilon} \qquad \text{Eq. 6.1}$$

where,

G = elastic modulus of a porous sample

G_o = elastic modulus of the material at zero porosity

ε = porosity

r = an empirical constant

The constant r may be considered as a measure of the change in the material's elastic modulus with respect to porosity.

Determination of the equation constants is facilitated by using Eq. 6.2:

$$\ln G = \ln G_o - r \cdot \varepsilon \qquad \text{Eq. 6.2}$$

Using Eq. 6.1, Spriggs (1961) reported a satisfactory fit of elastic modulus and porosity values for aluminium oxide. He obtained good agreement between the calculated values of elastic modulus at zero porosity and those reported by previous workers.

It was decided to test the fit of data of elastic modulus and viscosity coefficient obtained from creep experiments to Eq. 6.1, since both parameters were found here to vary with porosity. Figs. 6.8 and 6.9 illustrate these parameters plotted according to Eq. 6.2. In order to obtain values of each parameter which represent a material constant, it was decided to extrapolate the relationships to certain porosity values. Two meaningful options were recognised; firstly, porosity values were selected, different for each material, corresponding to the tapped density of the "loose" powders, and secondly, a fixed porosity value was chosen, common for all materials, at which they would all be partially consolidated. For this latter, a porosity value of 0.3 was chosen. Tables E.9 and E.10 show the extrapolated values of elastic modulus and viscosity coefficient at the two above-mentioned porosity conditions.

The plots of $\ln(G^*)$ against porosity (Fig. 6.8), reflect the increasing difficulty for each material to deform elastically as the porosity decreases and the available void space diminishes. The value of the slope for Emcompress was the highest, indicating a greater effect of porosity on its elastic properties than for the other materials. The particularly high value of elastic modulus at zero porosity, G_o^*, may well reflect

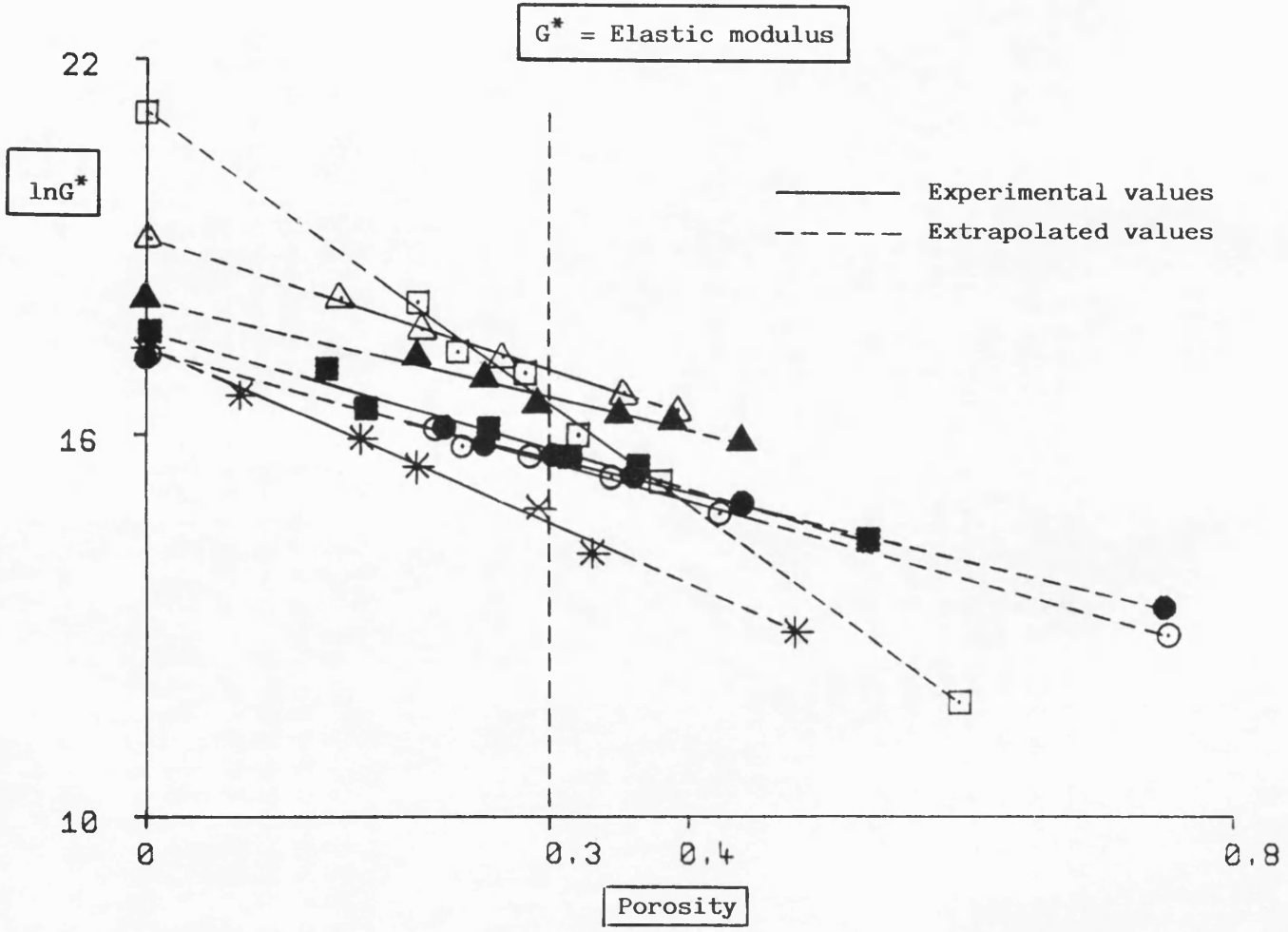

Fig. 6.8 Effect of porosity on $\ln G^*$ values.

(Key: page xxiii)

this material's relatively abrasive nature, which often results in scoring of the punches and dies used during its compression into compacts. On the other hand, Emcompress gave the lowest extrapolated value at the porosity corresponding to its tapped density condition (Table E.9). The exact significance of these latter results cannot so far be explained. However, the high negative slope obtained for this material can be attributed to the fine pore size distribution that may exist in compacts following extensive particle fragmentation.

The values of G_o^* for the other materials did not demonstrate sufficiently the differences in their elastic properties. Starch 1500 and sodium chloride gave relatively high values of the slope, indicating a marked dependence of their ability to undergo elastic deformation on porosity. In comparison, there was no significant difference between the values obtained for the two microcrystalline celluloses and sodium bicarbonate, the slopes being lower than for the other materials mentioned above.

The correlation coefficients obtained for the linear regressions of the plots of $\ln(\eta)$ against porosity (Fig. 6.9) for most materials (Table E.10), were higher than those for the corresponding plots of $\ln(G^*)$. However, sodium chloride gave a particularly low correlation coefficient. This can be explained by the slight curve apparent in the plot obtained for this material (Fig. 6.9). This "deviation" from linearity may be due to a change in the consolidation mechanism of sodium chloride as

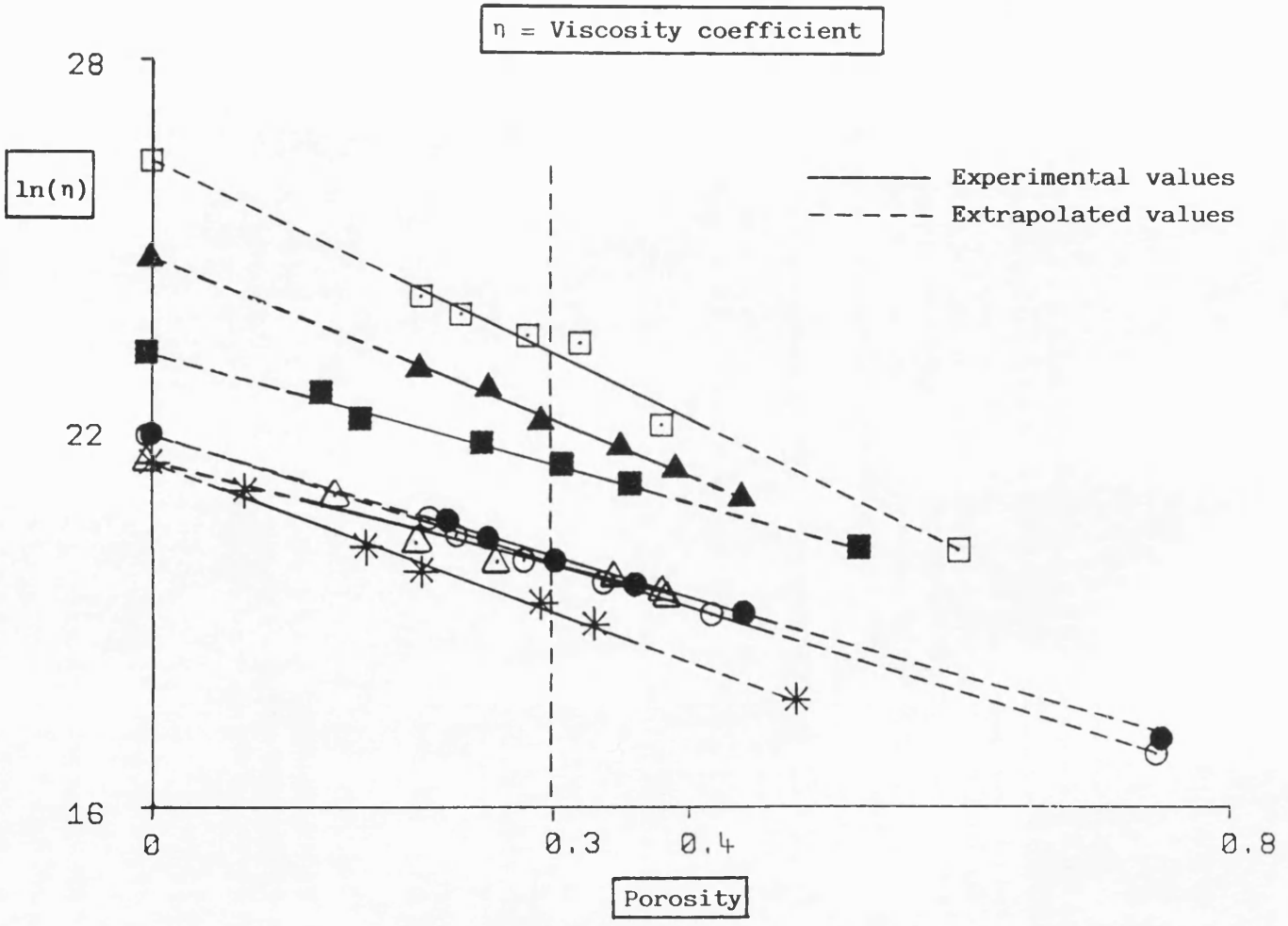

Fig. 6.9 Effect of porosity on ln η values.

(Key: page xxiii)

compaction proceeds, resulting in a reduced ability of this material to undergo plastic flow into the remaining void space. This may be attributed to work hardening effects, known to take place in sodium chloride crystals (Rees and Rue, 1978c).

Not surprisingly, the materials were ranked according to their ability to deform plastically. As already explained, the slope reflects the increasing resistance to plastic flow as the void space is reduced. No significant differences were observed for either the slope or the intercept values obtained for the two micocrystalline celluloses. Starch 1500 gave slightly higher values for the gradient (Table E.10), indicating a greater increase in its resistance to plastic deformation with decreasing porosity than for Avicel PH102 or Emcocel 90M. Also, Emcompress produced a higher slope value than the other materials which consolidate in a similar manner, such as anhydrous lactose and sodium bicarbonate. This suggests that the consolidation mechanism is not solely responsible for such differences. Pore size and size distribution within the materials may also be of importance.

It is interesting that the results for slopes listed in Table E.10, are of the same order of magnitude as the values of approximately -7, reported by Duckworth (1953) for a silicate porcelain. This suggests that this parameter may be independent of material. The results obtained here indicate that, other factors such as pore size may be responsible for the small differences observed between materials (Table E.10). Although

the overall porosity of the materials may be similar, different pore size and size distribution could account for the differences mentioned above.

The values of the intercept obtained from the linear regression of the plots illustrated in Fig. 6.9 provide a means of comparison of the ability of the materials to deform plastically at zero porosity. In principle, however, under the constrained conditions of the creep test, the viscosity coefficient at zero porosity would become infinite, since the materials would be unable to deform any further, due to lack of available void space. Therefore, the meaningful use of such intercept values is hereby questioned. One must, however, take also into account the fact that zero porosity is only an artificial limit, set by the particle density determined by gas pycnometric analysis of unconstrained powder samples. In practice, there may be intraparticle voids present which allow further deformation and even some molecular densification under high loads.

The extrapolated values of viscosity coefficient obtained for the materials at their tapped density condition, are most likely to represent their viscosity in an unconstrained condition. In this case, the materials were ranked as follows:

Emcocel 90M < Avicel PH102 < Starch 1500 < sodium chloride < Emcompress < anhydrous lactose < sodium bicarbonate

The relatively low extrapolated value of η_t, for Emcompress can be explained by the fairly low experimental

value obtained at 0.38 porosity. It is possible, that this reflects an ability of the material to undergo a certain amount of plastic deformation, for example at surface asperities, at very high porosity.

It must be emphasised that, caution is needed when interpreting extrapolated results without any evidence of the nature of the relationship between the two variables outside the data points used in the linear regression analysis.

For this reason, a more confident comparison of each material's ability to deform plastically is possible using the interpolated values at 0.3 porosity. The materials are then ranked as follows:

Starch 1500 < Emcocel 90M < Avicel PH102 < sodium chloride < anhydrous lactose < Emcompress

The viscoelastic properties of each material were assessed by means of the time constant k_2 and the asymptotic value J_i. As explained earlier (section 2.2.5.1), k_2 quantifies the retardation of the elastic strain in the viscoelastic region. A high k_2 value reflects a high degree of retardation, in other words, a low rate of retarded elastic deformation. So, a high k_2 value is indicative of a material with time-dependent characteristics.

The data for the time constant k_2 in the viscoelastic region are given in Tables E.7 and E.8. Fig. 6.10 shows the values for each material subjected to the creep test plotted versus relative density. Starch 1500, a material that is well

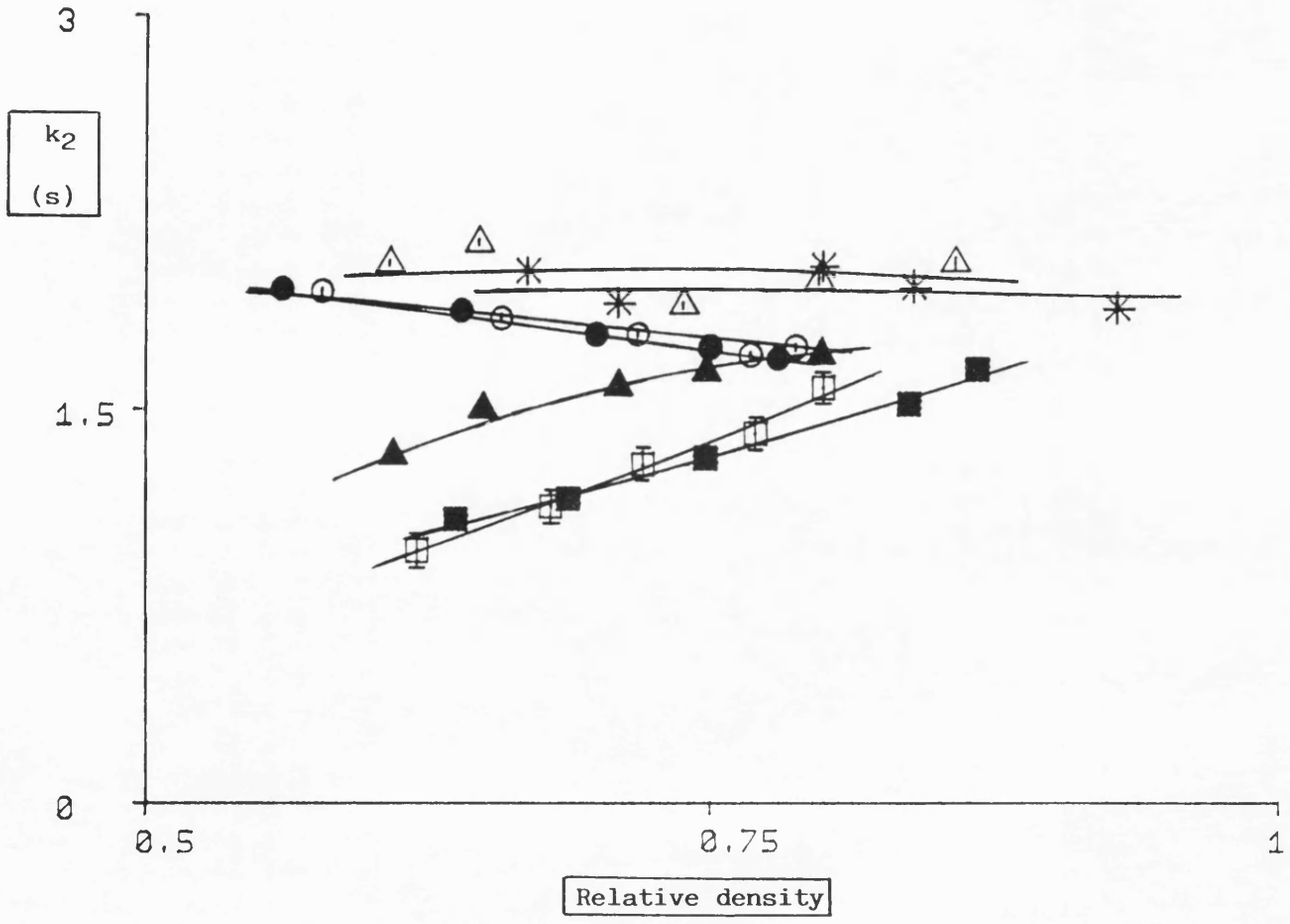

Fig. 6.10 k_2 values for the materials at a range of relative densities.

(Key: page xxiii)

known for its time-dependent nature, gave the highest values of k_2 across the full range of relative density. Interestingly, there was minimal change with compact porosity. The k_2 values for the two microcrystalline celluloses were lower, and for these materials there was a decrease with relative density. No significant differences were found between Avicel PH102 and Emcocel 90M. Sodium chloride values for k_2 were also very high, and showed very little variation with relative density. This is in agreement with previous findings of the material's time-dependent consolidation behaviour (Rees and Rue, 1978a). In contrast, brittle materials such as anhydrous lactose and Emcompress gave particularly low values of k_2, which in each case increased with density. Sodium bicarbonate values were also low suggesting a relatively low level of time-dependence.

The value of k_2 alone does not, however, characterise fully the viscoelastic behaviour of a material. The asymptotic value J_i must also be considered. J_i is the equilibrium value of creep compliance due to retarded elastic deformation at infinite time, that is, the total retarded elastic compliance.

The values obtained for the materials tested are shown in Tables E.7 and E.8. Not surprisingly, Starch 1500 gave the highest J_i values (Fig. 6.11). This indicates that the total potential for retarded elastic deformation of this material is greater than for any other. Avicel PH102, Emcocel 90M and sodium chloride also showed relatively high values suggesting that these materials too, are capable of a substantial amount of

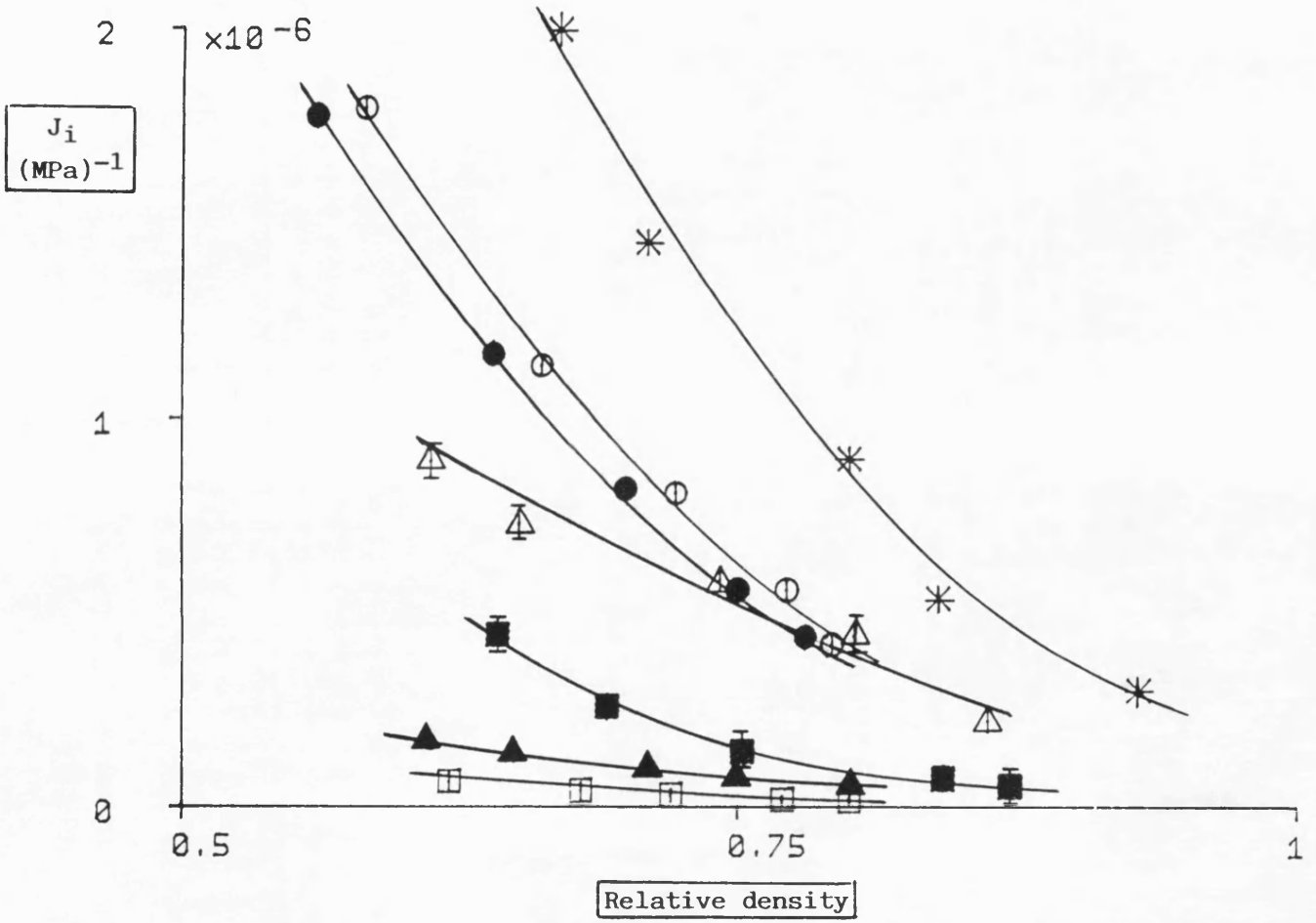

Fig. 6.11 J_i values for the materials at a range of relative densities.

(Key: page xxiii)

retarded elastic deformation. As one might expect, J_i values decreased as the compacts became more dense and the void space available for deformation diminished (Fig. 6.11). Understandably, the values for anhydrous lactose and Emcompress were particularly low as the extent of retarded deformation that these brittle materials undergo is very limited. The similarity between Figs. 6.4 and 6.11 is not unexpected, since J_r and J_i values reflect the amount of retarded elastic deformation of the materials at t=90s and infinity respectively.

In conclusion, creep analysis enables the separate quantification of the elastic, retarded elastic and plastic deformation of particulate materials, especially by means of the estimated elastic modulus, G^*, and the viscosity coefficient, η. The time constant k_2 of the viscoelastic region appears to be a particularly interesting parameter describing the time-dependent characteristics of materials. Further investigation of this parameter is called for.

Treatment of data using the approach proposed by Spriggs (1961), provide useful information regarding changes in parameters, such as elastic modulus and viscosity coefficient obtained from creep experiments, with porosity. Care is, however, necessary when considering extrapolated values, especially when there are changes in the consolidation behaviour of materials as densification proceeds.

6.3 SPECTRAL ANALYSIS OF CREEP DATA

6.3.1 Introduction

The Fourier transformation of a sequence supplies (Tukey, 1961; Jenkins and Watts, 1968; Bloomfield, 1976; Chatfield, 1984) the coefficients of the sinusoidal components into which a sequence may be analysed. In other words, spectral analysis is a method of decomposing a time series into its cyclical components and describing the tendency of a certain frequency to appear in the data. It gives a measure of the contribution of components characterised by a certain frequency to the total variation of the series.

The main characteristic of a time series, distinguishing it from a simple random sample, is that its observations depend on time. Furthermore, there is often a linear, exponential or polynomial trend, as well as seasonal fluctuation, i.e. single events that affect the observations. Both of the above must be removed from the data before any further analysis is done on the series. This filtering procedure is called prewhitening. The simplest way to achieve this is by autoregression, i.e. to linearly correlate each data point to its previous value. When obvious trends and seasonal fluctuation are removed, spectral analysis can be conducted on the residuals.

The first step involves the creation of the periodogram,

i.e. analysis of the time series at a range of frequencies which contribute to the variability of the series to different extents. The periodogram, however, fluctuates widely and generally needs to be modified and smoothed. Therefore, the final results depend not only on the prewhitening, but also on the smoothing methods. One way to smooth a periodogram is by a grouping procedure, i.e. choose a set of periodogram estimates in sets of size m and calculate their weighted average. In the frequency domain, such a weighting scheme is called a spectral window. The result is a smoothed spectrum with a statistical consistency. If the window chosen is too small, the estimated spectrum will be close to the periodogram with erratic variation. If, on the other hand, the window is too big, statistical errors are likely to increase. The choice of the bandwidth and, therefore, the size of the set of estimates used must maintain a balance between resolution and variance.

The spectrum produced consists of point estimates at different frequencies, showing the estimated contribution of each frequency to the total variance of the series. Whichever estimation method is adopted, the resulting estimates will be subjected to some error. There is, therefore, a need for the construction of confidence limits. The confidence interval for each point of the spectrum is given by the following values:

$$\frac{PS}{C^2\,(d.f.,\ p/2)} \qquad \text{to} \qquad \frac{PS}{C^2\,(d.f.,\ 1-p/2)}$$

where,

PS = power spectrum = σ^2 = variance of the series

$C^2 = \chi^2/d.f.$

χ^2 = values of the χ^2 distribution

d.f. = degrees of freedom of the spectral window = 2m

m = size of sets of estimates to be averaged

m = (bandwidth • N)/2

N = number of observations

bandwidth = width of the spectral window

In the case of a 99% confidence interval, for example,

$99 = 100 \cdot (1-p)$ and $p = 0.01$

The area under the spectrum equals the total variance in the series. The power spectrum indicates the proportion of variance accounted for at each frequency, being the area under the spectrum at that frequency. This shows why the power spectrum of a random series is flat. Since the series is random, all frequencies contribute equally to the variance and thus the power spectrum will be constant throughout the frequency range.

The significance of the peaks in a spectrum is tested by superimposing the power spectrum on the white noise spectrum which is a straight line, under which the area is equivalent to the total variance of the series. If this constant spectrum falls outside the confidence interval at a certain frequency, then the component at that frequency accounts for more variability than expected from a random process. The spectral peak at that frequency is then a significant peak (Fig. 6.12). If no peaks are significant, then the series is random.

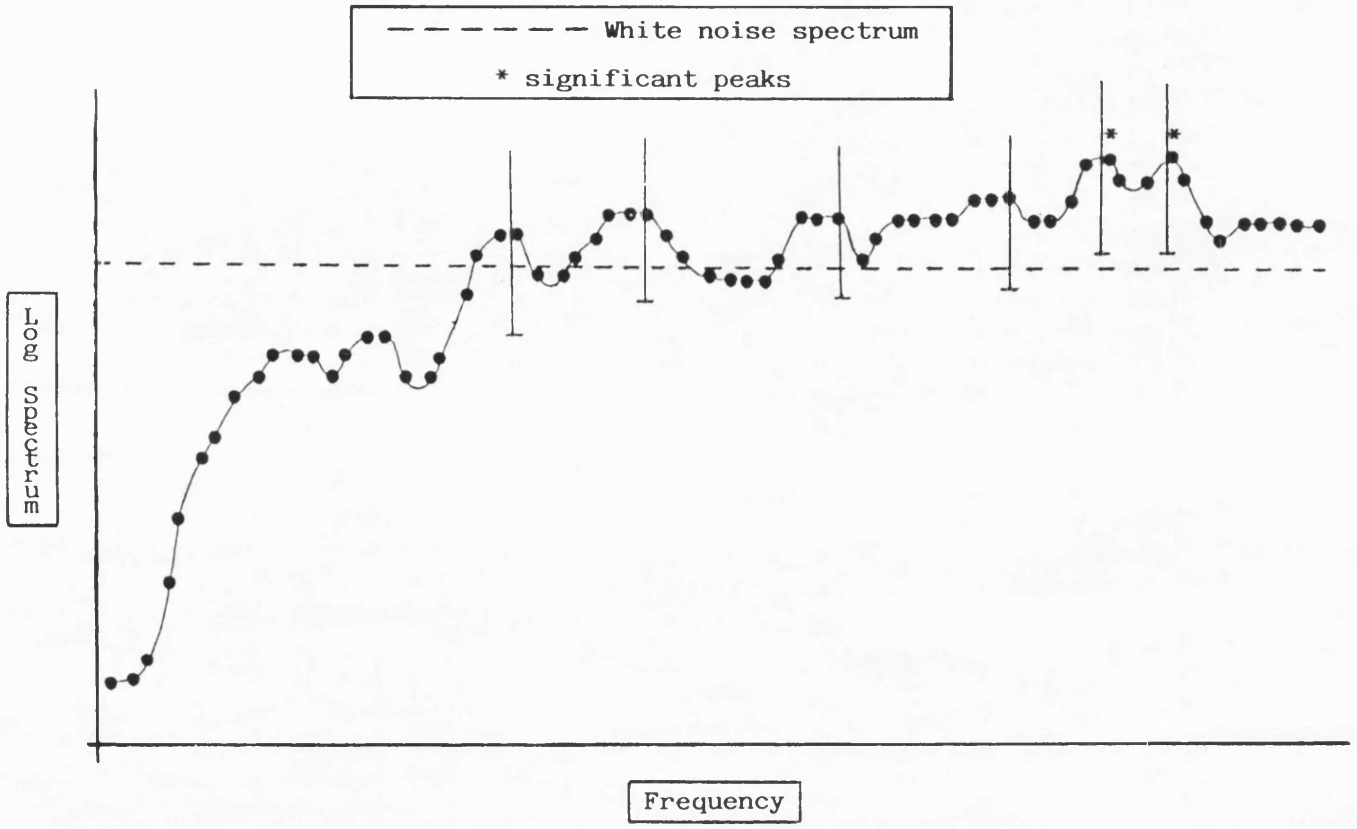

Fig. 6.12 Significance of peaks in a spectrum.

An example of spectral analysis of a time series in the field of economics, will be used as an introduction to spectral analysis. The time series shown in Fig. 6.13d, is the annual number of Canadian lynx trappings for the years 1821-1934. These data show an oscillatory behaviour with a cycle of approximately 10 years. Although a single sine wave fitted to the data matches the location of the peaks, it cannot mimic the irregular peak heights. If it did, then in the plot illustrated in Fig. 6.13cd, where the variation in the series is shown as the contribution of a range of frequencies, a single point at a frequency approximately 0.1 would represent the sine wave responsible for the variation in the series. In fact, a sum of sine waves is needed to improve the approximation to the data (Fig. 6.13bcd). Here, a number of points corresponding to a number of frequencies contribute to the variance of the series to different extents. Finally, the use of several smoothing techniques allows the creation of a spectrum (Fig. 6.13abcd), including the peak at frequency 0.1, which was obvious from the beginning. What has been achieved by using spectral analysis, is to detect hidden periodicities. This is where spectral analysis is at its most useful. It is not really worth applying it where large peaks speak for themselves. In fact, obvious effects of the data are often removed to allow the more subtle features to emerge. This is why this method was used; in order to reveal any cyclic components responsible for the variation in the time series, in this case, creep compliance against time.

a

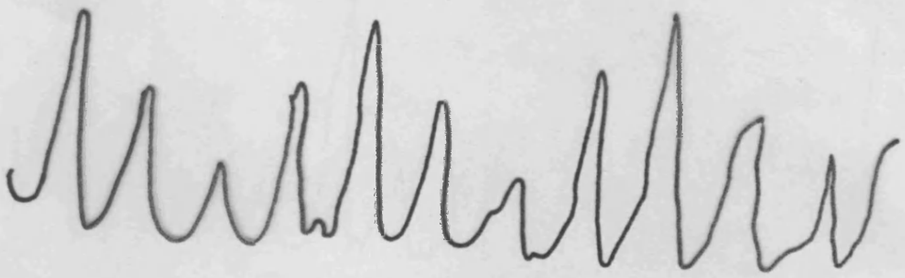

b

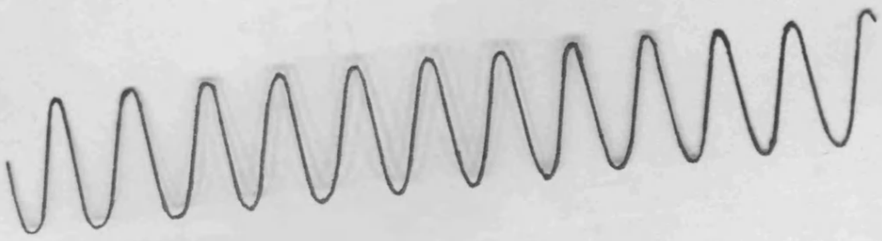

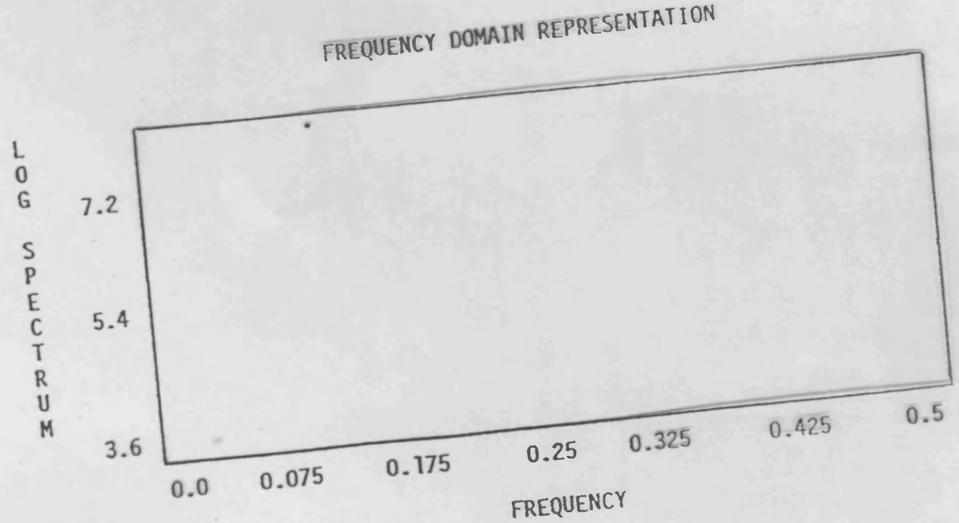
FREQUENCY DOMAIN REPRESENTATION
LOG SPECTRUM
7.2
5.4
3.6
0.0
0.075
0.175
0.25
0.325
0.425
0.5
FREQUENCY

c

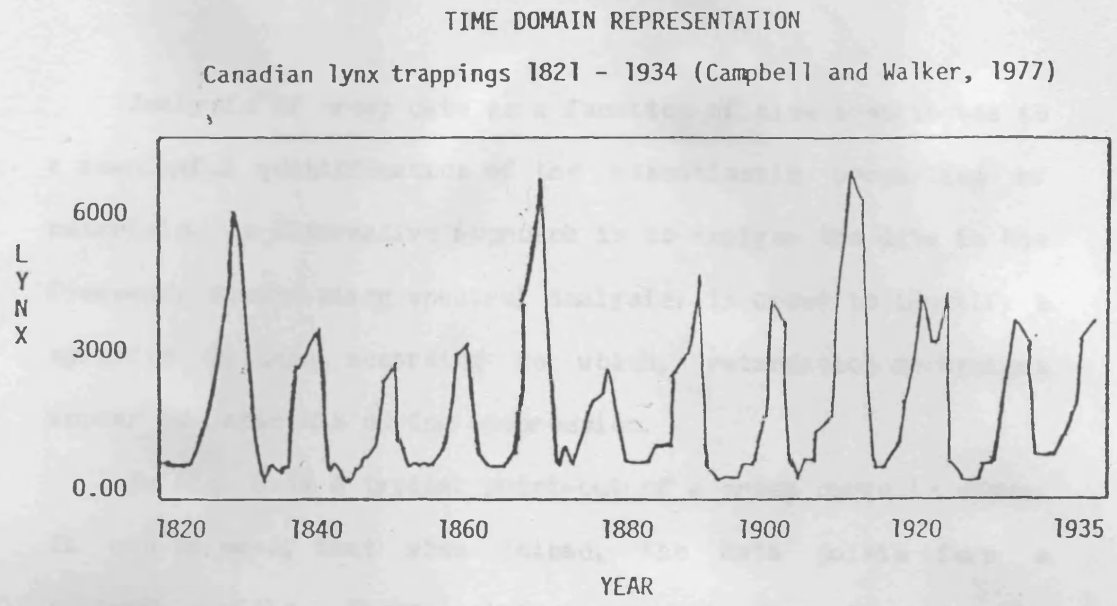

FIG. 6.13 d Example of spectral analysis of a time series.

6.3.2 Creep Spectra

Analysis of creep data as a function of time contributes to a meaningful quantification of the viscoelastic properties of materials. An alternative approach is to analyse the data in the frequency domain using spectral analysis, in order to identify a specific pattern according to which, retardation mechanisms appear in materials during compression.

In Fig. 6.14 a typical print-out of a creep curve is shown. It can be seen, that when joined, the data points form a sawtooth profile. These points represent data for which the force applied was within certain limits, in this case $\pm$98% of a set value. In itself, this variation exhibits a certain oscillatory behaviour and had, therefore, to be removed before spectral analysis was conducted on the residuals.

Fig. 6.15a illustrates the spectrum obtained for Emcompress. There are only two significant peaks at high frequencies, indicating that the only mechanisms which contribute to the variance of the series, are ones occuring at these two frequencies. The corresponding spectrum for anhydrous lactose is shown in Fig. 6.15b. It can be seen that it is very similar to that obtained for Emcompress. In the case of Starch 1500, however, several peaks are significant at the 99% level (Fig. 6.16a), indicating that events occuring at all these frequencies contribute to the variance of the series. It is

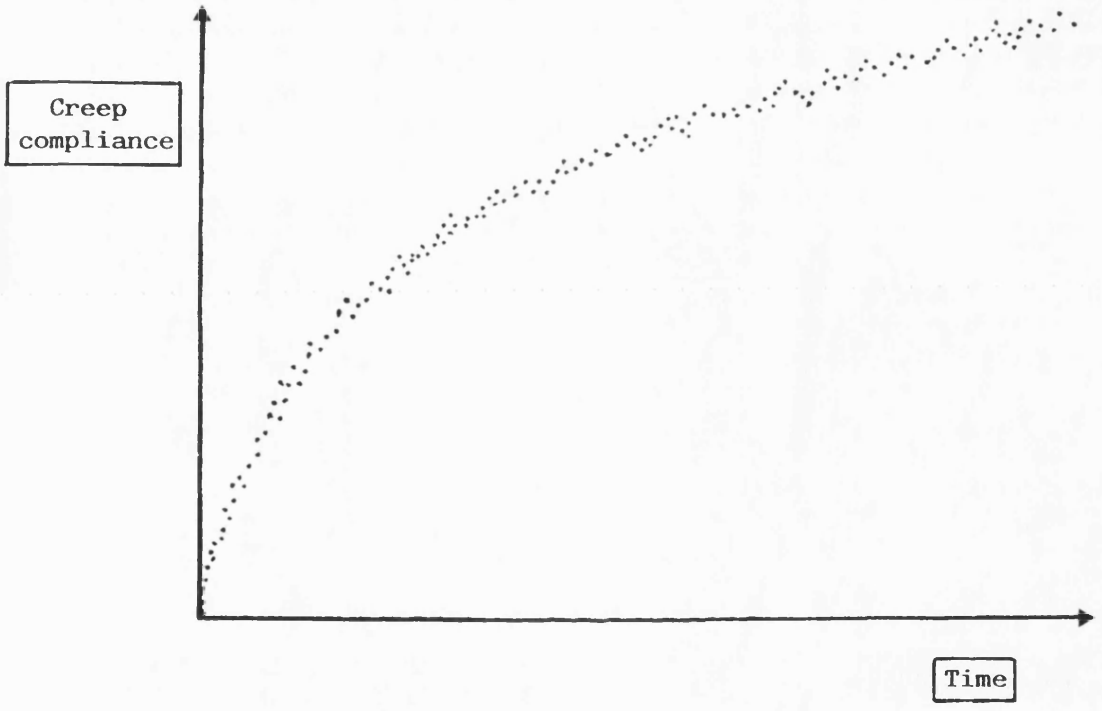

Fig. 6.14 Typical print-out of a creep curve.

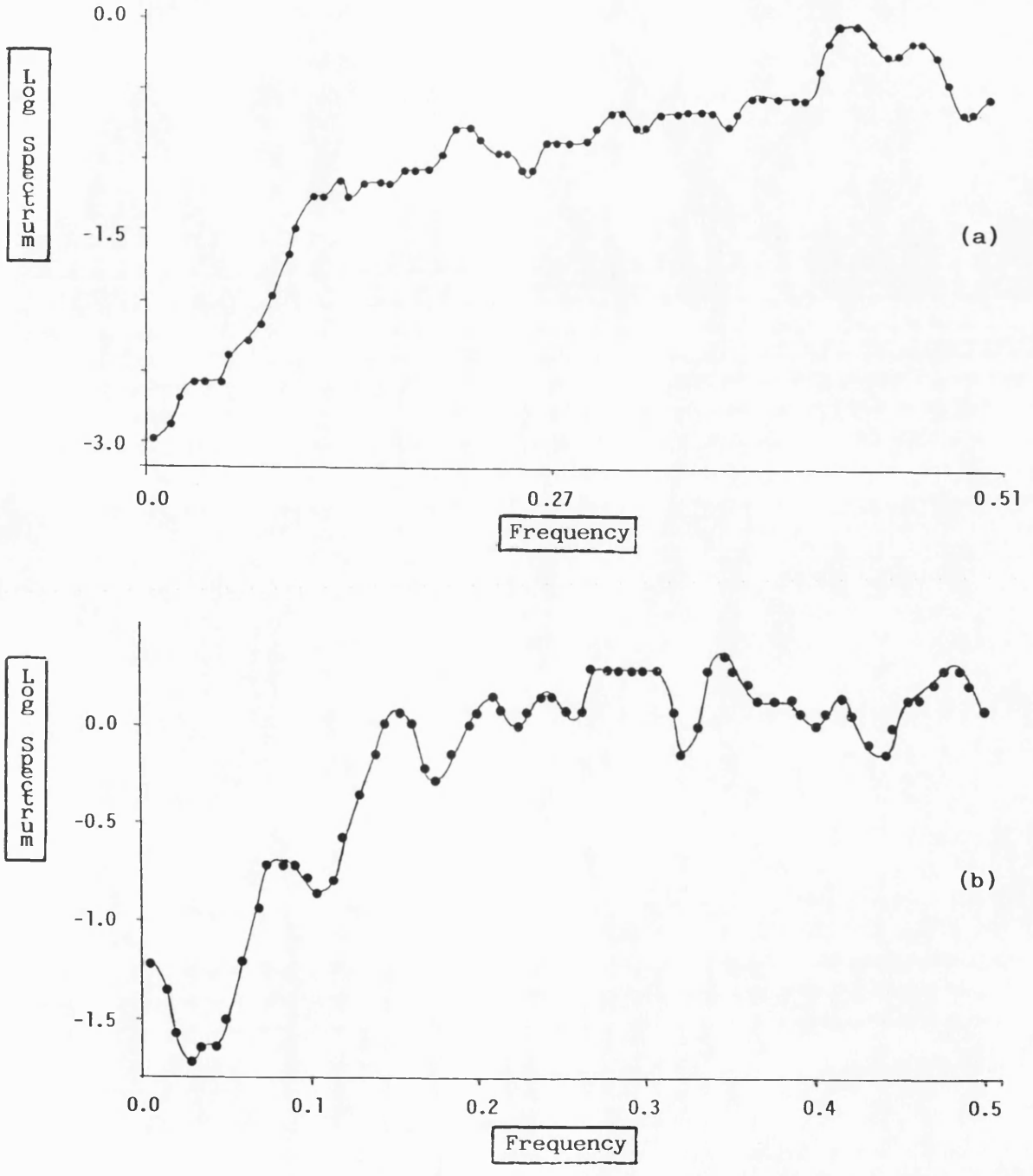

Fig. 6.15 Creep spectra for (a) Emcompress and (b) anhydrous lactose.

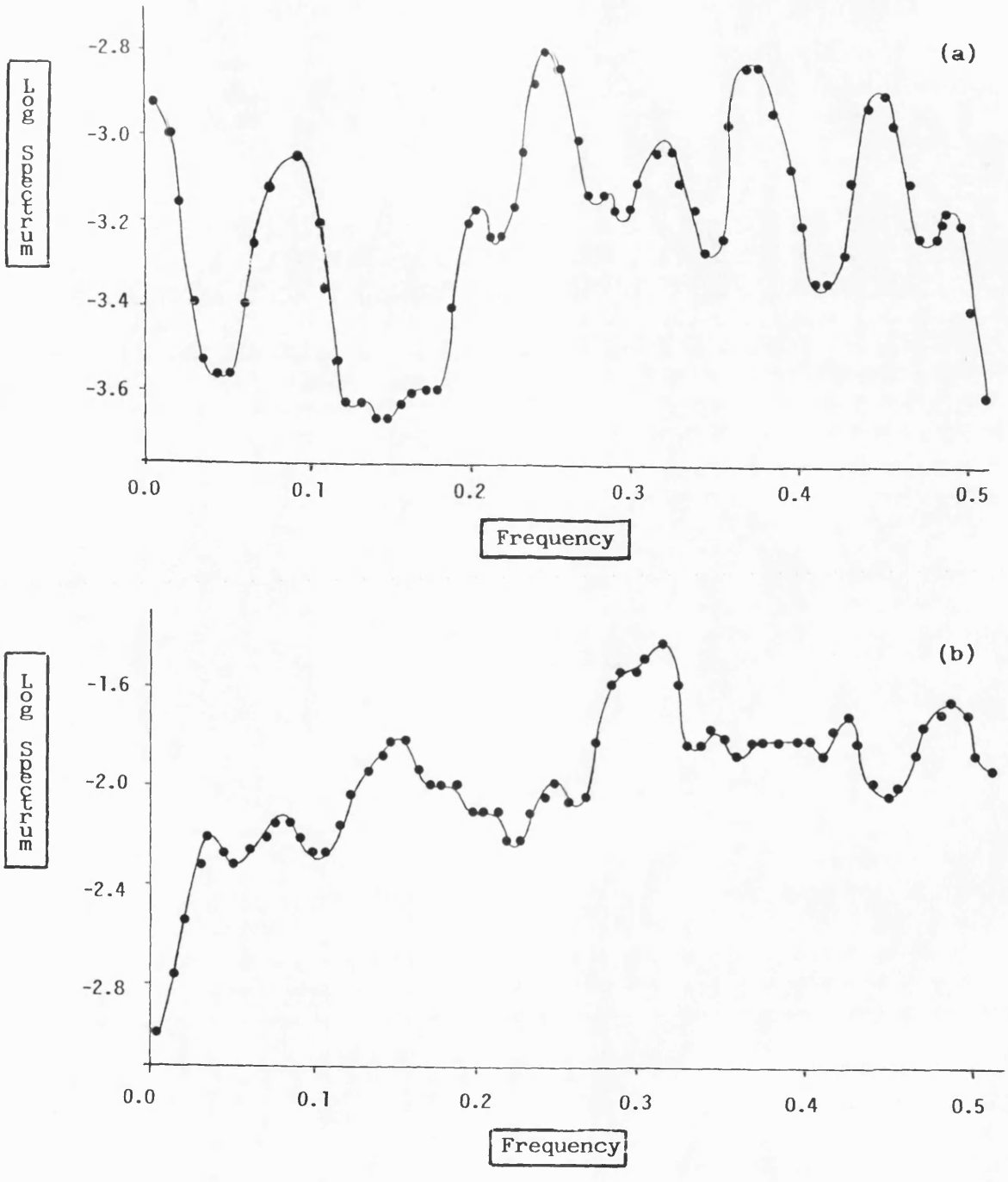

Fig. 6.16 Creep spectra for (a) Starch 1500 and (b) Avicel PH102.

believed that the presence of such a range of mechanisms is responsible for the material's viscoelastic properties. For Avicel PH102 samples, there are fewer significant peaks at intermediate and high frequencies and none at low frequencies (Fig. 6.16b). This confirms previous results according to which, Starch 1500 and Avicel PH102 exhibited different viscoelastic behaviour.

Although the spectra obtained for the materials tested showed distinct differences, it was found that replicate samples of the same material did not produce spectra with significant peaks at exactly the same frequencies. These were often shifted to either higher or lower frequency values. Whether this was due to actual differences in the samples related to their heterogeneous nature, or to the lack of reproducibility of the method, cannot so far be determined. As a result of the above, differentiation between materials using cross-spectral analysis techniques was not possible. Such an analysis would provide quantitative confirmation on whether spectra obtained for different materials are significantly uncorrelated, and at which frequencies this occurs.

It can be concluded, that apart from conventional creep analysis in the time domain, spectral analysis in the frequency domain may be used to reveal hidden periodicities of mechanisms possibly related to the viscoelastic behaviour of materials. It is clearly an approach that warrants more detailed investigation.

CHAPTER SEVEN

FACTORS AFFECTING THE PHYSICO-MECHANICAL PROPERTIES OF STARCH

7.1 INTRODUCTION

Starch is extracted from various plants through a sequence of processing steps (Whistler et al, 1984). It is a white, odourless and relatively tasteless powder with particles of a wide range of size and shape, depending on the plant source. Starch consists of two main chemical components: amylose and amylopectin. Amylose is a fairly low molecular weight linear polymer of D-glucose units linked with α-D-(1-4) glucocidic bonds whereas, high molecular weight amylopectin has a branched structure of glucose units linked by α-D-(1-6) bonds.

Starch granules contain crystalline and amorphous regions. Crystallites are formed when portions of amylose or amylopectin molecules are joined by hydrogen bonds between the hydroxyl groups of the glucose units. In the intermediate amorphous regions, the molecules are less closely packed. During cold water swelling, water penetrates into the amorphous regions of the granules and forms hydrogen bonds with the free hydroxyl

groups of the starch molecules (Radley, 1968).

Modified starch is widely used as an excipient in tablet formulations due to its binding and excellent swelling properties. It is modified by gelatinisation, an endothermic process which involves breaking down of the crystallites in the presence of moisture and heat (Radley, 1968). As a result, each glucose polymer and the unmodified starch are allowed to function separately when used in tablet formulations.

Although modified starches are known to undergo plastic deformation under load (Fuhrer et al, 1975; David and Augsburger, 1977; Duberg and Nystrom, 1982), their compacts possess inferior mechanical properties compared to many other excipients (Rees and Rue, 1978a). This is generally attributed to their extensive elastic recovery (Paronen and Juslin, 1983). Furthermore, starch products are well known for their time-dependent deformation (Rees and Rue, 1978a; Roberts and Rowe, 1985; Armstrong and Blundell, 1985) which may often cause serious problems during the development and the scaling-up of a formulation.

Maize starch, known as "corn starch" in the U.S.A., is obtained from Zea Mays L, a cultivated member of the grass family (Graminae). The aim of this study was to investigate the factors affecting the compaction properties and especially the viscoelastic behaviour of some modified corn starches. Such factors include both intrinsic characteristics of these materials as well as procedures employed in their manufacture.

7.2 PARTICLE SIZE

As mentioned in section 1.2.1.3, there have been reports on the effect of particle size on the compaction properties of materials. However, controversial results suggest that this effect is related to both the material's deformation mechanism and bonding ability and no general conclusions can be drawn.

The effect of particle size on the compressional behaviour of Starch 1500 was initially assessed by studying three particle size fractions obtained from the same original batch (B.N. 611002), consisting of particles <125μm, 125-180μm and >180μm. The data obtained during compaction at 6, 12 and 18kN are shown in Tables F.1-F.4. There was no significant effect of particle size on the parameters related to the energy involved in the compaction process (Tables F.1 and F.2). However, yield pressure values (Table F.4) for the original material were higher than those for the three fractions (Fig. 7.1), possibly due to a better packing of the material, as a result of a wider particle size distribution. Diametral loading results (Table F.5) showed no significant effect of particle size on either the tensile strength or the work of failure values (Fig. 7.2).

In order to investigate whether the above observations are also valid for Starch 1500 particles larger than those normally present in commercially available batches, two more size fractions were examined. These fractions, consisting of

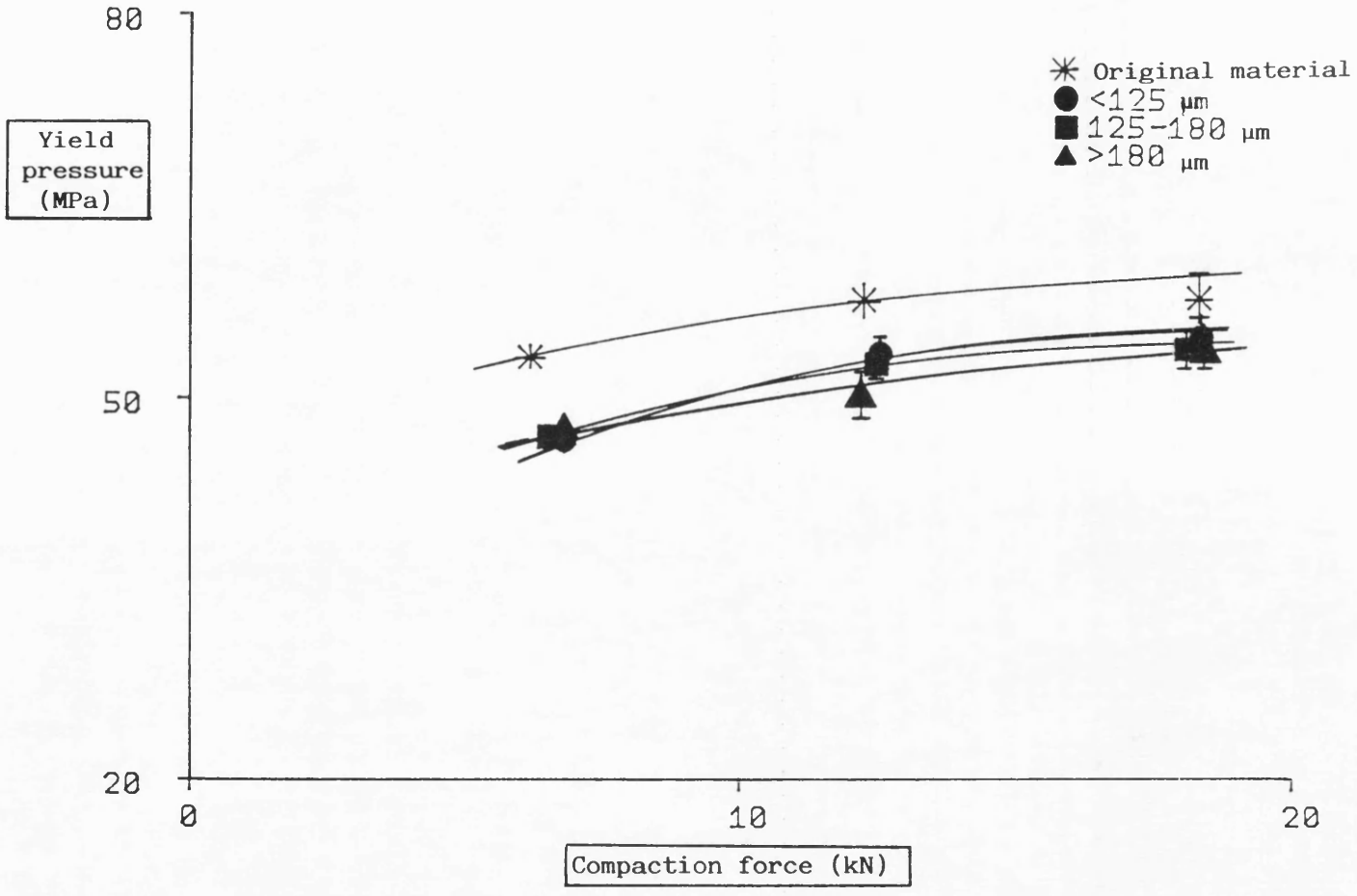

Fig. 7.1 Yield pressure values for some particle size fractions (<125µm, 125-180µm and >180µm) of Starch 1500.

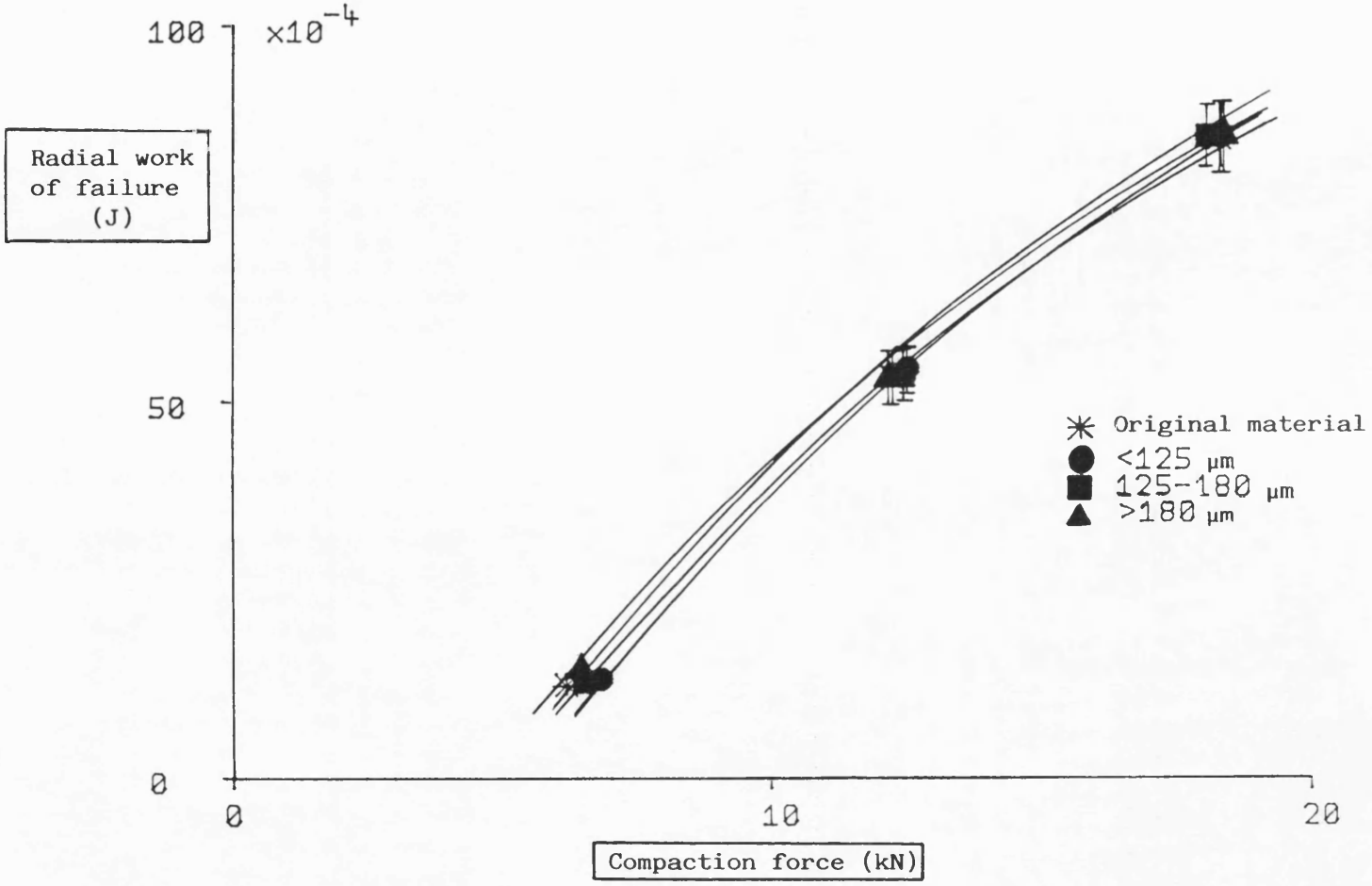

Fig. 7.2 Radial work of failure for some particle size fractions (<125µm, 125-180µm and >180µm) of Starch 1500.

particularly large particles, i.e. >710μm and >1680μm respectively (Figs. C.3 and C.4), had been selected during the process of manufacture of Starch 1500; such oversize particles are normally milled and included in the final product (Batch F).

Results obtained during compaction of these coarse particle size fractions and the final product are given in Tables F.6-F.9. Differences between the values of "true" work of compaction for these samples and the final product (Fig. 7.3) may be due to the presence of a large amount of flaws in the aggregates, leading to extensive plastic deformation during compaction. This was also demonstrated by the lower yield pressure values obtained for the two size fractions (Fig. 7.4).

Creep testing of these samples at a range of stress levels yielded the data in Tables F.10 and F.11. The small differences in elastic modulus (Fig. 7.5) and viscosity coefficient values (Fig. 7.6) for the particle size fractions and the final product decreased as the relative density of the compacts increased. This is attributed to the breakdown of the structure of the particle aggregates with increasing load, resulting in compacts of similar properties to those of the final product.

Diametral loading of the resulting compacts gave the results in Table F.12. Fig. 7.7 indicates that the two particle size fractions produced compacts of superior mechanical properties. This is attributed to the extensive plastic deformation of these samples during compaction, as evidenced by the yield pressure results, presented above.

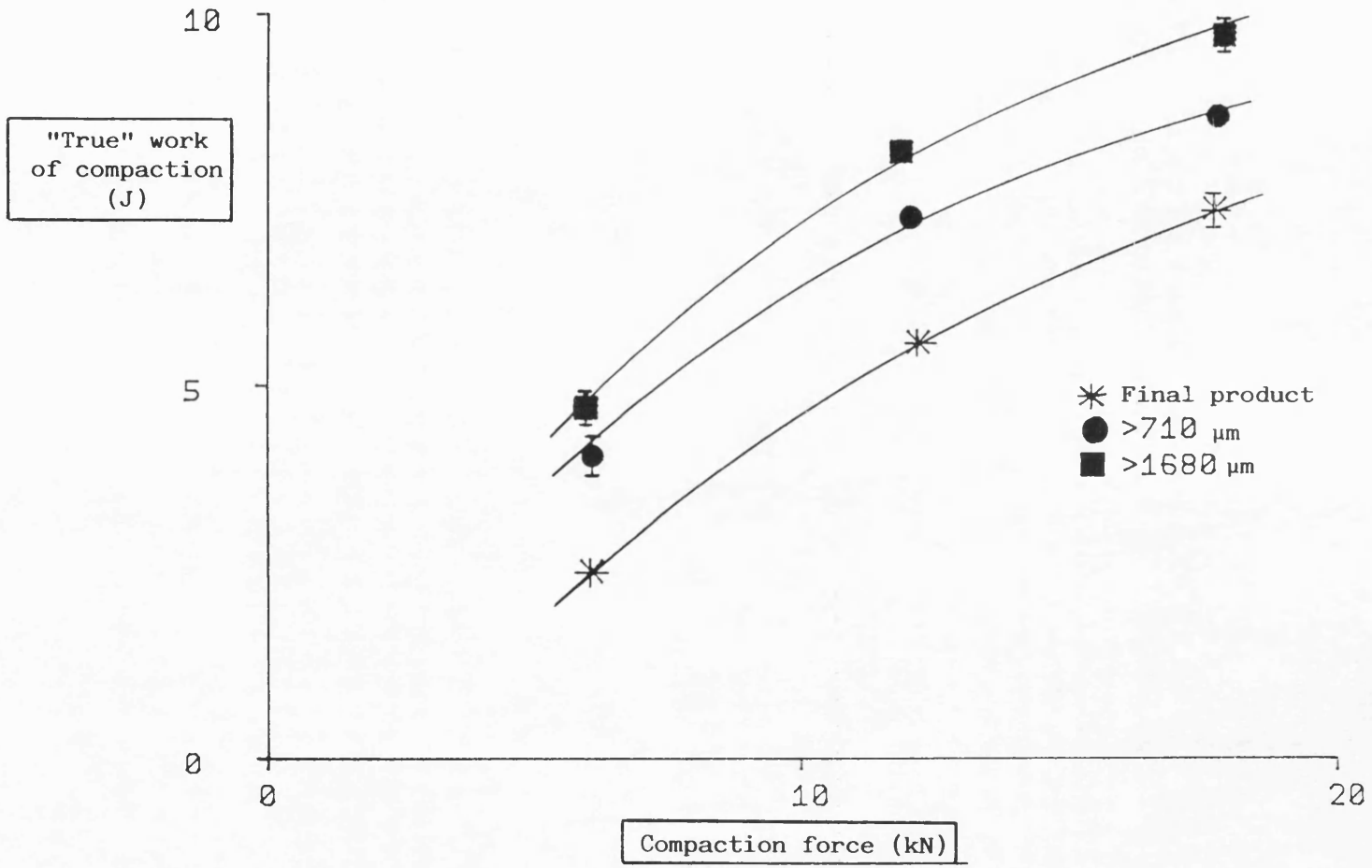

Fig. 7.3 "True" work of compaction for some coarse particle size fractions (>710µm and >1680µm) of Starch 1500.

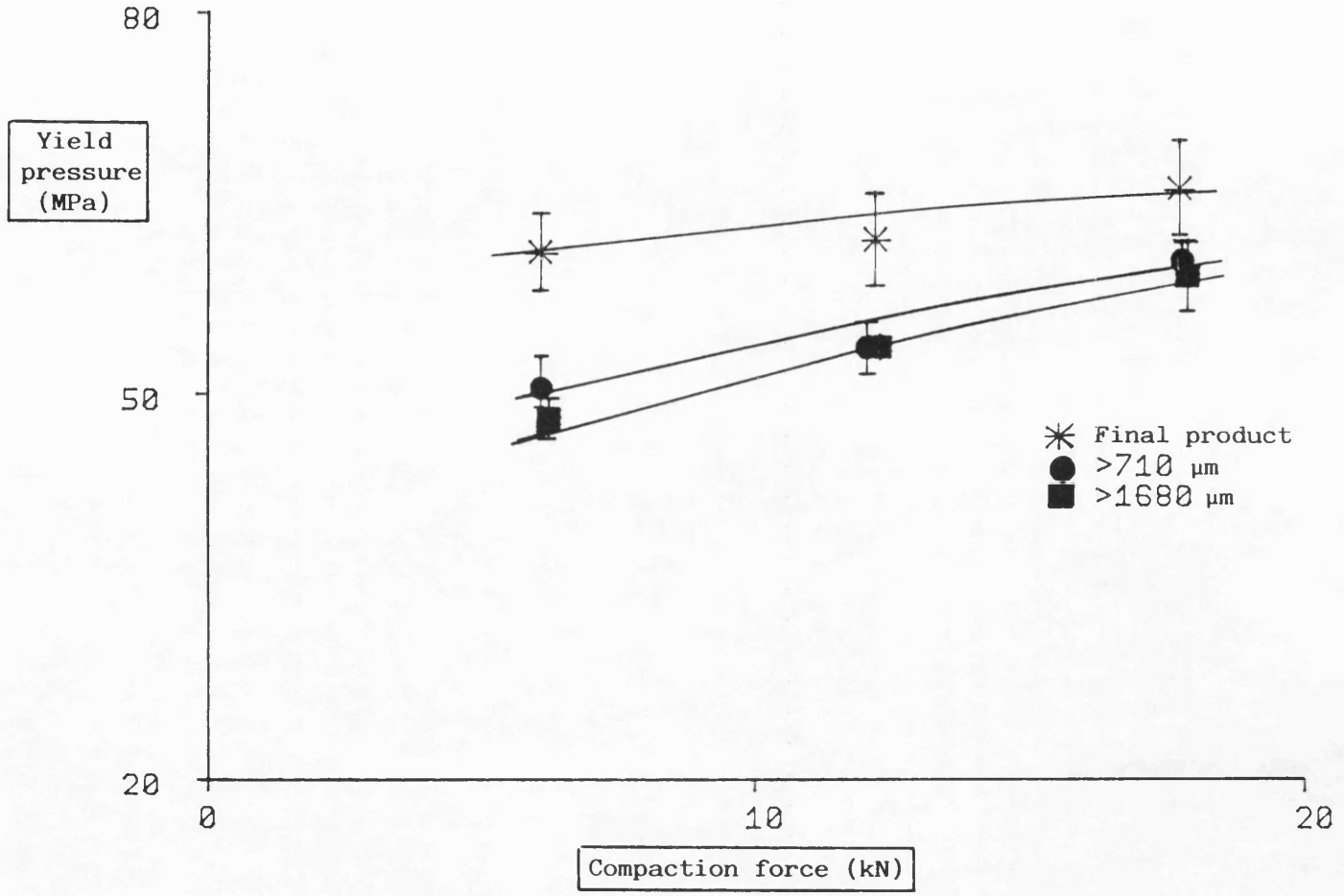

Fig. 7.4 Yield pressure values for some coarse particle size fractions (>710µm and >1680µm) of Starch 1500.

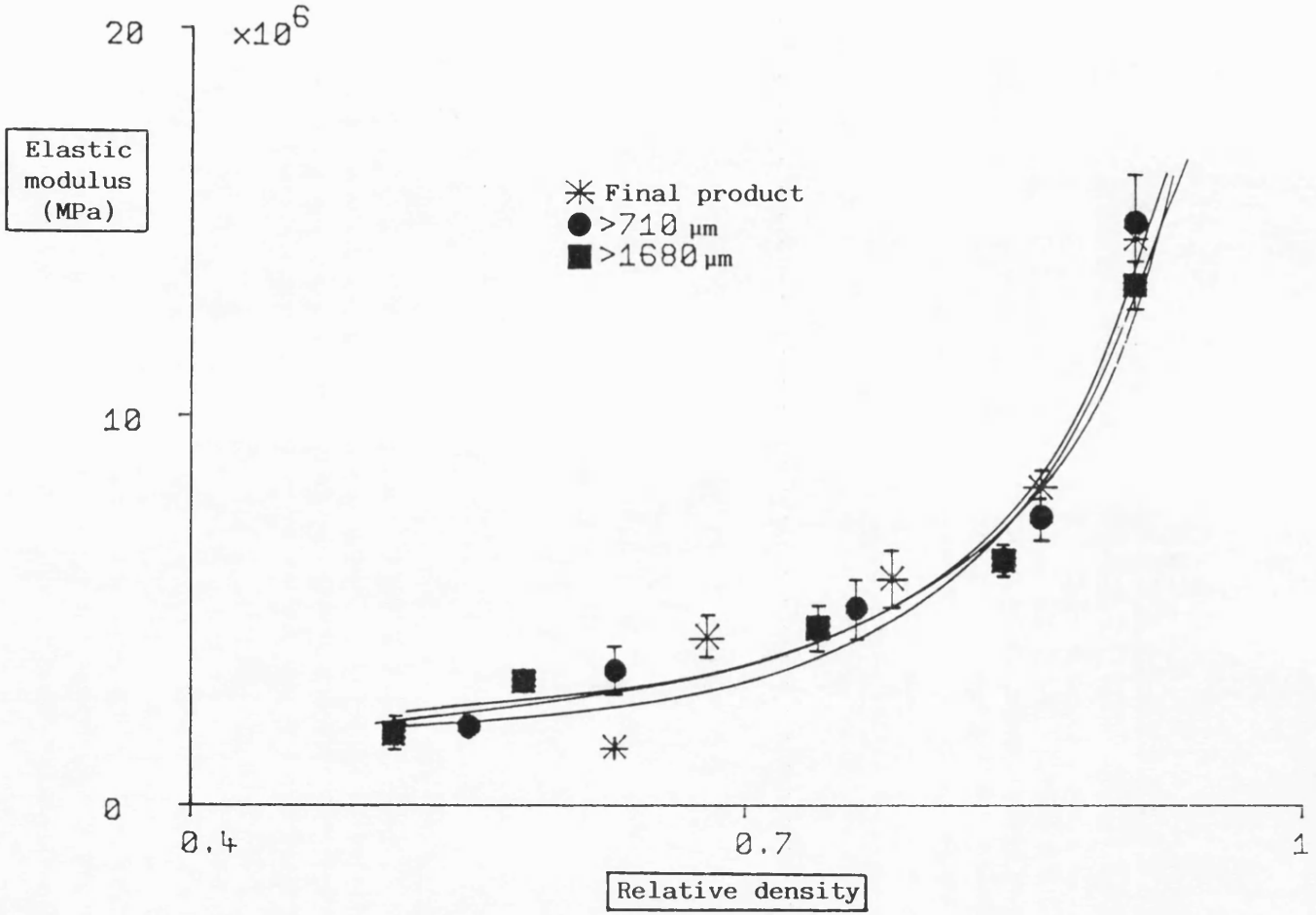

Fig. 7.5 Elastic modulus values for some coarse particle size fractions (>710µm and >1680µm) of Starch 1500.

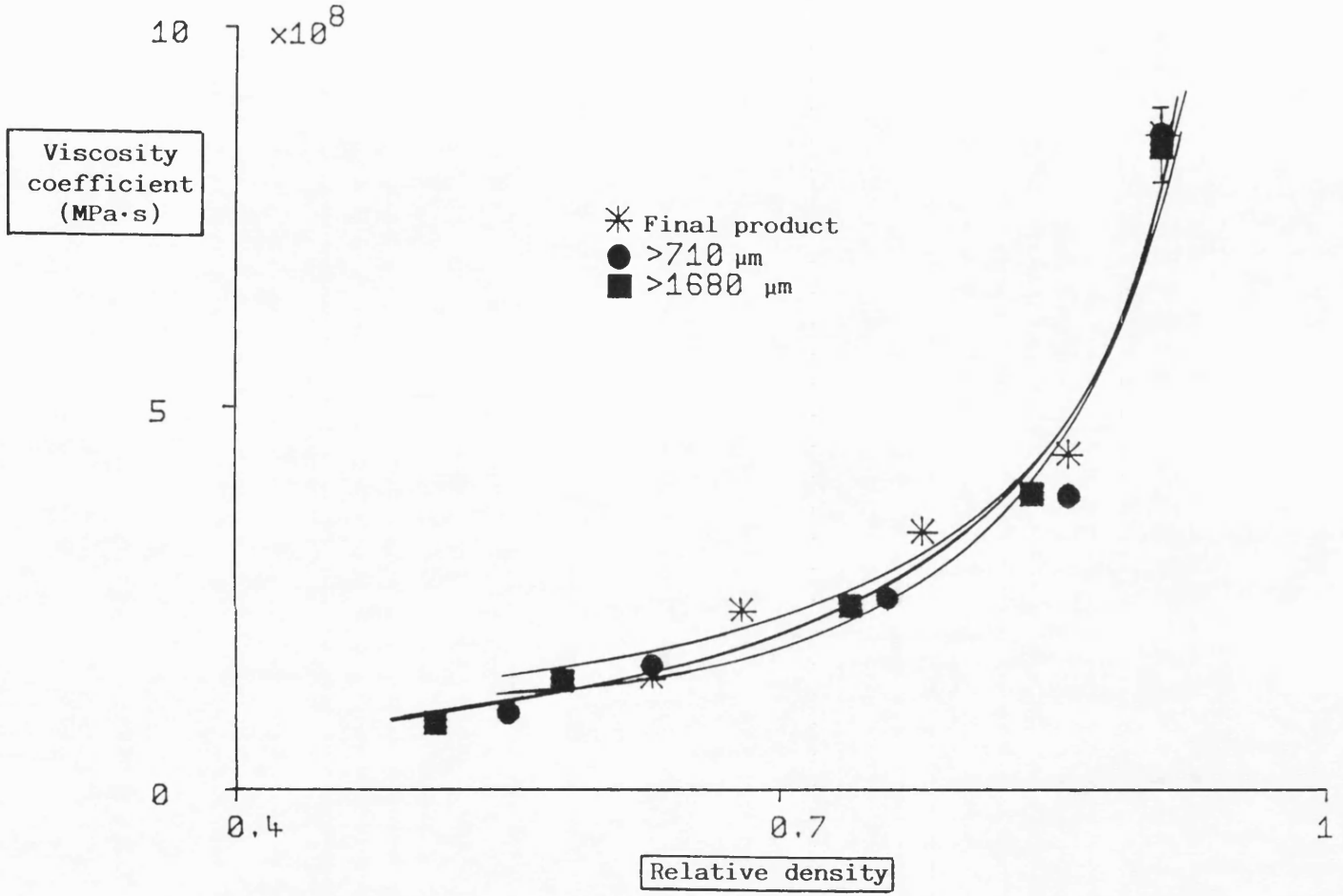

Fig. 7.6 Viscosity coefficient values for some coarse particle size fractions (>710µm and >1680µm) of Starch 1500.

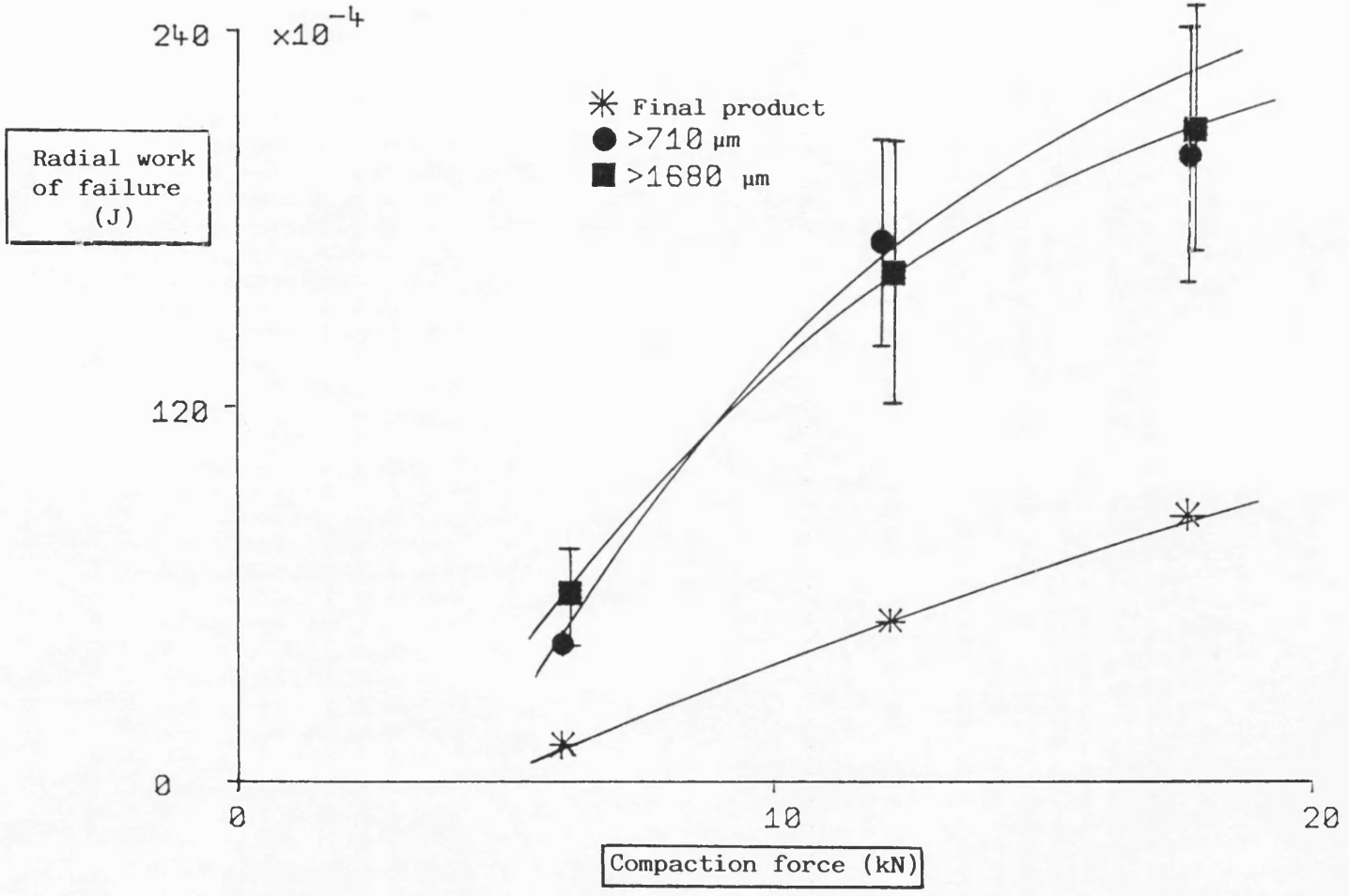

Fig. 7.7 Radial work of faiulure values for some coarse particle size fractions (>710µm and >1680µm) of Starch 1500.

7.3 MOISTURE CONTENT

As already mentioned in section 1.2.1.2, moisture is another factor reported to play an important role in the compaction properties of many pharmaceutical excipients. Corn starch as marketed, normally contains 10-14% (w/w) moisture.

Here, Starch 1500 samples were dried at 60C under vacuum for 24 hours and then equilibrated at a range of relative humidities (0, 22, 53, 80 and 94%) for a week. Moisture content was determined in triplicate by drying the powder to constant weight at 105C. The results are listed in Table F.13.

The samples were compressed at 6, 12 and 18kN. The data obtained during compaction are given in Tables F.14-F.17. The results showed, that moisture generally facilitated deformation of the material under load. This is particularly demonstrated by the decrease in yield pressure values with moisture (Fig. 7.8). This effect was, however, reversed at 94% relative humidity. In this case, as load increased, moisture seemed to prohibit deformation and powder cosolidation. This could be due to the increasing hydraulic resistance caused by the layers of water present on the surface of the starch particles.

Creep studies revealed the data given in Tables F.18 and F.19. Both elastic modulus and viscosity coefficient values for the material decreased as moisture increased (Figs. 7.9 and 7.10). This indicated that moisture facilitated both the elastic

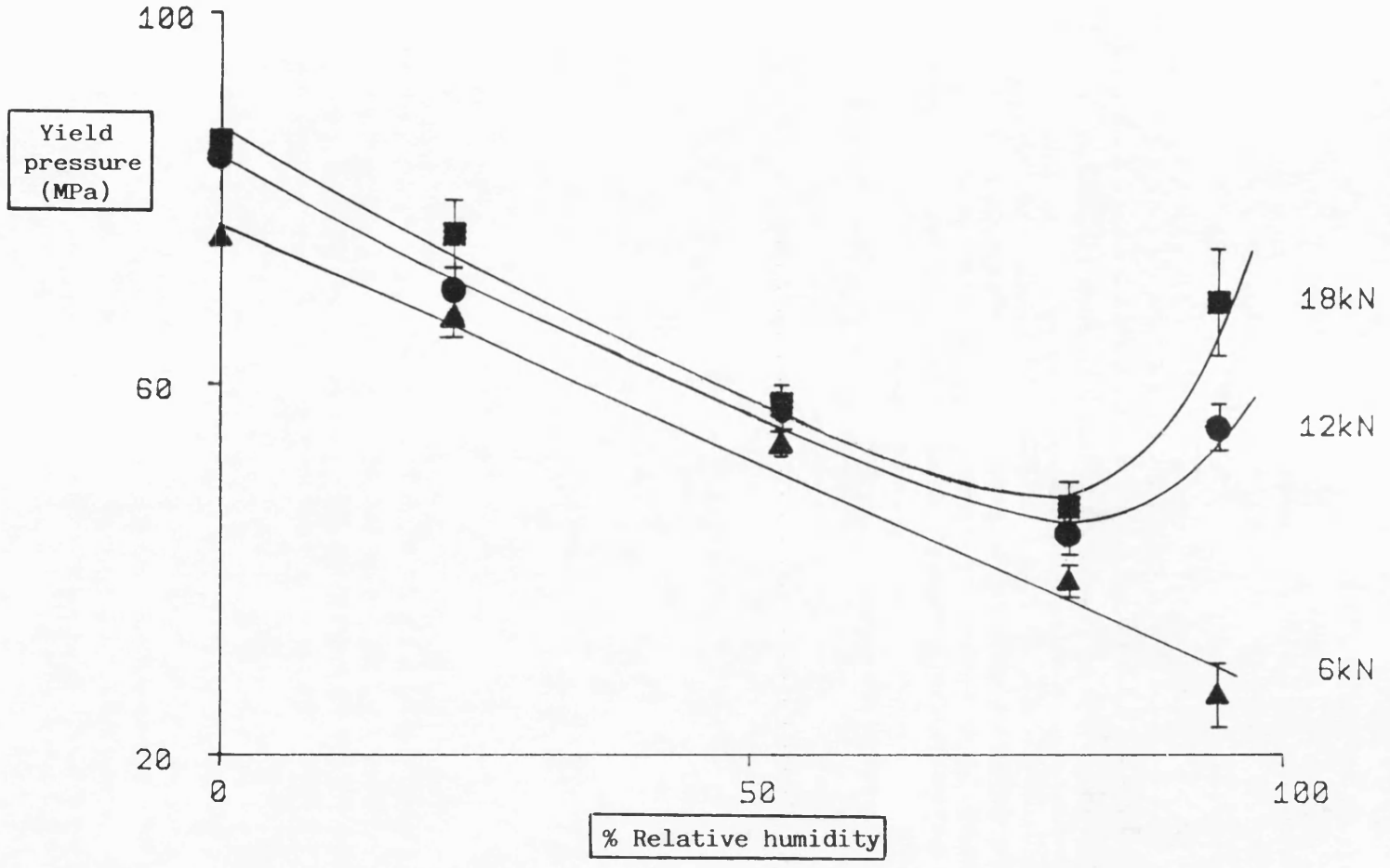

Fig. 7.8 Effect of moisture on the yield pressure of Starch 1500.

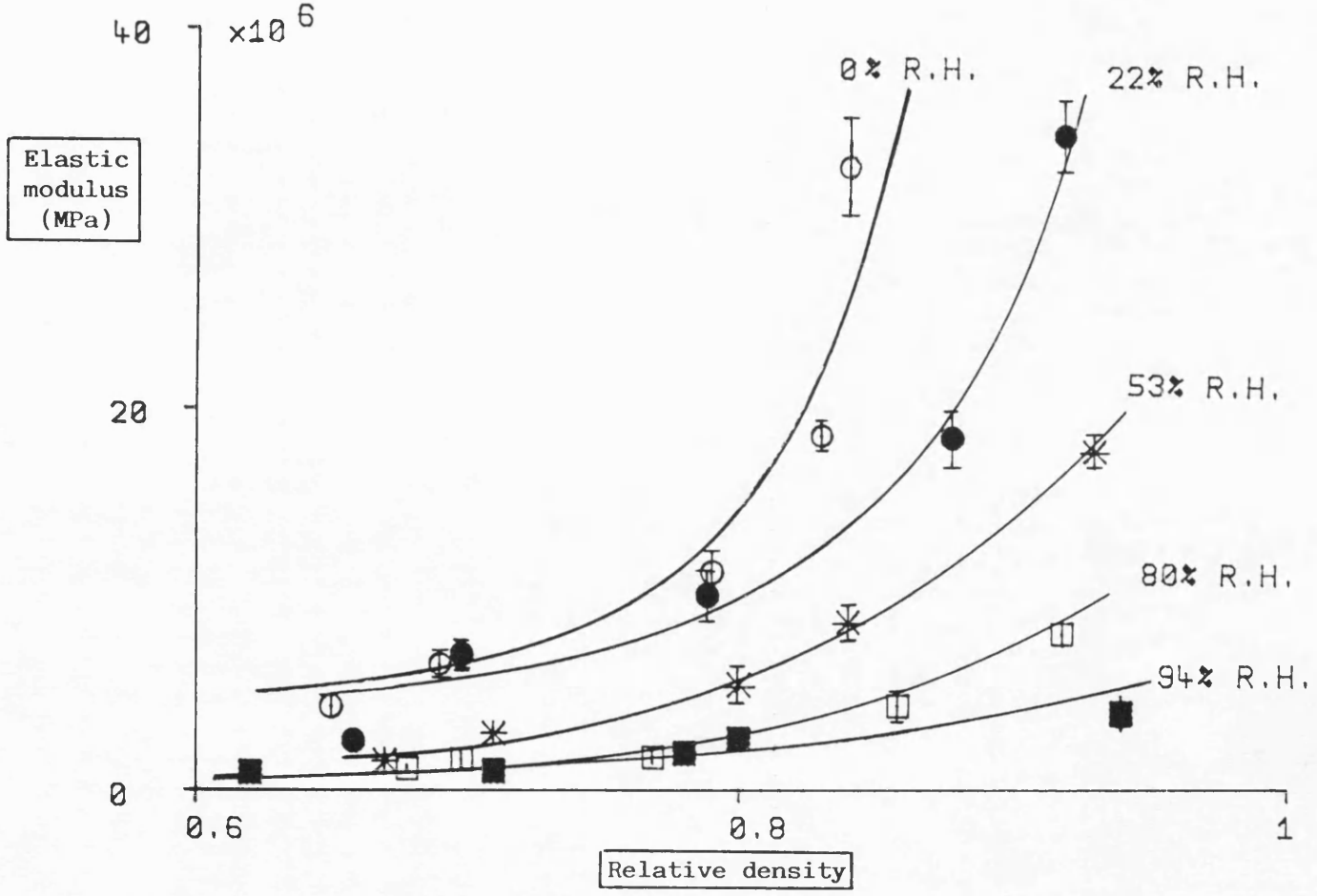

Fig. 7.9 Effect of moisture on the elastic modulus of Starch 1500.

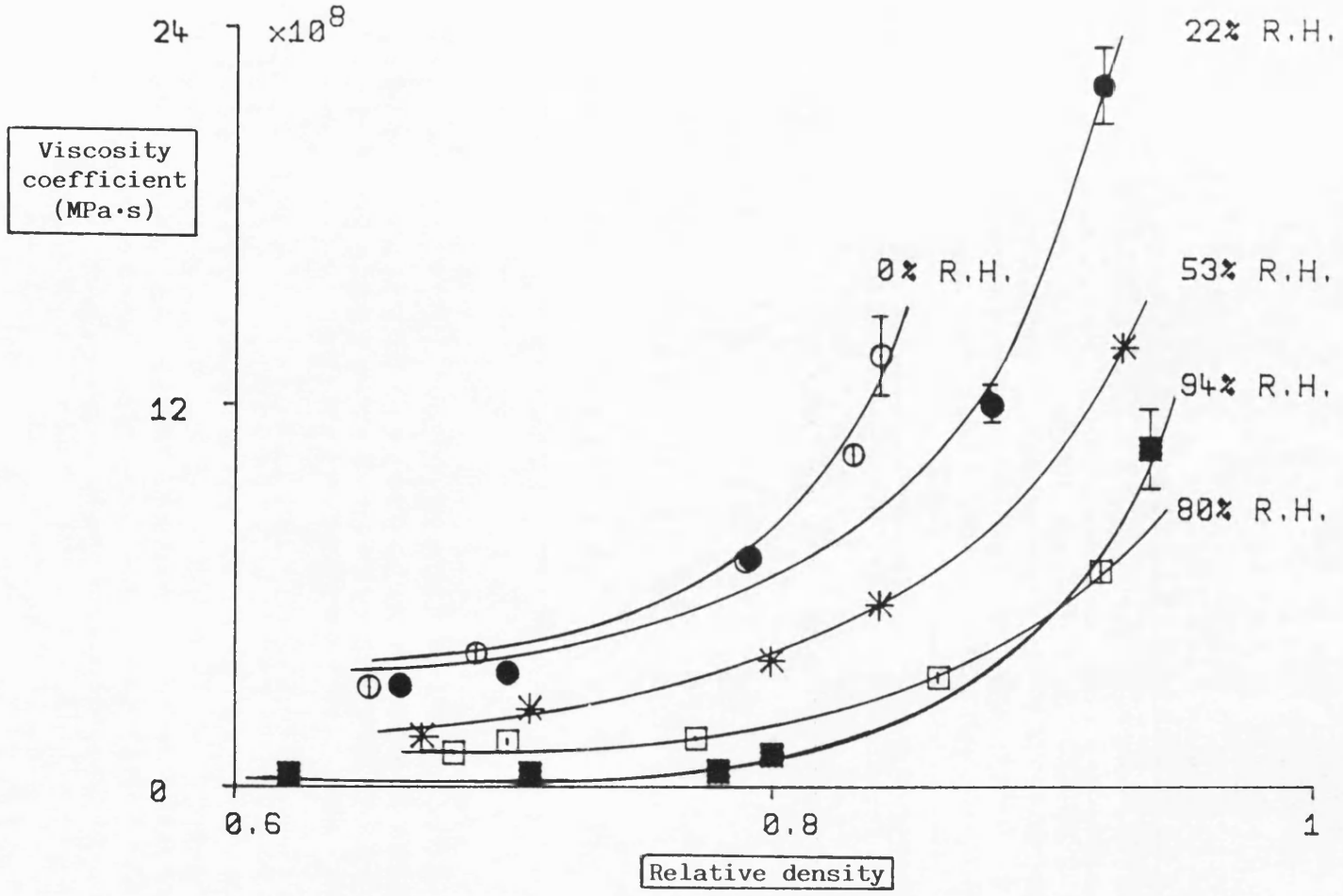

Fig. 7.10 Effect of moisture on the viscosity coefficient of Starch 1500.

and plastic deformation of the material. The effect of moisture on the viscoelastic properties of Starch 1500 was characterised by an increase in the asymptotic value J_i (Fig. 7.11), suggesting an increase in the material's potential for retarded elastic deformation. The k_2 values, however, showed a more complicated dependence on moisture (Fig. 7.12). They reached their lowest level at 22 and 53% and highest at 94%, while intermediate values were obtained at 0 and 80% relative humidity. This is attributed to gradually induced structural changes in the material as a result of starch-water interaction.

Diametral loading results obtained for the produced tablets can be seen in Table F.20. As mentioned above, moisture was shown to facilitate densification and produce tablets of lower porosity. Not unexpectedly, the mechanical properties of tablets, assessed by means of radial work of failure (Fig. 7.13), generally improved as moisture increased. However, at 94% relative humidity, values of this parameter decreased and, as a whole, a deterioration of the mechanical properties of tablets was observed. This confirms previous reports that high levels of moisture have a negative effect on the mechanical properties of tablets (Zografi et al, 1984; Ahlneck and Alderborn, 1989).

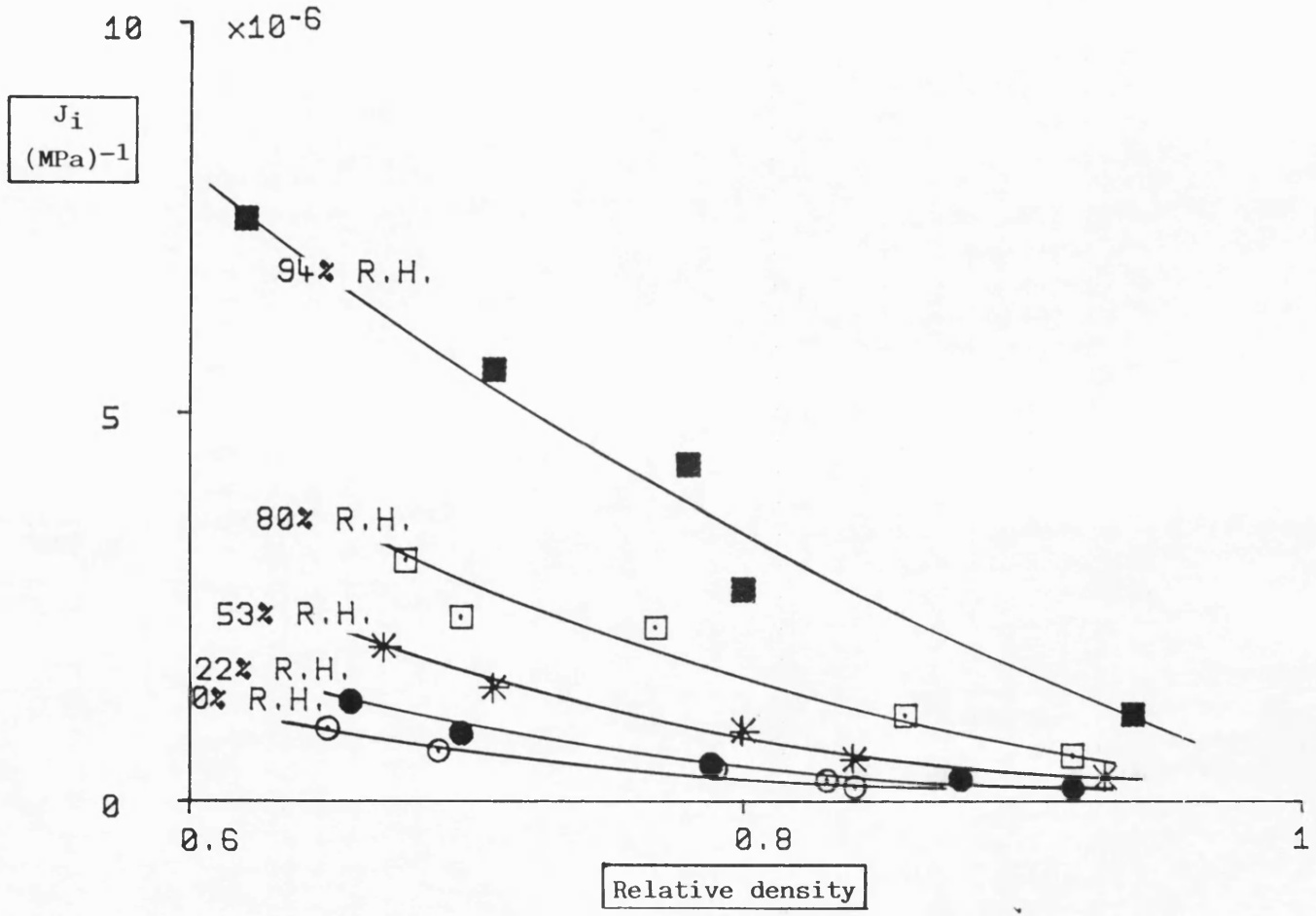

Fig. 7.11 Effect of moisture on the J_i values of Starch 1500.

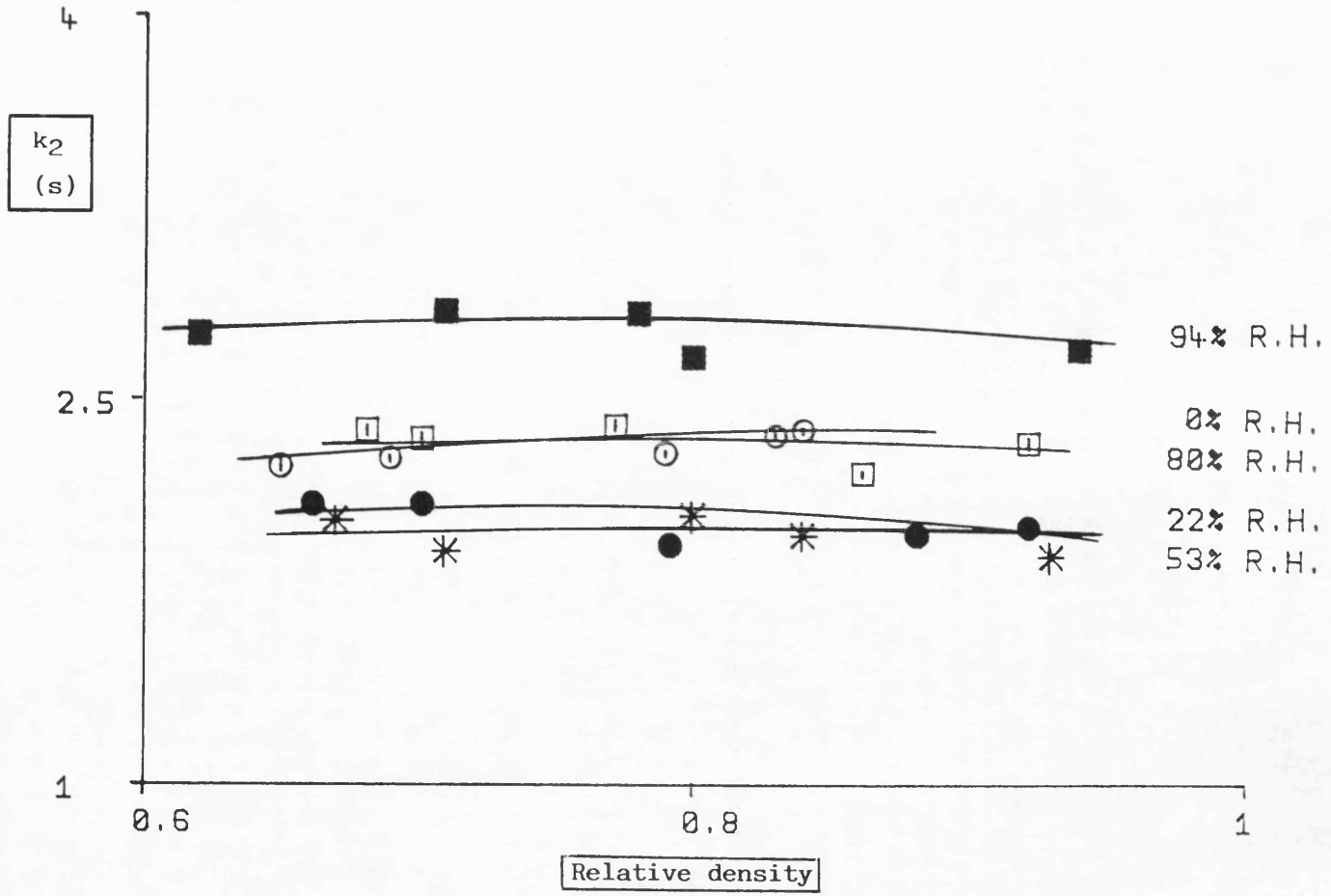

Fig. 7.12 Effect of moisture on the k_2 values of Starch 1500.

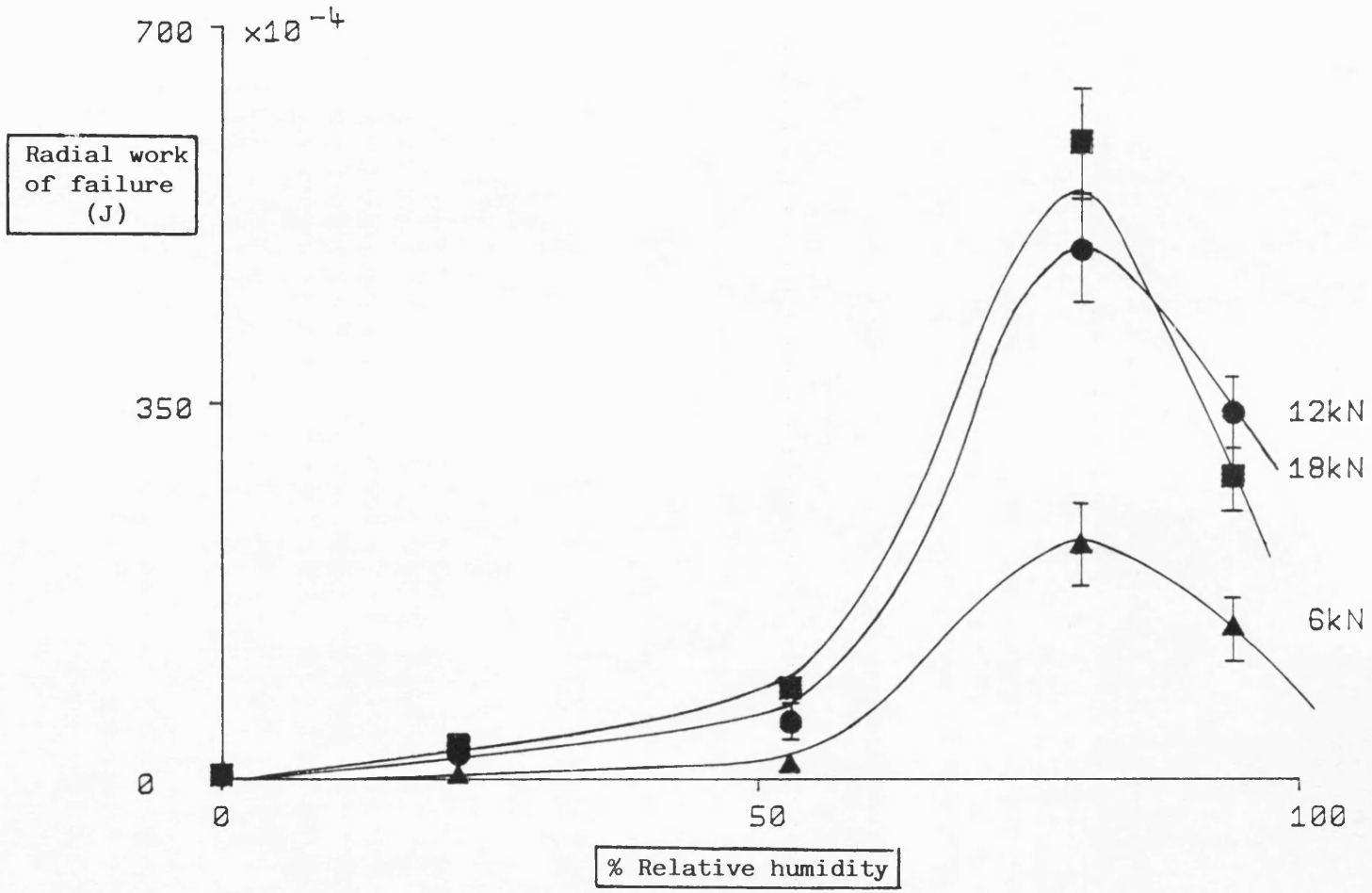

Fig. 7.13 Effect of moisture on the radial work of failure of Starch 1500.

7.4 DEGREE OF PREGELATINISATION

Starches from different sources differ in their amylose and amylopectin content (Whistler and Paschall, 1967). Such differences may be responsible for the difficulty in substituting various types of starch in a given formulation.

Pregelatinisation is a process involving the chemical or physical treatment of starch. During physical modification, starch is processed in the presence of water and heat and subsequently dried. As a result, all or part of the starch granules and, therefore, the amylose-amylopectin bonds are broken. Starch 1500 consists of approximately 5% amylose, 15% amylopectin and 80% unmodified starch.

Samples from four different batches (B.N. 807010, 811024, 801035 and 903025) were obtained, containing different amounts of cold water solubles, i.e. 15.4, 13.4, 12.6 and 10.9% respectively. These values were related to the amount of free amylopectin present (Evans, 1989) following pregelatinisation.

For comparative purposes, pure amylose and amylopectin were also tested along with the above-mentioned batches of Starch 1500. S.E.M. studies (Figs. C.5 and C.6) showed that both the amylose and amylopectin samples consisted of small, regularly shaped particles, loosely bonded together in large agglomerates. The samples were compressed to a peak load of 6, 12 and 18kN (section 2.2.1). The parameters related to work during

compaction, and results from extended Heckel plots are given in Tables F.21-F.24. No significant differences were found in any of the parameters for the four batches. Furthermore, amylose and amylopectin gave similar values for most parameters obtained during compaction (Tables F.25-F.27). However, yield pressure values for amylopectin (Table F.28) were slightly higher than for amylose (Fig. 7.14), indicating a higher resistance of amylopectin to consolidation during compaction.

Creep analysis was performed on samples of each material in order to determine differences in their viscoelastic behaviour. The data are presented in Tables F.29-F.32. The results yielded no evidence that the amount of cold water solubles affects the creep behaviour of Starch 1500. However, amylopectin samples showed higher values of viscosity coefficient than amylose throughout the porosity range (Fig. 7.15). This is in agreement with the observed higher yield pressure of amylopectin and indicates that this material is less able to undergo plastic deformation under load.

Diametral loading results are given in Tables F.33 and F.34. Amylose and, in particular, amylopectin tablets showed poor mechanical properties. This is not surprising, considering their lower ability to consolidate, as assessed by their yield pressure and viscosity coefficient values. In the case of the four batches of Starch 1500, neither tensile strength or work of failure values (Fig. 7.16) ranked the materials according to their cold water solubles content.

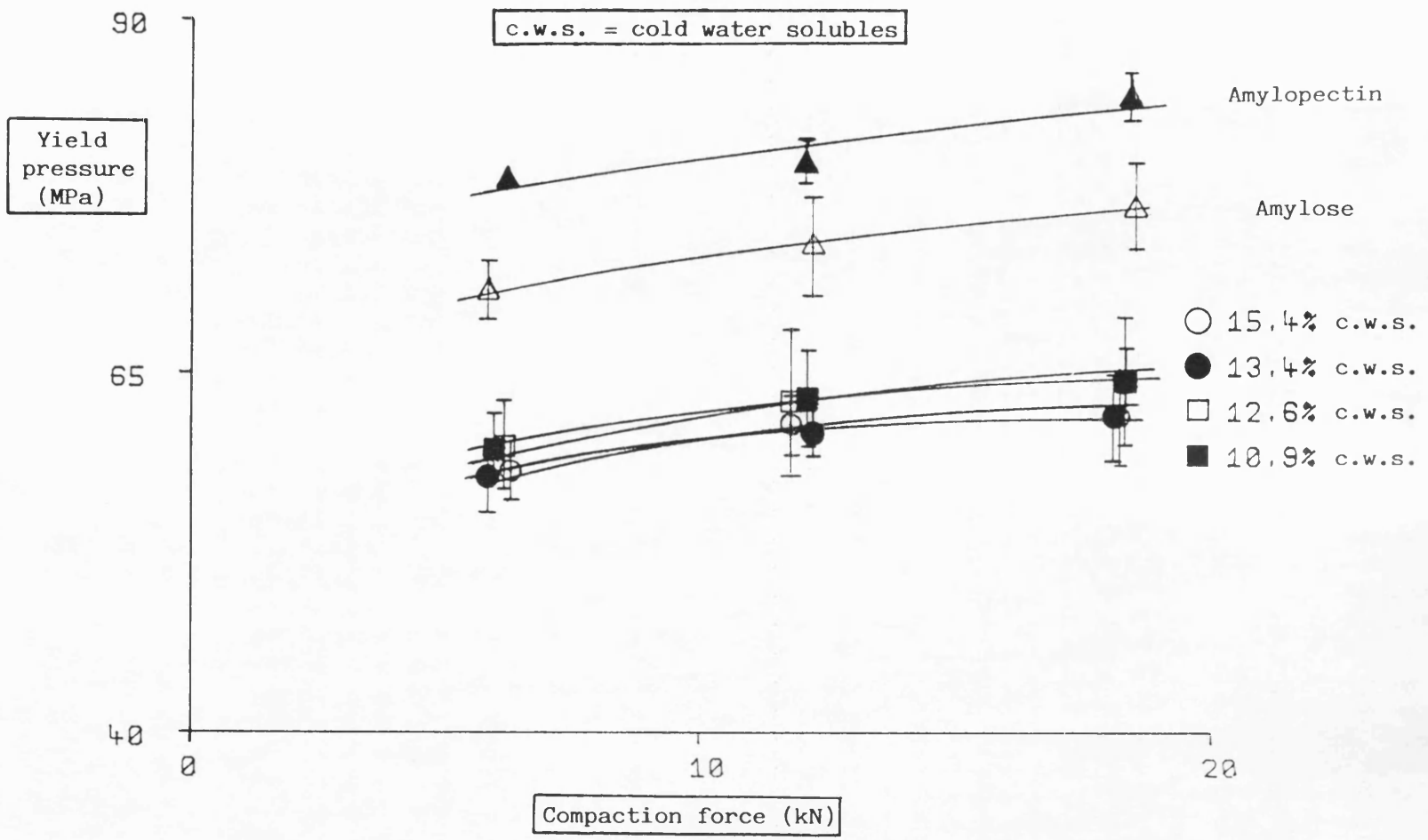

Fig. 7.14 Effect of the amount of cold water solubles on the yield pressure of Starch 1500.

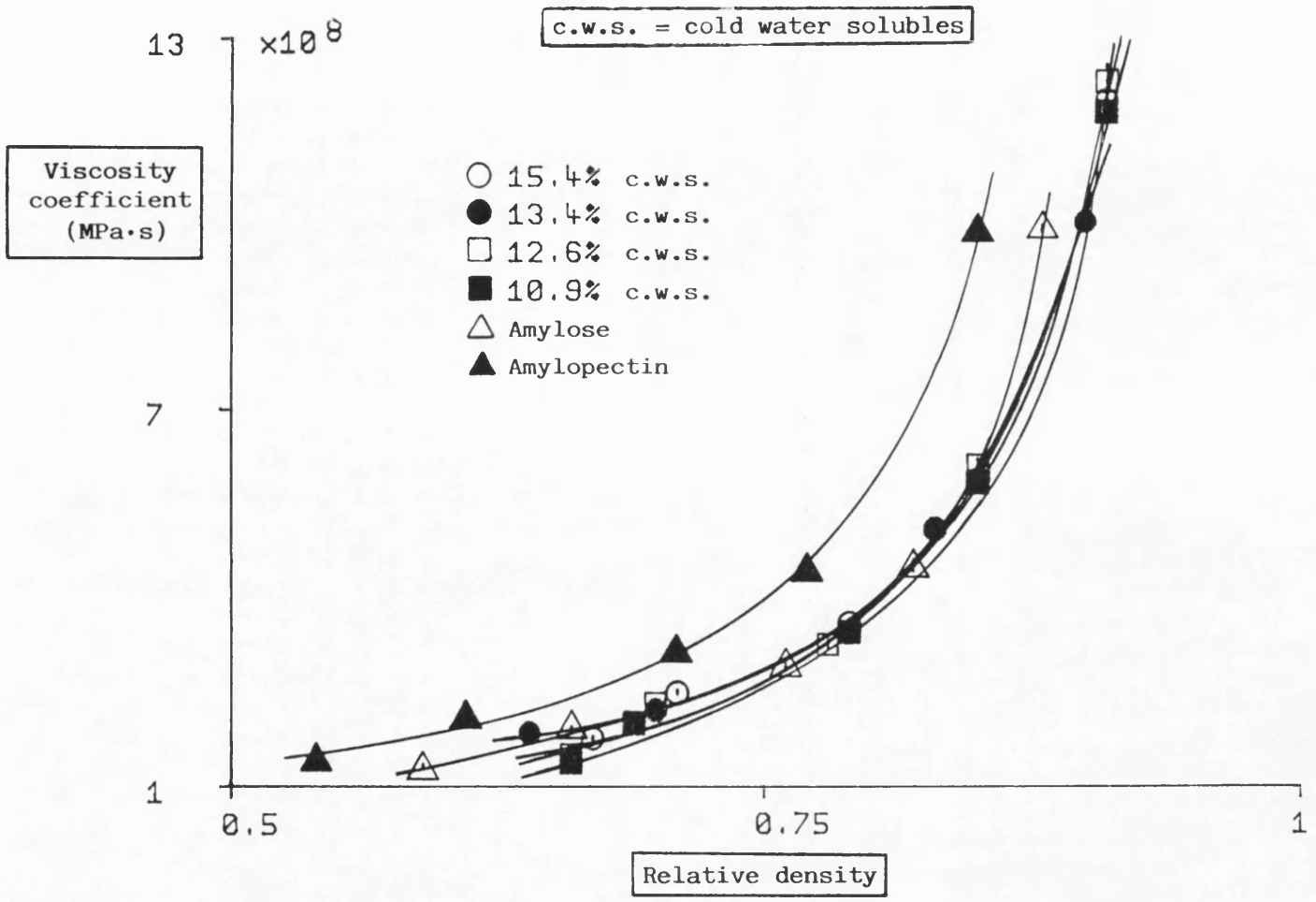

Fig. 7.15 Effect of the amount of cold water solubles on the viscosity coefficient of Starch 1500.

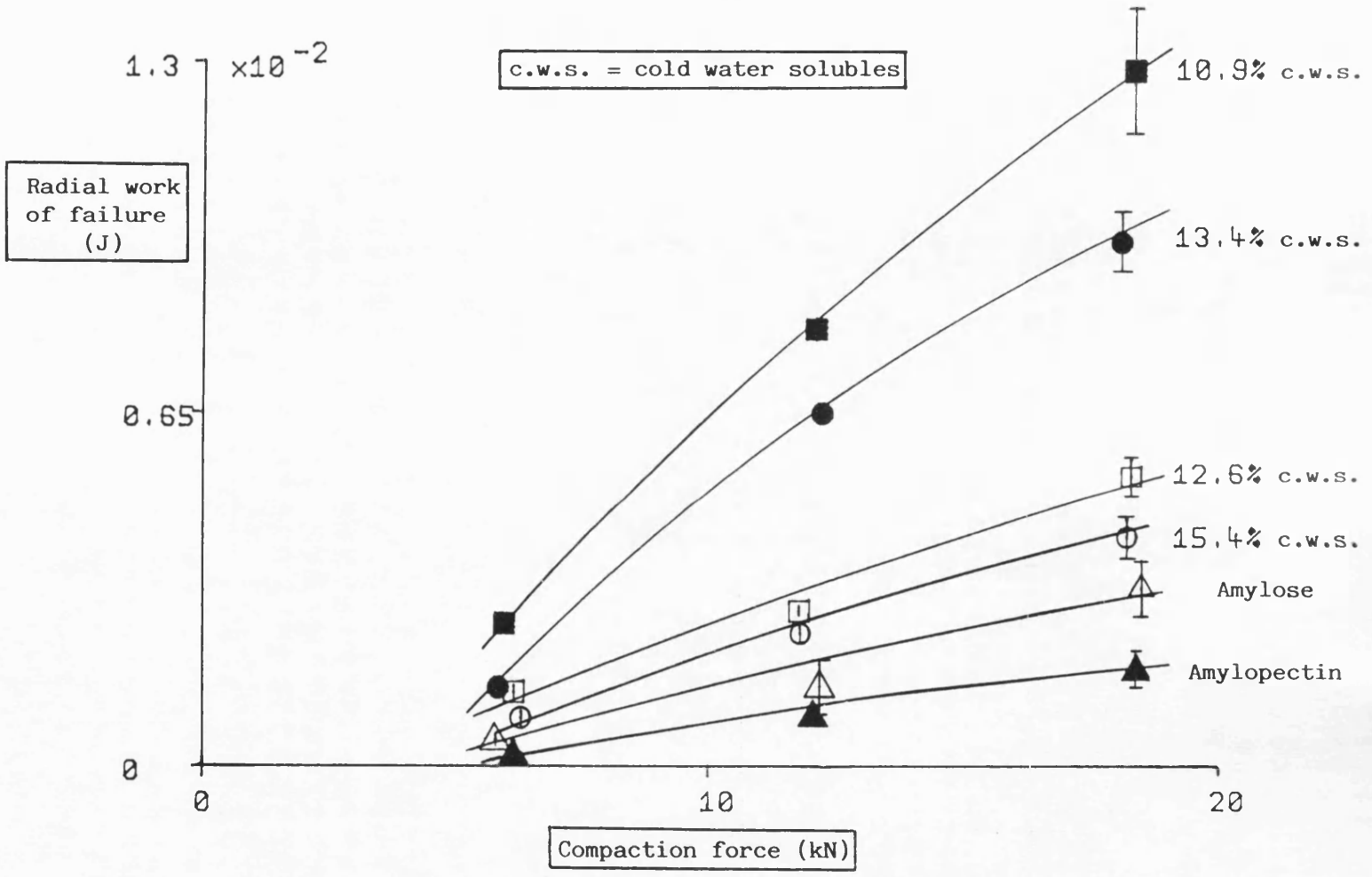

Fig. 7.16 Effect of the amount of cold water solubles on the radial work of failure of Starch 1500.

The results indicate, that for the range of samples studied, there is no effect of the amount of cold water solubles on the compaction properties of Starch 1500. This suggests that other factors are responsible for the observed differences. One possible explanation could be the variation in the particle size distribution of these samples (Table 2.4).

A partially pregelatinised starch, Starch 1500 (B.N. 306015) and a fully pregelatinised starch, National 1551, were also compared in order to assess the effect of the degree of pregelatinisation on the physico-mechanical properties of modified starch.

Work values and parameters from extended Heckel plots at three peak loads (6, 12 and 18kN) are presented in Table F.35. The lower mean yield pressure values obtained for National 1551 (Fig. 7.17) indicate that this material undergoes more deformation during compression than Starch 1500. On the other hand, chord area showed a larger increase with compaction force for National 1551 (Fig. 7.18), suggesting that this material undergoes a lot more continuing time-dependent deformation during decompression.

Creep data obtained for the two materials are given in Table F.36. Elastic modulus values for Starch 1500 were slightly lower at high porosities (Fig. 7.19) than those for National 1551. This indicates that at such porosities the latter undergoes less elastic deformation. Furthermore, no significant

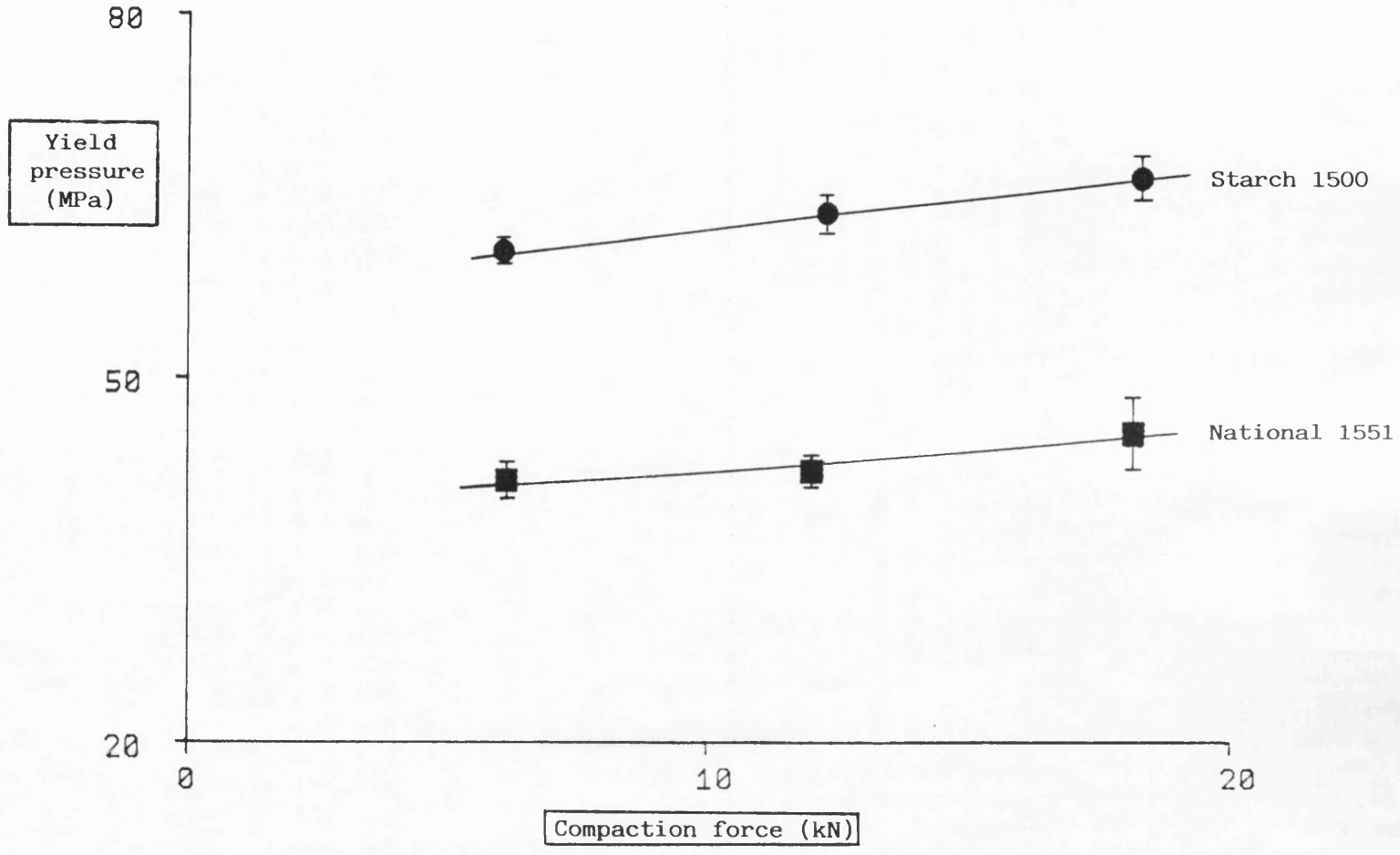

Fig. 7.17 Yield pressure values for Starch 1500 and National 1551 at a range of compaction forces.

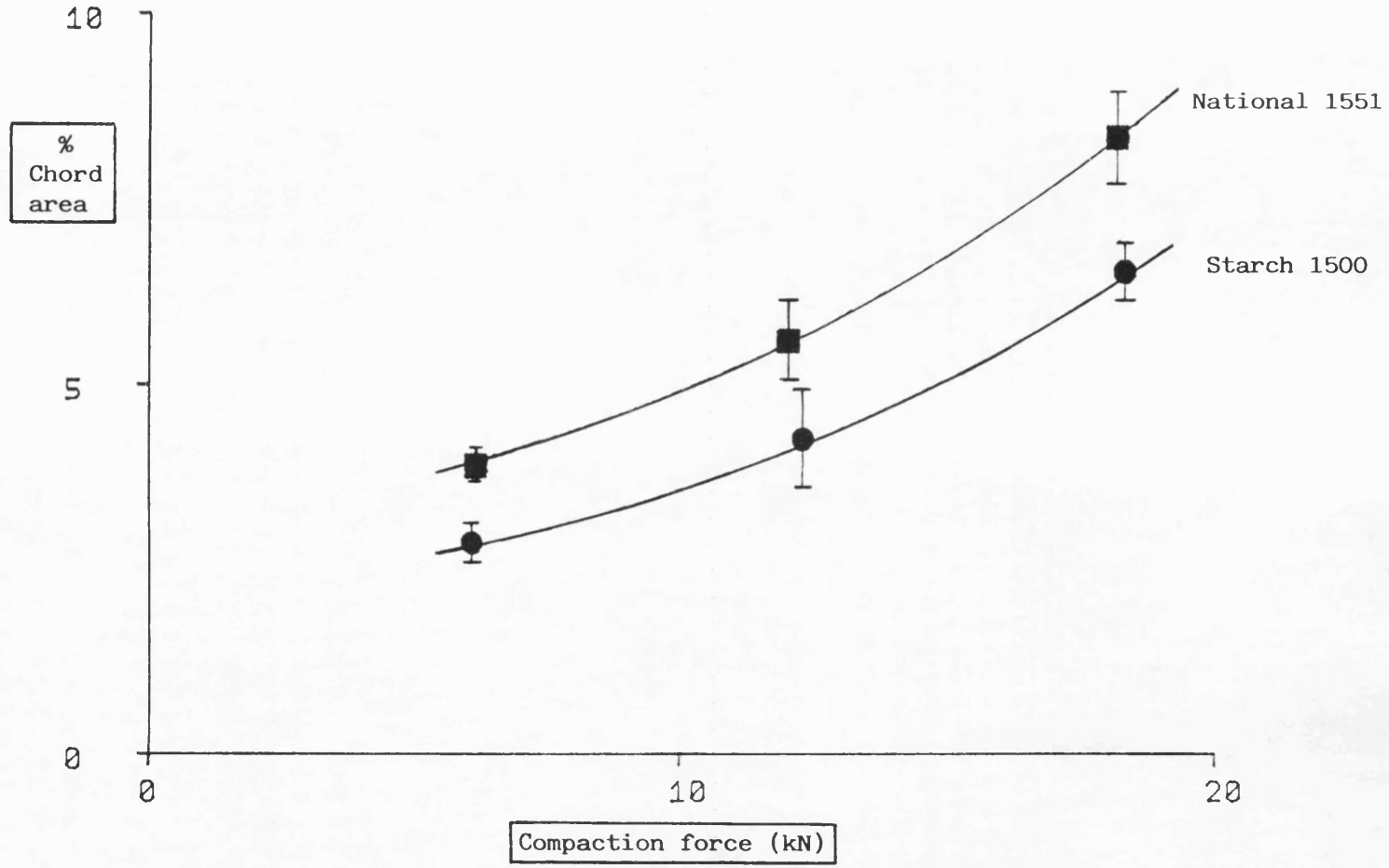

Fig. 7.18 % chord area values for Starch 1500 and National 1551 at a range of compaction forces.

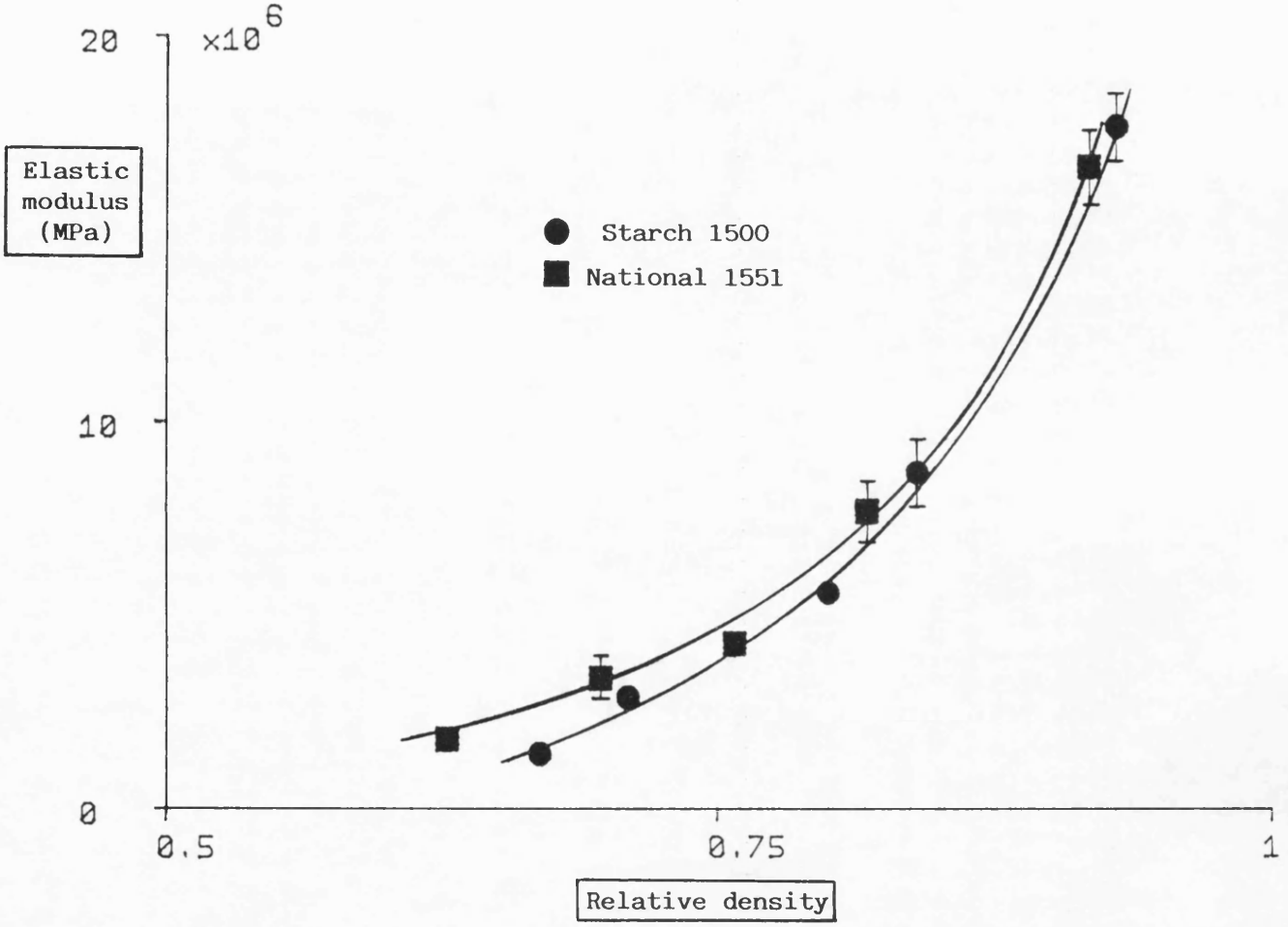

Fig. 7.19 Elastic modulus values for Starch 1500 and National 1551 at a range of relative densities.

differences were observed between the viscosity coefficient values for these two materials (Fig. 7.20). The same was true for the J_i values (Fig. 7.21). Except at the highest relative density, National 1551 showed higher k_2 values than Starch 1500 (Fig. 7.22), suggesting a stronger time-dependent nature. This is supported by the higher chord area values mentioned earlier.

Diametral loading results (Table F.37) showed that National 1551 formed tablets of superior mechanical properties. This was demonstrated by the higher tensile strength and work of failure values (Fig. 7.23) compared to those of Starch 1500. Since no major obvious differences seemed to exist in the deformation properties of these materials to justify the differences in the mechanical properties of their compacts, the extent and type of bonding within National 1551 compacts, possibly related to the pregelatinisation procedure, may be assumed to be the reason for the material's tableting performance. Differences in the surface characteristics between these two materials, as illustrated in Fig. C.2, may also play an important role. National 1551 particles showed a particularly high degree of surface irregularities, such as sharp projections and concavities, whereas Starch 1500 particles were generally smooth and relatively regular in their shape.

The above results suggest that the degree of pregelatinisation of starch products has an important effect on the mechanical properties of the produced compacts. It seems to be a field worthy of further study.

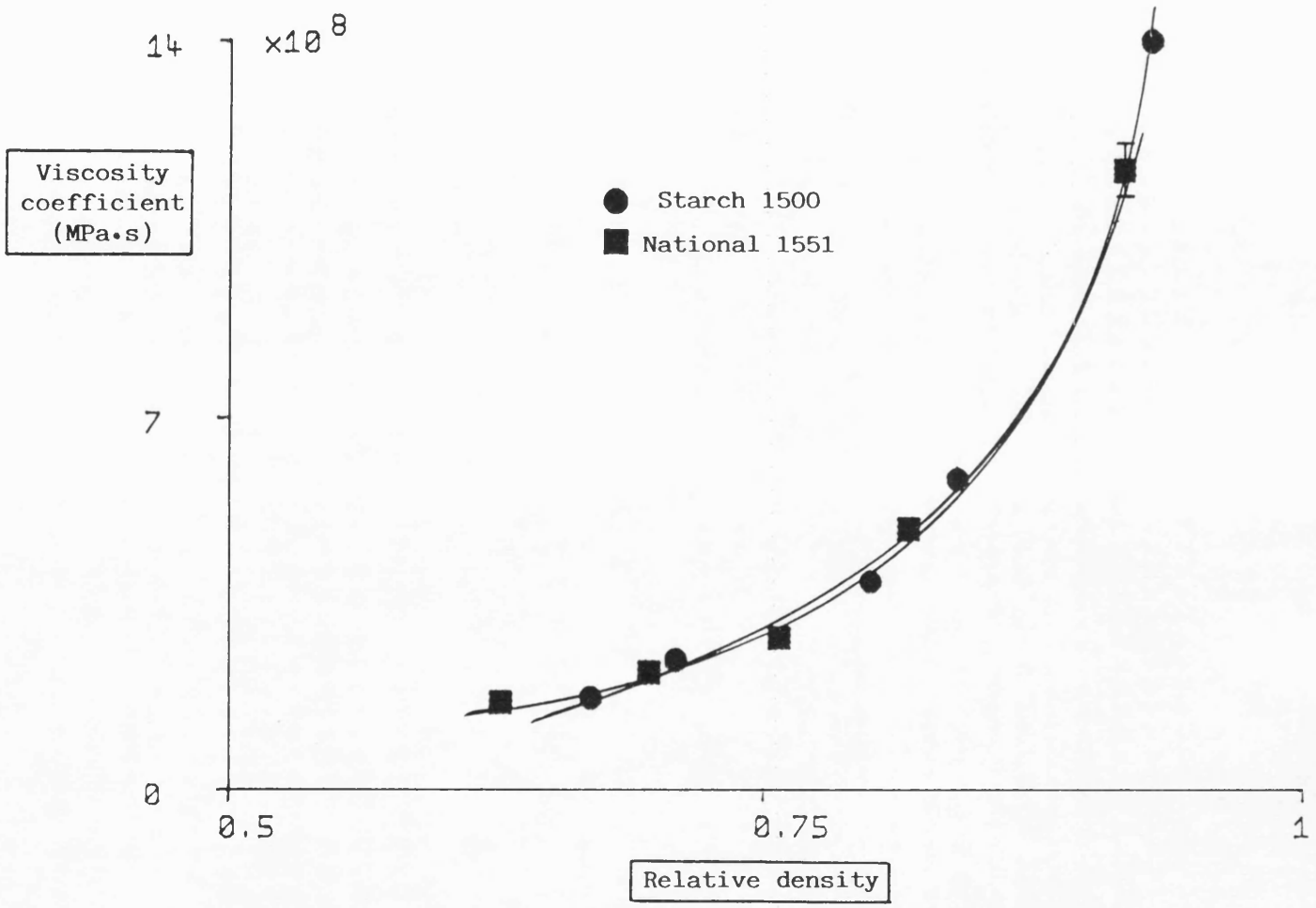

Fig. 7.20 Viscosity coefficient values for Starch 1500 and National 1551 at a range of relative densities.

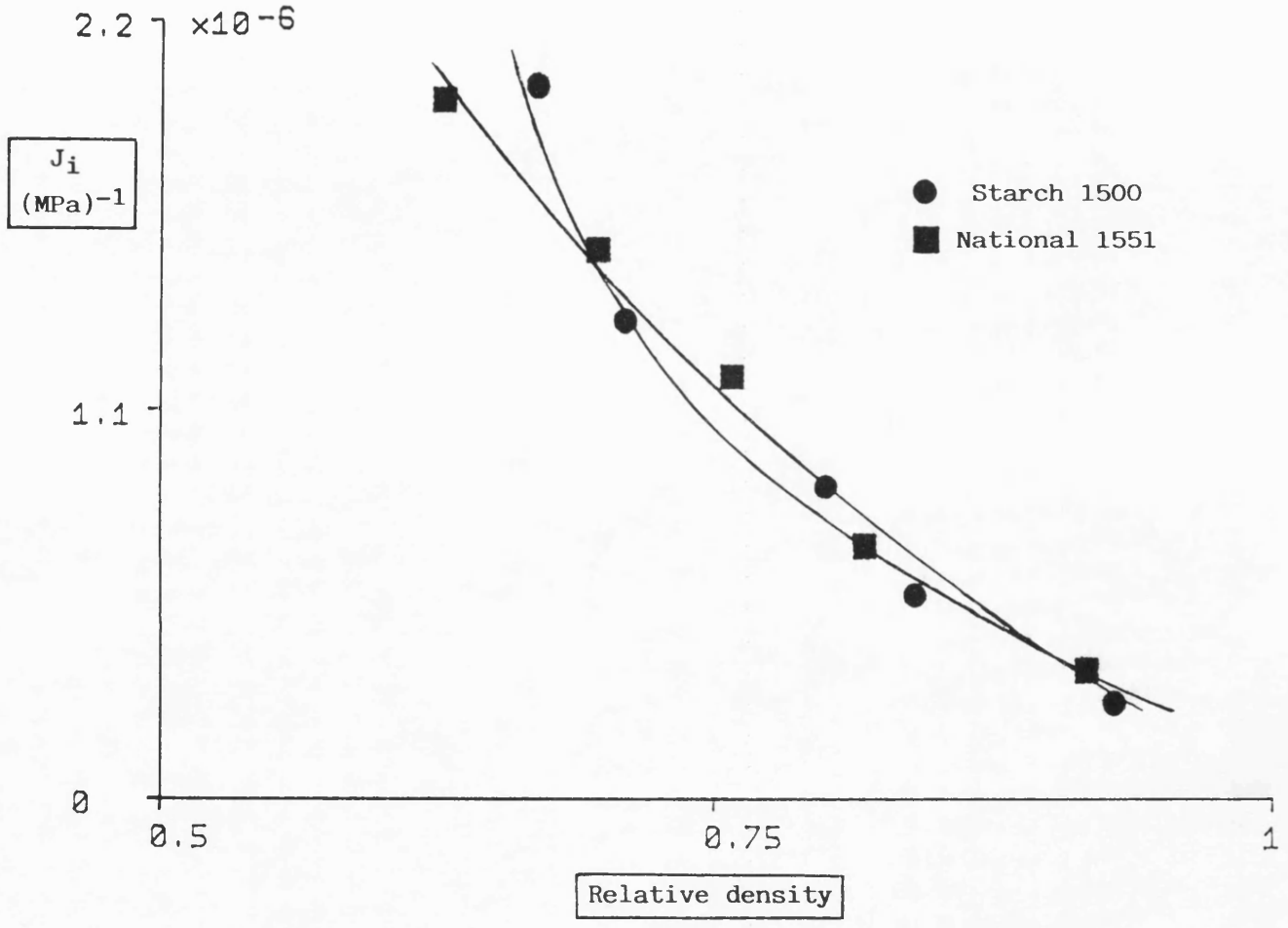

Fig. 7.21 J_i values for Starch 1500 and National 1551 at a range of relative densities.

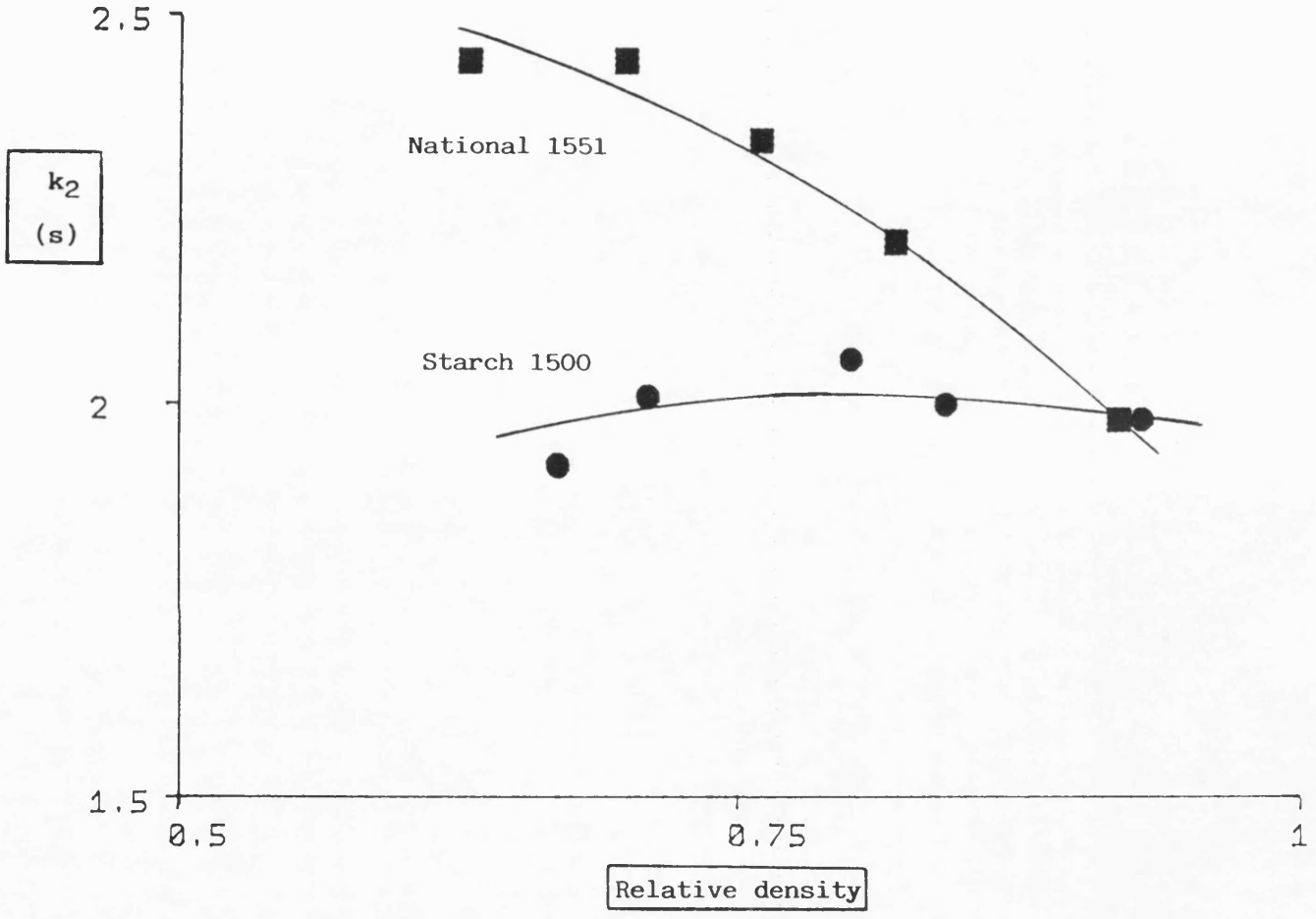

Fig. 7.22 k_2 values for Starch 1500 and National 1551 at a range of relative densities.

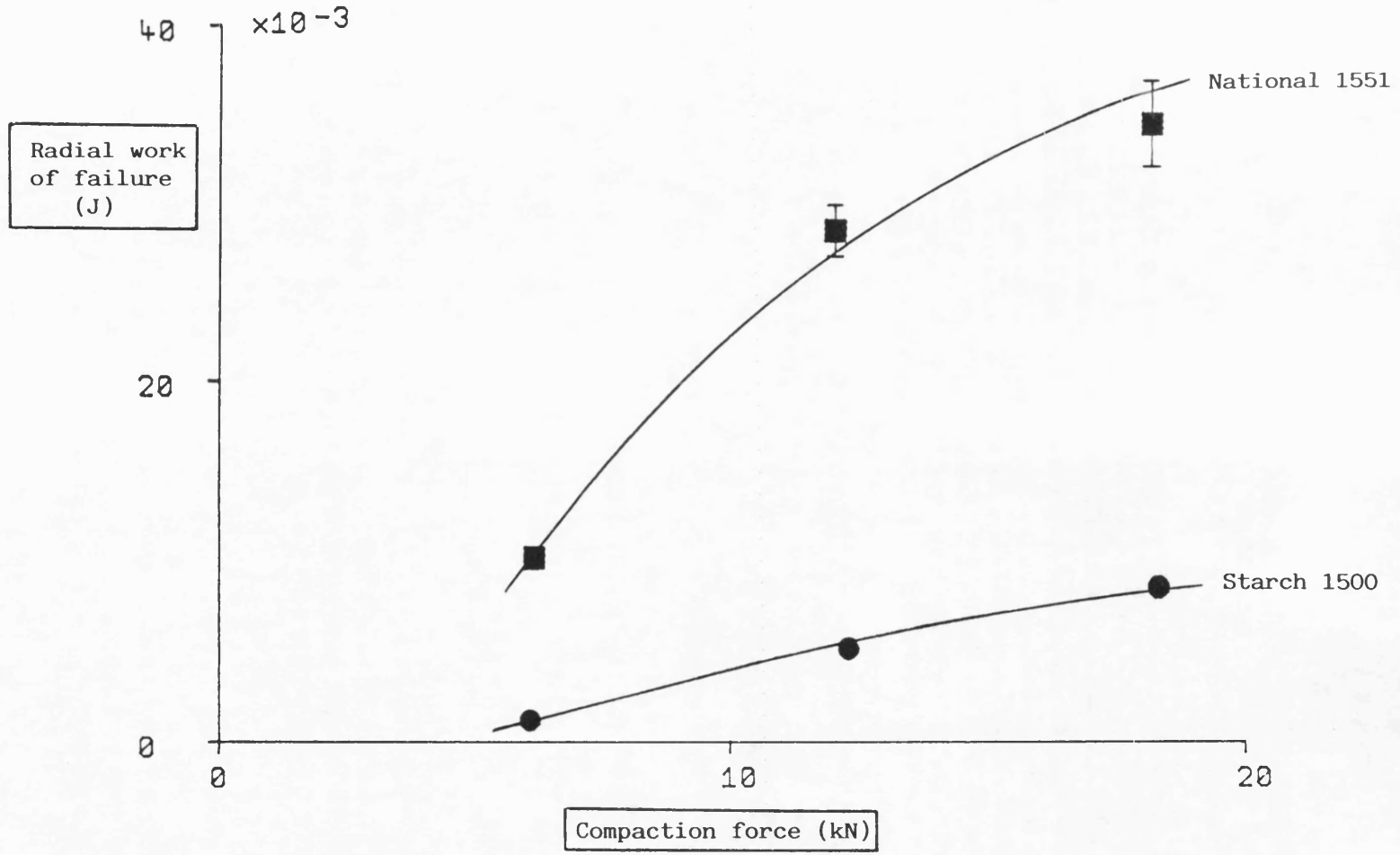

Fig. 7.23 Radial work of failure for Starch 1500 and National 1551 at a range of compaction forces.

CHAPTER EIGHT

CONCLUSIONS

Work measurements provided some information regarding the deformation properties of materials during compaction. Expansion work during decompression was used to rank the materials according to their ability to undergo elastic deformation. Energy utilisation during compaction was best assessed by means of the "true" work of compaction expressed as a percentage of the total work.

Values for conventional Heckel parameters were in agreement with previous results regarding the consolidation behaviour of the materials tested. The results showed that data derived from Heckel plots using the tablet-in-die-method, cannot differentiate between the discrete deformation mechanisms of materials, such as plastic and elastic deformation, for example, since they describe only the overall consolidation. Extended Heckel plots were used to characterise the behaviour of materials not only during compression, but also during decompression and after ejection. A number of new parameters were proposed for assessing the viscoelastic properties of

materials. The chord area quantified the curvature of decompression curves and reflected the combined effect of continuing plastic and viscoelastic deformation and the elastic recovery of materials during the decompression stage. The area under the compression curves and the area above the decompression curves of extended Heckel plots were also calculated and used to assess the deformation properties of materials. Such information, when considered with other data from conventional Heckel plots, contributes to a fuller understanding of the tableting behaviour of a material.

Standardisation of the experimental conditions during compaction studies is crucial. Values obtained from Heckel plots were strongly dependent on the applied pressure. Therefore, it is proposed that such information should accompany the results.

Diametral loading tests showed that the tensile strengths of tablets made at the same compaction force were higher for plastic than for brittle materials. Avicel PH102 and Emcocel 90M tablets showed the highest values for all the mechanical properties that were measured whereas, Emcompress gave particularly low values. This confirms that plastic deformation is an important factor in the formation of robust compacts. On the other hand, the results obtained for Starch 1500 indicate that plastic deformation alone does not guarantee compacts with adequate mechanical properties. Absence of extensive elastic deformation during compaction is also necessary.

The strength and toughness of tablets was measured in a

direct tension test as well as in a diametral loading test, in order to assess the degree of isotropicity with respect to these properties. The results showed that it is difficult to predict a tablet's mechanical properties from a knowledge of the consolidation mechanism alone. Bonding surface area and bond strength are also extremely important. Comparison between radial and axial strength values provided a useful means of assessing strength isotropy in tablets.

Stress relaxation results allowed the materials to be ranked according to their time-dependency. Fitting data to a hyperbolic equation enabled the asymptotic value of relaxed stress, and the rate of stress relaxation at short times immediately after peak load, to be determined. Such treatment of stress relaxation data is considered to be an improvement on methods proposed elsewhere (Baba and Nagafuji, 1964).

A method was developed to characterise the creep behaviour of particulate solids under load. Optimum experimental conditions were selected based on initial studies of factors such as test duration, powder mass, loading rate up to constant stress and the use of preformed compacts or loose powders Materials were compared over a range of relative densities.

Creep testing was shown to be extremely useful in assessing the deformation properties of particulate materials, since it is possible to quantify separately the elastic, viscoelastic and viscous deformation of materials under constant stress. Parameters such as the time constant k_2 in the viscoelastic

region and the asymptotic compliance value J_i quantify the rate and extent of retarded elastic deformation of materials under constant stress and thereby characterise their time-dependent characteristics.

Spectral analysis was used as an alternative approach to analyse creep data in the frequency domain. Characteristic spectral patterns, associated with the variance in the time series of creep compliance, provided evidence of specific mechanisms responsible for viscoelastic deformation in materials under load. For each material, a number of significant peaks were revealed, possibly related to physical changes within the materials which determine their time-dependent behaviour.

Extremely coarse particle size fractions of Starch 1500 showed lower yield pressure and higher work of failure values compared to the commercially available product. Moisture had a marked effect on the deformation characteristics of Starch 1500, but the amount of cold water soluble fraction in different samples of the material had no systematic effect on compression properties. Tablets of National 1551, a fully pregelatinised starch possessed superior mechanical properties to those formed from Starch 1500, a partially pregelatinised material.

SUGGESTIONS FOR FURTHER WORK

Determination of elastic moduli by creep analysis requires instantaneous loading of the materials. Further work should be performed to study the effect of greatly increased loading rates and if possible at rates approaching instantaneous loading.

The influence of contact time on the chord area obtained from the decompression curve of extended Heckel plots, would provide information on the time-dependency of materials. Also, the effect of contact time on the mechanical properties of tablets, measured in direct and indirect tension tests would assess time-dependency in both the axial and radial planes.

Further experiments are required at humidities between 53% and 94% R.H. to determine the exact point at which water results in a deterioration of the mechanical properties of Starch 1500. Furthermore, Differential Scanning Calorimetry studies of starch stored at various humidity conditions should provide information on the corresponding structural changes within the material.

The degree of pregelatinisation of modified starch was shown in this study to be an important factor affecting its physico-mechanical properties. More detailed study is needed of the manufacturing steps involved in the pregelatinisation process and their influence on the physical, chemical and mechanical properties of starch.

REFERENCES

- Ahlneck, C. and Alderborn, G., 1989

  Int. J. Pharm., 54, 131-141

- Alderborn, G., 1985

  "Studies on the importance and characterization of particle fragmentation during tableting"

  Ph. D. Thesis, University of Uppsala, Sweden

- Alderborn, G. and Nystrom, C., 1982a

  Acta Pharm. Suec., 19, 147-156

- Alderborn, G. and Nystrom, C., 1982b

  Acta Pharm. Suec., 19, 381-390

- Alderborn, G., Pasanen, K. and Nystrom, C., 1985

  Int. J. Pharm., 23, 79-86

- Armstrong, N.A. and Blundell, L.P., 1985

  J. Pharm. Pharmacol., 35, 320-321

- Armstrong, N.A. and Haines-Nutt, R.F., 1970

  J. Pharm. Pharmacol., 22, Suppl., 8S-10S

- Armstrong, N.A. and Haines-Nutt, R.F., 1974

  Proc. 1st Int. Conf. Comp. Consol. Part. Mat., Brighton

- Aulton, M.E., Tebby, H.G. and White, P.J.P., 1974

  J. Pharm. Pharmacol., 26, Suppl., 59P-60P

- Baba, M. and Nagafuji, N., 1965

Annu. Rept. Shionogi Res. Lab., No. 15, 147-151

- Bal'shin, Yu., 1938

Vestnik Metall., 18, 124-137

- Barry, B.W., 1970

J. Colloid. Interface Sci., 32, 551-560

- Barry, B.W., 1971

J. Soc. Cosmet. Chem., 22, 487-503

- Barry, B.W., 1974

"Advances in pharmaceutical sciences" Vol. 4

Academic Press, London

- Barry, B.W. and Grace, A.J., 1971a

Rheol. Acta, 10, 113-120

- Barry, B.W. and Grace, A.J., 1971b

J. Pharm. Sci., 60, 1198-1203

- Bateman, S.M., Rubinstein, M.H. and Wright, P., 1987

J. Pharm. Pharmacol., 39, 66P

- Bloomfield, P., 1976

"Fourier analysis of time series"

Wiley, New York

- Bowden, F.P. and Tabor, D., 1954

"The friction and lubrication of solids"

Clarendon Press

- Britten, J.R. and Pilpel, N., 1978

J. Pharm. Pharmacol., 30, 21P

- Carless, J.E. and Leigh, S., 1969

Feder. Int. Pharm., 29th Int. Congr. Pharm. Sci., London

- Carless, J.E. and Leigh, S., 1974

J. Pharm. Pharmacol., 26, 289-297

- Carneiro, F.F.L. and Barcellos, A., 1953

R.I.L.E.M Bull., No 18, p.99

- Carr, R.L., 1970

Brit. Chem. Eng., 15, 1541-1549

- Carstensen, J.T., 1980

"Mechanical properties and rate processes in solid pharmaceutics"

Academic Press, New York

- Carstensen, J.T., Marty, J.P., Puisieux, F. and Fessi, H., 1981

J. Pharm. Sci., 70, 222-223

- Carstensen, J.T. and Toure, P., 1980

Powder Technol., 26, 199-204

- Caspar, U. and Muller, F., 1984

Pharm. Acta Helv., 59, 329-

- Celik, M. and Travers, D.N., 1985

Drug Dev. Ind. Pharm., 11, 299-314

- Chatfield, C., 1984

"The analysis of time series: An introduction"

3rd Edn., Chapman and Hall Ltd., London

- Cole, E.T., Rees, J.E. and Hersey, J.A., 1975

Pharm. Acta Helv., 50, 28-32

- Cook, G.D. and Summers, M.P., 1986

J. Pharm. Pharmacol., 38, 76P

- Cook, J. and Gordon, J.E., 1964

Proc. Roy. Soc. A 282, 508

- Cottrell, A.H., 1953

"Dislocations and plastic flow in crystals"

Oxford University Press

- Coelho, M.C. and Harnby, N., 1978

Powder Technol., 7, 201-205

- David, S.T. and Augsburger, L.L., 1977

J. Pharm. Sci., 66, 155-159

- de Blaey, C.J. and Polderman, J., 1970

Pharm. Weekbl., 105, 241-250

- de Blaey, C.J. and Polderman, J., 1971a

Pharm. Weekbl., 106, 57-65

- de Blaey, C.J. and Polderman, J., 1971b

Pharm. Weekbl., 106, 589-596

- de Boer, A.H., Bolhuis, G.K. and Lerk, C.F., 1978

Powder Technol., 20, 75-82

- Doelker, E., Gurny, R., Mordier, D., Hart, J.P., Rees, J.E. and Aulton, M.E., 1987

Symposium on Tablet Technology, Stockholm

- Duberg, M. and Nystrom, C., 1982

Acta Pharm. Suec., 19, 421-436

- Duberg, M. and Nystrom, C., 1985

Int. J. Pharm. Tech. and Prod. Mfr., 6, 17-25

- Duckworth, W., 1953

J. AM. Ceram. Soc., 36, 68

- Evans, W.C., 1989

"Trease and Evans' Pharmacognosy"

13th Edn., Bailliere Tindall, London

- Fell, J.M. and Newton, J.M., 1968

J. Pharm. Pharmacol., 20, 657-658

- Fell, J.M. and Newton, J.M., 1970a

J. Pharm. Pharmacol., 22, 247-248

- Fell, J.T. and Newton, J.M., 1970b

J. Pharm. Sci., 59, 688-691

- Fell, J.T. and Newton, J.M., 1971

J. Pharm. Sci., 60, 1866-1869

- Ferry, J.D., 1970

"Visco-elastic properties of polymers"

2nd Edn., John Wiley, New York

- Forlano, A.J. and Chavkin, L., 1960

J. Am. Pharm. Ass. Sci. Ed., 49, 67-69

- Frocht, M.M., 1948

"Photoelasticity" Vol.2

Chapman and Hall Ltd., London

- Fuhrer, C., Nickel, E., Thiel, F., 1975

Acta Pharm. Technol., 21, 149-160

- Gatto, F., 1950

Alluminio, 19, 19-26

- Gordon, J.E., 1983

"The new science of strong materials"

2nd Ed., Penguin, Middlesex

- Gregory, H.R., 1962

Trans. Instn. Chem. Engrs., 40, 241-251

- Griffith, A.A., 1920

Phil. Trans. Roy. Soc. London, A 221, 163-198

- Guyot, J.C., 1978

Int. Conf. Powder Tech. Pharm., p.21

- Haleblian, J.K., 1975

J. Pharm. Sci., 64, 1269-1288

- Hardman, J.S. and Lilley, B.A., 1970

Nature, 228, 353-355

- Hardman, J.S. and Lilley, B.A., 1973

Proc. Roy. Soc. London, A 333, 183-199

- Heckel, R.W., 1961a

Trans. Met. Soc. AIME, 221, 671-675

- Heckel, R.W., 1961b

Trans. Met. Soc. AIME, 221, 1001-1008

- Henderson, B., 1972

"Defects in crystalline solids"

Edward Arnold

- Herrmann, W., 1971/1972

Powder Technol., 5, 25-30

- Hersey, J.A., Cole, E.T. and Rees, J.E., 1972

Proc. 1st Int. Conf. Comp. Consol. Part. Mat., London

- Hersey, J.A. and Krycer, I., 1980

Int. J. Pharm. Tech. and Prod. Mfr., 1, 18-21

- Hersey, J.A. and Rees, J.E., 1971

Nature Physical Science, 230, 96

- Hiestand, E.N., Bane, J.M.Jr. and Strzelinski, E.P., 1971

J. Pharm. Sci., 60, 758-763

- Hiestand, E.N. and Smith, D.P., 1984

Powder Technol., 38, 145-159

- Hiestand, E.N., Wells, J.E., Peot, C.B. and Ochs, J.F., 1977

J. Pharm. Sci., 66, 510-519

- Higuchi, T., Arnold, R.D., Tucker, S.J. and Busse, L.W., 1952

J. Am. Pharm. Ass. Sci. Ed., 41, 93-96

- Higuchi, T., Narsimha, A., Busse, L.W. and Swintosky, J.V., 1953

J. Am. Pharm. Ass. Sci. Ed., 42, 194-200

- Higuchi, T., Nelson, E. and Busse, L.W., 1954

J. Am. Pharm. Ass. Sci. Ed., 43, 344-348

- Higuchi, T., Shimamoto, T., Eriksen, S.P. and Yashiki, T., 1965

J. Pharm. Sci., 54, 111-118

- Ho, A.Y.K., 1986

"Time-dependent characteristics in tablet compaction"

Ph. D. Thesis, University of London

- Ho, A.Y.K. and Jones, T.M., 1982

Paper presented at Brit. Powd. Tech. Conf., London

- Huckle, P.D., 1985

"The use of stress relaxation data in the prediction of powder compactibility"

Ph. D. Thesis, University of London

- Huckle, P.D. and Summers, M.P., 1985

J. Pharm. Pharmacol., 37, 722-725

- Hunter, B.M., Fisher, D.G., Pratt, R.M. and Rowe, R.C., 1976

J. Pharm. Pharmacol., 28, 65P

- Huttenrauch, R., 1977

Pharmazie, 32, 130

- Huttenrauch, R., 1978

Acta Pharm. Technol., Suppl. 6, 55-127

- Huttenrauch, R. and Jacob, J., 1977

Pharmazie, 32, 49-50

- Huttenrauch, R. and Keiner, I., 1976a

Pharmazie, 31, 329-330

- Huttenrauch, R. and Keiner, I., 1976b

Pharmazie, 31, 330-331

- Huttenrauch, R. and Keiner, I., 1976c

Pharmazie, 31, 331

- Huttenrauch, R. and Keiner, I., 1976d

Pharmazie, 31, 651-652

- Huttenrauch, R. and Keiner, I., 1977

Pharmazie, 32, 129-130

- Huttenrauch, R. and Keiner, I., 1979a

Int. J. Pharm., 2, 59-60

- Huttenrauch, R. and Keiner, I., 1979b
  Powder Technol., 22, 289-290
- Jarosz, P.J. and Parrott, E.L., 1982
  Drug Dev. and Ind. Pharm., 8, 445-453
- Jayasinghe, S.S., Pilpel, N. and Harwood, C.F., 1969
  Mat. Sci. Eng., 5, 287-294
- Jenkins, G.M. and Watts, D.G., 1968
  "Spectral analysis and its applications"
  Holden-Day, San Fransisco
- Jetzer, W.E., Johnson, W.B. and Hiestand, E.N., 1985
  Int. J. Pharm., 26, 329-337
- Jetzer, W.E. and Leuenberger, H., 1984
  Pharm. Act Helv., 59, 2-7
- Johnson, K.L., Kendall, K. and Roberts, A.D., 1971
  Proc. Roy. Soc., London, A 324, 301-303
- Jones, T.M., 1977
  "Formulation and preparation of dosage forms"
  Polderman, J. North-Holland, Elsevier
- Jones, T.M., 1981
  Int. J. Pharm. Tech. and Prod. Mfr., 2, 17-24
- Kawakita, K. and Tsutsumi, Y., 1966
  Bull. Chem. Soc. Japan, 39, 1364-1368
- Khan, K.A., Musikabhumma, P. and Warr, J.P., 1981
  Drug Dev. Ind. Pharm., 7, 525-538

- Knoechel, E.L., Sperry, C.C., Ross, H.E. and Lintner, C.J., 1967a

J. Pharm. Sci., 56, 109-116

- Knoechel, E.L., Sperry, C.C. and Lintner, C.J., 1967b

J. Pharm. Sci., 56, 116-130

- Knudsen, F.P., 1959

J. Am. Ceram. Soc., 42, 376-387

- Kuhn, W., 1947

Helv. Chim. Acta, 30, 487-493

- Leigh, S., Carless, J.E. and Burt, B.W., 1967

J. Pharm. Sci., 56, 888-892

- Leuenberger, H., 1982

Int. J. Pharm., 12, 41-55

- Leuenberger, H., Hiestand, E.N. and Sucker, H., 1981

Chem. Ing. Tech., 53, 45-47

- Leuenberger, H. and Jetzer, W.E., 1984

Powder Technol., 37, 209-218

- Long, W.M., 1960

Powder Metall., 6, 73-86

- Mackenzie, J.K., 1950

Proc. Phys. Soc., 63 B, 2-11

- Malamataris, S., Bin Baie, S. and Pilpel, N., 1984

J. Pharm. Pharmacol., 36, 616-617

- Mann, S.C., Roberts, R.J., Rowe, R.C., Hunter, B.M. and Rees, J.E., 1983

J. Pharm. Pharmacol., 35, 44P

- Marshall, K. and Sixsmith, D., 1974

Drug Dev. Commun., 1, 51-71

- Mashadi, A. B., 1984

"Properties of lactose microgranulates showing the effect of incorporating Starch 1500 as binding agent by several process methods".

Final year honours project report for Bachelor of Pharmacy degree.

School of Pharmacy and Pharmacology, University of Bath

- McKenna, A. and McCafferty, D.F., 1982

J. Pharm. Pharmacol., 34, 347-351

- Milosovich, G., 1963

Drug. and Cosm. Ind., 92, 656-669

- Morii, M., Takeguchi, N. and Horikoshi, I., 1973

Chem. Pharm. Bull., 21, 589-593

- Moschos, A.E., 1985

"Mechanical properties of tablets in flexure and diametral loading"

M. Sc. Thesis, University of Bath

- Moschos, A.E. and Rees, J.E., 1985

J. Pharm. Pharmacol., 37, 32P

- Mullin, J.W., 1972

"Crystallisation"

2nd Edn., Butterworths, London

- Mullin, J.W., 1979

"Crystallisation"

3rd Edn., Plenum Press, New York

- Nelson, E., 1955

J. Am. Pharm. Ass. Sci. Ed., 44, 494-497

- Newton, I., 1721

"Opticks"

- Newton, J.M., 1974

J. Pharm. Pharmacol., 26, 215-216

- Newton, J.M., Ingham, S. and Onabajo, O.O., 1986

Acta Pharm. Technol., 32, 61-62

- Newton, J.M., Rowley, G. and Fell, J.T., 1972

J. Pharm. Pharmacol., 24, 503-504

- Newton, J.M., Rowley, G., Fell, J.T., Peacock, D.G. and Ridgway, K., 1971

J. Pharm. Pharmacol., 23, Suppl., 195S-201S

- Newton, J.M. and Stanley, P., 1974

J. Pharm. Pharmacol., 26, Suppl., 60P-61P

- Nyqvist, H., 1983

Int. J. Pharm. Tech. and Prod. Mfr., 4, 47-48

- Nystrom, C. Alex, W. and Malmqvist, K., 1977

Acta Pharm. Suec., 14, 317-320

- Nystrom, C., Malmqvist, K. and Mazur, J., 1978

Acta Pharm. Suec., 15, 226-232

- Obiorah, B.A. and Shotton, E., 1976

J. Pharm. Pharmacol., 28, 629-632

- Orr, C.Jr., 1966

"Particulate Technology"

The Mackillan Company, New York

Collier-Macmillan Ltd., London

- Parmentier, W., 1980

Pharm. Weekbl., 42, 752-756

- Paronen, P. and Juslin, M., 1983

J. Pharm. Pharmacol., 35, 627-635

- Patel, A.N. and Armstrong, N.A., 1987

J. Pharm. Pharmacol., 39, 11P

- Patel, C., 1986

"Design and characterization of direct compression excipients"

Ph. D. Thesis, University of Bath

- Patel, C. and Staniforth J.N., 1987

J. Pharm. Pharmacol., 39, 647-650

- Patel, C., Staniforth J.N. and Hart, J.P., 1985

J. Pharm. Pharmacol., 37, 30P

- Pitt, K.G., Newton, J.M. and Stanley, P., 1988

J. Mat. Sci., 23, 2723-2728

- Radley, J.A., 1968

"Starch and its derivatives"

4th Edn., Chapman and Hall Ltd., London

- Ragnarsson, G. and Sjogren, J., 1985

J. Pharm. Pharmacol., 37, 145-150

- Rankell, A.S. and Higuchi, T., 1968

J. Pharm. Sci., 57, 574-577

- Rees, J. E., 1970

J. Pharm. Pharmacol., 22, 245-246

- Rees, J.E. and Hersey, J.A., 1972

Pharm. Acta Helv., 47, 235-243

- Rees, J.E., Hersey, J.A. and Cole, E.T., 1972

J. Pharm. Sci., 61, 1313-1315

- Rees, J.E. and Rue, P.J., 1978a

J. Pharm. Pharmacol., 30, 601-607

- Rees, J.E. and Rue, P.J., 1978b

J. Pharm. Pharmacol., 30, 25P

- Rees, J.E. and Rue, P.J., 1978c

Drug Dev. Ind. Pharm., 4, 131-156

- Rees, J.E., Rue, P.J. and Richardson, S.C., 1977

J. Pharm. Pharmacol., 29, 38P

- Rees, J.E. and Shotton, E., 1970

J. Pharm. Pharmacol., 22, Suppl., 17S-23S

- Reier, G.E. and Shangraw, R., 1966

J. Pharm. Sci., 55, 510-514

- Ryshkewitch, E., 1953

J. Am. Ceram. Soc., 36, 65-68

- Ridgway, K., Glasby, J. and Rosser, P.H., 1969

J. Pharm. Pharmacol., 21, Suppl., 24S-29S

- Ritschel, W.A., Skinner, F.S. and Schlumpf, R., 1969

Pharm. Acta Helv., 44, 547-569

- Roberts, R.J. and Rowe, R.C., 1985

J. Pharm. Pharmacol., 37, 377-384

- Roberts, R.J. and Rowe, R.C., 1986a

J. Pharm. Pharmacol., 38, 526-528

- Roberts, R.J. and Rowe, R.C., 1986b

J. Pharm. Pharmacol., 38, 567-571

- Rosenberg, H.M., 1984

"The Solid State"

2nd Edn., Oxford University Press

- Rowe, R.C., Elworthy, P.H. and Ganderton, D., 1973

J. Pharm. Pharmacol., 25, Suppl., 12P-16P

- Rudnick, A., Hunter, A.R. and Holden, F.C., 1963

Mat. Res. Stand., 1, 283-289

- Rue, P.J. and Rees, J.E., 1978

J. Pharm. Pharmacol., 30, 642-643

- Rumpf, H., 1962

"Agglomeration", 379-418

Interscience, New York

- Schmid, S.M., 1976

Tectonophysics, 31, T21-28

- Schubert, H., Herrmann, W. and Rumpf, H., 1975

Powder Technol., 11, 121-131

- Schwarzkopf, P., 1947

"Powder metallurgy"

Macmillan, N. York

- Seelig, R.P. and Wulff, J., 1946

Trans. Am. Min. (Metall.) Engs., 166, 492

- Seitz, J.A. and Flessand, G.M., 1965

J. Pharm. Sci., 54, 1353-1357

- Seth, P.L., 1956

Ph. D. Thesis, Swiss Fed. Inst. Tech., Zurich

- Sherman, P., 1970

"Industrial rheology"

Academic Press, London

- Shlanta, S. and Milosovich, G., 1964

J. Pharm. Sci., 53, 562-564

- Shott, M., 1983

"The compaction of pharmaceutical powders"

Ph.D. Thesis, University of Nottingham

- Shotton, E., Deer, J.J. and Ganderton, D., 1963

J. Pharm. Pharmacol., 15, Suppl., 106T-114T

- Shotton, E. and Ganderton, D., 1961

J. Pharm. Pharmacol., 13, Suppl., 144P

- Shotton, E. and Obiorah, B. A., 1973

J. Pharm. Pharmacol., 25, Suppl., 37P-43P

- Shotton, E. and Rees, J.E., 1966

J. Pharm. Pharmacol., 18, Suppl., 160S-167S

- Sixsmith, D., 1980

J. Pharm. Pharmacol., 32, 854-855

- Sixsmith, D., 1982

J. Pharm. Pharmacol., 34, 345-346

- Smith, A.N., 1949

  Pharm. J., 163, 194

- Train, D., 1956

  J. Pharm. Pharmacol., 8, 745-761

- Train, D., 1957

  Trans. Inst. Chem. Eng., 35, 258-266

- Train, D. and Lewis, C.J., 1962

  Trans. Inst. Chem. Eng., 40, 235-240

- Travers, D.N., Celik, M. and Buttery, T.C., 1983

  Drug Dev. Ind. Pharm., 9, 139-157

- Tukey, J.W., 1961

  Technometrics, 3, 191-219

- Turner, G.A. and Balasubramanian, M., 1974

  Powder Technol., 10, 121-127

- Warburton, B. and Barry, B.W., 1968

  J. Pharm. Pharmacol., 20, 255-268

- Whistler, R.L., Bemiller, J.N. and Paschall, E.F., 1984

  "Starch: Chemistry and technology"

  Academic Press

- Whistler, R.L. and Paschall, E.F., 1967

  "Starch: Chemistry and technology"

  Academic Press

- Windheuser, J.J., Misra, J., Eriksen, S.P. and Higuchi, T.,

  1963

  J. Pharm. Sci., 52, 767-772

- York, P., 1981

  J. Pharm. Pharmacol., 33, 269-273

- York, P. and Grant, D.J.W., 1985

  Int. J. Pharm., 25, 57-72

- York, P. and Pilpel, N., 1972

  J. Pharm. Pharmacol., 24, Suppl., 47P-56P

- York, P. and Pilpel, N., 1973

  J. Pharm. Pharmacol., 25, Suppl., 1P-11P

- Zografi, G., 1988

  Drug Dev. and Ind. Pharm., 14, 1905-1926

- Zografi, G., Kontny, M.J., Yang, A.Y.S. and Brenner, G.S., 1984

  Int. J. Pharm., 18, 99-116

AUTHOR'S PUBLICATIONS

1. "Compression and recovery behaviour of compacts using extended Heckel plots" Tsardaka, K.D., Rees, J.E. and Hart, J.P., (1988) J. Pharm. Pharmacol., 40, 73P
   Presented at the British Pharmaceutical Conference, Aberdeen, U.K., September 1988

2. "Assessment of the viscoelastic behaviour of pharmaceutical particulate solids using mathematical analysis of creep data" Tsardaka, K.D. and Rees, J.E., (1988) Pharmaceutical Research, 5, S236
   Presented at the AAPS meeting, Orlando, Florida, U.S.A., October 1988

3. "Plastic deformation and retarded elastic deformation of particulate solids using creep experiments" Tsardaka, K.D. and Rees, J.E., (1989) J. Pharm. Pharmacol., 41, 28P
   Presented at the British Pharmaceutical Conference, Keele, U.K., September 1989.

4. "Effect of moisture on the viscoelastic properties of Starch 1500" Tsardaka, K.D. and Rees, J.E., (1989)
   Presented at the AAPS meeting, Atlanda, Georgia, U.S.A., October 1989

5. "Relations between viscoelastic parameters and compaction properties of two modified starches" Tsardaka, K.D. and Rees, J.E., (1990) J. Pharm. Pharmacol., 42, 77P
   Presented at the British Pharmaceutical Conference, Cardiff, U.K., September 1990.

6. "Effect of punch diameter and concavity on the creep behaviour of pharmaceutical particulate solids" Tsardaka, K.D. and Rees, J.E., (1990)
   Presented at the AAPS meeting, Las Vegas, Nevada, U.S.A., November 1990

APPENDICES

APPENDIX A

TABLE A.1 Work and related parameters obtained during compression for Avicel PH102, Emcocel 90M and Starch 1500. Numbers in parentheses represent ± confidence intervals at the 95% level.

Peak force (N)	Displ. (m)x10^{-3}	Upper punch work (J)	Lower punch work (J)	Total power of compaction (J/s)	True lower punch work (J)	True power of compaction (J/s)
			AVICEL PH102			
5998.2	3.53	5.88	5.65	5.05	5.50	6.32
(42.1)	(0.21)	(0.18)	(0.14)	(0.30)	(0.14)	(0.34)
11890.4	4.09	9.24	8.97	7.12	8.79	9.06
(79.8)	(0.16)	(0.13)	(0.09)	(0.35)	(0.04)	(0.37)
17900.1	4.15	11.10	10.80	7.88	10.61	9.99
(123.2)	(0.13)	(0.14)	(0.11)	(0.25)	(0.08)	(0.29)
			EMCOCEL 90M			
6097.5	3.86	6.02	5.38	5.17	5.23	6.32
(43.3)	(0.19)	(0.12)	(0.21)	(0.35)	(0.20)	(0.40)
12350.2	4.12	9.22	8.39	6.40	8.22	8.14
(184.3)	(0.13)	(0.20)	(0.07)	(0.61)	(0.09)	(0.66)
17670.0	4.14	10.79	9.83	6.73	9.63	8.75
(278.8)	(0.14)	(0.19)	(0.16)	(0.59)	(0.12)	(0.63)
			STARCH 1500			
6181.8	1.48	3.84	3.42	2.90	3.26	4.13
(78.9)	(0.02)	(0.06)	(0.06)	(0.15)	(0.06)	(0.20)
12279.6	1.63	7.11	6.89	5.94	6.65	8.07
(99.0)	(0.06)	(0.11)	(0.09)	(0.25)	(0.07)	(0.28)
18329.7	1.76	8.74	8.53	7.75	8.24	10.32
(252.9)	(0.03)	(0.05)	(0.07)	(0.48)	(0.10)	(0.64)

TABLE A.2 Work and related parameters obtained during compression for sodium chloride, sodium bicarbonate, anhydrous lactose and Emcompress. Numbers in parentheses represent ± confidence intervals at the 95% level.

Peak force (N)	Displ. (m)x10^{-3}	Upper punch work (J)	Lower punch work (J)	Total power of compaction (J/s)	True lower punch work (J)	True power of compaction (J/s)
			SODIUM CHLORIDE			
6489.6	0.83	2.65	2.57	2.82	2.55	3.97
(313.1)	(0.03)	(0.18)	(0.16)	(0.55)	(0.14)	(0.60)
12140.0	0.96	5.12	5.05	4.60	5.02	6.70
(73.5)	(0.03)	(0.06)	(0.06)	(0.82)	(0.07)	(1.04)
17579.6	1.16	7.42	7.12	5.79	7.09	8.29
(252.2)	(0.04)	(0.18)	(0.18)	(0.68)	(0.16)	(0.84)
			SODIUM BICARBONATE			
6098.9	0.83	2.18	2.06	3.17	2.01	4.44
(58.3)	(0.02)	(0.03)	(0.04)	(0.19)	(0.03)	(0.22)
12409.8	0.99	4.55	4.35	4.83	4.24	6.93
(101.7)	(0.05)	(0.09)	(0.07)	(0.74)	(0.06)	(0.81)
17700.0	1.10	6.39	6.11	5.36	5.95	7.82
(190.6)	(0.05)	(0.11)	(0.10)	(0.86)	(0.11)	(0.96)
			ANHYDROUS LACTOSE			
6804.1	1.06	2.52	2.43	3.33	2.37	4.71
(65.5)	(0.07)	(0.07)	(0.05)	(0.35)	(0.04)	(0.40)
12260.2	1.24	4.67	4.51	4.55	4.43	6.27
(67.3)	(0.05)	(0.07)	(0.07)	(0.28)	(0.04)	(0.33)
18070.4	1.34	6.87	6.64	5.35	6.52	7.43
(106.8)	(0.07)	(0.16)	(0.15)	(0.57)	(0.06)	(0.62)
			EMCOMPRESS			
6437.7	0.75	2.10	2.08	2.19	2.00	2.90
(157.3)	(0.07)	(0.11)	(0.10)	(0.17)	(0.09)	(0.20)
12290.0	0.87	4.21	3.98	3.65	3.87	4.72
(85.6)	(0.04)	(0.10)	(0.07)	(0.17)	(0.07)	(0.20)
17810.0	1.00	6.14	5.79	4.71	5.66	6.22
(975.1)	(0.08)	(0.44)	(0.43)	(0.35)	(0.41)	(0.37)

TABLE A.3 Results obtained for a rubber plug compressed at 18kN.

Total Work (J)	6.55 (0.15)
Work of Comp. (J)	0.04 (0.01)
Expansion Work (J)	6.51 (0.14)
Punch travel (m)x10^{-3}	0.001 (0.001)
Contact Time (s)	0.76 (0.05)
Rise Time (s)	0.55 (0.05)
Dwell Time (s)	0.01 (0.00)
Expansion Time (s)	0.19 (0.01)

TABLE A.4 Parameters related to elastic recovery, obtained during decompression for Avicel PH102, Emcocel 90M and Starch 1500. Numbers in parentheses represent ± confidence intervals at the 95% level.

Peak force (N)	Expansion work (J)	Expansion time (s)	Expansion rate $(m/s)x10^{-4}$	Power of expansion (J/s)
		AVICEL PH102		
5998.2	0.15	0.22	3.75	0.68
(42.1)	(0.01)	(0.03)	(0.26)	(0.05)
11890.4	0.18	0.26	2.85	0.69
(79.8)	(0.02)	(0.02)	(0.34)	(0.06)
17900.1	0.21	0.29	2.43	0.72
(123.2)	(0.03)	(0.02)	(0.33)	(0.07)
		EMCOCEL 90M		
6097.5	0.13	0.22	3.71	0.59
(43.3)	(0.01)	(0.03)	(0.29)	(0.05)
12350.2	0.17	0.28	2.77	0.60
(184.3)	(0.02)	(0.04)	(0.35)	(0.06)
17670.0	0.20	0.33	2.32	0.61
(278.8)	(0.02)	(0.05)	(0.22)	(0.05)
		STARCH 1500		
6181.8	0.15	0.31	4.03	0.50
(78.9)	(0.01)	(0.03)	(0.32)	(0.04)
12279.6	0.23	0.33	3.10	0.69
(99.0)	(0.02)	(0.03)	(0.30)	(0.06)
18329.7	0.29	0.33	2.80	0.96
(252.9)	(0.02)	(0.06)	(0.25)	(0.07)

TABLE A.5 Parameters related to elastic recovery, obtained during decompression for sodium chloride, sodium bicarbonate, anhydrous lactose and Emcompress. Numbers in parentheses represent ± confidence intervals at the 95% level.

Peak force (N)	Expansion work (J)	Expansion time (s)	Expansion rate $(m/s)x10^{-4}$	Power of expansion (J/s)
		SODIUM CHLORIDE		
6489.6	0.02	0.25	0.83	0.09
(313.1)	(0.00)	(0.04)	(0.14)	(0.01)
12140.0	0.03	0.31	0.21	0.10
(73.5)	(0.01)	(0.07)	(0.04)	(0.01)
17579.6	0.03	0.35	0.11	0.08
(252.2)	(0.01)	(0.04)	(0.03)	(0.01)
		SODIUM BICARBONATE		
6098.9	0.05	0.19	1.23	0.25
(58.3)	(0.01)	(0.02)	(0.24)	(0.02)
12409.8	0.11	0.26	1.17	0.43
(101.7)	(0.02)	(0.02)	(0.25)	(0.03)
17700.0	0.16	0.34	1.15	0.47
(190.6)	(0.02)	(0.04)	(0.16)	(0.04)
		ANHYDROUS LACTOSE		
6804.1	0.06	0.21	1.05	0.28
(65.5)	(0.01)	(0.02)	(0.25)	(0.01)
12260.2	0.08	0.27	0.71	0.32
(67.3)	(0.02)	(0.04)	(0.23)	(0.02)
18070.4	0.12	0.33	0.54	0.55
(106.8)	(0.02)	(0.07)	(0.21)	(0.04)
		EMCOMPRESS		
6437.7	0.08	0.23	1.50	0.36
(157.3)	(0.01)	(0.01)	(0.18)	(0.03)
12290.0	0.11	0.25	0.83	0.47
(85.6)	(0.02)	(0.02)	(0.13)	(0.04)
17810.0	0.13	0.26	0.36	0.49
(975.1)	(0.02)	(0.03)	(0.09)	(0.04)

TABLE A.6 Time-related parameters, obtained during compression for Avicel PH102, Emcocel 90M and Starch 1500. Numbers in parentheses represent ± confidence intervals at the 95% level.

Peak force (N)	Contact time (s)	Rise time (s)	Punch travel (m)x10^{-5}	Relaxation time (s)	Dwell time (s)
			AVICEL PH102		
5998.2	1.12	0.85	1.57	0.05	0.01
(42.1)	(0.08)	(0.06)	(0.41)	(0.02)	(0.00)
11890.4	1.26	0.97	1.13	0.03	0.02
(79.8)	(0.04)	(0.03)	(0.59)	(0.02)	(0.00)
17900.1	1.37	1.06	0.86	0.02	0.02
(123.2)	(0.06)	(0.05)	(0.47)	(0.02)	(0.00)
			EMCOCEL 90M		
6097.5	1.07	0.81	1.65	0.04	0.02
(49.3)	(0.05)	(0.04)	(0.53)	(0.02)	(0.01)
12350.2	1.31	1.01	0.96	0.02	0.01
(184.3)	(0.11)	(0.09)	(0.65)	(0.02)	(0.00)
17670.0	1.46	1.10	0.59	0.03	0.02
(278.8)	(0.09)	(0.08)	(0.44)	(0.03)	(0.01)
			STARCH 1500		
6181.8	1.18	0.79	2.51	0.08	0.04
(78.9)	(0.07)	(0.05)	(0.54)	(0.03)	(0.01)
12279.6	1.16	0.81	0.91	0.02	0.02
(99.0)	(0.06)	(0.03)	(0.57)	(0.01)	(0.01)
18329.7	1.10	0.81	0.34	0.01	0.02
(252.9)	(0.10)	(0.07)	(0.41)	(0.02)	(0.00)

TABLE A.7 Time-related parameters, obtained during compression for sodium chloride, sodium bicarbonate, anhydrous lactose and Emcompress. Numbers in parentheses represent ± confidence intervals at the 95% level.

Peak force (N)	Contact time (s)	Rise time (s)	Punch travel (m)x10^{-5}	Relaxation time (s)	Dwell time (s)
			SODIUM CHLORIDE		
6489.6	0.91	0.61	1.06	0.05	0.02
(313.1)	(0.11)	(0.09)	(0.49)	(0.02)	(0.04)
12140.0	1.09	0.75	0.91	0.03	0.01
(73.5)	(0.21)	(0.15)	(0.50)	(0.02)	(0.01)
17579.6	1.23	0.85	0.68	0.02	0.02
(252.2)	(0.11)	(0.10)	(0.26)	(0.02)	(0.01)
			SODIUM BICARBONATE		
6098.9	0.65	0.45	0.49	0.01	0.02
(58.3)	(0.02)	(0.02)	(0.36)	(0.01)	(0.01)
12409.8	0.90	0.63	0.32	0.00	0.02
(101.7)	(0.09)	(0.08)	(0.15)	(0.10)	(0.00)
17700.0	1.14	0.81	0.20	0.00	0.01
(190.6)	(0.13)	(0.12)	(0.13)	(0.02)	(0.00)
			ANHYDROUS LACTOSE		
6804.1	0.73	0.50	0.65	0.02	0.02
(65.5)	(0.05)	(0.03)	(0.41)	(0.02)	(0.01)
12260.2	0.99	0.68	0.94	0.04	0.02
(67.3)	(0.05)	(0.04)	(0.52)	(0.02)	(0.01)
18070.4	1.24	0.86	1.45	0.04	0.02
(106.8)	(0.11)	(0.07)	(0.93)	(0.04)	(0.01)
			EMCOMPRESS		
6437.7	0.95	0.69	0.60	0.02	0.02
(157.3)	(0.05)	(0.04)	(0.33)	(0.01)	(0.01)
12290.0	1.09	0.82	0.51	0.02	0.02
(85.6)	(0.04)	(0.03)	(0.36)	(0.02)	(0.01)
17810.0	1.23	0.91	0.43	0.01	0.01
(975.1)	(0.12)	(0.09)	(0.26)	(0.02)	(0.00)

TABLE A.8 Extended Heckel plot results for Avicel PH102, Emcocel 90M and Starch 1500. Numbers in parentheses represent ± confidence intervals at the 95% level.

Peak force (N)	Correl. coeff.	Yield pressure (MPa)	Interc. A	Square area	% Under rising F area	% Above falling F area	% Chord area
			AVICEL PH102				
5998.2	0.997	61.02	0.50	76.69	64.11	2.26	2.49
(42.1)	(0.001)	(0.91)	(0.02)	(0.69)	(0.71)	(0.23)	(0.39)
11890.4	0.996	69.08	0.57	237.50	59.31	4.69	3.00
(79.8)	(0.001)	(1.45)	(0.03)	(3.39)	(0.80)	(0.41)	(0.34)
17900.1	0.997	70.19	0.54	492.70	55.37	5.14	4.31
(123.2)	(0.001)	(1.81)	(0.04)	(10.21)	(0.93)	(0.68)	(0.61)
			EMCOCEL 90M				
6097.5	0.996	62.86	0.53	77.95	64.80	2.16	2.00
(43.3)	(0.002)	(1.18)	(0.02)	(0.56)	(0.59)	(0.23)	(0.08)
12350.2	0.996	68.81	0.56	250.10	59.75	4.32	2.73
(184.3)	(0.001)	(3.02)	(0.05)	(3.02)	(0.72)	(0.39)	(0.35)
17670.0	0.997	70.28	0.55	466.91	56.95	5.01	4.53
(278.8)	(0.001)	(1.95)	(0.03)	(9.88)	(1.02)	(0.59)	(0.32)
			STARCH 1500				
6181.8	0.999	53.31	0.70	80.59	67.50	2.63	3.84
(78.9)	(0.001)	(0.89)	(0.02)	(0.69)	(0.72)	(0.24)	(0.39)
12279.6	0.997	57.83	0.71	258.43	55.36	5.12	4.43
(99.0)	(0.001)	(1.32)	(0.02)	(3.22)	(0.83)	(0.43)	(0.35)
18329.7	0.991	58.00	0.73	462.75	51.45	7.93	6.64
(252.9)	(0.003)	(1.87)	(0.03)	(11.02)	(0.89)	(0.57)	(0.61)

TABLE A.9 Extended Heckel plot results for sodium chloride, sodium bicarbonate, anhydrous lactose and Emcompress. Numbers in parentheses represent ± confidence intervals at the 95% level.

Peak force (N)	Correl. coeff.	Yield pressure (MPa)	Interc. A	Square area	% Under rising F area	% Above falling F area	% Chord area
			SODIUM CHLORIDE				
6489.6	0.999	69.93	0.89	82.98	68.73	0.92	0.23
(313.1)	(0.000)	(2.18)	(0.02)	(5.58)	(1.20)	(0.09)	(0.08)
12140.0	0.999	73.78	0.90	217.52	63.77	1.02	0.36
(73.5)	(0.001)	(2.40)	(0.02)	(2.64)	(0.61)	(0.11)	(0.23)
17579.6	0.998	74.27	0.86	411.74	58.71	1.06	0.97
(252.2)	(0.001)	(5.21)	(0.06)	(6.45)	(1.01)	(0.12)	(0.26)
			SODIUM BICARBONATE				
6098.9	0.997	99.04	0.92	65.17	77.23	0.75	0.34
(58.3)	(0.000)	(3.27)	(0.01)	(0.65)	(0.99)	(0.09)	(0.12)
12409.8	0.998	118.10	1.02	180.11	73.31	1.45	0.66
(101.7)	(0.000)	(8.51)	(0.02)	(3.46)	(0.68)	(0.12)	(0.10)
17700.0	0.998	130.13	1.09	302.73	70.99	1.96	1.34
(190.6)	(0.001)	(12.81)	(0.05)	(2.79)	(0.54)	(0.16)	(0.49)
			ANHYDROUS LACTOSE				
6804.1	0.993	95.38	0.94	78.61	78.65	0.92	0.35
(65.5)	(0.002)	(2.99)	(0.01)	(0.54)	(0.59)	(0.08)	(0.03)
12260.2	0.994	120.22	1.00	175.32	74.91	1.27	0.62
(67.3)	(0.002)	(5.75)	(0.02)	(1.18)	(0.38)	(0.12)	(0.17)
18070.4	0.996	143.25	1.05	297.06	72.26	1.70	0.81
(106.8)	(0.001)	(6.38)	(0.03)	(2.67)	(0.58)	(0.16)	(0.25)
			EMCOMPRESS				
6437.7	0.979	93.64	0.92	72.19	78.83	1.04	0.54
157.3)	(0.003)	(4.25)	(0.02)	(1.59)	(0.35)	(0.09)	(0.03)
12290.0	0.966	154.42	1.00	155.02	78.87	1.09	0.42
(85.6)	(0.005)	(10.71)	(0.01)	(5.22)	(0.62)	(0.11)	(0.05)
17810.0	0.964	194.40	1.05	245.13	78.50	1.05	0.56
975.1)	(0.002)	(14.93)	(0.03)	(7.34)	(0.30)	(0.12)	(0.07)

TABLE A.10 Yield pressure values for Tablettose, obtained at 50-200MPa using various high speed compaction simulators (Bateman et al, 1988).

Institution	Yield pressure (MPa)	% Error from mean
ICI Pharm. Division	172.95	- 8.046
The Boots Co. PLC	198.30	+ 5.431
School of Pharmacy Liverpool polytechnic	181.93	- 3.272
The Wellcome Foundation Ltd	169.26	- 10.009
Smith Kline & French Labs	234.75	+ 24.811

TABLE A.11 Yield pressure values for Tablettose at a range of compaction forces. Numbers in brackets represent ± confidence intervals at the 95% level.

Peak force (N)	Yield pressure (MPa)
5895.4 (97.2)	94.43 (3.25)
12330.7 (144.3)	130.28 (9.86)
18070.5 (173.6)	144.36 (10.22)
24236.9 (211.4)	178.37 (12.23)

APPENDIX B

TABLE B.1 Diametral loading results for Avicel PH102, Emcocel 90M and Starch 1500. Numbers in parentheses represent ± confidence intervals at the 95% level.

	Peak force (N)	Rel. dens.	Break. force (N)	Tensile strength (MPa)	Deform. before failure $(m)\times10^{-4}$	Work of failure $(J)\times10^{-4}$	Corr. work of failure (J/m^2)	Power of failure $(J/s)\times10^{-4}$	Apparent failure viscosity (MPa·s)	Area ratio
	5998.2	0.73	194.6	3.22	3.38	412.3	682.2	31.7	41.8	0.80
	(42.1)	(0.00)	(3.8)	(0.07)	(0.16)	(31.2)	(51.1)	(18.7)	(1.7)	(0.02)
AVICEL	11890.4	0.84	326.3	6.22	4.63	993.5	1892.8	59.9	103.4	0.76
PH102	(79.8)	(0.00)	(7.2)	(0.12)	(0.30)	(75.4)	(140.7)	(23.0)	(3.3)	(0.02)
	17900.1	0.89	394.4	7.92	4.82	1350.2	2708.1	75.7	141.2	0.70
	(123.2)	(0.00)	(4.2)	(0.10)	(0.13)	(54.4)	(114.3)	(20.3)	(2.8)	(0.02)
	6097.5	0.74	211.9	3.56	3.45	445.4	748.1	33.1	47.9	0.82
	(43.3)	(0.00)	(3.7)	(0.07)	(0.12)	(27.2)	(46.2)	(18.2)	(1.3)	(0.01)
EMCOCEL	12350.2	0.85	354.5	6.83	4.53	1070.1	2065.3	63.7	115.4	0.75
90M	(184.3)	(0.00)	(7.5)	(0.17)	(0.30)	(99.8)	(177.0)	(34.4)	(4.7)	(0.03)
	17670.0	0.89	399.2	8.09	5.18	1540.3	3128.2	82.1	151.8	0.67
	(278.8)	(0.00)	(2.9)	(0.07)	(0.16)	(12.9)	(255.4)	(70.1)	(3.7)	(0.06)
	6181.8	0.67	15.4	0.23	1.62	12.4	18.7	2.8	1.0	0.92
	(78.9)	(0.00)	(0.8)	(0.01)	(0.11)	(0.8)	(1.3)	(0.2)	(0.1)	(0.05)
STARCH	12279.6	0.76	44.3	0.76	2.12	53.2	90.2	8.2	4.9	0.89
1500	(99.0)	(0.00)	(1.3)	(0.02)	(0.10)	(3.2)	(5.5)	(0.2)	(0.3)	(0.02)
	18329.7	0.81	65.8	1.19	2.53	85.1	152.8	10.8	9.4	0.93
	(252.9)	(0.00)	(1.9)	(0.03)	(0.02)	(4.5)	(8.8)	(0.4)	(0.5)	(0.02)

TABLE B.2 Diametral loading results for sodium chloride and sodium bicarbonate. Numbers in parentheses represent ± confidence intervals at the 95% level.

	Peak force (N)	Rel. dens.	Break. force (N)	Tensile strength (MPa)	Deform. before failure (m)x10^{-4}	Work of failure (J)x10^{-4}	Corr. work of failure (J/m^2)	Power of failure (J/s)x10^{-4}	Apparent failure viscosity (MPa·s)	Area ratio
	6489.6	0.81	58.9	1.08	0.51	26.4	48.4	15.3	1.9	0.67
	(313.1)	(0.00)	(2.0)	(0.04)	(0.16)	(6.2)	(5.2)	(0.7)	(0.2)	(0.05)
SODIUM	12140.0	0.89	108.8	2.20	0.76	63.0	127.1	16.6	8.2	0.60
CHLORIDE	(73.5)	(0.00)	(5.1)	(0.10)	(0.04)	(3.5)	(7.2)	(0.9)	(0.7)	(0.06)
	17579.6	0.93	148.3	3.14	0.82	70.1	147.9	17.1	12.9	0.55
	(252.2)	(0.00)	(6.2)	(0.13)	(0.04)	(4.3)	(10.9)	(1.7)	(0.9)	(0.09)
	6098.9	0.73	19.7	0.33	0.66	8.6	14.4	4.8	0.6	0.74
	(58.3)	(0.00)	(1.5)	(0.15)	(0.14)	(3.5)	(5.9)	(2.1)	(0.3)	(0.07)
SODIUM	12409.8	0.80	32.9	0.60	0.88	17.8	32.7	7.1	1.5	0.81
BICARBONATE	(101.7)	(0.00)	(2.5)	(0.04)	(0.05)	(2.6)	(4.8)	(0.7)	(0.2)	(0.03)
	17700.0	0.84	51.4	0.99	1.11	34.2	65.7	9.2	3.7	0.84
	(190.6)	(0.00)	(4.6)	(0.09)	(0.08)	(5.9)	(11.5)	(1.0)	(0.6)	(0.06)

TABLE B.3 Diametral loading results for lactose and Emcompress. Numbers in parentheses represent ± confidence intervals at the 95% level.

	Peak force (N)	Rel. dens.	Break. force (N)	Tensile strength (MPa)	Deform. before failure $(m)\times10^{-4}$	Work of failure $(J)\times10^{-4}$	Corr. work of failure (J/m^2)	Power of failure $(J/s)\times10^{-4}$	Apparent viscosity (MPa·s)	Area ratio
	6804.1	0.76	84.7	1.46	0.96	54.7	94.2	14.2	5.6	0.74
	(65.5)	(0.00)	(1.9)	(0.03)	(0.05)	(3.0)	(5.1)	(0.9)	(0.2)	(0.07)
ANHYDROUS	12260.2	0.82	128.7	2.39	0.98	76.7	142.5	17.1	10.7	0.81
LACTOSE	(67.3)	(0.00)	(3.1)	(0.07)	(0.05)	(3.9)	(7.2)	(0.7)	(0.5)	(0.02)
	18070.4	0.86	184.2	3.58	1.14	124.3	241.7	24.2	18.4	0.84
	(106.8)	(0.00)	(8.9)	(0.17)	(0.14)	(17.3)	(17.3)	(2.3)	(1.9)	(0.04)
	6437.7	0.68	14.6	0.25	0.84	8.2	13.8	3.6	0.6	0.75
	(157.3)	(0.00)	(1.0)	(0.02)	(0.04)	(1.1)	(1.8)	(0.6)	(0.1)	(0.09)
EMCOMPRESS	12290.0	0.70	34.1	0.60	0.98	22.3	39.3	6.8	2.1	0.74
	(85.6)	(0.00)	(2.8)	(0.05)	(0.06)	(2.3)	(3.2)	(0.4)	(0.2)	(0.04)
	17810.0	0.76	44.8	0.82	1.17	30.5	56.1	7.8	3.2	0.86
	(975.1)	(0.00)	(4.0)	(0.55)	(0.08)	(3.8)	(6.7)	(0.3)	(0.5)	(0.05)

TABLE B.4 Effect of platen rate on the radial tensile strength (MPa) of Avicel PH102 compacts. Numbers in brackets represent ± confidence intervals at the 95% level.

Platen rate (mm/min)	Force (kN)				
	4	10	15	20	25
1	2.29 (0.04)	5.07 (0.06)	6.43 (0.10)	8.42 (0.16)	9.35 (0.10)
2.2	2.25 (0.02)	4.97 (0.06)	6.33 (0.07)	8.35 (0.09)	9.27 (0.12)
6	2.33 (0.03)	5.02 (0.07)	6.60 (0.15)	8.78 (0.10)	9.53 (0.11)
16	2.42 (0.03)	5.46 (0.08)	7.00 (0.10)	8.96 (0.10)	9.74 (0.17)
35	2.48 (0.07)	5.50 (0.07)	7.08 (0.09)	8.98 (0.13)	9.78 (0.17)
45	2.48 (0.07)	5.51 (0.09)	7.16 (0.03)	9.06 (0.08)	9.85 (0.18)

TABLE B.5 Effect of platen rate on the radial work of failure ($Jx10^{-2}$) of Avicel PH102 compacts. Numbers in brackets represent ± confidence intervals at the 95% level.

Platen rate (mm/min)	Force (kN)				
	4	10	15	20	25
1	3.9 (0.3)	8.6 (0.5)	11.2 (0.7)	14.6 (0.7)	16.5 (0.7)
2.2	3.8 (0.3)	8.5 (0.3)	10.9 (0.7)	14.5 (1.0)	16.2 (0.8)
6	4.1 (0.3)	8.6 (0.3)	11.9 (0.6)	15.1 (0.6)	17.1 (0.9)
16	4.2 (0.2)	9.7 (0.3)	12.6 (0.6)	15.5 (0.9)	17.2 (0.9)
35	4.3 (0.1)	10.1 (0.2)	13.2 (0.4)	15.5 (0.6)	17.4 (1.1)
45	4.3 (0.3)	10.3 (0.1)	13.7 (0.1)	15.8 (0.6)	17.6 (0.9)

TABLE B.6 Direct tension results for Avicel PH102, Emcocel 90M and Starch 1500. Numbers in parentheses represent ± confidence intervals at the 95% level.

	Peak force (N)	Rel. dens.	Break. force (N)	Tensile strength (MPa)	Deform. before failure $(m)x10^{-4}$	Work of failure $(J)x10^{-4}$	Corr. work of failure (J/m^2)
	5998.2	0.73	207.6	1.64	0.84	139.6	231.2
	(42.1)	(0.00)	(5.6)	(0.03)	(0.03)	(12.0)	(20.2)
AVICEL	11890.4	0.84	369.6	2.92	1.09	281.0	537.6
PH102	(79.8)	(0.00)	(9.2)	(0.05)	(0.09)	(24.4)	(40.2)
	17900.1	0.89	452.8	3.56	1.20	368.8	739.6
	(123.2)	(0.00)	(9.0)	(0.08)	(0.03)	(32.0)	(60.2)
	6097.5	0.74	234.1	1.85	0.86	160.8	270.5
	(43.3)	(0.00)	(5.3)	(0.03)	(0.03)	(12.5)	(23.7)
EMCOCEL	12350.2	0.85	418.2	3.28	1.13	338.0	652.4
90M	(184.3)	(0.00)	(9.3)	(0.07)	(0.09)	(32.0)	(57.7)
	17670.0	0.89	471.2	3.72	1.29	401.6	812.1
	(278.8)	(0.00)	(8.2)	(0.03)	(0.03)	(38.7)	(72.4)
	6181.8	0.67	12.8	0.10	0.40	4.4	6.8
	(78.9)	(0.00)	(0.9)	(0.01)	(0.03)	(0.4)	(0.4)
STARCH	12279.6	0.76	40.4	0.32	0.53	18.0	30.8
1500	(99.0)	(0.00)	(1.2)	(0.01)	(0.02)	(0.8)	(2.5)
	18329.7	0.81	60.8	0.48	0.63	33.6	60.8
	(252.9)	(0.00)	(1.9)	(0.02)	(0.01)	(2.4)	(5.2)

TABLE B.7 Direct tension results for sodium chloride and sodium bicarbonate. Numbers in parentheses represent ± confidence intervals at the 95% level.

	Peak force (N)	Rel. dens.	Break. force (N)	Tensile strength (MPa)	Deform. before failure (m)x10^{-4}	Work of failure (J)x10^{-4}	Corr. work of failure (J/m^2)
	6489.6	0.81	61.0	0.49	0.13	4.0	7.6
	(313.1)	(0.00)	(5.0)	(0.02)	(0.03)	(0.4)	(0.8)
SODIUM	12140.0	0.89	120.1	0.95	0.19	13.6	27.6
CHLORIDE	(73.5)	(0.00)	(8.2)	(0.06)	(0.01)	(0.8)	(2.4)
	17579.6	0.93	159.7	1.26	0.20	26.5	55.2
	(252.2)	(0.00)	(9.8)	(0.07)	(0.01)	(2.0)	(4.8)
	6098.9	0.73	15.2	0.12	0.16	1.6	2.8
	(58.3)	(0.00)	(2.8)	(0.05)	(0.03)	(0.3)	(0.4)
SODIUM	12409.8	0.80	26.4	0.21	0.41	4.4	8.0
BICARBONATE	(101.7)	(0.00)	(5.1)	(0.03)	(0.01)	(0.4)	(0.8)
	17700.0	0.84	41.6	0.33	0.27	8.8	17.2
	(190.6)	(0.00)	(8.0)	(0.05)	(0.02)	(0.8)	(1.5)

TABLE B.8 Direct tension results for anhydrous lactose and Emcompress. Numbers in parentheses represent ± confidence intervals at the 95% level.

	Peak force (N)	Rel. dens.	Break. force (N)	Tensile strength (MPa)	Deform. before failure $(m)x10^{-4}$	Work of failure $(J)x10^{-4}$	Corr. work of failure (J/m^2)
	6804.1	0.76	149.2	1.18	0.24	25.3	43.6
	(65.5)	(0.00)	(3.9)	(0.01)	(0.01)	(2.0)	(3.6)
ANHYDROUS	12260.2	0.82	239.2	1.89	0.27	49.6	91.6
LACTOSE	(67.3)	(0.00)	(5.2)	(0.03)	(0.01)	(4.0)	(8.3)
	18070.4	0.86	353.2	2.79	0.29	84.8	164.8
	(106.8)	(0.00)	(12.9)	(0.08)	(0.03)	(7.6)	(13.5)
	6437.7	0.68	32.8	0.26	0.22	5.2	8.8
	(157.3)	(0.00)	(2.5)	(0.01)	(0.01)	(0.4)	(0.8)
EMCOMPRESS	12290.0	0.70	76.0	0.60	0.25	13.2	23.2
	(85.6)	(0.00)	(5.3)	(0.02)	(0.01)	(1.2)	(0.2)
	17810.0	0.76	102.4	0.81	0.30	24.8	45.6
	(975.1)	(0.00)	(8.6)	(0.20)	(0.02)	(2.0)	(0.4)

TABLE B.9 Strength isotropy ratio values for the materials subjected to both a direct and an indirect tension test. Numbers in parentheses represent ± confidence intervals at the 95% level.

Material	6kN	12kN	18kN
AVICEL PH102	0.51(0.01)	0.47(0.01)	0.45(0.02)
EMCOCEL 90M	0.52(0.01)	0.48(0.01)	0.46(0.01)
STARCH 1500	0.43(0.01)	0.42(0.01)	0.40(0.01)
SODIUM CHLORIDE	0.45(0.01)	0.43(0.01)	0.40(0.01)
SODIUM BICARBONATE	0.36(0.02)	0.35(0.01)	0.33(0.02)
ANHYDROUS LACTOSE	0.81(0.01)	0.79(0.02)	0.78(0.02)
EMCOMPRESS	1.04(0.02)	1.00(0.01)	0.99(0.02)

APPENDIX C

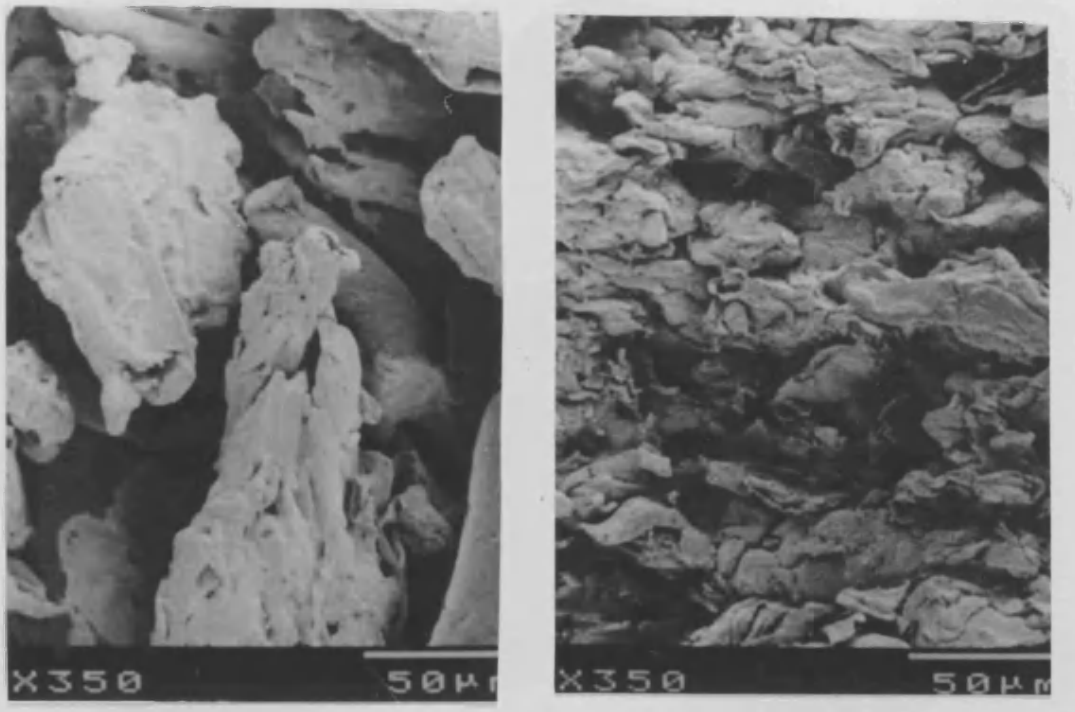

(a) (b)

Avicel PH102

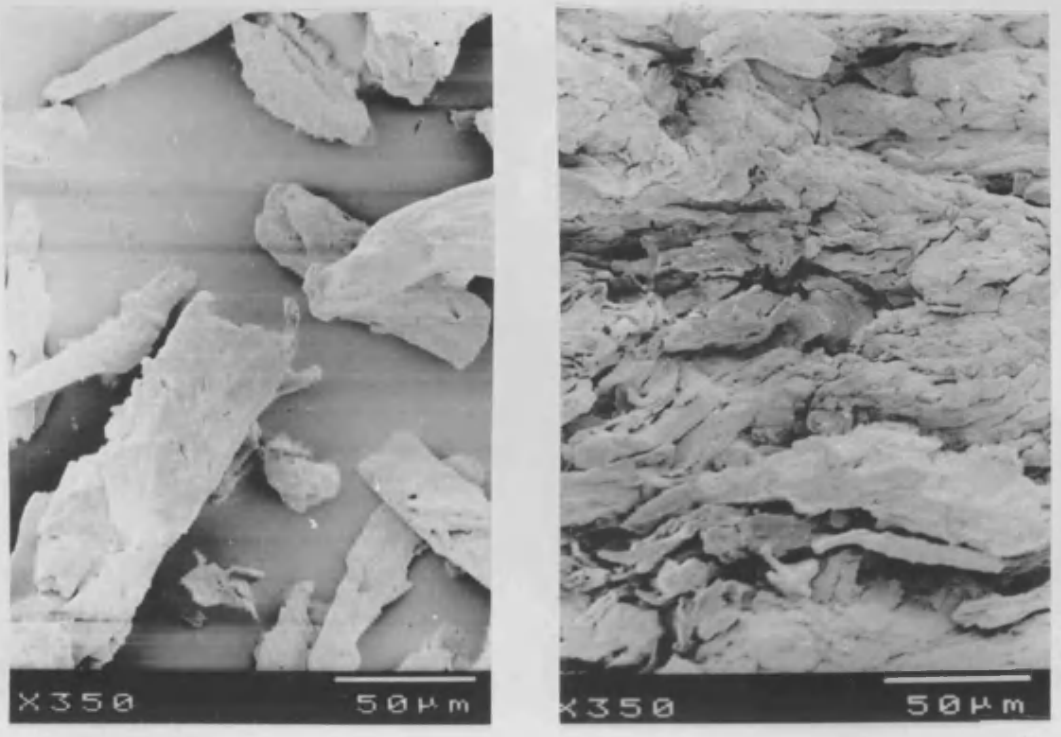

(a) (b)

Emcocel 90M

FIG. C.1 Scanning electron micrographs of Avicel PH102 and Emcocel 90M powder (a) and surface of a fractured tablet (b).

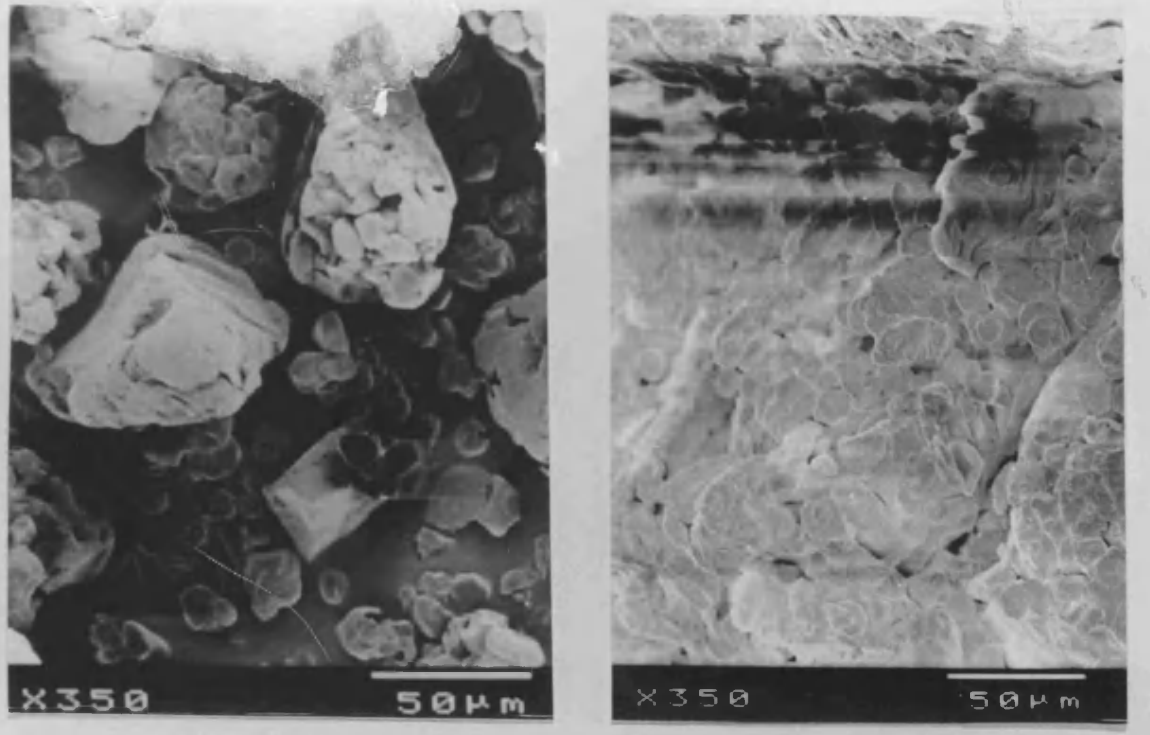

(a) (b)

Starch 1500

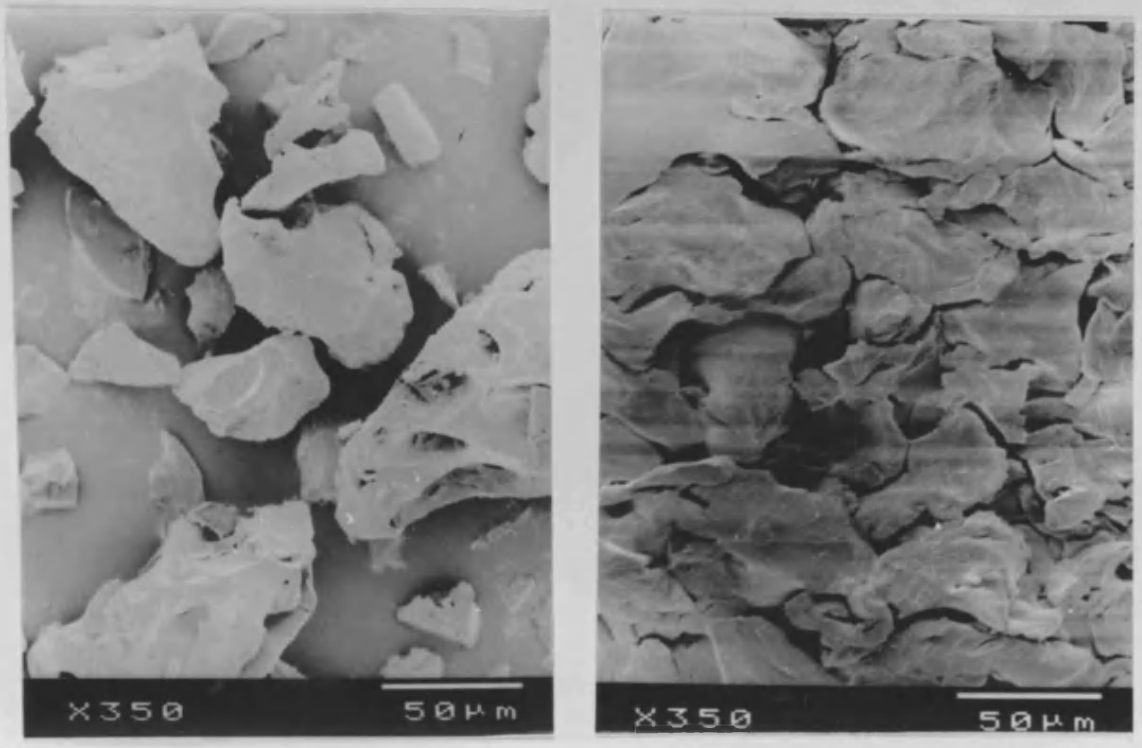

(a) (b)

National 1551

FIG. C.2 Scanning electron micrographs of Starch 1500 and National 1551 powder (a) and surface of a fractured tablet (b).

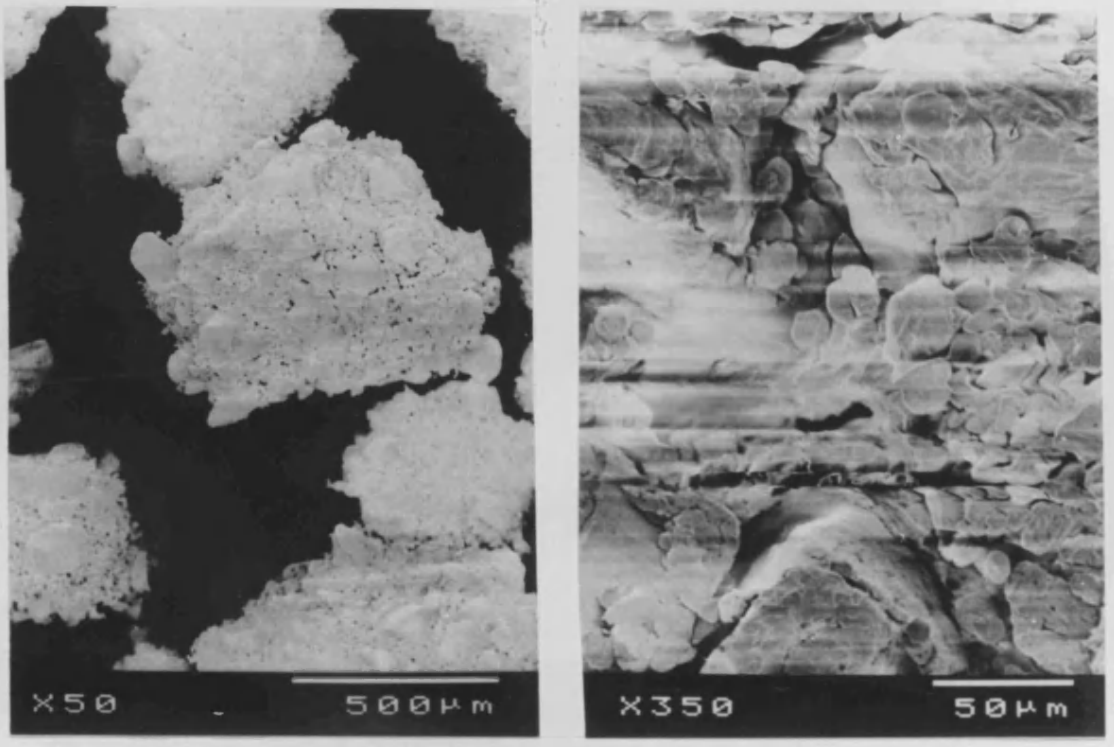

(a) (b)

FIG. C.3 Scanning electron micrographs of Starch 1500 (>710µm) powder (a) at low and high magnification, and surface of a fractured tablet (b).

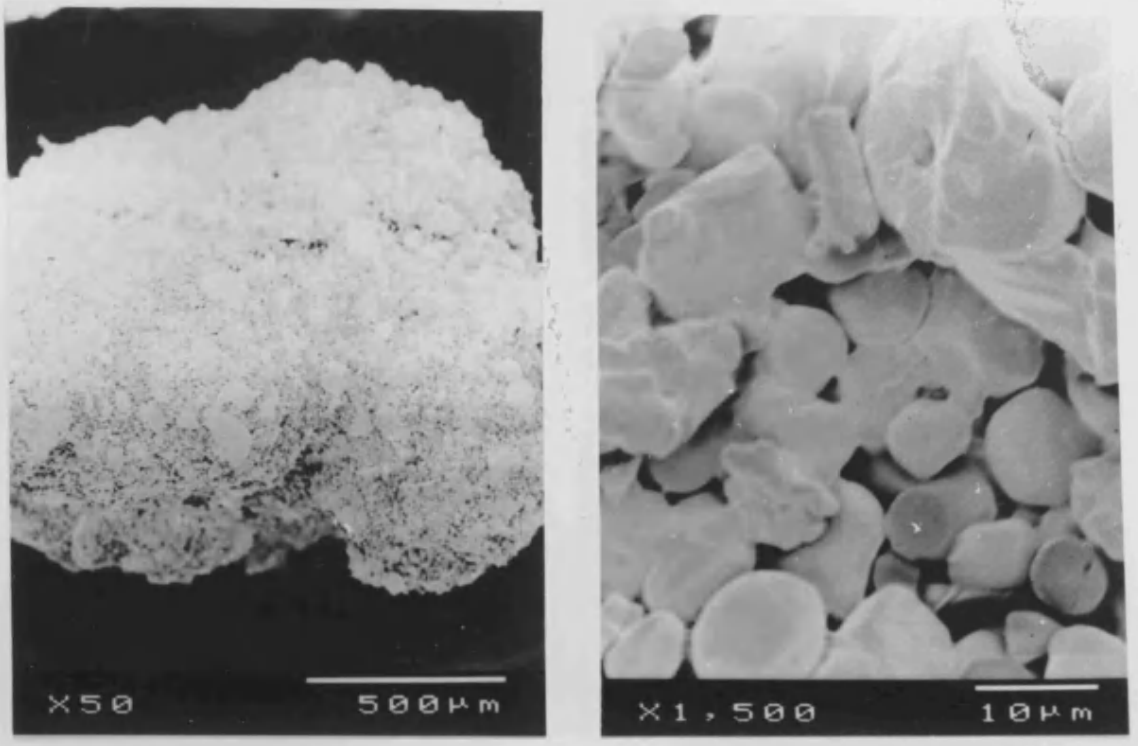

(a)

(b)

FIG. C.4 Scanning electron micrographs of Starch 1500 (>1680µm) powder (a) at low and high magnification, and surface of a fractured tablet (b).

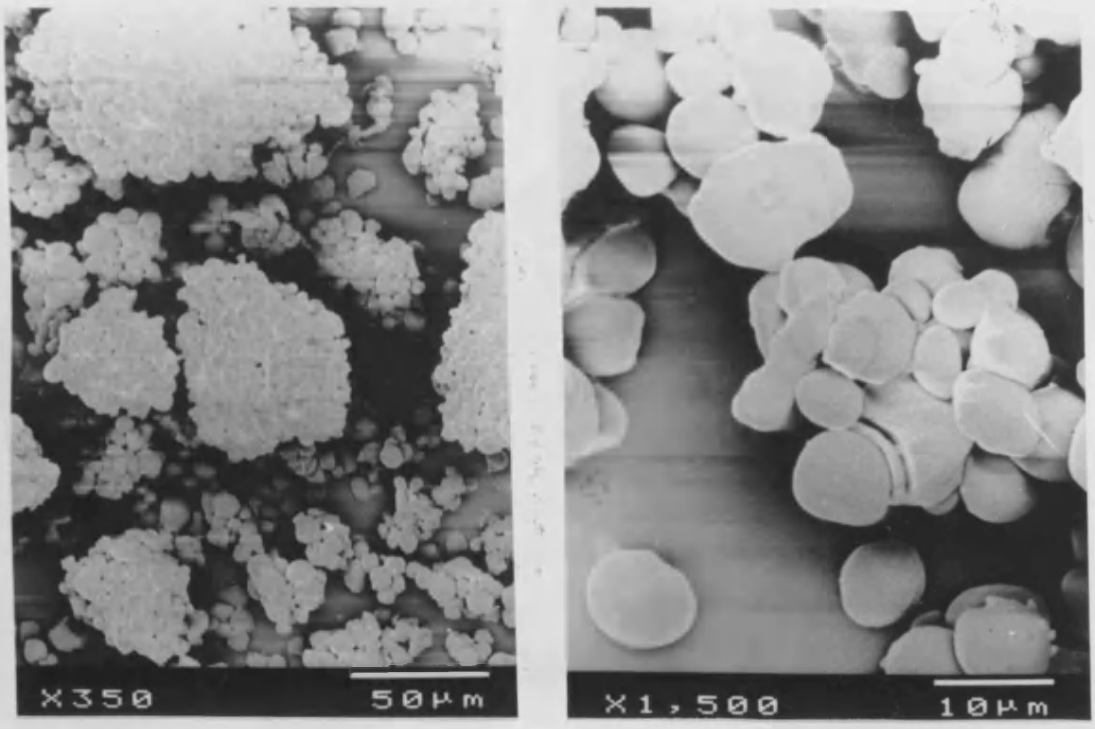

(a)

(b)

FIG. C.5 Scanning electron micrographs of amylose powder (a) at low and high magnification, and surface of a fractured tablet (b).

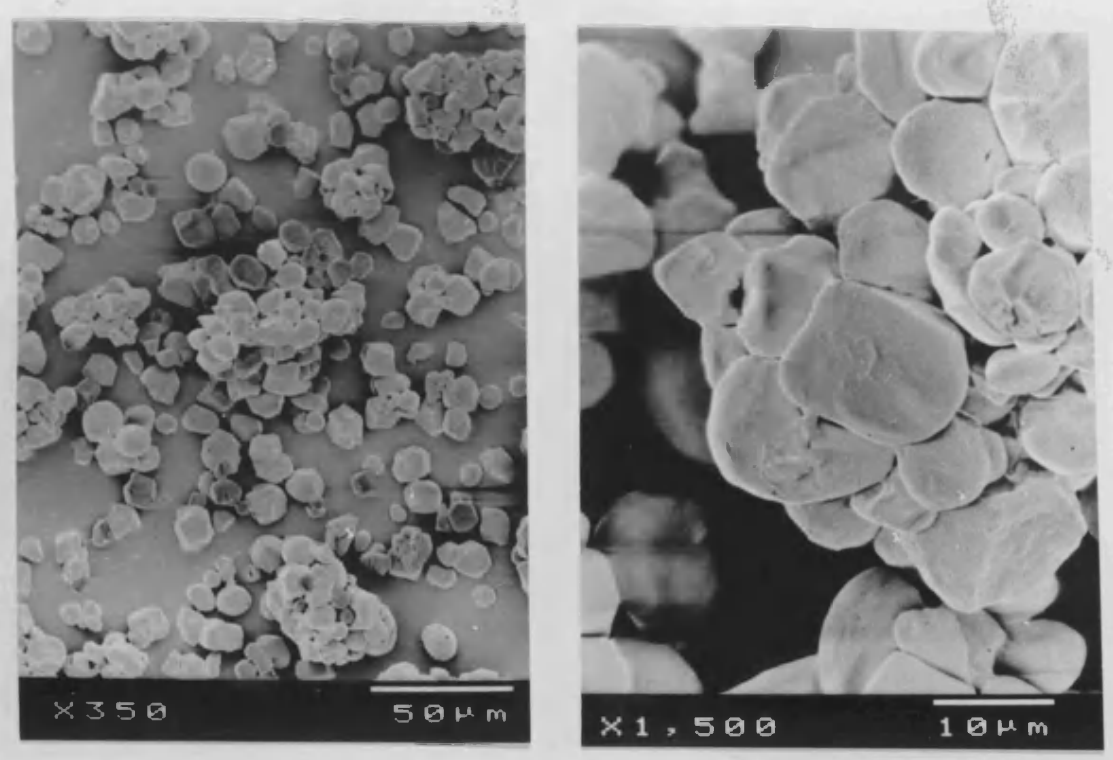

(a)

(b)

FIG. C.6 Scanning electron micrographs of amylopectin powder (a) at low and high magnification, and surface of a fractured tablet (b).

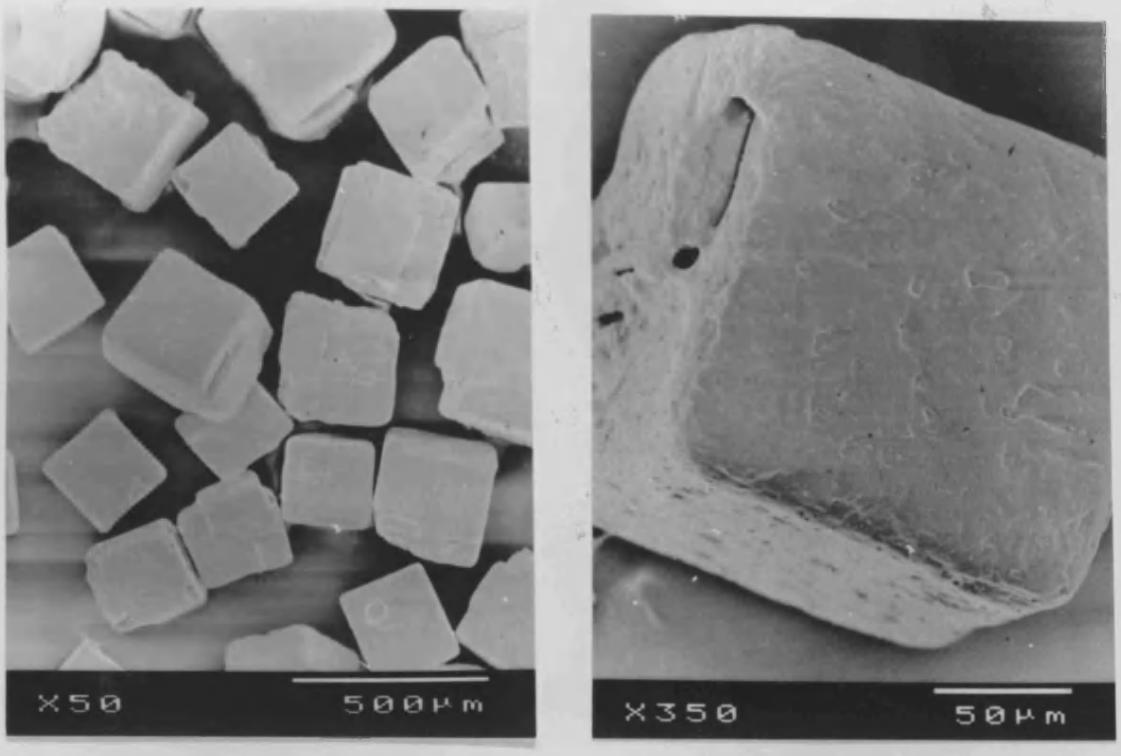

(a)

(b)

FIG. C.7 Scanning electron micrographs of sodium chloride powder (a) at low and high magnification, and surface of a fractured tablet (b).

(a) (b)

Sodium bicarbonate

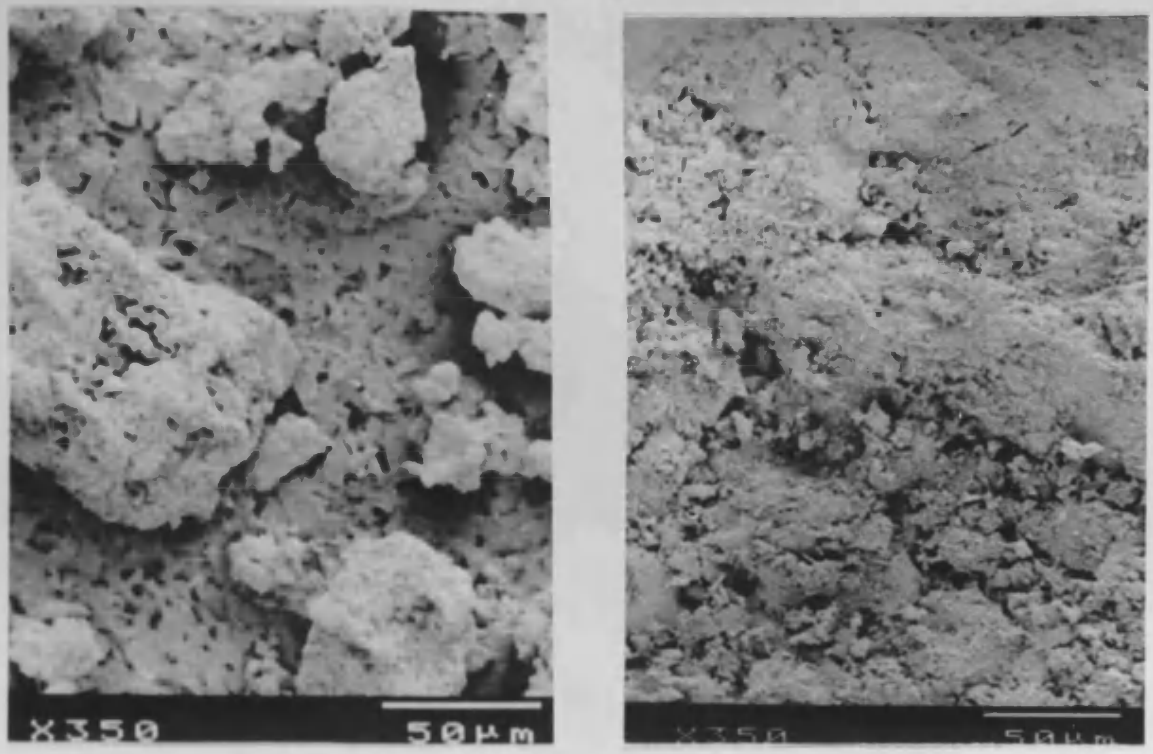

(a) (b)

Anhydrous lactose

FIG. C.8 Scanning electron micrographs of sodium bicarbonate and anhydrous lactose powder (a) and surface of a fractured tablet (b).

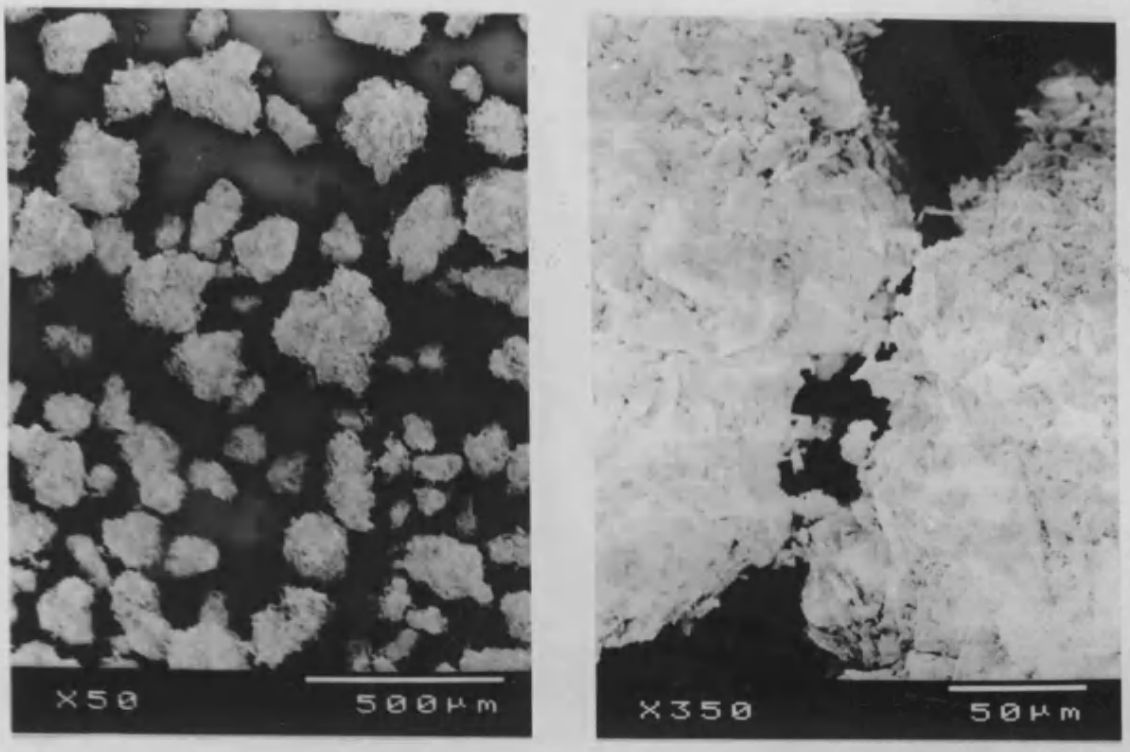

(a)

(b)

FIG. C.9 Scanning electron micrographs of Emcompress powder (a) at low and high magnification, and surface of a fractured tablet (b).

APPENDIX D

TABLE D.1 Stress relaxation results. Numbers in parentheses represent ± confidence intervals at the 95% level.

Platen rate (mm/min)	Max. force (N)	Rel. dens.	Total force drop (N)	Relative force drop	Rate of force decay to half force drop (N/s)
			AVICEL PH102		
10	2088	0.61	452	0.216	49
	(5)	(0.00)	(11)	(0.001)	(1.2)
50	2091	0.62	456	0.218	66
	(17)	(0.01)	(8)	(0.001)	(2.1)
10	6039	0.89	915	0.152	88
	(7)	(0.01)	(14)	(0.001)	(2.2)
50	6110	0.90	929	0.152	137
	(42)	(0.01)	(13)	(0.001)	(3.2)
			STARCH 1500		
10	2021	0.71	476	0.235	53
	(5)	(0.01)	(8)	(0.001)	(1.3)
50	2027	0.71	468	0.231	67
	(25)	(0.01)	(13)	(0.001)	(2.2)
10	6042	0.91	1221	0.202	125
	(4)	(0.01)	(13)	(0.001)	(2.9)
50	6048	0.90	1249	0.207	195
	(14)	(0.01)	(19)	(0.001)	(4.3)
			ANHYDROUS LACTOSE		
10	2041	0.72	220	0.108	39
	(10)	(0.01)	(14)	(0.001)	(0.9)
50	2020	0.73	239	0.118	43
	(12)	(0.03)	(10)	(0.002)	(1.1)
10	6017	0.91	477	0.079	39
	(4)	(0.02)	(23)	(0.002)	(1.0)
50	6244	0.92	536	0.086	54
	(30)	(0.03)	(25)	(0.002)	(1.4)
			EMCOMPRESS		
10	2016	0.65	57	0.028	4
	(7)	(0.00)	(3)	(0.001)	(0.2)
50	2184	0.66	69	0.031	4
	(18)	(0.01)	(5)	(0.002)	(0.1)
10	6056	0.82	143	0.024	7
	(7)	(0.01)	(6)	(0.002)	(0.5)
50	6258	0.80	159	0.025	13
	(225)	(0.01)	(9)	(0.002)	(0.7)

TABLE D.2 Results obtained from linearisation of stress relaxation data. Numbers in parentheses represent ± confidence intervals at the 95% level.

		[F_t/F_{min} vs lnt]			[$t/(F_{max}-F_t)$ vs t]		
Platen rate (mm/min)	Max. force (N)	Corr. coeff.	Slope $x10^{-2}$	Intercept	Corr. coeff.	Slope $x10^{-3}$ $(N)^{-1}$	Intercept $x10^{-2}$ (s/N)
				AVICEL PH102			
10	2088	0.990	-3.4	1.19	0.999	2.19	2.84
	(5)		(0.1)	(0.00)		(0.05)	(0.11)
50	2091	0.986	-3.1	1.18	0.999	2.19	2.61
	(17)		(0.1)	(0.00)		(0.03)	(0.10)
10	6039	0.992	-2.2	1.13	0.999	1.06	1.54
	(7)		(0.0)	(0.00)		(0.02)	(0.07)
50	6110	0.989	-2.0	1.12	0.999	1.05	1.36
	(42)		(0.0)	(0.00)		(0.01)	(0.04)
				STARCH 1500			
10	2021	0.988	-3.6	1.21	0.999	2.06	2.61
	(5)		(0.1)	(0.00)		(0.04)	(0.13)
50	2027	0.983	-3.4	1.19	0.999	2.10	2.41
	(25)		(0.1)	(0.00)		(0.07)	(0.13)
10	6042	0.990	-3.1	1.17	0.999	0.80	1.06
	(4)		(0.0)	(0.00)		(0.01)	(0.03)
50	6048	0.987	-2.9	1.16	0.999	0.78	0.96
	(14)		(0.0)	(0.00)		(0.01)	(0.05)
				ANHYDROUS LACTOSE			
10	2041	0.970	-1.3	1.07	0.999	4.65	4.43
	(10)		(0.1)	(0.00)		(0.24)	(0.63)
50	2020	0.964	-1.4	1.08	0.999	4.28	3.46
	(12)		(0.1)	(0.00)		(0.16)	(0.79)
10	6017	0.992	-1.1	1.06	0.999	2.06	3.17
	(4)		(0.0)	(0.00)		(0.09)	(0.34)
50	6244	0.991	-1.2	1.07	0.999	1.84	2.72
	(30)		(0.1)	(0.00)		(0.09)	(0.33)
				EMCOMPRESS			
10	2016	0.900	-0.4	1.02	0.987	20.74	9.24
	(7)		(0.0)	(0.00)		(1.40)	(1.31)
50	2184	0.913	-0.4	1.02	0.993	16.87	11.95
	(18)		(0.0)	(0.00)		(1.53)	(1.29)
10	6056	0.961	-0.3	1.02	0.994	7.32	10.63
	(7)		(0.0)	(0.00)		(0.37)	(0.95)
50	6258	0.952	-0.3	1.02	0.996	6.57	8.01
	(225)		(0.0)	(0.00)		(0.41)	(0.90)

APPENDIX E

TABLE E.1 Effect of test duration on the parameters derived from creep data for Starch 1500 and Emcompress. Numbers in parentheses represent ± confidence intervals at the 95% level.

(* indicates insufficient linear region)

Time (s)	Relative density (t=0)	Elastic modulus (MPa) x10^{6}	Viscosity coefficient (MPa s) x10^{8}	J_i (MPa)$^{-1}$ x10^{-6}	k_2 (s)
		STARCH 1500 (24MPa applied stress)			
60	0.77(0.02)	4.07(0.28)	*	*	*
90	0.76(0.01)	3.76(0.39)	3.08(0.10)	1.23(0.05)	2.00(0.04)
120	0.75(0.02)	3.62(0.71)	3.12(0.11)	1.25(0.07)	2.11(0.02)
300	0.74(0.01)	3.51(0.92)	3.19(0.09)	1.17(0.04)	2.05(0.03)
600	0.75(0.01)	3.45(1.40)	3.27(0.06)	1.26(0.08)	2.14(0.04)
		EMCOMPRESS (64MPa applied stress)			
60	0.76(0.02)	34.14(0.68)	*	*	*
90	0.77(0.01)	33.86(1.12)	242.43(28.24)	0.03(0.01)	1.35(0.03)
120	0.75(0.02)	27.09(1.43)	255.45(26.13)	0.02(0.02)	1.26(0.04)
300	0.75(0.02)	25.56(1.65)	247.65(25.18)	0.02(0.01)	1.29(0.04)
600	0.76(0.02)	24.33(2.13)	251.32(24.03)	0.02(0.01)	1.32(0.04)

TABLE E.2 Effect of powder mass on the parameters derived from creep data for Starch 1500 and Emcompress. Numbers in parentheses represent ± confidence intervals at the 95% level.

Mass (mg)	Relative density (t=0)	Elastic modulus (MPa) x10^6	Viscosity coefficient (MPa s) x10^8	J_i (MPa)$^{-1}$ x10^{-6}	k_2 (s)
		STARCH 1500 (24MPa applied stress)			
105	0.77(0.02)	3.61(0.92)	3.41(0.18)	1.62(0.16)	2.16(0.07)
211	0.77(0.01)	3.12(0.67)	3.22(0.11)	1.37(0.13)	2.17(0.04)
423	0.75(0.01)	3.24(0.30)	3.26(0.03)	1.46(0.08)	2.11(0.02)
634	0.76(0.01)	3.33(0.28)	3.19(0.03)	1.43(0.07)	2.04(0.02)
		EMCOMPRESS (64MPa applied stress)			
161	0.77(0.02)	36.01(2.33)	235.43(44.21)	0.03(0.02)	1.24(0.08)
322	0.75(0.02)	24.16(1.91)	261.32(36.90)	0.02(0.01)	1.31(0.06)
644	0.76(0.01)	27.83(1.03)	249.23(31.17)	0.02(0.01)	1.37(0.03)
966	0.76(0.01)	25.28(0.24)	257.31(21.19)	0.02(0.01)	1.34(0.03)

TABLE E.3 Effect of upper punch concavity on the parameters derived from creep data for Starch 1500 and Emcompress. Numbers in parentheses represent ± confidence intervals at the 95% level.

Radius (mm)	Relative density (t=0)	Elastic modulus (MPa) x10^6	Viscosity coefficient (MPa s) x10^8	J_i (MPa)$^{-1}$ x10^{-6}	k_2 (s)
STARCH 1500 (24MPa applied stress)					
16.5	0.76(0.01)	3.76(0.59)	3.11(0.14)	1.16(0.05)	2.07(0.01)
8.00	0.74(0.01)	3.70(0.71)	3.16(0.16)	1.25(0.07)	1.95(0.01)
6.35	0.76(0.01)	3.51(0.52)	3.01(0.16)	1.21(0.04)	2.05(0.03)
∞	0.75(0.01)	3.65(0.30)	3.08(0.03)	1.30(0.08)	2.00(0.02)
EMCOMPRESS (64MPa applied stress)					
16.5	0.75(0.01)	33.41(0.91)	234.32(26.91)	0.02(0.01)	1.12(0.04)
8.00	0.78(0.01)	25.36(1.13)	203.26(34.12)	0.03(0.01)	1.27(0.03)
6.35	0.75(0.03)	26.18(1.64)	217.31(40.06)	0.02(0.01)	1.04(0.05)
∞	0.76(0.02)	28.00(1.33)	225.45(30.23)	0.02(0.01)	1.36(0.04)

TABLE E.4 Effect of punch and die diameter on the parameters derived from creep data for Starch 1500 and Emcompress. Numbers in parentheses represent ± confidence intervals at the 95% level.

Diam. (mm)	Relative density (t=0)	Elastic modulus (MPa) x10^{6}	Viscosity coefficient (MPa s) x10^{8}	J_i (MPa)$^{-1}$ x10^{-6}	k_2 (s)
		STARCH 1500 (24MPa applied stress)			
7.9	0.74(0.01)	0.57(0.52)	0.83(0.16)	10.20(0.01)	2.31(0.01)
10.0	0.75(0.01)	1.18(0.71)	1.41(0.16)	4.39(0.01)	2.22(0.01)
12.7	0.77(0.01)	3.43(0.59)	2.86(0.06)	1.24(0.01)	2.02(0.01)
14.2	0.78(0.01)	3.92(0.30)	3.38(0.03)	0.78(0.01)	1.94(0.02)
		EMCOMPRESS (64MPa applied stress)			
7.9	0.77(0.01)	25.78(2.17)	250.00(15.11)	0.02(0.01)	1.33(0.02)
10.0	0.75(0.01)	33.44(1.21)	273.96(27.74)	0.02(0.01)	1.28(0.04)
12.7	0.76(0.02)	27.02(2.33)	245.06(33.23)	0.02(0.01)	1.36(0.04)
14.2	0.75(0.03)	26.24(1.54)	257.11(41.05)	0.03(0.01)	1.24(0.05)

TABLE E.5 Creep results for Avicel PH102, Emcocel 90M and Starch 1500. Numbers in parentheses represent ± confidence intervals at the 95% level.

Load (kN)	Relative density (t=0)	J_o^* $(MPa)^{-1}$ $x10^{-7}$	J_r $(MPa)^{-1}$ $x10^{-7}$	J_n $(MPa)^{-1}$ $x10^{-7}$	$\frac{J_n}{J_o^* + J_r}$
		AVICEL PH102			
2	0.56(0.01)	3.37(0.49)	14.23(0.49)	4.53(0.14)	0.26(0.01)
3	0.64(0.00)	2.15(0.28)	9.47(0.30)	2.87(0.06)	0.25(0.01)
4	0.70(0.01)	1.53(0.10)	6.62(0.16)	2.02(0.05)	0.25(0.01)
5	0.75(0.00)	1.29(0.14)	4.25(0.23)	1.43(0.03)	0.26(0.01)
6	0.78(0.01)	0.98(0.07)	3.46(0.09)	1.09(0.04)	0.25(0.01)
		EMCOCEL 90M			
2	0.58(0.00)	3.93(0.52)	13.91(0.61)	4.65(0.09)	0.26(0.00)
3	0.66(0.00)	2.24(0.42)	9.16(0.41)	2.82(0.09)	0.25(0.01)
4	0.72(0.00)	1.55(0.09)	6.42(0.18)	2.01(0.05)	0.25(0.01)
5	0.77(0.01)	1.36(0.17)	4.23(0.26)	1.42(0.03)	0.25(0.01)
6	0.79(0.01)	1.01(0.11)	3.25(0.11)	1.07(0.04)	0.25(0.01)
		STARCH 1500			
1	0.67(0.00)	6.58(0.33)	13.21(0.34)	6.40(0.28)	0.31(0.02)
2	0.71(0.00)	3.41(0.33)	10.14(0.45)	4.21(0.07)	0.31(0.00)
4	0.80(0.01)	1.84(0.39)	7.10(0.09)	2.79(0.07)	0.31(0.01)
6	0.84(0.01)	1.14(0.16)	4.54(0.16)	1.89(0.10)	0.33(0.02)
10	0.93(0.01)	0.56(0.03)	2.10(0.09)	0.81(0.06)	0.30(0.02)

TABLE E.6 Creep results for sodium chloride, sodium bicarbonate, anhydrous lactose and Emcompress. Numbers in parentheses represent ± confidence intervals at the 95% level.

Load (kN)	Relative density (t=0)	J_o^* $(MPa)^{-1}$ $x10^{-7}$	J_r $(MPa)^{-1}$ $x10^{-7}$	J_n $(MPa)^{-1}$ $x10^{-7}$	$\frac{J_n}{J_o^* + J_r}$
		SODIUM CHLORIDE			
1	0.61(0.01)	0.76(0.10)	7.08(0.37)	3.39(0.31)	0.43(0.05)
2	0.65(0.01)	0.56(0.05)	5.75(0.21)	2.62(0.18)	0.41(0.03)
4	0.74(0.01)	0.32(0.02)	4.88(0.15)	2.06(0.08)	0.40(0.01)
6	0.80(0.01)	0.21(0.03)	3.56(0.14)	1.54(0.05)	0.41(0.01)
10	0.86(0.01)	0.12(0.00)	1.83(0.06)	0.76(0.04)	0.40(0.02)
		SODIUM BICARBONATE			
1	0.61(0.00)	0.80(0.04)	1.01(0.11)	0.87(0.21)	0.48(0.09)
2	0.65(0.00)	0.76(0.01)	0.85(0.07)	0.54(0.07)	0.34(0.07)
4	0.71(0.01)	0.65(0.02)	0.70(0.04)	0.47(0.07)	0.35(0.06)
6	0.75(0.02)	0.43(0.01)	0.58(0.07)	0.32(0.07)	0.32(0.07)
10	0.80(0.01)	0.30(0.01)	0.32(0.02)	0.16(0.01)	0.26(0.03)
		ANHYDROUS LACTOSE			
1	0.64(0.00)	1.81(0.11)	2.08(0.27)	1.64(0.49)	0.42(0.14)
2	0.69(0.00)	1.54(0.07)	1.39(0.15)	0.83(0.10)	0.28(0.04)
4	0.75(0.01)	1.01(0.11)	1.01(0.06)	0.45(0.06)	0.23(0.03)
10	0.84(0.01)	0.71(0.06)	0.55(0.03)	0.28(0.05)	0.22(0.06)
14	0.87(0.01)	0.39(0.03)	0.43(0.02)	0.18(0.02)	0.22(0.06)
		EMCOMPRESS			
2	0.62(0.00)	2.35(0.22)	0.30(0.10)	0.48(0.10)	0.18(0.10)
4	0.68(0.00)	1.10(0.11)	0.25(0.08)	0.34(0.10)	0.25(0.06)
6	0.72(0.00)	0.41(0.03)	0.22(0.03)	0.28(0.02)	0.44(0.11)
10	0.77(0.00)	0.29(0.02)	0.13(0.04)	0.17(0.03)	0.41(0.14)
14	0.80(0.01)	0.13(0.01)	0.12(0.01)	0.12(0.03)	0.48(0.11)

TABLE E.7 Parameters derived from creep data for Avicel PH102, Emcocel 90M and Starch 1500. Numbers in parentheses represent ± confidence intervals at the 95% level.

Load (kN)	Relative density (t=0)	Elastic modulus (MPa) x10^6	Viscosity coefficient (MPa s) x10^8	J_i $(MPa)^{-1}$ x10^{-6}	k_2 (s)
		AVICEL PH102			
2	0.56(0.01)	3.07(0.41)	2.04(0.07)	1.78(0.03)	1.96(0.01)
3	0.64(0.00)	4.79(0.59)	3.16(0.07)	1.17(0.03)	1.88(0.01)
4	0.70(0.01)	6.61(0.47)	4.62(0.11)	0.82(0.02)	1.79(0.01)
5	0.75(0.00)	7.87(0.76)	6.58(0.18)	0.56(0.03)	1.74(0.01)
6	0.78(0.01)	10.31(0.72)	8.61(0.28)	0.44(0.03)	1.70(0.01)
		EMCOCEL 90M			
2	0.58(0.00)	2.64(0.43)	2.01(0.06)	1.80(0.02)	1.95(0.01)
3	0.66(0.00)	4.71(0.75)	3.26(0.12)	1.14(0.02)	1.85(0.01)
4	0.72(0.00)	6.49(0.39)	4.63(0.10)	0.81(0.02)	1.79(0.01)
5	0.77(0.01)	7.55(0.81)	6.70(0.18)	0.56(0.02)	1.71(0.01)
6	0.79(0.01)	10.13(0.84)	8.87(0.25)	0.42(0.03)	1.74(0.01)
		STARCH 1500			
1	0.67(0.00)	1.52(0.08)	1.62(0.14)	2.00(0.04)	2.03(0.01)
2	0.71(0.00)	2.93(0.27)	2.47(0.08)	1.46(0.03)	1.91(0.01)
4	0.80(0.01)	5.44(0.20)	4.01(0.05)	0.90(0.03)	2.05(0.01)
6	0.84(0.01)	8.74(0.81)	5.79(0.26)	0.54(0.01)	1.97(0.01)
10	0.93(0.01)	17.71(0.86)	13.86(0.13)	0.30(0.01)	1.89(0.01)

TABLE E.8 Parameters derived from creep data for sodium chloride, sodium bicarbonate, anhydrous lactose and Emcompress. Numbers in parentheses represent ± confidence intervals at the 95% level.

Load (kN)	Relative density (t=0)	Elastic modulus (MPa) x10^{6}	Viscosity coefficient (MPa s) x10^{8}	J_i $(MPa)^{-1}$ x10^{-7}	k_2 (s)
		SODIUM CHLORIDE			
1	0.61(0.01)	13.81(1.98)	2.92(0.32)	8.92(0.39)	2.06(0.01)
2	0.65(0.01)	18.12(1.46)	3.65(0.20)	7.30(0.32)	2.14(0.01)
4	0.74(0.01)	31.68(1.99)	4.54(0.18)	5.86(0.25)	1.90(0.01)
6	0.80(0.01)	49.93(2.54)	6.11(0.18)	4.43(0.33)	2.00(0.02)
10	0.86(0.01)	81.56(1.39)	12.79(0.71)	2.20(0.27)	2.06(0.02)
		SODIUM BICARBONATE			
1	0.61(0.00)	12.50(0.30)	19.65(2.11)	1.76(0.26)	1.34(0.02)
2	0.65(0.00)	13.22(0.62)	27.42(2.12)	1.40(0.23)	1.51(0.03)
4	0.71(0.01)	15.41(2.45)	42.44(1.72)	1.02(0.17)	1.59(0.02)
6	0.75(0.02)	23.35(1.61)	72.00(1.37)	0.78(0.22)	1.66(0.03)
10	0.80(0.01)	33.28(5.14)	96.27(1.30)	0.44(0.20)	1.71(0.02)
		ANHYDROUS LACTOSE			
1	0.64(0.00)	5.48(0.30)	15.51(3.38)	4.47(0.40)	1.08(0.02)
2	0.69(0.00)	6.51(0.29)	21.41(4.58)	2.58(0.33)	1.16(0.01)
4	0.75(0.01)	10.10(1.11)	30.00(5.33)	1.41(0.48)	1.32(0.02)
10	0.84(0.01)	14.13(1.02)	43.89(1.88)	0.72(0.31)	1.53(0.02)
14	0.87(0.01)	26.33(2.53)	66.41(7.55)	0.54(0.38)	1.66(0.02)
		EMCOMPRESS			
2	0.62(0.00)	4.32(0.40)	40.51(7.97)	0.63(0.23)	0.96(0.06)
4	0.68(0.00)	9.10(1.21)	151.01(15.6)	0.40(0.19)	1.13(0.06)
6	0.72(0.00)	24.57(1.85)	169.19(18.3)	0.30(0.15)	1.29(0.05)
10	0.77(0.00)	34.50(4.49)	238.24(42.8)	0.19(0.09)	1.41(0.05)
14	0.80(0.01)	76.88(6.63)	318.11(67.5)	0.17(0.06)	1.59(0.05)

TABLE E.9 Elastic modulus values obtained using the mathematical treatment proposed by Spriggs (1961). Numbers in parentheses represent ± confidence intervals at the 95% level.

Material	Corr. coeff.	Slope	$\ln G_o^*$	G_o^* (MPa) $\times 10^6$	$G_{0.3}^*$ (MPa) $\times 10^6$	G_t^* (MPa) $\times 10^6$
AVICEL PH102	0.992	-5.28 (0.27)	17.268 (0.088)	31.58	6.48	0.60
EMCOCEL 90M	0.979	-5.93 (0.51)	17.317 (0.153)	33.16	5.60	0.39
STARCH 1500	0.982	-9.29 (0.73)	17.395 (0.168)	35.85	2.21	0.41
SODIUM CHLORIDE	0.997	-7.03 (0.23)	19.158 (0.066)	209.03	25.36	13.47
SODIUM BICARBONATE	0.908	-5.24 (0.96)	18.266 (0.292)	85.67	17.80	8.55
ANH. LACTOSE	0.932	-6.24 (0.98)	17.689 (0.251)	48.11	7.39	1.76
EMCOMPRESS	0.974	-15.61 (1.48)	21.170 (0.429)	1563.20	14.47	0.13

G_o^* = Elastic modulus at zero porosity

$G_{0.3}^*$ = Elastic modulus at 0.3 porosity

G_t^* = Elastic modulus for powders at tapped density

TABLE E.10 Extrapolated viscosity coefficient values using the mathematical treatment proposed by Spriggs (1961). Numbers in parentheses represent ± confidence intervals at the 95% level.

Material	Corr. coeff.	Slope	$\ln\eta_o$	η_o (MPa s) $\times 10^8$	$\eta_{0.3}$ (MPa s) $\times 10^8$	η_t (MPa s) $\times 10^8$
AVICEL PH102	0.993	-6.47 (0.30)	21.937 (0.098)	33.66	4.83	0.26
EMCOCEL 90M	0.985	-6.77 (0.48)	21.923 (0.146)	33.19	4.35	0.21
STARCH 1500	0.986	-7.81 (0.54)	21.497 (0.125)	21.68	2.08	0.51
SODIUM CHLORIDE	0.900	-5.28 (1.02)	21.480 (0.288)	21.31	4.88	2.72
SODIUM BICARBONATE	0.989	-8.62 (0.52)	24.749 (0.158)	560.21	42.23	12.64
ANH. LACTOSE	0.977	-5.85 (0.52)	23.273 (0.134)	128.04	22.11	5.75
EMCOMPRESS	0.890	-10.43 (2.12)	26.378 (0.612)	2856.40	124.89	5.46

η_o = Viscosity coefficient at zero porosity

$\eta_{0.3}$ = Viscosity coefficient at 0.3 porosity

η_t = Viscosity coefficient for powders at tapped density

APPENDIX F

TABLE F.1 Work and related parameters obtained during compression for some Starch 1500 (B.N. 611002) particle size fractions. Numbers in parentheses represent ± confidence intervals at the 95% level.

Peak force (N)	Displ. (m)x10^{-3}	Upper punch work (J)	Lower punch work (J)	Total power of compaction (J/s)	True lower punch work (J)	True power of compaction (J/s)
			ORIGINAL PRODUCT			
6181.8	1.48	3.84	3.42	2.90	3.26	4.13
(78.9)	(0.02)	(0.06)	(0.06)	(0.15)	(0.06)	(0.20)
12279.6	1.63	7.11	6.89	5.94	6.65	8.07
(99.0)	(0.06)	(0.11)	(0.09)	(0.25)	(0.07)	(0.28)
18329.7	1.76	8.74	8.53	7.75	8.24	10.28
(252.9)	(0.03)	(0.05)	(0.07)	(0.48)	(0.10)	(0.64)
			<125μm			
6838.2	1.56	4.53	4.42	3.76	4.21	5.69
(60.1)	(0.07)	(0.10)	(0.09)	(0.61)	(0.08)	(0.15)
12560.5	1.88	7.78	7.52	5.91	7.23	9.51
(236.9)	(0.07)	(0.07)	(0.08)	(0.31)	(0.11)	(0.36)
18360.3	2.06	9.69	9.36	9.06	9.05	11.71
(176.8)	(0.07)	(0.17)	(0.17)	(0.61)	(0.11)	(0.60)
			125-180μm			
6550.0	1.46	4.26	4.07	3.46	3.89	5.19
(197.8)	(0.13)	(0.17)	(0.15)	(0.54)	(0.15)	(0.99)
12500.3	1.83	7.47	6.90	5.23	6.66	8.76
(212.7)	(0.08)	(0.07)	(0.10)	(0.69)	(0.06)	(0.68)
18119.9	2.05	9.47	9.10	8.46	8.81	11.30
(327.7)	(0.06)	(0.16)	(0.20)	(0.41)	(0.14)	(0.42)
			>180μm			
6494.5	1.54	4.21	3.99	3.40	3.82	5.23
(69.8)	(0.06)	(0.08)	(0.04)	(0.47)	(0.04)	(0.47)
12220.2	1.85	7.20	6.91	5.65	6.67	9.14
(49.4)	(0.06)	(0.07)	(0.08)	(0.37)	(0.07)	(0.36)
18430.3	1.90	9.21	8.92	8.91	8.62	10.9
(137.6)	(0.04)	(0.13)	(0.13)	(0.95)	(0.10)	(0.91)

TABLE F.2 Parameters related to elastic recovery, obtained during decompression for some Starch 1500 (B.N. 611002) particle size fractions. Numbers in parentheses represent ± confidence intervals at the 95% level.

Peak force (N)	Expansion work (J)	Expansion time (s)	Expansion rate $(m/s)x10^{-4}$	Power of expansion (J/s)
		ORIGINAL PRODUCT		
6181.8	0.15	0.31	4.03	0.50
(78.9)	(0.01)	(0.03)	(0.32)	(0.04)
12279.6	0.23	0.33	3.10	0.69
(99.0)	(0.02)	(0.03)	(0.30)	(0.06)
18329.7	0.29	0.33	2.80	0.96
(252.9)	(0.02)	(0.06)	(0.25)	(0.07)
		<125µm		
6838.2	0.21	0.30	4.13	0.78
(60.1)	(0.01)	(0.02)	(0.22)	(0.04)
12560.5	0.29	0.32	3.21	0.90
(236.9)	(0.02)	(0.03)	(0.25)	(0.03)
18360.3	0.31	0.33	2.77	0.94
(176.8)	(0.03)	(0.04)	(0.22)	(0.04)
		125-180µm		
6550.0	0.18	0.27	3.98	0.67
(197.8)	(0.02)	(0.03)	(0.24)	(0.03)
12500.3	0.24	0.32	3.13	0.75
(212.7)	(0.03)	(0.02)	(0.23)	(0.05)
18119.9	0.29	0.33	2.83	0.89
(327.7)	(0.03)	(0.04)	(0.20)	(0.04)
		>180µm		
6494.5	0.17	0.29	4.01	0.59
(69.8)	(0.01)	(0.02)	(0.17)	(0.02)
12220.2	0.24	0.31	3.01	0.77
(49.4)	(0.03)	(0.03)	(0.26)	(0.04)
18430.3	0.30	0.33	2.71	0.91
(137.6)	(0.02)	(0.05)	(0.20)	(0.05)

TABLE F.3 Time-related parameters, obtained during compression for some Starch 1500 (B.N. 611002) particle size fractions. Numbers in parentheses represent ± confidence intervals at the 95% level.

Peak force (N)	Contact time (s)	Rise time (s)	Punch travel $(m)x10^{-5}$	Relaxation time (s)	Dwell time (s)
		ORIGINAL PRODUCT			
6181.8	1.18	0.79	2.51	0.08	0.04
(78.9)	(0.07)	(0.05)	(0.54)	(0.03)	(0.01)
12279.6	1.16	0.81	0.91	0.02	0.02
(99.0)	(0.06)	(0.03)	(0.57)	(0.01)	(0.01)
18329.7	1.10	0.81	0.34	0.01	0.02
(252.9)	(0.10)	(0.07)	(0.41)	(0.02)	(0.00)
		<125μm			
6838.2	1.11	0.74	2.36	0.07	0.03
(60.1)	(0.04)	(0.05)	(0.45)	(0.02)	(0.02)
12560.5	1.10	0.76	0.96	0.02	0.02
(236.9)	(0.02)	(0.04)	(0.52)	(0.01)	(0.01)
18360.3	1.12	0.77	0.36	0.02	0.02
(176.8)	(0.08)	(0.03)	(0.44)	(0.01)	(0.01)
		125-180μm			
6550.0	1.10	0.75	2.41	0.08	0.04
(197.8)	(0.04)	(0.06)	(0.47)	(0.03)	(0.01)
12500.3	1.11	0.76	0.90	0.03	0.02
(212.7)	(0.03)	(0.03)	(0.51)	(0.02)	(0.02)
18119.9	1.13	0.78	0.35	0.02	0.01
(327.7)	(0.07)	(0.02)	(0.39)	(0.02)	(0.00)
		>180μm			
6494.5	1.08	0.73	2.45	0.06	0.03
(69.8)	(0.05)	(0.04)	(0.51)	(0.02)	(0.01)
12220.2	1.11	0.78	0.93	0.02	0.02
(49.4)	(0.03)	(0.03)	(0.59)	(0.02)	(0.01)
18430.3	1.13	0.79	0.32	0.01	0.02
(137.6)	(0.10)	(0.04)	(0.40)	(0.01)	(0.00)

TABLE F.4 Extended Heckel plot results for some Starch 1500 (B.N. 611002) particle size fractions. Numbers in parentheses represent ± confidence intervals at the 95% level.

Peak force (N)	Correl. coeff.	Yield pressure (MPa)	Interc. A	Square area	% Under rising F area	% Above falling F area	% Chord area
			ORIGINAL PRODUCT				
6181.8	0.999	53.31	0.70	80.59	67.50	2.63	3.84
(78.9)	(0.001)	(0.89)	(0.03)	(1.00)	(0.72)	(0.24)	(0.39)
12279.6	0.997	57.83	0.71	258.43	55.36	5.12	4.43
(99.0)	(0.001)	(1.32)	(0.02)	(3.01)	(0.83)	(0.43)	(0.35)
18329.7	0.991	58.00	0.73	462.75	51.45	7.93	6.64
(252.9)	(0.003)	(1.87)	(0.03)	(11.02)	(2.47)	(0.57)	(0.61)
			<125μm				
6838.2	0.999	46.82	0.58	95.82	60.61	3.67	3.34
(60.1)	(0.000)	(0.97)	(0.03)	(0.73)	(0.71)	(0.27)	(0.36)
12560.5	0.997	53.61	0.64	266.43	57.54	5.38	4.90
(236.9)	(0.001)	(1.12)	(0.02)	(2.76)	(0.92)	(0.56)	(0.44)
18360.3	0.999	54.95	0.62	518.07	54.03	8.33	6.33
(176.8)	(0.001)	(1.67)	(0.03)	(10.59)	(0.97)	(0.87)	(0.60)
			125-180μm				
6550.0	0.999	47.02	0.64	91.50	62.81	3.36	3.45
(197.8)	(0.001)	(0.84)	(0.02)	(0.69)	(0.69)	(0.31)	(0.27)
12500.3	0.998	52.81	0.74	284.36	57.02	6.02	4.18
(212.7)	(0.001)	(1.06)	(0.03)	(3.12)	(0.87)	(0.70)	(0.36)
18119.9	0.998	53.95	0.65	549.27	51.64	8.56	5.85
(327.7)	(0.001)	(1.36)	(0.03)	(10.27)	(1.05)	(0.98)	(0.58)
			>180μm				
6494.5	0.998	47.05	0.63	90.82	64.33	3.30	3.68
(69.8)	(0.001)	(0.88)	(0.02)	(0.71)	(0.70)	(0.25)	(0.28)
12220.2	0.998	50.12	0.60	256.08	58.62	5.09	4.91
(49.4)	(0.002)	(1.43)	(0.03)	(3.05)	(0.89)	(0.69)	(0.39)
18430.3	0.999	54.23	0.62	540.19	53.10	8.90	6.41
(137.6)	(0.001)	(1.72)	(0.04)	(11.14)	(1.03)	(0.71)	(0.63)

TABLE F.5 Diametral loading results for some Starch 1500 (B.N. 611002) particle size fractions. Numbers in parentheses represent ± confidence intervals at the 95% level.

	Peak force (N)	Rel. dens.	Break. force (N)	Tensile strength (MPa)	Deform. before failure $(m)\times10^{-4}$	Work of failure $(J)\times10^{-4}$	Corr. work of failure (J/m^2)	Power of failure $(J/s)\times10^{-4}$	Apparent failure viscosity (MPa·s)	Area ratio
	6181.8	0.67	15.4	0.23	1.62	12.4	18.7	2.8	1.0	0.92
	(78.9)	(0.00)	(0.8)	(0.01)	(0.11)	(0.8)	(1.3)	(0.2)	(0.1)	(0.05)
ORIGINAL	12279.6	0.76	44.3	0.76	2.12	53.2	90.2	8.2	4.9	0.89
PRODUCT	(99.0)	(0.00)	(1.3)	(0.02)	(0.10)	(3.2)	(5.5)	(0.2)	(0.3)	(0.02)
	18329.7	0.81	65.8	1.19	2.53	85.1	152.8	10.8	9.4	0.93
	(252.9)	(0.00)	(1.9)	(0.03)	(0.02)	(4.5)	(8.8)	(0.4)	(0.5)	(0.02)
	6838.2	0.68	16.3	0.24	1.69	13.0	20.3	3.1	1.0	0.91
	(60.1)	(0.00)	(0.6)	(0.01)	(0.10)	(0.8)	(1.4)	(0.2)	(0.1)	(0.04)
<125μm	12560.5	0.77	45.4	0.68	2.14	54.5	92.4	8.1	4.6	0.90
	(236.9)	(0.01)	(1.1)	(0.01)	(0.08)	(2.9)	(5.6)	(0.3)	(0.3)	(0.01)
	18360.3	0.80	66.6	0.99	2.60	85.4	156.9	11.0	7.7	0.94
	(176.8)	(0.00)	(1.9)	(0.03)	(0.07)	(4.0)	(9.3)	(0.4)	(0.4)	(0.02)

TABLE F.5 Diametral loading results for some Starch 1500 particle size fractions. Numbers in parentheses represent ± confidence intervals at the 95% level.

(continued)

	Peak force (N)	Rel. dens.	Break. force (N)	Tensile strength (MPa)	Deform. before failure (m)x10^{-4}	Work of failure (J)x10^{-4}	Corr. work of failure (J/m^2)	Power of failure (J/s)x10^{-4}	Apparent failure viscosity (MPa·s)	Area ratio
	6550.0	0.70	16.1	0.24	1.67	12.8	19.3	2.9	1.1	0.90
	(197.8)	(0.00)	(0.7)	(0.01)	(0.12)	(0.8)	(1.2)	(0.2)	(0.1)	(0.02)
125-180µm	12500.3	0.80	44.7	0.67	2.09	53.7	91.8	8.4	4.3	0.89
	(212.7)	(0.01)	(1.4)	(0.02)	(0.10)	(3.1)	(5.0)	(0.3)	(0.2)	(0.03)
	18119.9	0.82	66.9	1.00	2.58	85.3	155.5	10.8	7.9	0.92
	(327.7)	(0.01)	(1.8)	(0.02)	(0.04)	(4.0)	(8.6)	(0.4)	(0.4)	(0.05)
	6494.5	0.68	17.1	0.25	1.70	13.8	20.8	3.1	1.1	0.90
	(69.8)	(0.00)	(0.7)	(0.02)	(0.09)	(0.9)	(1.3)	(0.2)	(0.1)	(0.04)
>180µm	12220.2	0.80	45.7	0.68	2.15	54.4	92.2	8.2	4.5	0.91
	(49.4)	(0.00)	(1.2)	(0.03)	(0.09)	(3.3)	(5.3)	(0.3)	(0.3)	(0.02)
	18430.3	0.81	66.7	1.00	2.62	85.2	154.4	10.6	8.0	0.90
	(137.6)	(0.01)	(1.7)	(0.03)	(0.06)	(4.6)	(8.3)	(0.4)	(0.4)	(0.03)

TABLE F.6 Work and related parameters obtained during compression for some Starch 1500 (Batch F) particle size fractions. Numbers in parentheses represent ± confidence intervals at the 95% level.

Peak force (N)	Displ. (m)x10^{-3}	Upper punch work (J)	Lower punch work (J)	Total power of compaction (J/s)	True lower punch work (J)	True power of compaction (J/s)
			FINAL PRODUCT			
6064.4	0.91	2.83	2.66	3.69	2.50	5.31
(87.9)	(0.04)	(0.06)	(0.04)	(0.29)	(0.04)	(0.32)
12200.0	1.26	6.21	5.78	5.96	5.60	8.33
(70.8)	(0.06)	(0.09)	(0.07)	(0.51)	(0.07)	(0.57)
17739.7	1.48	8.16	7.63	6.87	7.39	9.69
(125.5)	(0.03)	(0.11)	(0.11)	(0.31)	(0.04)	(0.37)
			>710μm			
6080.7	1.86	4.56	4.19	4.60	4.05	5.99
(75.4)	(0.22)	(0.26)	(0.24)	(0.14)	(0.24)	(0.18)
12060.1	2.00	8.00	7.47	6.73	7.28	8.80
(222.8)	(0.13)	(0.18)	(0.13)	(0.24)	(0.14)	(0.30)
17789.9	2.30	9.43	8.91	7.61	8.62	10.58
(152.2)	(0.11)	(0.20)	(0.19)	(0.55)	(0.14)	(0.61)
			>1680μm			
5998.1	2.39	5.38	4.85	4.75	4.71	5.99
(69.8)	(0.17)	(0.15)	(0.16)	(0.20)	(0.15)	(0.23)
11889.6	2.76	8.95	8.35	6.96	8.16	9.20
(180.7)	(0.10)	(0.19)	(0.16)	(0.24)	(0.14)	(0.28)
17900.3	2.81	10.62	9.98	7.39	9.70	9.90
(251.5)	(0.13)	(0.26)	(0.24)	(0.70)	(0.19)	(0.80)

TABLE F.7 Parameters related to elastic recovery, obtained during decompression for some Starch 1500 (Batch F) particle size fractions. Numbers in parentheses represent ± confidence intervals at the 95% level.

Peak force (N)	Expansion work (J)	Expansion time (s)	Expansion rate $(m/s)x10^{-4}$	Power of expansion (J/s)
		FINAL PRODUCT		
6064.4	0.16	0.26	5.99	0.61
(87.9)	(0.01)	(0.01)	(0.47)	(0.05)
12200.0	0.18	0.28	3.81	0.64
(70.8)	(0.02)	(0.02)	(0.44)	(0.06)
17739.7	0.24	0.32	2.86	0.76
(125.5)	(0.03)	(0.03)	(0.33)	(0.06)
		>710µm		
6080.7	0.14	0.21	5.54	0.68
(75.4)	(0.01)	(0.02)	(0.67)	(0.06)
12060.1	0.19	0.26	3.53	0.76
(222.8)	(0.02)	(0.03)	(0.54)	(0.06)
17789.9	0.29	0.33	3.00	0.89
(152.2)	(0.02)	(0.03)	(0.42)	(0.07)
		>1680µm		
6257.1	0.14	0.21	5.30	0.67
(23.7)	(0.01)	(0.01)	(0.37)	(0.06)
12310.3	0.19	0.26	3.27	0.73
(61.3)	(0.02)	(0.04)	(0.42)	(0.06)
17890.5	0.28	0.34	3.02	0.84
(85.3)	(0.02)	(0.03)	(0.44)	(0.08)

TABLE F.8 Time-related parameters, obtained during compression for some Starch 1500 (Batch F) particle size fractions. Numbers in parentheses represent ± confidence intervals at the 95% level.

Peak force (N)	Contact time (s)	Rise time (s)	Punch travel (m)x10^{-5}	Relaxation time (s)	Dwell time (s)
			FINAL PRODUCT		
6064.4	0.72	0.45	1.46	0.05	0.02
(87.9)	(0.04)	(0.03)	(0.31)	(0.01)	(0.01)
12200.0	0.97	0.65	1.38	0.05	0.01
(70.8)	(0.05)	(0.05)	(0.33)	(0.01)	(0.00)
17739.7	1.11	0.76	0.79	0.03	0.02
(125.5)	(0.05)	(0.04)	(0.26)	(0.02)	(0.01)
			>710µm		
6080.7	0.91	0.64	2.18	0.06	0.02
(75.4)	(0.05)	(0.05)	(0.39)	(0.01)	(0.01)
12060.1	1.11	0.82	0.95	0.03	0.01
(222.8)	(0.03)	(0.03)	(0.20)	(0.01)	(0.00)
17789.9	1.17	0.84	0.85	0.00	0.01
(152.2)	(0.05)	(0.04)	(0.52)	(0.02)	(0.00)
			>1680µm		
6257.1	1.02	0.75	1.95	0.06	0.02
(23.7)	(0.05)	(0.04)	(0.41)	(0.01)	(0.00)
12310.3	1.20	0.89	1.14	0.02	0.01
(61.3)	(0.03)	(0.02)	(0.62)	(0.01)	(0.00)
17890.5	1.35	1.00	0.82	0.01	0.02
(85.3)	(0.07)	(0.07)	(0.46)	(0.02)	(0.01)

TABLE F.9 Extended Heckel plot results for some Starch 1500 (Batch F) particle size fractions. Numbers in parentheses represent ± confidence intervals at the 95% level.

Peak force (N)	Correl. coeff.	Yield pressure (MPa)	Interc. A	Square area	% Under rising F area	% Above falling F area	% Chord area
			FINAL PRODUCT				
6064.4	0.999	61.47	0.65	72.57	68.49	2.60	2.67
(87.9)	(0.000)	(3.08)	(0.02)	(0.81)	(0.86)	(0.18)	(0.17)
12200.0	0.998	62.46	0.71	225.12	60.86	3.85	4.26
(70.8)	(0.000)	(3.47)	(0.06)	(1.50)	(0.45)	(0.29)	(0.24)
17739.7	0.997	66.39	0.78	443.24	56.49	8.15	6.42
(125.5)	(0.001)	(3.66)	(0.08)	(18.31)	(1.05)	(0.82)	(0.35)
			>710μm				
6080.7	0.999	50.48	0.60	75.37	65.02	2.30	3.40
(75.4)	(0.000)	(2.51)	(0.03)	(0.92)	(0.32)	(0.22)	(0.16)
12060.1	0.999	53.78	0.61	232.54	60.11	4.26	4.49
(222.8)	(0.000)	(2.04)	(0.03)	(2.04)	(0.67)	(0.28)	(0.22)
17789.9	0.999	60.74	0.68	442.61	57.44	8.47	6.51
(152.2)	(0.000)	(1.29)	(0.02)	(7.81)	(0.94)	(1.02)	(1.02)
			>1680μm				
6257.1	0.999	48.10	0.53	77.28	64.27	2.23	3.21
(23.7)	(0.000)	(1.50)	(0.02)	(0.87)	(0.47)	(0.12)	(0.09)
12310.3	0.999	53.86	0.56	236.53	59.36	4.18	4.98
(61.3)	(0.000)	(1.01)	(0.02)	(4.03)	(0.89)	(0.70)	(0.32)
17890.5	0.999	59.59	0.62	435.25	58.07	8.80	6.81
(85.3)	(0.000)	(2.92)	(0.06)	(9.66)	(0.79)	(0.79)	(0.50)

TABLE F.10 Creep results for some Starch 1500 (Batch F) particle size fractions. Numbers in parentheses represent ± confidence intervals at the 95% level.

Load (kN)	Relative density (t=0)	J_o^* $(MPa)^{-1}$ $x10^{-7}$	J_r $(MPa)^{-1}$ $x10^{-7}$	J_n $(MPa)^{-1}$ $x10^{-7}$	$\frac{J_n}{J_o^* + J_r}$
		FINAL PRODUCT			
1	0.63(0.00)	6.55(0.44)	12.71(0.39)	6.12(0.20)	0.32(0.01)
2	0.68(0.01)	2.33(0.29)	9.24(0.30)	3.81(0.10)	0.33(0.01)
4	0.78(0.01)	1.76(0.26)	6.48(0.29)	2.66(0.12)	0.32(0.01)
6	0.86(0.01)	1.23(0.07)	4.83(0.16)	2.05(0.09)	0.34(0.02)
10	0.91(0.01)	0.70(0.10)	2.52(0.08)	1.05(0.03)	0.33(0.01)
		>710μm			
1	0.55(0.01)	5.17(1.11)	22.44(1.49)	8.90(0.26)	0.32(0.01)
2	0.63(0.01)	3.07(0.78)	13.93(0.59)	5.52(0.23)	0.32(0.01)
4	0.76(0.01)	2.03(0.26)	8.68(0.36)	3.55(0.22)	0.33(0.01)
6	0.86(0.01)	1.36(0.10)	5.76(0.20)	2.33(0.09)	0.33(0.01)
10	0.91(0.01)	0.67(0.06)	2.55(0.12)	1.05(0.03)	0.33(0.01)
		>1680μm			
1	0.51(0.01)	5.82(1.32)	26.56(1.35)	10.32(0.36)	0.32(0.01)
2	0.58(0.00)	3.12(0.30)	16.49(0.27)	6.13(0.14)	0.31(0.00)
4	0.74(0.01)	2.21(0.24)	9.46(0.34)	4.71(0.14)	0.32(0.01)
6	0.84(0.01)	1.59(0.08)	5.80(0.13)	2.29(0.07)	0.31(0.01)
10	0.91(0.01)	0.75(0.03)	2.63(0.09)	1.08(0.05)	0.32(0.01)

TABLE F.11 Parameters derived from creep data for some Starch 1500 (Batch F) particle size fractions. Numbers in parentheses represent ± confidence intervals at the 95% level.

Load (kN)	Relative density (t=0)	Elastic modulus (MPa) x10^6	Viscosity coefficient (MPa s) x10^8	J_i (MPa)$^{-1}$ x10^{-6}	k_2 (s)
			FINAL PRODUCT		
1	0.63(0.00)	1.54(0.10)	1.49(0.06)	1.96(0.01)	2.11(0.01)
2	0.68(0.01)	4.38(0.48)	2.38(0.08)	1.18(0.01)	2.14(0.01)
4	0.78(0.01)	5.86(0.74)	3.42(0.17)	0.84(0.01)	2.06(0.01)
6	0.86(0.01)	8.19(0.46)	4.43(0.18)	0.62(0.01)	2.10(0.01)
10	0.91(0.01)	14.58(1.65)	8.66(0.34)	0.33(0.01)	2.08(0.01)
			>710μm		
1	0.55(0.01)	2.04(0.30)	1.01(0.03)	2.82(0.01)	2.38(0.01)
2	0.63(0.01)	3.50(0.59)	1.63(0.06)	1.74(0.01)	2.35(0.02)
4	0.76(0.01)	5.09(0.71)	2.54(0.16)	1.10(0.01)	2.29(0.02)
6	0.86(0.01)	7.41(0.52)	3.88(0.16)	0.73(0.01)	2.23(0.01)
10	0.91(0.01)	15.00(1.23)	8.64(0.24)	0.33(0.01)	2.16(0.02)
			>1680μm		
1	0.51(0.01)	1.87(0.40)	0.88(0.04)	3.34(0.01)	2.37(0.02)
2	0.58(0.00)	3.25(0.32)	1.43(0.03)	2.02(0.01)	2.35(0.01)
4	0.74(0.01)	4.62(0.54)	2.43(0.09)	1.20(0.01)	2.20(0.01)
6	0.84(0.01)	6.33(0.33)	3.90(0.13)	0.76(0.01)	2.18(0.01)
10	0.91(0.01)	13.38(0.56)	8.49(0.41)	0.34(0.01)	2.16(0.02)

TABLE F.12 Diametral loading results for some Starch 1500 (Batch F) particle size fractions. Numbers in parentheses represent ± confidence intervals at the 95% level.

	Peak force (N)	Rel. dens.	Break. force (N)	Tensile strength (MPa)	Deform. before failure (m)x10^{-4}	Work of failure (J)x10^{-4}	Corr. work of failure (J/m^2)	Power of failure (J/s)x10^{-4}	Apparent failure viscosity (MPa·s)	Area ratio
	6064.4	0.66	14.4	0.22	1.59	12.3	18.5	2.8	0.9	0.93
	(87.9)	(0.00)	(0.8)	(0.01)	(0.12)	(0.9)	(1.3)	(0.3)	(0.1)	(0.07)
FINAL	12200.0	0.76	43.8	0.75	2.11	52.3	89.7	8.1	4.8	0.88
PRODUCT	(70.8)	(0.00)	(1.4)	(0.02)	(0.09)	(3.4)	(5.8)	(0.2)	(0.3)	(0.02)
	17739.7	0.80	66.1	1.20	2.50	86.0	155.8	11.0	9.4	0.96
	(125.5)	(0.00)	(1.9)	(0.04)	(0.01)	(4.8)	(9.0)	(0.4)	(0.5)	(0.01)
	6080.7	0.64	22.9	0.34	2.89	44.5	65.2	5.7	2.6	0.75
	(75.4)	(0.01)	(1.0)	(0.01)	(0.31)	(4.0)	(5.7)	(0.5)	(0.2)	(0.05)
>710µm	12060.1	0.74	75.1	1.27	3.61	172.2	291.6	15.1	14.5	0.80
	(222.8)	(0.00)	(3.6)	(0.06)	(0.25)	(32.6)	(53.0)	(1.8)	(2.0)	(0.09)
	17789.9	0.78	83.4	1.51	3.56	200.0	357.7	17.1	17.6	0.78
	(152.2)	(0.00)	(1.9)	(0.04)	(0.26)	(40.8)	(73.4)	(2.4)	(1.8)	(0.00)
	6257.1	0.62	22.3	0.32	3.51	60.9	87.3	6.3	3.1	0.65
	(23.7)	(0.01)	(3.9)	(0.06)	(0.47)	(13.9)	(20.3)	(1.6)	(0.5)	(0.07)
>1680µm	12310.3	0.73	65.3	1.08	4.06	162.5	269.5	12.8	13.7	0.84
	(61.3)	(0.00)	(6.1)	(0.10)	(0.35)	(41.6)	(69.7)	(2.2)	(2.5)	(0.10)
	17890.5	0.77	86.4	1.49	4.10	208.4	365.2	15.9	20.0	0.84
	(85.3)	(0.00)	(9.9)	(0.26)	(0.32)	(39.6)	(70.0)	(2.0)	(4.7)	(0.07)

TABLE F.13 Moisture content of Starch 1500 at a range of relative humidities.

% Relative humidity	% Moisture content
0	5.6
22	8.1
53	10.6
80	14.3
94	19.7

TABLE F.14 Work and related parametters obtained during compression for Starch 1500 stored at different humidity conditions. Numbers in parentheses represent ± confidence intervals at the 95% level.

Peak force (N)	Displ. (m)x10^{-3}	Upper punch work (J)	Lower punch work (J)	Total power of compaction (J/s)	True lower punch work (J)	True power of compaction (J/s)
			0% Relative Humidity			
6012.7	0.62	2.21	2.07	3.00	1.90	4.63
(192.8)	(0.03)	(0.11)	(0.10)	(0.29)	(0.09)	(0.33)
12389.9	1.01	5.97	5.50	5.34	5.14	7.77
(169.0)	(0.03)	(0.15)	(0.12)	(0.41)	(0.08)	(0.48)
17990.2	1.13	8.68	8.11	6.59	7.65	9.36
(213.8)	(0.03)	(0.16)	(0.16)	(0.88)	(0.12)	(1.01)
			22% Relative Humidity			
6392.8	1.37	3.69	3.31	2.98	3.08	4.11
(82.9)	(0.04)	(0.07)	(0.05)	(0.15)	(0.04)	(0.18)
12449.9	1.60	7.37	6.85	5.39	6.50	6.53
(109.5)	(0.05)	(0.07)	(0.05)	(0.48)	(0.08)	(0.56)
18000.0	1.73	9.92	9.33	6.81	8.89	9.51
(373.3)	(0.01)	(0.13)	(0.13)	(1.25)	(0.12)	(1.69)
			53% Relative Humidity			
6181.8	1.48	3.84	3.42	2.90	3.26	4.13
(78.9)	(0.02)	(0.06)	(0.06)	(0.15)	(0.06)	(0.20)
12279.6	1.63	7.11	6.89	5.94	6.65	8.07
(99.0)	(0.06)	(0.11)	(0.09)	(0.25)	(0.07)	(0.28)
18329.7	1.76	8.74	8.53	7.75	8.24	10.32
(252.9)	(0.03)	(0.05)	(0.07)	(0.48)	(0.10)	(0.64)
			80% Relative Humidity			
6291.1	1.74	3.95	3.41	2.86	3.45	3.75
(184.2)	(0.03)	(0.10)	(0.08)	(0.30)	(0.07)	(0.33)
12190.1	1.90	5.57	4.98	3.80	4.78	5.02
(103.8)	(0.07)	(0.09)	(0.04)	(0.31)	(0.03)	(0.35)
18020.3	1.93	5.81	5.65	4.83	5.39	6.57
(147.8)	(0.06)	(0.08)	(0.13)	(0.32)	(0.15)	(0.38)
			94% Relative Humidity			
6146.6	1.11	3.04	2.74	3.70	2.70	4.97
(425.9)	(0.07)	(0.24)	(0.24)	(0.21)	(0.23)	(0.25)
12120.0	1.21	3.51	3.20	3.72	3.01	5.37
(535.4)	(0.03)	(0.14)	(0.16)	(0.41)	(0.13)	(0.45)
18759.9	1.24	3.55	3.28	3.01	2.94	4.26
(800.7)	(0.07)	(0.20)	(0.21)	(0.41)	(0.19)	(0.46)

TABLE F.15 Parameters related to elastic recovery, obtained during decompression for Starch 1500 stored at different humidity conditions. Numbers in parentheses represent ± confidence intervals at the 95% level.

Peak force (N)	Expansion work (J)	Expansion time (s)	Expansion rate $(m/s)x10^{-4}$	Power of expansion (J/s)
		0% Relative Humidity		
6012.7	0.17	0.24	6.36	0.70
(192.8)	(0.01)	(0.02)	(0.81)	(0.07)
12389.9	0.36	0.31	5.34	1.18
(169.0)	(0.02)	(0.03)	(0.83)	(0.09)
17990.2	0.46	0.35	4.58	1.37
(213.8)	(0.03)	(0.05)	(0.79)	(0.11)
		22% Relative Humidity		
6392.8	0.23	0.31	5.32	0.75
(82.9)	(0.01)	(0.02)	(0.47)	(0.07)
12449.9	0.35	0.33	4.25	1.05
(109.5)	(0.02)	(0.03)	(0.49)	(0.09)
18000.0	0.44	0.36	3.91	1.28
(373.3)	(0.03)	(0.03)	(0.78)	(0.11)
		53% Relative Humidity		
6181.8	0.15	0.31	4.03	0.50
(78.9)	(0.01)	(0.03)	(0.32)	(0.04)
12279.6	0.23	0.33	3.10	0.69
(99.0)	(0.02)	(0.03)	(0.30)	(0.06)
18329.7	0.29	0.33	2.80	0.96
(252.9)	(0.02)	(0.06)	(0.25)	(0.07)
		80% Relative Humidity		
6291.1	0.06	0.27	2.11	0.24
(184.2)	(0.01)	(0.02)	(0.22)	(0.02)
12190.1	0.19	0.31	1.46	0.63
(103.8)	(0.01)	(0.03)	(0.21)	(0.05)
18020.3	0.26	0.31	1.33	0.88
(147.8)	(0.02)	(0.06)	(0.19)	(0.07)
		94% Relative Humidity		
6146.6	0.04	0.19	2.05	0.23
(425.9)	(0.01)	(0.02)	(0.46)	(0.02)
12120.0	0.19	0.26	1.54	0.76
(535.4)	(0.01)	(0.02)	(0.34)	(0.06)
18759.9	0.34	0.31	1.65	1.10
(800.7)	(0.02)	(0.03)	(0.21)	(0.10)

TABLE F.16 Time-related parameters, obtained during compression for Starch 1500 stored at different humidity conditions. Numbers in parentheses represent ± confidence intervals at the 95% level.

Peak force (N)	Contact time (s)	Rise time (s)	Punch travel (m)x10^{-5}	Relaxation time (s)	Dwell time (s)
		0% Relative Humidity			
6012.7	0.69	0.39	1.19	0.05	0.01
(192.8)	(0.03)	(0.02)	(0.28)	(0.02)	(0.00)
12389.9	1.03	0.66	1.05	0.05	0.02
(169.0)	(0.06)	(0.06)	(0.52)	(0.03)	(0.01)
17990.2	1.23	0.84	0.98	0.04	0.02
(213.8)	(0.12)	(0.10)	(0.46)	(0.02)	(0.01)
		22% Relative Humidity			
6392.8	1.11	0.74	1.73	0.07	0.03
(82.9)	(0.04)	(0.04)	(0.67)	(0.02)	(0.01)
12449.9	1.27	0.86	1.63	0.08	0.02
(109.5)	(0.11)	(0.08)	(0.59)	(0.02)	(0.01)
18000.0	1.37	0.94	1.58	0.07	0.02
(373.3)	(0.07)	(0.05)	(0.54)	(0.03)	(0.01)
		53% Relative Humidity			
6181.8	1.18	0.79	2.51	0.08	0.04
(78.9)	(0.07)	(0.05)	(0.54)	(0.03)	(0.01)
12279.6	1.16	0.81	0.91	0.02	0.02
(99.0)	(0.06)	(0.03)	(0.57)	(0.01)	(0.01)
18329.7	1.16	0.81	0.34	0.01	0.02
(252.9)	(0.10)	(0.07)	(0.41)	(0.02)	(0.00)
		80% Relative Humidity			
6291.1	1.19	0.86	1.71	0.05	0.03
(184.2)	(0.08)	(0.07)	(0.33)	(0.01)	(0.01)
12190.1	1.31	0.97	0.63	0.03	0.03
(103.8)	(0.08)	(0.07)	(0.33)	(0.00)	(0.01)
18020.3	1.17	0.86	0.31	0.01	0.01
(147.8)	(0.07)	(0.04)	(0.18)	(0.02)	(0.00)
		94% Relative Humidity			
6146.6	0.74	0.51	1.22	0.04	0.02
(425.9)	(0.03)	(0.02)	(0.36)	(0.01)	(0.01)
12120.0	0.86	0.61	0.88	0.03	0.02
(535.4)	(0.04)	(0.02)	(0.52)	(0.01)	(0.01)
18759.9	1.09	0.78	0.72	0.01	0.02
(800.7)	(0.07)	(0.06)	(0.41)	(0.02)	(0.00)

TABLE F.17 Extended Heckel plot results for Starch 1500 stored at different humidity conditions. Numbers in parentheses represent ± confidence intervals at the 95% level.

Peak force (N)	Correl. coeff.	Yield pressure (MPa)	Interc. A	Square area	% Under rising F area	% Above falling F area	% Chord area
			0% Relative Humidity				
6012.7	0.999	76.11	0.82	64.67	66.92	3.66	2.86
(192.8)	(0.000)	(5.78)	(0.02)	(1.78)	(0.65)	(0.20)	(0.14)
12389.9	0.997	84.79	0.78	196.75	63.96	6.19	5.25
(169.0)	(0.001)	(5.99)	(0.04)	(4.90)	(0.80)	(0.65)	(0.30)
17990.2	0.994	86.51	0.81	384.22	58.01	10.00	9.99
(213.8)	(0.001)	(5.26)	(0.07)	(5.59)	(0.68)	(0.90)	(0.33)
			22% Relative Humidity				
6392.8	0.999	67.01	0.75	76.00	69.61	3.24	3.57
(82.9)	(0.000)	(1.65)	(0.01)	(0.92)	(0.26)	(0.09)	(0.28)
12449.9	0.997	70.45	0.74	240.84	59.11	6.11	5.45
(109.5)	(0.001)	(2.82)	(0.05)	(3.18)	(0.39)	(0.60)	(0.43)
18000.0	0.995	76.38	0.75	433.31	51.27	8.96	8.46
(373.3)	(0.002)	(3.48)	(0.07)	(30.22)	(1.46)	(1.23)	(0.91)
			53% Relative Humidity				
6181.8	0.999	53.31	0.70	80.59	67.50	2.63	3.84
(78.9)	(0.001)	(0.89)	(0.02)	(1.00)	(0.72)	(0.24)	(0.39)
12279.6	0.997	57.83	0.71	258.43	55.36	5.12	4.43
(99.0)	(0.001)	(1.32)	(0.02)	(3.01)	(0.83)	(0.43)	(0.35)
18329.7	0.991	58.00	0.73	462.75	51.45	7.93	6.64
(252.9)	(0.003)	(1.87)	(0.03)	(11.02)	(2.47)	(0.57)	(0.61)
			80% Relative Humidity				
6291.1	0.999	38.95	0.50	119.65	60.05	2.70	3.60
(184.2)	(0.000)	(1.12)	(0.02)	(2.92)	(0.61)	(0.42)	(0.35)
12190.1	0.999	43.85	0.73	351.70	57.98	4.61	2.16
(103.8)	(0.000)	(1.45)	(0.02)	(4.79)	(0.89)	(0.91)	(0.56)
18020.3	0.996	46.71	0.90	507.42	47.96	6.19	2.22
(147.8)	(0.002)	(2.66)	(0.05)	(29.96)	(3.47)	(3.11)	(2.03)
			94% Relative Humidity				
6146.6	0.997	26.46	0.71	133.91	57.20	2.37	3.33
(425.9)	(0.001)	(3.06)	(0.05)	(3.91)	(1.50)	(0.41)	(0.38)
12120.0	0.975	55.36	1.30	284.21	61.72	4.61	0.74
(535.4)	(0.010)	(2.14)	(0.21)	(16.60)	(2.94)	(1.61)	(0.43)
18759.9	0.921	69.21	2.09	418.55	60.55	6.54	1.47
(800.7)	(0.010)	(5.51)	(0.23)	(9.15)	(1.87)	(1.69)	(0.73)

TABLE F.18 Creep results for Starch 1500 stored at different humidity conditions. Numbers in parentheses represent ± confidence intervals at the 95% level.

Load (kN)	Relative density (t=0)	J_o^* $(MPa)^{-1}$ $x10^{-7}$	J_r $(MPa)^{-1}$ $x10^{-7}$	J_n $(MPa)^{-1}$ $x10^{-7}$	$\frac{J_n}{J_o^* + J_r}$
		0% Relative Humidity			
1	0.65(0.00)	2.39(0.29)	6.84(0.34)	3.05(0.23)	0.33(0.03)
2	0.69(0.00)	1.56(0.14)	4.79(0.14)	2.17(0.11)	0.34(0.01)
6	0.79(0.01)	0.90(0.09)	3.12(0.08)	1.28(0.03)	0.32(0.01)
10	0.83(0.01)	0.54(0.02)	2.10(0.07)	0.87(0.03)	0.33(0.01)
14	0.84(0.02)	0.31(0.02)	1.46(0.05)	0.58(0.05)	0.33(0.04)
		22% Relative Humidity			
1	0.66(0.01)	4.02(0.38)	8.75(0.44)	3.17(0.46)	0.25(0.03)
2	0.70(0.00)	1.46(0.15)	7.40(0.25)	2.67(0.27)	0.30(0.03)
6	0.79(0.01)	1.02(0.13)	3.57(0.13)	1.34(0.06)	0.29(0.01)
10	0.88(0.01)	0.55(0.04)	2.25(0.07)	0.83(0.06)	0.30(0.02)
14	0.92(0.01)	0.29(0.01)	1.35(0.05)	0.44(0.02)	0.26(0.02)
		53% Relative Humidity			
1	0.67(0.00)	6.58(0.33)	13.21(0.34)	6.40(0.28)	0.31(0.02)
2	0.71(0.00)	3.41(0.33)	10.14(0.45)	4.21(0.07)	0.31(0.00)
4	0.80(0.01)	1.84(0.39)	7.10(0.09)	2.79(0.07)	0.31(0.01)
6	0.84(0.01)	1.14(0.16)	4.54(0.16)	1.89(0.10)	0.33(0.02)
10	0.93(0.01)	0.56(0.03)	2.10(0.09)	0.81(0.06)	0.30(0.02)
		80% Relative Humidity			
1	0.68(0.00)	9.44(1.26)	21.31(1.56)	8.42(0.34)	0.27(0.01)
1.5	0.70(0.00)	6.83(1.06)	16.69(0.83)	6.48(0.16)	0.28(0.01)
2	0.77(0.00)	6.12(0.84)	16.22(0.78)	6.07(0.13)	0.27(0.01)
4	0.86(0.01)	2.41(0.42)	8.38(0.56)	2.74(0.10)	0.25(0.01)
6	0.92(0.01)	1.25(0.10)	4.50(0.13)	1.40(0.06)	0.24(0.02)
		94% Relative Humidity			
0.5	0.62(0.00)	13.38(4.89)	47.13(8.90)	22.11(4.10)	0.36(0.02)
1	0.71(0.01)	12.91(2.75)	41.64(2.93)	20.44(1.04)	0.38(0.01)
1.5	0.78(0.01)	5.35(0.76)	36.50(2.32)	15.39(0.65)	0.37(0.01)
2	0.80(0.01)	4.02(0.68)	22.61(1.17)	8.85(0.40)	0.33(0.02)
4	0.94(0.01)	2.70(0.53)	7.84(1.14)	3.63(0.38)	0.34(0.03)

TABLE F.19 Parameters derived from creep data for Starch 1500 stored at different humidity conditions. Numbers in parentheses represent ± confidence intervals at the 95% level.

Load (kN)	Relative density (t=0)	Elastic modulus (MPa) x10^6	Viscosity coefficient (MPa s) x10^8	J_i (MPa)$^{-1}$ x10^{-6}	k_2 (s)
		0% Relative Humidity			
1	0.65(0.00)	4.30(0.54)	3.15(0.29)	0.94(0.01)	2.24(0.02)
2	0.69(0.00)	6.50(0.60)	4.21(0.22)	0.65(0.01)	2.27(0.01)
6	0.79(0.01)	11.30(1.07)	7.10(0.19)	0.41(0.01)	2.29(0.01)
10	0.83(0.01)	18.56(0.66)	10.43(0.31)	0.27(0.01)	2.36(0.01)
14	0.84(0.02)	32.77(2.52)	13.56(1.17)	0.18(0.01)	2.38(0.01)
		22% Relative Humidity			
1	0.66(0.01)	2.53(0.25)	3.20(0.33)	1.28(0.02)	2.09(0.01)
2	0.70(0.00)	7.00(0.77)	3.58(0.19)	0.87(0.01)	2.09(0.01)
6	0.79(0.01)	10.11(1.20)	7.21(0.14)	0.46(0.01)	1.93(0.01)
10	0.88(0.01)	18.42(1.43)	12.01(0.51)	0.28(0.01)	1.97(0.01)
14	0.92(0.01)	34.35(1.77)	22.13(1.17)	0.16(0.01)	2.00(0.01)
		53% Relative Humidity			
1	0.67(0.00)	1.52(0.08)	1.62(0.14)	2.00(0.04)	2.03(0.01)
2	0.71(0.00)	2.93(0.27)	2.47(0.08)	1.46(0.03)	1.91(0.01)
4	0.80(0.01)	5.44(0.20)	4.01(0.05)	0.90(0.03)	2.05(0.01)
6	0.84(0.01)	8.74(0.81)	5.79(0.26)	0.54(0.01)	1.97(0.01)
10	0.93(0.01)	17.71(0.86)	13.86(0.13)	0.30(0.01)	1.89(0.01)
		80% Relative Humidity			
1	0.68(0.00)	1.10(0.19)	1.09(0.04)	3.11(0.01)	2.38(0.02)
1.5	0.70(0.00)	1.56(0.34)	1.43(0.06)	2.38(0.01)	2.35(0.02)
2	0.77(0.00)	1.71(0.31)	1.52(0.04)	2.24(0.01)	2.40(0.02)
4	0.86(0.01)	4.36(0.76)	3.44(0.13)	1.09(0.01)	2.21(0.01)
6	0.92(0.01)	8.11(0.64)	6.79(0.24)	0.58(0.01)	2.33(0.02)
		94% Relative Humidity			
0.5	0.62(0.00)	0.94(0.36)	0.43(0.08)	7.50(0.03)	2.76(0.01)
1	0.71(0.01)	1.00(0.29)	0.44(0.02)	5.56(0.02)	2.85(0.01)
1.5	0.78(0.01)	1.94(0.27)	0.48(0.02)	4.33(0.02)	2.84(0.01)
2	0.80(0.01)	2.63(0.49)	1.01(0.06)	2.73(0.01)	2.67(0.01)
4	0.94(0.01)	4.00(0.87)	10.66(1.21)	1.11(0.01)	2.70(0.01)

TABLE F.20 Diametral loading results for Starch 1500 stored at different humidity conditions. Numbers in parentheses represent ± confidence intervals at the 95% level.
(* indicates tablets of inadequate strength)

	Peak force (N)	Rel. dens.	Break. force (N)	Tensile strength (MPa)	Deform. before failure $(m)\times10^{-4}$	Work of failure $(J)\times10^{-4}$	Corr. work of failure (J/m^2)	Power of failure $(J/s)\times10^{-4}$	Apparent failure viscosity (MPa·s)	Area ratio
	6012.7	0.57	*	*	*	*	*	*	*	*
0%	(192.8)	(0.01)	*	*	*	*	*	*	*	*
Relative	12389.9	0.69	7.0	0.11	1.07	3.5	5.6	1.1	0.4	1.08
humidity	(169.0)	(0.01)	(0.6)	(0.01)	(0.12)	(0.5)	(0.8)	(0.2)	(0.0)	(0.04)
	17990.2	0.75	11.1	0.20	1.16	4.7	8.4	1.3	0.5	0.99
	(213.8)	(0.03)	(1.2)	(0.03)	(0.15)	(0.5)	(1.5)	(0.2)	(0.1)	(0.05)
	6392.8	0.59	6.7	0.10	1.41	5.3	7.8	1.3	0.4	0.91
22%	(82.9)	(0.02)	(0.3)	(0.05)	(0.25)	(0.5)	(0.8)	(0.2)	(0.1)	(0.09)
Relative	12449.9	0.73	27.6	0.47	1.43	23.7	40.5	5.7	2.0	0.83
humidity	(109.5)	(0.01)	(4.1)	(0.07)	(0.16)	(0.4)	(6.6)	(0.7)	(0.4)	(0.05)
	18000.0	0.76	38.5	0.69	1.45	32.7	58.9	7.6	3.0	0.83
	(373.3)	(0.00)	(2.2)	(0.04)	(0.08)	(2.5)	(4.5)	(0.5)	(0.2)	(0.03)
	6181.8	0.67	15.4	0.23	1.62	12.4	18.7	2.8	1.0	0.92
53%	(78.9)	(0.00)	(0.8)	(0.01)	(0.11)	(0.8)	(1.3)	(0.2)	(0.1)	(0.05)
Relative	12279.6	0.76	44.3	0.76	2.12	53.2	90.2	8.2	4.9	0.89
humidity	(99.0)	(0.00)	(1.3)	(0.02)	(0.10)	(3.2)	(5.5)	(0.2)	(0.3)	(0.02)
	18329.7	0.81	65.8	1.19	2.53	85.1	152.8	10.8	9.4	0.93
	(252.9)	(0.00)	(1.9)	(0.03)	(0.02)	(4.5)	(8.8)	(0.4)	(0.5)	(0.02)

TABLE F.20 Diametral loading results for Starch 1500 stored at different humidity conditions. Numbers in parentheses represent ± confidence intervals at the 95% level.

(continued)

	Peak force (N)	Rel. dens.	Break. force (N)	Tensile strength (MPa)	Deform. before failure (m)x10^{-4}	Work of failure (J)x10^{-4}	Corr. work of failure (J/m^2)	Power of failure (J/s)x10^{-4}	Apparent failure viscosity (MPa·s)	Area ratio
	6291.1	0.80	127.3	2.20	3.25	218.0	377.1	18.1	26.6	0.95
80%	(184.2)	(0.01)	(8.8)	(0.15)	(0.24)	(17.6)	(34.3)	(1.3)	(4.0)	(0.04)
Relative	12190.1	0.87	219.0	4.06	3.83	492.3	912.5	31.6	63.4	0.86
humidity	(103.8)	(0.01)	(17.3)	(0.32)	(0.28)	(34.2)	(117.2)	(3.2)	(11.0)	(0.03)
	18020.3	0.88	230.5	4.32	4.36	593.2	1114.3	36.6	69.9	0.85
	(147.8)	(0.00)	(13.6)	(0.25)	(0.24)	(34.2)	(110.0)	(3.7)	(8.2)	(0.02)
	6146.6	0.83	73.8	1.36	3.04	141.1	258.4	12.8	15.0	0.84
94%	(425.9)	(0.04)	(33.1)	(0.29)	(0.25)	(21.6)	(28.9)	(1.2)	(1.9)	(0.02)
Relative	12120.0	0.87	138.4	2.64	4.17	341.5	654.4	22.8	41.7	0.85
humidity	(535.4)	(0.01)	(10.1)	(0.21)	(0.37)	(33.0)	(35.1)	(2.6)	(3.1)	(0.05)
	18759.9	0.85	114.1	2.80	4.04	281.4	534.6	18.0	34.1	0.82
	(800.7)	(0.01)	(7.3)	(0.13)	(0.27)	(27.1)	(36.8)	(1.8)	(2.3)	(0.04)

TABLE F.21 Work and related parameters obtained during compression for batches of Starch 1500 containing different proportions of cold water solubles (c.w.s.). Numbers in parentheses represent ± confidence intervals at the 95% level.

Peak force (N)	Displ. (m)x10^{-3}	Upper punch work (J)	Lower punch work (J)	Total power of compaction (J/s)	True lower punch work (J)	True power of compaction (J/s)
			15.4% c.w.s. (B.N. 807010)			
6285.5	1.11	2.98	2.74	3.65	2.59	5.31
(144.4)	(0.16)	(0.10)	(0.08)	(0.28)	(0.07)	(0.32)
11829.7	1.31	5.78	5.39	6.57	5.17	9.34
(174.2)	(0.09)	(0.10)	(0.12)	(0.41)	(0.11)	(0.46)
18230.0	1.57	8.13	7.67	6.73	7.39	9.63
(248.3)	(0.10)	(0.18)	(0.17)	(0.62)	(0.15)	(0.68)
			13.4% c.w.s. (B.N. 811024)			
5848.2	1.17	2.91	2.71	3.82	2.56	5.29
(134.3)	(0.08)	(0.11)	(0.10)	(0.40)	(0.09)	(0.44)
12259.6	1.32	6.35	5.95	6.40	5.72	9.17
(108.7)	(0.05)	(0.10)	(0.08)	(0.56)	(0.07)	(0.64)
18100.1	1.59	8.40	7.98	6.94	7.66	9.75
(217.3)	(0.09)	(0.12)	(0.10)	(0.49)	(0.09)	(0.55)
			12.6% c.w.s. (B.N. 801035)			
6174.8	1.06	3.02	2.77	3.69	2.60	5.16
(154.1)	(0.07)	(0.06)	(0.06)	(0.14)	(0.05)	(0.18)
11810.0	1.23	5.96	5.46	6.35	5.21	9.01
(142.3)	(0.12)	(0.11)	(0.09)	(0.37)	(0.08)	(0.46)
18330.5	1.50	8.71	8.15	7.21	7.81	10.19
(240.8)	(0.11)	(0.12)	(0.15)	(0.86)	(0.14)	(0.95)
			10.9% c.w.s. (B.N. 903025)			
5975.5	1.10	2.85	2.66	3.80	2.54	5.33
(64.3)	(0.09)	(0.06)	(0.04)	(0.22)	(0.04)	(0.24)
12120.0	1.39	6.13	5.68	6.17	5.47	8.75
(97.8)	(0.10)	(0.07)	(0.07)	(0.57)	(0.05)	(0.65)
18349.9	1.61	8.23	7.76	7.12	7.41	10.48
(338.4)	(0.12)	(0.17)	(0.15)	(0.64)	(0.06)	(0.72)

TABLE F.22 Parameters related to elastic recovery, obtained during decompression for batches of Starch 1500 containing different proportions of cold water solubles (c.w.s.). Numbers in parentheses represent ± confidence intervals at the 95% level.

Peak force (N)	Expansion work (J)	Expansion time (s)	Expansion rate $(m/s)x10^{-4}$	Power of expansion (J/s)
		15.4% c.w.s. (B.N. 807010)		
6285.5	0.15	0.23	5.42	0.69
(144.4)	(0.01)	(0.02)	(0.89)	(0.06)
11829.7	0.22	0.24	4.74	0.93
(174.2)	(0.02)	(0.02)	(0.53)	(0.08)
18230.0	0.28	0.28	3.49	1.00
(248.3)	(0.03)	(0.04)	(0.55)	(0.10)
		13.4% c.w.s. (B.N. 811024)		
5848.2	0.15	0.20	6.10	0.77
(134.3)	(0.01)	(0.01)	(0.20)	(0.07)
12259.6	0.23	0.27	3.57	0.86
(108.7)	(0.02)	(0.02)	(0.41)	(0.08)
18100.1	0.32	0.33	3.66	1.01
(217.3)	(0.03)	(0.03)	(0.43)	(0.10)
		12.6% c.w.s. (B.N. 801035)		
6174.8	0.17	0.21	6.04	0.78
(154.1)	(0.01)	(0.02)	(0.72)	(0.08)
11810.0	0.25	0.25	5.06	1.00
(142.3)	(0.02)	(0.02)	(0.47)	(0.09)
18330.5	0.34	0.33	3.89	1.09
(240.8)	(0.03)	(0.04)	(0.61)	(0.10)
		10.9% c.w.s. (B.N. 903025)		
5975.5	0.12	0.20	5.07	0.61
(64.3)	(0.01)	(0.02)	(0.54)	(0.05)
12120.0	0.21	0.27	3.89	0.79
(97.8)	(0.02)	(0.02)	(0.53)	(0.06)
18349.9	0.35	0.34	2.97	1.01
(338.4)	(0.03)	(0.03)	(0.26)	(0.09)

TABLE F.23 Time-related parameters, obtained during compression for batches of Starch 1500 containing different proportions of cold water solubles (c.w.s.). Numbers in parentheses represent ± confidence intervals at the 95% level.

Peak force (N)	Contact time (s)	Rise time (s)	Punch travel (m)x10^{-5}	Relaxation time (s)	Dwell time (s)
			15.4% c.w.s. (B.N. 807010)		
6285.5	0.75	0.47	2.04	0.05	0.02
(144.4)	(0.04)	(0.03)	(0.49)	(0.02)	(0.00)
11829.7	0.82	0.55	1.17	0.03	0.01
(174.2)	(0.04)	(0.03)	(0.20)	(0.01)	(0.00)
18230.0	1.14	0.79	0.67	0.02	0.02
(248.3)	(0.10)	(0.06)	(0.39)	(0.03)	(0.01)
			13.4% c.w.s. (B.N. 811024)		
5848.2	0.71	0.46	1.87	0.06	0.02
(134.3)	(0.04)	(0.04)	(0.44)	(0.01)	(0.01)
12259.6	0.93	0.63	0.93	0.02	0.02
(108.7)	(0.05)	(0.04)	(0.33)	(0.02)	(0.01)
18100.1	1.15	0.82	0.39	0.01	0.02
(217.3)	(0.06)	(0.05)	(0.33)	(0.02)	(0.01)
			12.6% c.w.s. (B.N. 801035)		
6174.8	0.75	0.48	1.73	0.05	0.01
(154.1)	(0.02)	(0.02)	(0.91)	(0.02)	(0.00)
11810.0	0.86	0.59	0.96	0.02	0.02
(142.3)	(0.05)	(0.04)	(0.62)	(0.01)	(0.00)
18330.5	1.13	0.77	0.73	0.03	0.02
(240.8)	(0.07)	(0.05)	(0.49)	(0.03)	(0.01)
			10.9% c.w.s. (B.N. 903025)		
5975.5	0.70	0.46	1.59	0.05	0.02
(64.3)	(0.01)	(0.02)	(0.36)	(0.01)	(0.01)
12120.0	0.92	0.63	1.01	0.02	0.02
(97.8)	(0.04)	(0.04)	(0.70)	(0.02)	(0.01)
18349.9	1.09	0.76	0.70	0.02	0.01
(338.4)	(0.05)	(0.04)	(0.57)	(0.02)	(0.00)

TABLE F.24 Extended Heckel plot results for batches of Starch 1500 containing different proportions of cold water solubles (c.w.s.). Numbers in parentheses represent ± confidence intervals at the 95% level.

Peak force (N)	Correl. coeff.	Yield pressure (MPa)	Interc. A	Square area	% Under rising F area	% Above falling F area	% Chord area
			15.4% c.w.s. (B.N. 807010)				
6285.5	0.999	58.18	0.74	80.89	66.15	2.90	3.30
(144.4)	(0.000)	(2.35)	(0.02)	(2.01)	(0.72)	(0.50)	(0.17)
11829.7	0.998	61.44	0.77	219.03	60.73	3.98	5.00
(174.2)	(0.000)	(2.14)	(0.02)	(3.00)	(0.53)	(0.52)	(0.42)
18230.0	0.998	62.00	0.79	457.85	57.17	6.94	7.72
(248.3)	(0.001)	(3.41)	(0.05)	(12.54)	(0.88)	(0.75)	(0.52)
			13.4% c.w.s. (B.N. 811024)				
5848.2	0.999	58.12	0.76	66.20	68.96	2.37	2.72
(134.3)	(0.000)	(2.55)	(0.02)	(1.28)	(0.70)	(0.17)	(0.16)
12259.6	0.999	61.15	0.77	210.42	62.67	3.80	3.72
(108.7)	(0.000)	(1.53)	(0.02)	(1.46)	(0.40)	(0.31)	(0.35)
18100.1	0.999	62.34	0.79	372.83	62.75	7.20	5.44
(217.3)	(0.000)	(3.11)	(0.03)	(3.64)	(0.47)	(0.77)	(0.19)
			12.6% c.w.s. (B.N. 801035)				
6174.8	0.999	60.20	0.68	74.15	67.96	2.75	2.98
(154.1)	(0.000)	(3.33)	(0.01)	(1.50)	(0.67)	(0.32)	(0.15)
11810.0	0.996	63.42	0.71	199.67	62.44	3.76	4.55
(142.3)	(0.000)	(5.06)	(0.06)	(2.26)	(0.90)	(0.45)	(0.34)
18330.5	0.997	64.86	0.74	422.51	58.14	6.57	6.95
(240.8)	(0.000)	(4.89)	(0.08)	(6.64)	(0.78)	(0.72)	(0.25)
			10.9% c.w.s. (B.N. 903025)				
5975.5	0.997	59.97	0.70	69.94	67.56	3.14	2.52
(64.3)	(0.000)	(2.41)	(0.02)	(0.69)	(0.57)	(0.22)	(0.13)
12120.0	0.996	63.63	0.76	198.86	63.97	4.15	3.59
(97.8)	(0.000)	(3.49)	(0.03)	(1.78)	(0.77)	(1.01)	(0.24)
18349.9	0.997	64.91	0.83	375.84	63.35	7.12	4.65
(338.4)	(0.000)	(2.34)	(0.03)	(10.93)	(0.79)	(1.00)	(0.28)

TABLE F.25 Work and related parameters obtained during compression for amylose and amylopectin. Numbers in parentheses represent ± confidence intervals at the 95% level.

Peak force (N)	Displ. (m)x10^{-3}	Upper punch work (J)	Lower punch work (J)	Total power of compaction (J/s)	True lower punch work (J)	True power of compaction (J/s)
			AMYLOSE			
5817.8	1.06	3.09	2.86	4.21	2.66	6.03
(130.0)	(0.07)	(0.11)	(0.08)	(0.28)	(0.07)	(0.32)
12230.5	1.50	7.48	6.96	7.17	6.67	10.11
(207.5)	(0.07)	(0.14)	(0.14)	(0.61)	(0.11)	(0.66)
18530.2	1.64	10.62	9.89	7.91	9.53	11.00
(285.4)	(0.06)	(0.22)	(0.21)	(0.85)	(0.18)	(0.99)
			AMYLOPECTIN			
6187.3	0.94	3.37	3.17	4.40	2.94	6.38
(137.0)	(0.03)	(0.08)	(0.12)	(0.41)	(0.10)	(0.46)
12089.9	1.38	8.04	7.42	7.81	7.16	10.90
(101.1)	(0.05)	(0.14)	(0.12)	(0.52)	(0.12)	(0.57)
18400.2	1.61	11.51	10.69	8.56	10.41	11.71
(229.7)	(0.05)	(0.23)	(0.22)	(0.86)	(0.17)	(1.04)

TABLE F.26 Parameters related to elastic recovery, obtained during decompression for amylose and amylopectin. Numbers in parentheses represent ± confidence intervals at the 95% level.

Peak force (N)	Expansion work (J)	Expansion time (s)	Expansion rate (m/s)x10^{-4}	Power of expansion (J/s)
		AMYLOSE		
5817.8	0.20	0.20	7.10	0.99
(130.0)	(0.02)	(0.02)	(1.00)	(0.10)
12230.5	0.29	0.28	4.34	1.04
(207.5)	(0.02)	(0.01)	(0.46)	(0.11)
18530.2	0.36	0.34	3.41	1.06
(285.4)	(0.03)	(0.04)	(0.53)	(0.09)
		AMYLOPECTIN		
6187.3	0.23	0.24	7.70	0.96
(137.0)	(0.02)	(0.02)	(0.76)	(0.09)
12089.9	0.26	0.26	5.30	0.99
(101.1)	(0.02)	(0.02)	(0.63)	(0.10)
18400.2	0.33	0.33	3.81	1.03
(229.7)	(0.03)	(0.03)	(0.52)	(0.10)

TABLE F.27 Time-related parameters, obtained during compression for amylose and amylopectin. Numbers in parentheses represent ± confidence intervals at the 95% level.

Peak force (N)	Contact time (s)	Rise time (s)	Punch travel (m)x10^{-5}	Relaxation time (s)	Dwell time (s)
			AMYLOSE		
5817.8	0.68	0.43	1.88	0.04	0.01
(130.0)	(0.02)	(0.01)	(0.41)	(0.02)	(0.01)
12230.5	0.97	0.66	1.22	0.03	0.02
(207.5)	(0.06)	(0.04)	(0.41)	(0.01)	(0.00)
18530.2	1.25	0.86	1.14	0.04	0.01
(285.4)	(0.11)	(0.07)	(0.54)	(0.03)	(0.00)
			AMYLOPECTIN		
6187.3	0.72	0.45	1.85	0.05	0.02
(137.0)	(0.02)	(0.02)	(0.62)	(0.02)	(0.01)
12089.9	0.95	0.64	1.18	0.04	0.02
(101.1)	(0.02)	(0.02)	(0.44)	(0.02)	(0.00)
18400.2	1.25	0.88	0.77	0.04	0.01
(229.7)	(0.11)	(0.08)	(0.26)	(0.02)	(0.00)

TABLE F.28 Extended Heckel plot results for amylose and amylopectin. Numbers in parentheses represent ± confidence intervals at the 95% level.

Peak force (N)	Correl. coeff.	Yield pressure (MPa)	Interc. A	Square area	% Under rising F area	% Above falling F area	% Chord area
			AMYLOSE				
5817.8	0.999	71.21	0.54	61.34	70.06	2.73	2.69
(130.0)	(0.001)	(2.04)	(0.01)	(1.19)	(1.06)	(0.21)	(0.21)
12230.5	0.997	74.33	0.63	200.42	61.89	3.63	4.34
(207.5)	(0.001)	(3.81)	(0.02)	(2.70)	(0.35)	(0.20)	(0.34)
18530.2	0.994	77.11	0.71	444.83	54.33	5.68	7.15
(285.4)	(0.001)	(3.00)	(0.15)	(11.93)	(1.03)	(0.58)	(0.52)
			AMYLOPECTIN				
6187.3	0.999	79.16	0.54	59.14	65.57	2.26	2.69
(137.0)	(0.001)	(0.91)	(0.02)	(1.20)	(1.17)	(0.24)	(0.21)
12089.9	0.998	80.13	0.57	176.12	59.75	4.69	4.16
(101.1)	(0.001)	(1.32)	(0.02)	(1.57)	(0.48)	(0.61)	(0.35)
18400.2	0.997	84.88	0.64	363.55	56.91	8.74	5.91
(229.7)	(0.001)	(1.80)	(0.03)	(6.52)	(0.62)	(0.74)	(0.36)

TABLE F.29 Creep results for batches of Starch 1500 containing different proportions of cold water solubles (c.w.s.). Numbers in parentheses represent ± confidence intervals at the 95% level.

Load (kN)	Relative density (t=0)	J_o^* $(MPa)^{-1}$ $x10^{-7}$	J_r $(MPa)^{-1}$ $x10^{-7}$	J_n $(MPa)^{-1}$ $x10^{-7}$	$\frac{J_n}{J_o^* + J_r}$
		15.4% c.w.s. (B.N. 807010)			
1	0.67(0.01)	7.14(0.78)	13.01(1.10)	6.35(0.93)	0.32(0.02)
2	0.71(0.01)	3.64(0.68)	10.15(0.59)	4.11(0.36)	0.30(0.01)
4	0.79(0.01)	2.16(0.27)	7.46(0.30)	2.86(0.24)	0.30(0.01)
6	0.85(0.01)	1.10(0.13)	4.33(0.26)	1.70(0.22)	0.31(0.02)
10	0.91(0.01)	0.68(0.09)	2.97(0.21)	1.11(0.09)	0.30(0.01)
		13.4% c.w.s. (B.N. 811024)			
1	0.64(0.00)	8.77(1.15)	15.38(1.15)	7.09(0.22)	0.29(0.01)
2	0.70(0.01)	4.10(0.30)	11.07(0.30)	4.72(0.26)	0.31(0.01)
4	0.79(0.01)	2.14(0.40)	7.54(0.48)	2.91(0.27)	0.30(0.01)
6	0.83(0.01)	1.23(0.11)	4.86(0.26)	2.17(0.11)	0.35(0.01)
10	0.90(0.01)	0.83(0.14)	3.33(0.18)	1.13(0.11)	0.27(0.02)
		12.6% c.w.s. (B.N. 801035)			
1	0.66(0.01)	7.63(2.32)	13.87(2.22)	6.68(0.70)	0.31(0.02)
2	0.70(0.01)	3.89(0.39)	11.67(0.34)	4.57(0.26)	0.29(0.01)
4	0.78(0.01)	2.32(0.19)	8.65(0.28)	3.10(0.21)	0.28(0.01)
6	0.85(0.01)	1.10(0.15)	4.21(0.19)	1.73(0.15)	0.33(0.01)
10	0.91(0.01)	0.67(0.08)	3.08(0.17)	1.16(0.08)	0.31(0.01)
		10.9% c.w.s. (B.N. 903025)			
1	0.66(0.01)	8.40(1.43)	14.14(1.43)	7.01(0.41)	0.31(0.01)
2	0.69(0.00)	4.52(0.68)	11.52(0.86)	5.42(0.29)	0.34(0.01)
4	0.79(0.01)	2.18(0.32)	7.56(0.44)	2.98(0.15)	0.31(0.01)
6	0.85(0.01)	1.04(0.11)	4.31(0.26)	1.68(0.14)	0.31(0.01)
10	0.91(0.01)	0.65(0.07)	3.23(0.20)	1.04(0.10)	0.27(0.02)

TABLE F.30 Parameters derived from creep data for batches of Starch 1500 containing different proportions of cold water solubles (c.w.s.). Numbers in parentheses represent ± confidence intervals at the 95% level.

Load (kN)	Relative density (t=0)	Elastic modulus (MPa) x10^6	Viscosity coefficient (MPa s) x10^8	J_i (MPa)$^{-1}$ x10^{-6}	k_2 (s)
		15.4% c.w.s. (B.N. 807010)			
1	0.67(0.01)	1.40(0.06)	1.77(0.03)	2.10(0.01)	2.04(0.01)
2	0.71(0.01)	2.75(0.12)	2.49(0.03)	1.47(0.01)	2.13(0.01)
4	0.79(0.01)	4.63(0.25)	3.59(0.05)	1.13(0.01)	2.19(0.01)
6	0.85(0.01)	9.09(0.20)	5.89(0.07)	0.58(0.01)	1.98(0.01)
10	0.91(0.01)	14.67(0.62)	12.03(0.03)	0.36(0.00)	1.96(0.02)
		13.4% c.w.s. (B.N. 811024)			
1	0.64(0.00)	1.14(0.11)	1.48(0.01)	2.34(0.01)	2.07(0.01)
2	0.70(0.01)	2.44(0.05)	2.21(0.03)	1.62(0.01)	2.13(0.01)
4	0.79(0.01)	4.67(0.31)	3.44(0.06)	0.99(0.01)	2.10(0.01)
6	0.83(0.01)	8.13(0.20)	5.11(0.08)	0.63(0.01)	1.97(0.01)
10	0.90(0.01)	11.98(0.98)	10.06(0.04)	0.41(0.00)	2.01(0.02)
		12.6% c.w.s. (B.N. 801035)			
1	0.66(0.01)	1.31(0.27)	1.51(0.03)	2.11(0.01)	2.02(0.01)
2	0.70(0.01)	2.57(0.16)	2.31(0.03)	1.63(0.01)	2.10(0.01)
4	0.78(0.01)	4.31(0.17)	3.25(0.06)	1.24(0.01)	2.10(0.01)
6	0.85(0.01)	9.10(0.28)	6.12(0.10)	0.57(0.01)	1.95(0.01)
10	0.91(0.01)	14.88(0.56)	12.33(0.25)	0.35(0.00)	2.01(0.01)
		10.9% c.w.s. (B.N. 903025)			
1	0.66(0.01)	1.19(0.11)	1.38(0.02)	2.16(0.01)	2.06(0.01)
2	0.69(0.00)	2.21(0.14)	2.01(0.04)	1.68(0.01)	2.12(0.01)
4	0.79(0.01)	4.58(0.22)	3.45(0.03)	0.97(0.01)	2.12(0.01)
6	0.85(0.01)	9.58(0.20)	5.84(0.08)	0.55(0.01)	2.00(0.01)
10	0.91(0.01)	15.41(0.53)	11.85(0.28)	0.34(0.00)	1.99(0.02)

TABLE F.31 Creep results for amylose and amylopectin. Numbers in parentheses represent ± confidence intervals at the 95% level.

Load (kN)	Relative density (t=0)	J_o^* $(MPa)^{-1}$ $\times 10^{-7}$	J_r $(MPa)^{-1}$ $\times 10^{-7}$	J_n $(MPa)^{-1}$ $\times 10^{-7}$	$\frac{J_n}{J_o^* + J_r}$
		AMYLOSE			
1	0.59(0.00)	4.38(0.92)	16.01(0.81)	6.51(0.12)	0.32(0.01)
2	0.66(0.01)	2.99(0.26)	11.73(0.33)	4.71(0.08)	0.32(0.01)
4	0.76(0.01)	1.93(0.19)	8.02(0.32)	3.11(0.08)	0.31(0.01)
6	0.82(0.01)	1.43(0.52)	5.23(0.04)	1.99(0.03)	0.30(0.00)
10	0.88(0.01)	0.68(0.30)	2.31(0.05)	0.91(0.05)	0.31(0.01)
		AMYLOPECTIN			
1	0.54(0.00)	3.92(0.75)	15.02(0.76)	6.36(0.17)	0.33(0.01)
2	0.61(0.00)	3.24(0.55)	10.11(0.69)	4.37(0.18)	0.33(0.01)
4	0.71(0.00)	1.93(0.14)	7.35(0.20)	2.90(0.05)	0.31(0.00)
6	0.77(0.01)	1.43(0.06)	5.20(0.20)	2.03(0.04)	0.31(0.01)
10	0.85(0.01)	0.73(0.04)	2.47(0.09)	1.01(0.03)	0.32(0.01)

TABLE F.32 Parameters derived from creep data for amylose and amylopectin. Numbers in parentheses represent ± confidence intervals at the 95% level.

Load (kN)	Relative density (t=0)	Elastic modulus (MPa) $\times 10^{6}$	Viscosity coefficient (MPa s) $\times 10^{8}$	J_i $(MPa)^{-1}$ $\times 10^{-6}$	k_2 (s)
		AMYLOSE			
1	0.59(0.00)	2.44(0.43)	1.32(0.03)	2.09(0.01)	2.21(0.01)
2	0.66(0.01)	3.39(0.31)	1.92(0.03)	1.50(0.01)	2.23(0.01)
4	0.76(0.01)	5.27(0.51)	2.90(0.07)	1.02(0.01)	2.19(0.01)
6	0.82(0.01)	7.02(0.26)	4.52(0.08)	0.68(0.01)	2.19(0.01)
10	0.88(0.01)	14.69(0.68)	9.94(0.06)	0.31(0.01)	2.13(0.01)
		AMYLOPECTIN			
1	0.54(0.00)	2.71(0.49)	1.42(0.03)	1.94(0.01)	2.19(0.01)
2	0.61(0.00)	3.25(0.58)	2.07(0.09)	1.37(0.01)	2.22(0.01)
4	0.71(0.00)	5.22(0.37)	3.09(0.05)	0.96(0.01)	2.20(0.01)
6	0.77(0.01)	7.01(0.28)	4.46(0.10)	0.68(0.01)	2.14(0.01)
10	0.85(0.01)	13.67(0.79)	9.87(0.03)	0.33(0.01)	2.05(0.01)

TABLE F.33 Diametral loading results for batches of Starch 1500 containing different proportions of cold water solubles (c.w.s.). Numbers in parentheses represent ± confidence intervals at the 95% level.

	Peak force (N)	Rel. dens.	Break. force (N)	Tensile strength (MPa)	Deform. before failure $(m)\times10^{-4}$	Work of failure $(J)\times10^{-4}$	Corr. work of failure (J/m^2)	Power of failure $(J/s)\times10^{-4}$	Apparent failure viscosity (MPa·s)	Area ratio
	6285.5	0.68	12.7	0.20	1.30	8.8	13.7	2.4	0.7	0.94
	(144.4)	(0.00)	(1.5)	(0.02)	(0.07)	(1.2)	(2.3)	(0.3)	(0.1)	(0.02)
15.4% c.w.s.	11829.7	0.75	27.8	0.48	1.60	24.1	41.6	5.4	2.1	0.92
(B.N. 807010)	(174.2)	(0.00)	(1.0)	(0.02)	(0.05)	(1.8)	(3.1)	(0.2)	(0.1)	(0.02)
	18230.0	0.79	39.9	0.73	1.88	41.7	76.0	7.8	3.9	0.90
	(248.3)	(0.00)	(1.4)	(0.03)	(0.06)	(3.3)	(6.2)	(0.3)	(0.3)	(0.02)
	5848.2	0.68	18.1	0.27	1.49	14.2	21.4	3.6	1.1	0.95
	(134.3)	(0.00)	(1.1)	(0.02)	(0.08)	(1.6)	(2.4)	(0.2)	(0.1)	(0.04)
13.4% c.w.s.	12259.6	0.78	53.0	0.92	2.27	64.9	112.2	9.5	6.3	0.93
(B.N. 811024)	(108.7)	(0.00)	(1.1)	(0.02)	(0.07)	(1.5)	(2.5)	(0.1)	(0.3)	(0.04)
	18100.1	0.81	73.8	1.33	2.52	96.9	174.9	12.2	10.5	0.96
	(217.3)	(0.00)	(3.1)	(0.06)	(0.10)	(5.3)	(9.7)	(0.4)	(0.7)	(0.04)

TABLE F.33 Diametral loading results for batches of Starch 1500 containing different proportions of cold water solubles (c.w.s.). Numbers in parentheses represent ± confidence intervals at the 95% level.

(continued)

	Peak force (N)	Rel. dens.	Break. force (N)	Tensile strength (MPa)	Deform. before failure (m)x10^{-4}	Work of failure (J)x10^{-4}	Corr. work of failure (J/m^2)	Power of failure (J/s)x10^{-4}	Apparent viscosity (MPa·s)	Area ratio
	6174.8	0.67	16.6	0.25	1.48	13.4	20.4	3.2	1.0	0.91
	(154.1)	(0.00)	(0.9)	(0.01)	(0.10)	(1.2)	(1.9)	(0.2)	(0.1)	(0.02)
12.6% c.w.s.	11810.0	0.73	27.5	0.45	1.82	28.1	46.5	5.7	2.2	0.89
(B.N. 801035)	(142.3)	(0.00)	(0.4)	(0.01)	(0.07)	(0.8)	(1.4)	(0.2)	(0.1)	(0.04)
	18330.5	0.78	44.9	0.79	2.11	52.9	93.6	8.5	4.9	0.90
	(240.8)	(0.00)	(1.5)	(0.03)	(0.08)	(3.5)	(6.3)	(0.2)	(0.4)	(0.03)
	5975.5	0.70	28.7	0.45	1.68	25.9	40.4	5.5	2.1	0.93
	(64.3)	(0.00)	(0.7)	(0.01)	(0.05)	(1.2)	(1.9)	(0.2)	(0.1)	(0.02)
10.9% c.w.s.	12120.0	0.79	22.8	1.14	2.29	80.7	140.7	11.2	8.2	0.93
(B.N. 903025)	(97.8)	(0.00)	(3.5)	(0.02)	(0.04)	(2.1)	(3.1)	(0.1)	(0.2)	(0.01)
	18349.9	0.84	41.0	1.53	2.72	128.2	235.0	14.4	13.6	0.88
	(338.4)	(0.00)	(3.5)	(0.02)	(0.18)	(11.2)	(20.8)	(0.7)	(0.9)	(0.04)

TABLE F.34 Diametral loading results for amylose and amylopectin. Numbers in parentheses represent ± confidence intervals at the 95% level.

	Peak force (N)	Rel. dens.	Break. force (N)	Tensile strength (MPa)	Deform. before failure $(m)\times10^{-4}$	Work of failure $(J)\times10^{-4}$	Corr. work of failure (J/m^2)	Power of failure $(J/s)\times10^{-4}$	Apparent failure viscosity (MPa·s)	Area ratio
	5817.8	0.60	7.7	0.10	1.00	4.9	6.7	1.7	0.3	0.78
	(130.0)	(0.01)	(0.9)	(0.01)	(0.11)	(0.9)	(1.2)	(0.2)	(0.06)	(0.05)
AMYLOSE	12230.5	0.70	22.8	0.36	1.12	14.5	22.9	4.5	1.15	0.90
	(207.5)	(0.00)	(3.5)	(0.06)	(0.16)	(4.2)	(6.6)	(0.8)	(0.30)	(0.03)
	18530.2	0.76	41.0	0.70	1.45	32.4	55.3	8.0	2.88	0.92
	(285.4)	(0.00)	(3.5)	(0.06)	(0.24)	(4.9)	(8.3)	(1.0)	(0.68)	(0.11)
	6187.3	0.54	2.6	0.03	0.89	1.7	2.1	0.6	0.09	0.70
	(137.0)	(0.01)	(0.3)	(0.00)	(0.16)	(0.4)	(0.5)	(0.1)	(0.02)	(0.04)
AMYLOPECTIN	12089.9	0.66	16.5	0.25	1.10	9.2	14.2	3.0	0.79	0.98
	(101.1)	(0.00)	(0.8)	(0.01)	(0.05)	(0.8)	(1.2)	(0.2)	(0.07)	(0.06)
	18400.2	0.70	27.4	0.38	1.27	17.3	23.6	4.9	1.34	1.01
	(229.7)	(0.02)	(2.7)	(0.08)	(0.10)	(2.8)	(4.3)	(0.5)	(0.74)	(0.05)

TABLE F.35 Parameters obtained during compaction for Starch 1500 (B.N. 306015) and National 1551. Numbers in parentheses represent ± confidence intervals at the 95% level.

	STARCH 1500			NATIONAL 1551		
Peak force (N)	6064.2	12313.5	18330.0	6250.2	12120.0	18269.8
	(67.8)	(95.1)	(225.6)	(58.4)	(81.3)	(87.2)
Work of compaction (lower punch) (J)	4.82	5.78	7.73	4.30	7.25	8.64
	(0.18)	(0.11)	(0.13)	(0.11)	(0.15)	(0.16)
True work of compaction (J) (lower punch)	4.98	5.52	7.39	4.17	7.04	8.34
	(0.06)	(0.08)	(0.11)	(0.11)	(0.14)	(0.11)
Expansion work (J)	0.16	0.26	0.34	0.13	0.22	0.30
	(0.02)	(0.04)	(0.05)	(0.02)	(0.03)	(0.09)
Expansion rate $(m/s)x10^{-4}$	4.13	2.72	2.61	5.46	3.28	2.96
	(0.39)	(0.36)	(0.49)	(0.65)	(0.42)	(0.46)
Punch travel $(m)x10^{-5}$	2.38	0.98	0.44	2.44	0.91	0.57
	(0.39)	(0.38)	(0.32)	(0.38)	(0.26)	(0.36)
Intercept A	0.69	0.70	0.73	0.55	0.55	0.57
	(0.01)	(0.01)	(0.01)	(0.02)	(0.04)	(0.09)
Yield pressure (MPa)	60.51	63.55	66.53	41.68	42.41	45.50
	(0.91)	(1.30)	(1.67)	(1.44)	(1.13)	(2.95)
% chord area	2.87	4.27	6.53	3.90	5.60	8.33
	(0.24)	(0.65)	(0.36)	(0.18)	(0.67)	(0.61)

TABLE F.36 Parameters derived form creep data for Starch 1500 (B.N. 306015) and National 1551. Numbers in parentheses represent ± confidence intervals at the 95% level.

Load (kN)	Relative density (t=0)	Elastic modulus (MPa) x10^6	Viscosity coefficient (MPa s) x10^8	J_i (MPa)$^{-1}$ x10^{-6}	k_2 (s)
		STARCH 1500			
1	0.67(0.00)	1.40(0.07)	1.72(0.11)	2.02(0.03)	1.92(0.01)
2	0.71(0.00)	2.86(0.28)	2.43(0.06)	1.36(0.03)	2.01(0.01)
4	0.80(0.01)	5.58(0.20)	3.93(0.07)	0.88(0.02)	2.06(0.01)
6	0.84(0.01)	8.66(0.85)	5.85(0.22)	0.57(0.03)	2.00(0.01)
10	0.93(0.01)	17.60(0.84)	13.98(0.14)	0.27(0.03)	1.98(0.01)
		NATIONAL 1551			
1	0.63(0.00)	1.81(0.08)	1.65(0.05)	1.98(0.02)	2.44(0.01)
2	0.70(0.00)	3.39(0.51)	2.21(0.05)	1.56(0.02)	2.44(0.01)
4	0.76(0.00)	4.27(0.12)	2.87(0.05)	1.20(0.02)	2.34(0.01)
6	0.82(0.00)	7.67(0.73)	4.93(0.08)	0.71(0.02)	2.21(0.01)
10	0.92(0.01)	16.58(0.89)	11.61(0.45)	0.36(0.03)	1.98(0.01)

TABLE F.37 Diametral loading results for Starch 1500 (B.N. 306015) and National 1551. Numbers in parentheses represent ± confidence intervals at the 95% level.

	STARCH 1500			NATIONAL 1551		
Compaction force (N)	6064.2 (67.8)	12313.5 (95.1)	18330.0 (225.6)	6250.2 (58.4)	12120.0 (81.3)	18269.8 (87.2)
Relative density	0.66 (0.00)	0.76 (0.00)	0.80 (0.00)	0.70 (0.00)	0.81 (0.00)	0.84 (0.00)
Breaking force (N)	14.4 (0.8)	43.8 (1.4)	66.1 (1.9)	73.7 (1.2)	162.4 (2.7)	191.1 (3.2)
Tensile strength (MPa)	0.22 (0.01)	0.75 (0.02)	1.20 (0.04)	1.18 (0.02)	2.97 (0.05)	3.64 (0.06)
Deformation before failure (m)x10^{-4}	1.59 (0.12)	2.11 (0.09)	2.50 (0.06)	2.53 (0.08)	3.27 (0.07)	3.33 (0.13)
Work of failure (J)x10^{-3}	1.23 (0.09)	5.23 (0.34)	8.60 (0.48)	10.21 (0.16)	28.51 (1.31)	34.50 (2.28)
Corrected work of failure (J/m^2)	18.5 (1.3)	89.7 (5.8)	156.4 (9.1)	163.1 (2.5)	522.2 (24.5)	658.4 (43.5)